



Universitat de Girona

REACTIVITY OF WELL-DEFINED ORGANOMETALLIC COPPER (III) COMPLEXES IN CARBON- HETEROATOM BOND FORMING REACTIONS

Alícia CASITAS MONTERO

Dipòsit legal: GI. 1042-2012

<http://hdl.handle.net/10803/81985>

ADVERTIMENT. L'accés als continguts d'aquesta tesi doctoral i la seva utilització ha de respectar els drets de la persona autora. Pot ser utilitzada per a consulta o estudi personal, així com en activitats o materials d'investigació i docència en els termes establerts a l'art. 32 del Text Refós de la Llei de Propietat Intel·lectual (RDL 1/1996). Per altres utilitzacions es requereix l'autorització prèvia i expressa de la persona autora. En qualsevol cas, en la utilització dels seus continguts caldrà indicar de forma clara el nom i cognoms de la persona autora i el títol de la tesi doctoral. No s'autoritza la seva reproducció o altres formes d'explotació efectuades amb finalitats de lucre ni la seva comunicació pública des d'un lloc aliè al servei TDX. Tampoc s'autoritza la presentació del seu contingut en una finestra o marc aliè a TDX (framing). Aquesta reserva de drets afecta tant als continguts de la tesi com als seus resums i índexs.

ADVERTENCIA. El acceso a los contenidos de esta tesis doctoral y su utilización debe respetar los derechos de la persona autora. Puede ser utilizada para consulta o estudio personal, así como en actividades o materiales de investigación y docencia en los términos establecidos en el art. 32 del Texto Refundido de la Ley de Propiedad Intelectual (RDL 1/1996). Para otros usos se requiere la autorización previa y expresa de la persona autora. En cualquier caso, en la utilización de sus contenidos se deberá indicar de forma clara el nombre y apellidos de la persona autora y el título de la tesis doctoral. No se autoriza su reproducción u otras formas de explotación efectuadas con fines lucrativos ni su comunicación pública desde un sitio ajeno al servicio TDR. Tampoco se autoriza la presentación de su contenido en una ventana o marco ajeno a TDR (framing). Esta reserva de derechos afecta tanto al contenido de la tesis como a sus resúmenes e índices.

WARNING. Access to the contents of this doctoral thesis and its use must respect the rights of the author. It can be used for reference or private study, as well as research and learning activities or materials in the terms established by the 32nd article of the Spanish Consolidated Copyright Act (RDL 1/1996). Express and previous authorization of the author is required for any other uses. In any case, when using its content, full name of the author and title of the thesis must be clearly indicated. Reproduction or other forms of for profit use or public communication from outside TDX service is not allowed. Presentation of its content in a window or frame external to TDX (framing) is not authorized either. These rights affect both the content of the thesis and its abstracts and indexes.

Tesi Doctoral

**Reactivity of Well-Defined Organometallic Copper(III)
Complexes in Carbon-Heteroatom Bond Forming Reactions**

ALICIA CASITAS MONTERO

March 2012

Programa de Doctorat en Ciències Experimentals i Sostenibilitat

Directors de Tesi:

Dr. Xavi Ribas Salamaña

Dr. Miquel Costas Salgueiro

Memòria presentada per a optar al títol de **Doctora**
per la **Universitat de Girona**.

Els sotasignants **Dr. Xavi Ribas Salamaña** i **Dr. Miquel Costas Salgueiro**, Professor Agregat i Professor Titular del Departament de Química de la Universitat de Girona, respectivament,

CERTIFIQUEN, que la memòria que porta per títol “Reactivity of well-defined organometallic copper(III) complexes in Carbon-Heteroatom bond forming reactions” que presenta l'**Alicia Casitas Montero**, ha estat realitzada sobre la seva direcció i constitueix la seva memòria de Tesi Doctoral per aspirar al grau de Doctora amb Menció Europea.

I perquè així consti, signen aquest certificat.

Dr. Xavi Ribas Salamaña

Dr. Miquel Costas Salgueiro

Girona, 30 de març del 2012.

*Els descobriments sempre es produeixen per casualitat...
si treballes suficientment com per provocar-la.*

Mario Capecchi – Premi Nobel de Medicina 2007

Als meus pares i germans

Agraïments

Doncs ja ha arribat el moment de fer balanç de tots aquests anys de doctorat i d'agrair a tota la gent que ha col·laborat de mil i una maneres diferents en la realització d'aquesta tesi, no només en el camp professional però també en el camp personal on, segurament, aquestes línies no seran suficients.

Volia començar agraint sincerament als meus directors de tesi, Xavi i Miquel, per donar-me l'oportunitat de realitzar la tesi en el seu grup, per tots els seus esforços i dedicació per a que la tesi anés sempre cap a la bona direcció i per tot el que m'han ensenyat al llarg d'aquests anys. A en Miquel, per la seva manera inhata d'entusiasmar-me a fer bona recerca i, perquè encara que vagi de bólit, sempre té temps per donar-me bons consells. A en Xavi, per seguir dia a dia els meus experiments (tant els fructuosos com els fracassos absoluts), per estar disponible a resoldre dubtes i ajudar en tot moment, i pel seu recolzament no només per a tirar endavant la química del coure(III) però també a nivell personal.

També vull agrair al professor Shannon S. Stahl per la seva col·laboració durant tots aquests anys de tesi. També per poder fer una estada de tres mesos al seu grup a Madison, que va ser molt aprofitosa, i també a la gent del seu grup, especialment la Lauren, que em van acollir molt bé en el laboratori.

Ara toca agrair a tots els QBISencs, perquè els bons companys de feina són imprescindibles per a disfrutar del doctorat i dels quals conservo molts bons records tant a dins com fora del laboratori. A l'Anna (sempre disposada a ajudar i a posar seny al QBIS quan fa falta), la Laura (quants bons moments juntes! I quants congressos!), l'Isaac (espero que li vagi molt bé el post-doc per Baltimore) i l'Irene (ja saps que ets la propera, sort!), amb tots ells he compartit la major part de la tesi. Encara m'enrecordo dels primers anys de doctorat comprimits al laboratori de la tercera planta de la facultat de ciències, dels esmorzars a can Paco, de les bromes de la M^aÁngeles, les hores al departx amb la resta d'inorgànics, dels sopars amb tots els becaris del departament... A la Mercè (i el seu bon humor i pels seus crits pel lab!), a la Cristina (amiga tant al laboratori com fora, amb qui sempre estic parlant de roba, fent plans de futur, explicant xafarderies...), a en Marc (amb qui comparteixo el coure(III), per la seva ajuda durant l'últim any, al final hem aconseguit un *Copper Team!*), a en Julio (i la seva passió per la química que va encomanant a tothom), a en Zoel (quin fenomen! No paris de fer oxigen!), a l'Olaf (sempre amb les seves catàlisi, bromes i bestieses). I a tots els que acabeu de començar en el grup us dono molts ànims: Mireia, Gerard, Joan, Arnau, David, Imma, Ming, Ferran, Marta. I a la

nova secretaria del grup Raquel, sense la qual segurament el manteniment del grup seria un desastre, no t'estressis per posar-ho tot en ordre!

No em vull oblidar de la resta persones del Departament de Química. Als becaris de l'àrea d'inorgànica (Jordi, Mónica, Isabel, Arnau, Pep Antón...) així com a la resta de becaris que formen part de moltes hores a la facultat i de molts bons moments. A també a les professores d'inorgànica, M^aÁngeles i Montse, que durant els primers anys a la facultat van ser de gran ajuda. I al professor Miquel Solà per col·laborar amb els estudis computacionals.

També vull agrair al Dr. Gaunt de la Universitat de Cambridge per poder realitzar una estada al seu laboratori l'estiu passat. A en Marcos per dirigir la meva recerca durant la meva estada i per totes les xerrades filosòfiques en el laboratori sobre química, política, i la vida en general. I a tota la gent del grup (Elise, Cathy, Lily, Elliot, Alice, Aurélien, Lindsey...) que em van incorporar molt ràpidament en el seu grup i van fer molt agradable l'estada. I no em puc oblidar de la *Spanish Mafia* (Amadeo, Marcos, Albert, Lena, Azucena, Aurélien...) per tots els dinars al *College*, barbacoes, sopars per gairebé tots els restaurants de Cambridge, les nits al Regal, Kambar... La veritat és que m'ho vaig passar molt bé, no sempre es comença i es termina una estada amb una festa!

Dins i fora de l'àmbit de la química volia agrair a l'Ester i l'Imma que vaig conèixer durant la carrera i amb les quals ha sorgit una molt bona amistat amb el pas del temps i que espero que continui durant molts anys més. I a la Mireia, pels bons moments al llarg d'aquest anys d'amistat. I també a la colla Tutsworld i la colla de Banyoles per tots els sopars, barbacoes, bicicletades... que fan més divertits els caps de setmana! També a les amigues de la infància, Lourdes i María José, que encara que sigui difícil, sempre trobem temps per trobar-nos i explicar-nos la vida. A l'Anna que ha marxat a viure lluny però que ens continuem trucant per telèfon, a veure si ens veiem aviat!

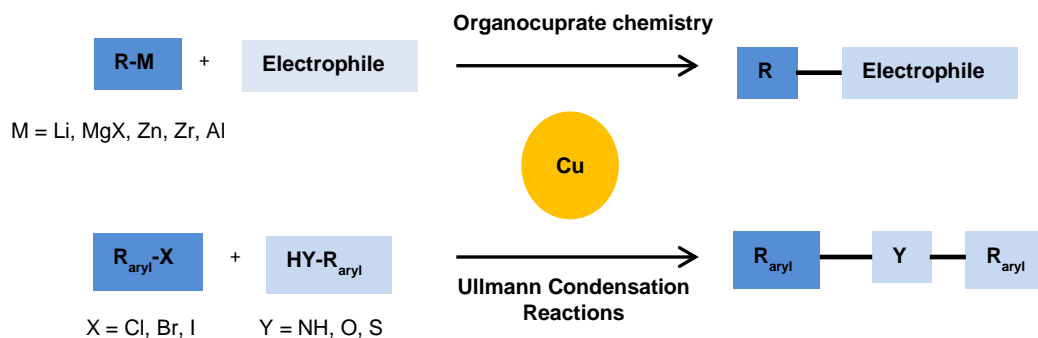
Finalment, aquesta tesi no hagués estat possible sense la meva família. Als meus pares i germans perquè sempre estan al meu costat tant les coses vagin bé com malament. A la meva germana que sé que puc comptar amb ella en tot. Al meu germà, per totes les hores junts, compartint *hobbies*, veient sèries de TV, pel·lícules, xerrant de coses *frikies*, de com solucionar el món...

Moltes gràcies a tots,

Alicia

Graphical Abstract

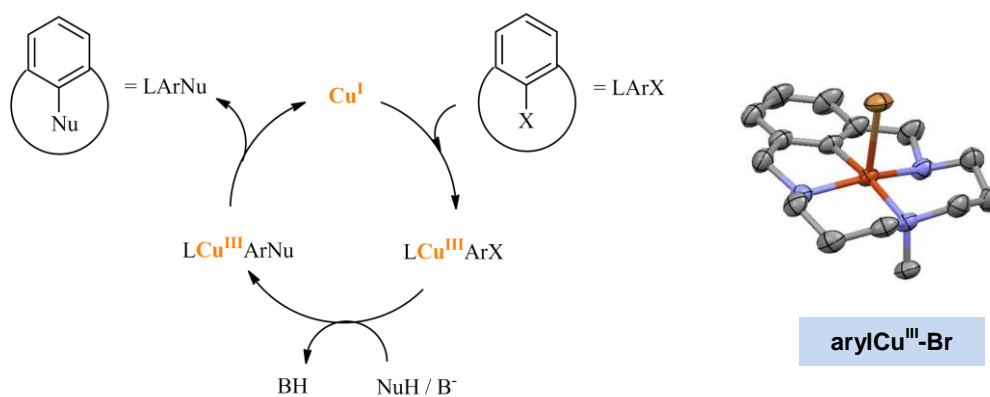
CHAPTER I. General Introduction (p. 27)



In this chapter we will focus on copper-catalyzed C-C and C-heteroatom bond forming reactions where copper(III) complexes have been proposed to have an important role. Moreover, recent relevant copper-catalyzed C-H functionalization reactions where copper(III) has also been invoked will be summarized. The reader will be introduced to the comprehension of these reactions from a mechanistic point of view. The aim of this chapter is to highlight the involvement of organometallic copper(III) complexes in organic transformations as the framework for the results disclosed in this thesis.

CHAPTER II. Objectives (p. 85)

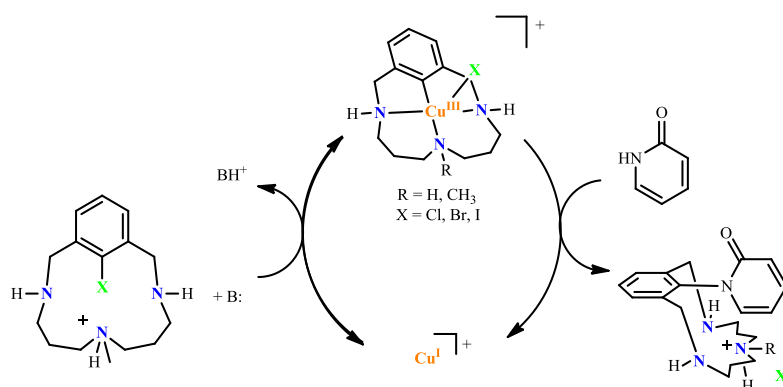
CHAPTER III. Results and Discussion (p. 89)



A general outlook of the results presented in chapters IV-VII will be provided here. The most important results will be summarized, and relevant additional information not included in the papers will be also added to improve the clarity of the discussion.

CHAPTER IV. (p. 141)

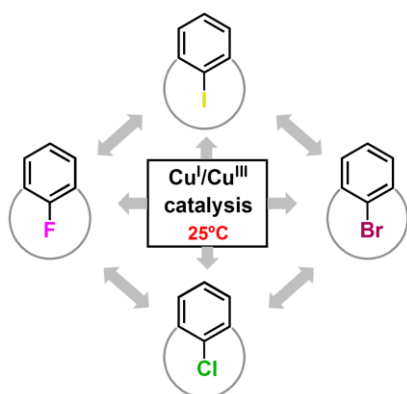
Direct observation of Cu^I/Cu^{III} redox steps relevant to Ullmann-type coupling reactions



The synthesis and characterization of a family of arylCu^{III}-halide complexes (X = Cl, Br, I) is described in this chapter. Their preparation has enabled the direct observation of aryl halide reductive elimination from Cu^{III} and the reversal oxidative addition at Cu^I. *In situ* spectroscopic studies (¹H-NMR and UV-Vis) of a Cu-catalyzed C-N coupling provides clear evidences for the involvement of an arylCu^{III}-halide intermediate in the catalytic mechanism.

CHAPTER V. (p. 149)

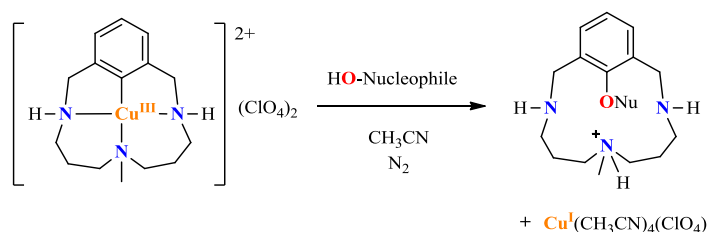
Nucleophilic aryl fluorination and aryl halide exchange mediated by a Cu^I/Cu^{III} catalytic cycle



Copper-catalyzed halide exchange reactions towards both heavier and lighter halides have been accomplished under very mild reaction conditions in a family of model aryl halide substrates. Aromatic fluorination of aryl halide substrates have also been achieved using common nucleophilic fluoride sources. Experimental and computational data support a mechanism based on two electron redox Cu^I/Cu^{III} catalytic cycle.

CHAPTER VI. (p. 159)

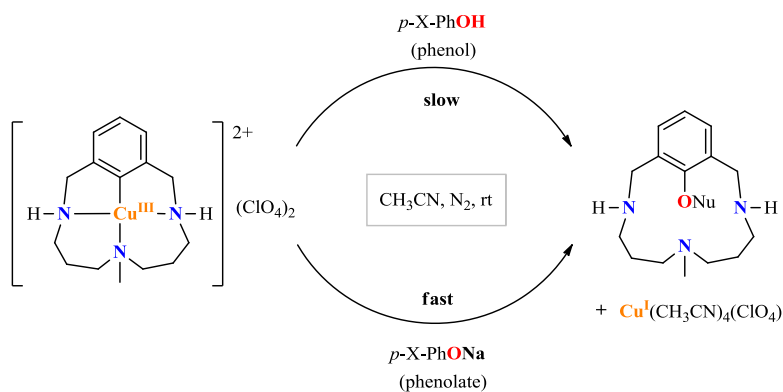
Observation and mechanistic study of facile C–O bond formation between a well-defined aryl-copper(III) complex and oxygen nucleophiles



The reactivity of arylCu^{III} complex with oxygen nucleophiles (carboxylic acids, phenols and aliphatic alcohols) to form the corresponding C–O coupled products has been explored and studied from a mechanistic point of view. Detailed kinetic data supports a reaction pathway that depends on the pK_A of the nucleophile.

CHAPTER VII. (p. 169)

Aryl-O reductive elimination from reaction of well-defined aryl-copper(III) species with phenolates: the importance of ligand reactivity



ArylCu^{III} complex undergoes rapid reductive elimination upon reaction with phenolates (⁻OPh) to form aryl-OPh cross-coupling products. The pH-active macrocyclic ligand undergoes an initial amine deprotonation that triggers a faster reactivity in comparison to phenols substrates. The detection of EPR active species will be discussed in detail.

CHAPTER VIII. General Discussion (p. 175)

CHAPTER IX. General Conclusions (p. 181)

Table of contents

Summary.....	17
Resum.....	19
Full List of Publications	21
Glossary of Abbreviations	23
Acknowledgements.....	25
Chapter I. General introduction	27
I. The role of organometallic copper(III) complexes in organic transformations.....	29
I.1 Copper in oxidation state +3.....	29
I.1.1 Organometallic copper(III) complexes	32
I.2 Nucleophilic organocuprate chemistry for C-C bond formation.....	34
I.2.1 General mechanism of C-C bond forming reactions with organocuprates	35
I.2.1.1 Conjugated additions to enones.....	37
I.2.1.2 S _N 2 alkylation reactions.....	38
I.2.1.3 S _N 2' allylic alkylations	40
I.3 Ullmann Condensation Reaction: C-heteroatom bond formation.....	42
I.3.1 Oxidation state of copper	44
I.3.2 Studies related to the active catalyst structure	45
I.3.3 Studies focusing on the activation of the aryl halide.....	49
I.3.3.1 Mechanism Involving σ -Bond Metathesis	50
I.3.3.2 Mechanism Involving π -Complexation of Copper(I) to Aryl Halides	51
I.3.3.3 One Electron Redox Processes via Cu ^I /Cu ^{II} : SET and AT.....	52
I.3.3.4 Oxidative Addition/Reductive elimination Cu ^I /Cu ^{III} pathway.....	57
I.3.4 Reactivity of well-defined arylcopper(III) complexes.....	62
I.4 Halide Exchange reactions catalyzed by copper	64
I.4.1 Fluorine insertion catalyzed by copper: a very challenging reaction	66

I.5	Direct C-H activation through copper complexes	69
I.5.1	Electrophilic C-H functionalization reactions.....	70
I.5.2	Intramolecular C-H activation in macrocyclic ligands as mechanistic models.	75
I.6	References.....	77

Chapter II. Main Objectives 85

Chapter III. Results and Discussion..... 89

III.1	Direct Observation of Cu ^I /Cu ^{III} redox steps relevant to Ullmann-type coupling reactions.....	91
III.1.1	Synthesis of arylCu ^{III} -halide complexes.....	91
III.1.2	Characterization of aryl-Cu ^{III} -halide complexes	92
III.1.2.1	Solid state structures	92
III.1.2.2	NMR characterization	94
III.1.2.3	UV-Visible spectroscopy	94
III.1.2.4	Electronic properties determined by Cyclic Voltammetry	95
III.1.3	Acid triggered C-halogen bond formation from well-defined arylCu ^{III} -halide complexes	97
III.1.3.1	Kinetic analysis.....	97
III.1.3.2	Characterization of intermediates in the reductive elimination reaction	99
III.1.3.3	Computational studies on C-Cl reductive elimination triggered by triflic acid .	102
III.1.4	Reversible oxidative addition of aryl halides to copper(I)	103
III.1.5	Catalytic intramolecular C-N reductive elimination reaction	104
III.2	Nucleophilic aryl fluorination and aryl halide exchange mediated by a Cu ^I /Cu ^{III} catalytic cycle	107
III.2.1	C-Halogen Reductive Elimination Triggered by External Ligands.....	107
III.2.2	Halide Exchange in Aryl-X Model Substrates (X = Cl, Br, I).....	108
III.2.2.1	DFT calculations on C-Cl reductive elimination reaction.....	113
III.2.3	Stoichiometric C-F bond forming reactions.....	114
III.2.3.1	DFT calculations on C-F reductive elimination reaction.....	116

III.2.4	Catalytic C-F bond forming reactions.....	117
III.2.5	Defluorination of Aryl Fluoride to Afford Aryl Chloride	119
III.3	Observation and mechanistic study of facile C–O bond formation between a well-defined arylcopper(III) complex and oxygen nucleophiles.....	121
III.3.1	Stoichiometric Carbon-Oxygen bond forming reactions	121
III.3.2	Kinetic analysis of C-O bond forming reaction.....	123
III.3.2.1	Carboxylic acids	124
III.3.2.2	Phenols	125
III.3.3	Efforts to identify arylCu ^{III} -nucleophile adducts.....	126
III.3.4	Mechanistic proposal	128
III.3.5	Catalytic C-O bond forming reaction.....	130
III.4	Aryl-O reductive elimination from reaction of well-defined aryl-copper(III) species with phenolates: the importance of ligand reactivity.....	131
III.4.1	Stoichiometric reactions with phenolates	131
III.4.2	Kinetic analysis of stoichiometric reactions with phenolates	132
III.4.3	Reactivity of arylcopper(III) complex with bases.....	134
III.4.4	Low Temperature NMR studies of intermediates	136
III.4.5	EPR experiments: detection of a Cu ^{II} complex.....	136
III.4.6	Mechanistic proposal	138
III.5	References.....	139

Chapter IV.	Direct observation of Cu ^I /Cu ^{III} redox steps relevant to Ullmann-type coupling reactions.....	141
--------------------	---	-----

Chapter V.	Nucleophilic aryl fluorination and aryl halide exchange mediated by a Cu ^I /Cu ^{III} catalytic cycle.....	149
-------------------	---	-----

Chapter VI.	Observation and mechanistic study of facile C–O bond formation between a well-defined aryl-copper(III) complex and oxygen nucleophiles	159
--------------------	--	-----

Chapter VII. Aryl-O reductive elimination from reaction of well-defined aryl-copper(III) species with phenolates: the importance of ligand reactivity.	169
Chapter VIII. General Discussion	175
Chapter VIII. General Conclusions	181
Annex	187
Supporting Information Chapter IV	189
Supporting Information Chapter V	203
Supporting Information Chapter VI	219
Supporting Information Chapter VII	235

Supplementary Digital Information

- pdf file of the Ph.D. Dissertation
- pdf file of the Digital Annex containing additional NMR spectra and theoretical data.
- cif files for each crystal structure presented in this thesis

Summary

This thesis is focused on the unexplored field of organometallic Cu^{III} chemistry, and especially on arylCu^{III} complexes. The synthesis and isolation of stable organometallic Cu^{III} complexes remains a challenging goal that has been achieved only in a limited number of systems. On the other hand, arylCu^{III} species have been proposed as key intermediates in Ullmann Condensation reactions. This reaction consists in the coupling of aryl halides and heteroatom nucleophiles catalyzed by copper, in the presence of a base, an auxiliary ligand and usually at high temperatures. The study of the reactivity of well-defined arylCu^{III} complexes may provide a better understanding of the mechanism of Ullmann Condensation reactions, which is still under intense debate.

The first part of this thesis (Chapter IV) deals with the synthesis and characterization of a family of arylCu^{III}-halide complexes (Cl, Br, I), which are stabilized within triazamacrocyclic ligands. C_{aryl}-halogen reductive elimination from arylCu^{III}-halide complexes as well as the reversal oxidative addition has been studied in depth, and the molecular details of these fundamental processes have been well-established in our systems. We have shown that arylCu^{III}-Br complexes are intermediates in copper-catalyzed C-N bond forming reaction in model aryl halide substrates. Our study represents the first direct observation of these fundamental two electron redox steps, which have been proposed in the mechanism of Ullmann Condensation Reactions.

Furthermore, we have explored halide exchange reactions in aryl halide model substrates based on a Cu^I/Cu^{III} catalytic cycle (Chapter V). Halide exchange reactions towards both heavier and lighter halides have been accomplished under very mild reactions conditions. Nucleophilic aromatic fluorination catalyzed by copper has also been achieved for the first time, and the intermediacy of arylCu^{III}-halide complexes has been demonstrated.

In the third part of the thesis, we have explored the reactivity of arylCu^{III} complex in C-O bond forming reactions using oxygen nucleophiles, including carboxylic acids, phenols and aliphatic alcohols (Chapter VI). Mechanistic studies have revealed a reaction pathway that depends on the pK_A of the nucleophile. Besides we have developed copper-catalyzed C-O bond forming reactions with a Cu^I/Cu^{III} catalytic cycle in aryl halide model substrates.

Finally, the fourth part of this thesis aimed at study the differences in reactivity for deprotonated O-nucleophiles with our isolated arylCu^{III} complex, in concrete, using phenolate derivatives (Chapter VI). The non-innocent role of the macrocyclic ligand of the complex, caused by its acid/base properties, is reflected by a faster C-O coupling reaction with phenolates than the corresponding phenols. The pH-dependent reactivity of the complex might be a strategy to consider in the development of novel catalytic processes.

Therefore, we have shown the feasibility of arylCu^{III} complexes to participate in C_{aryl}-heteroatom bond forming reactions at very mild conditions. The obtained results with our

model systems, with the remarkable characterization of arylCu^{III}-halide species under catalytic conditions for the first time, are relevant in Ullmann Condensation Reactions from a mechanistic and fundamental point of view. This work also opens the door to the exploration of copper-catalyzed nucleophilic fluorinations of aryl halides. Furthermore, the results obtained in aryl halide model substrates open an interesting approach for the development of new copper catalysts that may operate under milder reaction conditions, based on two electron redox Cu^I/Cu^{III} catalytic cycle.

Resum

Aquesta tesi es centra en el camp de la química organometàl·lica del Cu^{III} que roman sense explorar, concretament en complexos $\text{arilCu}^{\text{III}}$. La síntesi i l'aïllament de complexos organometàl·lics estables de Cu^{III} és encara un objectiu desafiant que només s'ha aconseguit en un nombre limitat de sistemes. Tanmateix, les espècies $\text{arilCu}^{\text{III}}$ s'han proposat com a intermedis clau en les reaccions de Condensació Ullmann. Aquesta reacció consisteix en l'acoblament d'halurs d'aril i nucleòfils amb heteroàtoms catalitzats per coure, en presència de base, lligand auxiliar i, generalment, a altes temperatures. L'estudi de la reactivitat de complexos d' $\text{arilCu}^{\text{III}}$ ben definits pot proporcionar una millor comprensió del mecanisme de les reaccions de Condensació Ullmann, el qual està encara sota debat intens.

La primera part de la tesi (Capítol IV) consisteix en la síntesi i la caracterització d'una família de complexos $\text{arilCu}^{\text{III}}$ -halur (Cl, Br, I), els quals s'estabilitzen amb lligands triazamacrocíclics. L'eliminació reductiva C_{aril} -halogen, a partir de complexos $\text{arilCu}^{\text{III}}$ -halur, així com l'addició oxidant, que és la reacció inversa, s'han estudiat en profunditat i els detalls moleculars d'aquests processos fonamentals s'han establert en els nostres sistemes. Hem demostrat que els complexos $\text{arilCu}^{\text{III}}$ -Br són intermedis en la reacció de formació d'enllaç C-N catalitzada per coure en substrats models d'halur d'aril. El nostre estudi representa la primera observació directa d'aquests processos redox fonamentals a dos electrons, els quals s'han proposat en el mecanisme de les reaccions de Condensació Ullmann.

A continuació, s'han explorat les reaccions d'intercanvi d'halurs en substrats model d'halurs d'aril basats en un cicle catalític $\text{Cu}^{\text{I}}/\text{Cu}^{\text{III}}$ (Capítol V). Les reaccions d'intercanvi d'halurs, tant cap a halurs més pesants com cap a halurs més lleugers, s'han aconseguit en condicions de reacció molt suaus. La fluoració aromàtica nucleofílica catalitzada amb coure també s'ha aconseguit per primera vegada, i s'ha demostrat que els complexos $\text{arilCu}^{\text{III}}$ -halur estan involucrats en la reacció.

En la tercera part de la tesi, s'ha explorat la reactivitat del complex $\text{arilCu}^{\text{III}}$ en reaccions de formació d'enllaç C-O utilitzant nucleòfils basats en oxigen, on s'inclouen àcids carboxílics, fenols i alcohols alifàtics (Capítol VI). Els estudis mecanístics han revelat un mecanisme de reacció que depèn del pK_{A} del nucleòfil. A més a més, s'han desenvolupat reaccions de formació d'enllaç C-O catalitzades per coure i basades en un cicle catalític $\text{Cu}^{\text{I}}/\text{Cu}^{\text{III}}$ en substrats model d'halurs d'aril.

Finalment, la quarta part de la tesi té l'objectiu d'estudiar les diferències de reactivitat dels nucleòfils basats en oxigen desprotonats amb el complex aïllat $\text{arilCu}^{\text{III}}$, utilitzant, concretament, derivats fenolats (Capítol VI). El paper no innocent del lligand macrocíclic del complex, causat per les seves propietats àcid/base, es reflexa per una reacció de formació d'enllaç C-O més ràpida amb fenolats que amb els corresponents fenols. La reactivitat del

complex dependent del pH pot ser una estratègia a considerar en el desenvolupament de nous processos catalítics.

Per tant, s'ha demostrat la viabilitat dels complexos $\text{arylCu}^{\text{III}}$ per a participar en reaccions de formació d'enllaç C_{aryl} -heteroàtom en condicions suaus de reacció. Els resultats obtinguts en els nostres sistemes models, amb la remarcable caracterització per primer cop de les espècies $\text{arylCu}^{\text{III}}$ -halur sota condicions catalítiques, són rellevants en les reaccions de Condensació d'Ullmann des d'un punt de vista mecanístic i fonamental. A més a més, aquest treball obre les portes a explorar les fluoracions nucleofíliques catalitzades per coure en halurs d'aryl. Finalment, els resultats obtinguts en els substrats model d'halurs d'aryl poden iniciar un interessant apropament cap al desenvolupament de nous catalitzadors de coure que puguin operar en condicions de reacció suaus, sota un cicle catalític $\text{Cu}^{\text{I}}/\text{Cu}^{\text{III}}$ basat en processos redox a dos electrons.

Full list of publications

This thesis is based on the following publications:

Chapter IV

1. Direct observation of Cu^I/Cu^{III} redox steps relevant to Ullmann-type coupling reactions. Casitas, A.; King, A. E.; Parella, T.; Costas, M.; Stahl, S. S.; Ribas, X. *Chem. Sci.* **2010**, *1*, 326.

Chapter V

2. Nucleophilic aryl fluorination and aryl halide exchange mediated by a Cu^I/Cu^{III} catalytic cycle. Casitas, A.; Canta, M.; Solà, M.; Costas, M.; Ribas, X. *J. Am. Chem. Soc.* **2011**, *133*, 19386.

Chapter VI

3. Observation and mechanistic study of facile C–O bond formation between a well-defined aryl-copper(III) complex and oxygen nucleophiles. Huffman, L. M.; Casitas, A.; Font, M.; Canta, M.; Costas, M.; Ribas, X.; Stahl, S. S. *Chem. Eur. J.* **2011**, *17*, 10643.

Chapter VII

4. Aryl-O reductive elimination from reaction of well-defined arylCu^{III} species with phenolates: the importance of ligand reactivity. Casitas, A.; Ioannidis, N.; Mitrikas, G.; Costas, M.; Ribas, X. *Dalton Trans.*, **2011**, *40*, 8796.

Publications not included in this thesis:

5. Copper-Catalyzed Aerobic Oxidative Functionalization of an Arene C-H Bond: Evidence for an Aryl-Copper(III) Intermediate. King, A. E.; Huffman, L. M.; Casitas, A.; Costas, M.; Ribas, X.; Stahl, S. S. *J. Am. Chem. Soc.* **2010**, *132*, 12068.

6. Facile C-H Bond Cleavage via a Proton-Coupled Electron Transfer Involving a C-H...Cu^{II} Interaction. Ribas, X.; Calle, C.; Poater, A.; Casitas, A.; Gómez, L.; Xifra, R.; Parella, T.; Benet-Buchholz, J.; Schweiger, A.; Mitrikas, G.; Solà, M.; Llobet, A.; Stack, T. D. P. *J. Am. Chem. Soc.* **2010**, *132*, 12299.

7. Molecular mechanism of acid-triggered aryl-halide cross-coupling reaction via reductive elimination in well-defined arylCu^{III}-halide species. Casitas, A.; Poater, A.; Solà, M.; Stahl, S. S.; Costas, M.; Ribas, X. *Dalton Trans.*, **2010**, *39*, 10458.

Glossary of Abbreviations

abs	absorbance
Ac	Acetyl
acac	acetylacetonate
AQH	anthraquinone
AQBr	1-bromoanthraquinone
AQBr ⁻	1-bromoanthraquinone radical anion
Ar	Aryl
AT	Atom Transfer
AU	Atomic Unit
B	Base
Bu	Butyl
CCDD	Cambridge Crystallographic Data Centre
COSY	Correlation Spectroscopy (2D NMR experiment)
Cy	cyclohexanyl
CV	Cyclic Voltammetry
cw	continuous wave
DFT	Density Functional Theory
DMF	<i>N,N'</i> -Dimethylformamide
DMSO	Dimethylsulfoxide
ENDOR	Electron-Nuclear Double Resonance (EPR experiment)
$E_{1/2}$	Half-wave potential
E _{pa}	anodic peak potential
E _{pc}	cathodic peak potential
EPR	Electron Paramagnetic Resonance
equiv	equivalents
ESI-MS	ElectroSpray Ionization Mass Spectrometry
ESI-HRMS	ElectroSpray Ionization High-Resolution Mass Spectrometry
Fc/Fc ⁺	Ferrocene/Ferrocinium
GC/MS	Gas Chromatography/Mass Spectrometry
h	hour
HMBC	Heteronuclear Multiple Bond Correlation (2D NMR experiment)
HMPA	Hexamethylphosphoramide
HSQC	Heteronuclear Single Quantum Coherence (2D NMR experiment)
HYSCORE	Hyperfine Sublevel Correlation (EPR experiment)
IAT	Iodine Atom Transfer
ⁱ Pr	isopropyl

KIE	Kinetic Isotope Effect
L	Ligand
LMCT	Ligand to Metal Charge Transfer
Me	Methyl
min	minutes
<i>m/z</i>	mass/charge
NHC	N-heterocyclic carbene
NMP	N-methyl-pyrrolidinone
NMR	Nuclear Magnetic Resonance
NOESY	Nuclear Overhauser effect spectroscopy (2D NMR experiment)
norm abs	Normalized absorbance
Nu	nucleophile
OTf	trifluoromethanesulfonate anion
p	page
PCET	Proton-Coupled Electron Transfer
PCM	Polarizable continuous solvation model
PET	Positron Emission Tomography
Ph	Phenyl
phen	1,10-phenanthroline
Proton-sponge [®]	1,8-Bis(dimethylamino)naphthalene
SET	Single Electron Transfer
SM	Starting Material
SSCE	Saturated Sodium Calomel Electrode
RDS	Rate-Determining Step
RMN	Nuclear Magnetic Resonance
rt	room temperature
TBAP	tetrabutylammonium phosphate
TEMPO	2,2,6,6-tetramethylpiperidine-1-oxyl
THF	tetrahydrofuran
TMEDA	<i>N,N,N,N</i> -tetramethylethylenediamine
UV-Vis	Ultraviolet-Visible
vs.	versus
XAS	X-Ray Absorption Spectroscopy

Acknowledgements

This work would not have been possible without the following collaborations:

- Serveis Tècnics de Recerca from Universitat de Girona for technical support.
- Prof. Dr. Shannon S. Stahl, Dr. Lauren M. Huffman and Dr. Amanda E. King from University of Wisconsin-Madison for hosting a scientific visit and the collaborative work in the reactivity of copper(III) complexes.
- Dr. George Mitrikas and Nikolaos Ioannidis from Institute of Materials Science at NCSR Demokritos (Athens), for EPR spectroscopy experiments.
- Dr. Teodor Parella from Servei de NMR at Universitat Autònoma de Barcelona for some NMR experiments and helping discussions.
- Dr. Albert Poater and Prof. Dr. Miquel Solà from Institut de Química Computacional and Mercè Cantà from Departament de Química of Universitat de Girona for DFT calculations.
- MICINN of Spain for financial support through projects CTQ2006-05367/BQU and CTQ2009-08464/BQU, and MICINN for a PhD FPU Grant AP2007-01954.



CHAPTER I.
General Introduction

The role of organometallic copper(III) complexes in organic transformations

Copper catalysis in organic transformations is one of the most successful and useful strategies to effect C-C and C-Heteroatom bond formation. Among the hundreds of reactions catalyzed or mediated by copper, we want to highlight some of the most useful types, with a focused interest in the mechanistic understanding of these processes, and specifically, the mechanistic role of the copper metal center. The type of reactions that will be covered in the introduction of this thesis include nucleophilic organocuprate chemistry for C-C bond formation and C-Heteroatom cross-coupling reactions (Ullmann Condensation reactions and Halide-exchange processes). Moreover, we will highlight some direct C-H bond functionalizations catalyzed by copper with or without the presence of external oxidants.

The limited stability of copper(III) complexes have precluded to study the organometallic chemistry of these complexes for a long time. Nevertheless, growing evidences of the participation of copper(III) complexes in these organic transformations, especially in organocuprate chemistry, have increased the interest of researchers in copper in oxidation state +3.

I.1 Copper in oxidation state +3

Copper as a late transition metal is known in a wide range of coordination numbers and oxidation states (from Cu^0 to Cu^{IV}), as reflected by the uncountable number of copper compounds described in the literature.^{1,2} While copper complexes in oxidation states +1 and +2 are the most common, copper complexes in oxidation state +3 are known in a narrow number of complexes. Hereafter we will briefly summarize the most important contributions in the synthesis and characterization of Cu^{III} complexes. It is worth to mention that several Cu^{III} species have been characterized upon oxygen activation in low-molecular weight chemical models of copper metalloenzymes, but those will not be discussed in this thesis.^{3,4}

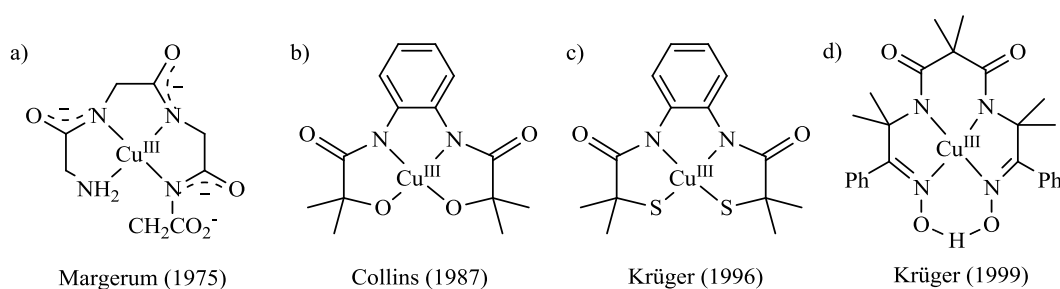
Most of copper(III) complexes show coordination number four in a square-planar geometry, which is the most stable environment for a d^8 electronic configuration, in agreement with the Ligand-Field Theory.⁵ On the other hand, there are several examples reporting axial coordination affording pentacoordinated square-pyramidal geometry. Whereas copper(III) complexes in both square-planar and square-pyramidal geometries are diamagnetic, complexes with octahedral geometry exhibit paramagnetic properties, for instance, $\text{K}_3[\text{Cu}^{\text{III}}\text{F}_6]$ that has been described in text books² and the heterometallic compound $[\text{LCu}^{\text{III}}\text{Cu}^{\text{III}}\text{Co}^{\text{III}}\text{L}](\text{ClO}_4)_3$, where the ligand is the hexadentate macrocyclic trianion 1,4,7-tris(4-*tert*-butyl-2-sulfidobenzyl)-1,4,7-triazacyclononane.⁶ Takui and coworkers reported

the diamagnetic-to-paramagnetic conversion of a tris(2-pyridylthio)methylcopper(III) through a geometry change from trigonal bipyramidal to octahedral upon addition of chloride.⁷

With regard to the stability of copper(III), early reports described complexes that are only stable in the solid state, for instance, $\text{NaCu}^{\text{III}}\text{O}_2$, Cu^{III} -bis-biuret and Cu^{III} -bis-oxamide.⁸⁻¹⁰ Some copper(III) complexes were generated in aqueous media or acetonitrile by electrochemical experiments in the presence of macrocyclic amines^{11,12} or by pulse radiolytic experiments,¹³⁻¹⁵ but they decompose spontaneously in solution towards copper(II) species. Moreover, copper(III) is considered a strong oxidant, and, in fact, $\text{K}_7\text{Cu}^{\text{III}}(\text{IO}_6)_2$ and $\text{K}_9\text{Cu}^{\text{III}}(\text{TeO}_6)_2$, generated in alkaline solutions, have been used as oxidizing reagents for inorganic compounds as well as organic substrates.^{16,17}

In 1975, Margerum and coworkers reported the first characterization of long-lived copper(III) complex in aqueous solution using a deprotonated tetraglycine ligand (Scheme I.1.1, a). The Cu^{III} -peptide complex was formed by chemical oxidation using IrCl_6^{2-} and it has a half-life of about 2h at 25° C. The strong electron donor properties of the ligand and the favorable square planar geometry stabilize the Cu^{III} -peptide complex, as indicated by the low $\text{Cu}^{\text{III}}/\text{Cu}^{\text{II}}$ redox potential.¹⁸ Since then, Margerum reported the synthesis of several copper(III) complexes bearing peptides ligands and studied their properties.¹⁹⁻²³

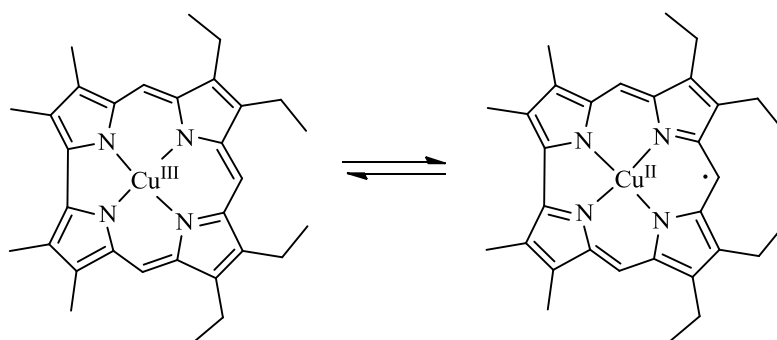
The strategy of using anionic ligands that force square planar geometry has been widely used in order to stabilize other copper(III) complexes, which have been obtained by electrochemical or chemical oxidation methods (i.e. Scheme I.1.1, b-d). Therefore, several copper(III) complexes bearing ligands with strong σ -donor groups such as carboxylate, amido, thiolate, alkoxide, phenolate, oxime and hydrazide groups have been isolated.²⁴⁻²⁷ The comparison of several $\text{Cu}^{\text{III}}/\text{Cu}^{\text{II}}$ redox potentials in water and CH_3CN indicates the general trend of enhanced stabilization of copper(III) complexes by increasing the number of anionic donor atoms and by introducing thiolate donor groups.²⁶



Scheme I.1.1. Examples of copper(III) complexes bearing anionic square-planar ligands.

Porphyrins and corrole ligands have also been used to stabilize copper in high oxidation states but the non-innocent role of these ligands has been debated.²⁸⁻³⁰ Ambiguity in

formal oxidation state assignments can arise when a metal center is bound to an unsaturated ligand with an extended π system that is mixed with the metal orbitals. In this context, Gross and coworkers reported the synthesis of diamagnetic copper(III) complexes using corrole ligands that were in equilibrium with the corresponding paramagnetic Cu^{II} π -cation radical complexes at high temperature (Scheme I.1.2).²⁸ Ghosh calculated that the ground-state of the corrole copper complex is best described as a diamagnetic Cu^{III} , being the Cu^{II} π -cation radical state higher in energy.²⁹ This behavior was shown to be general in many corrole complexes.³⁰ The non-innocent role of ligand have also been questioned in square-planar copper(III) complexes based on bis-1,2-dithiolene and bis-1,2-diselenolene ligands.³¹⁻³³

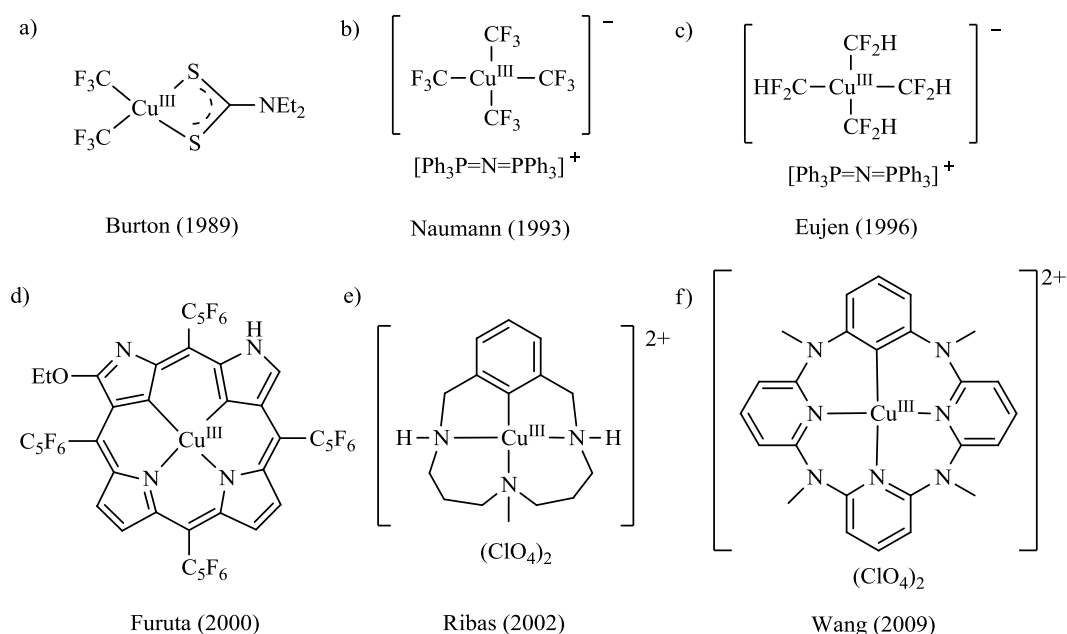


Scheme I.1.2. Equilibrium between ground state copper(III) complex and copper(II) π -cation radical complex proposed by Gross.

Several common spectroscopic methods used for characterizing copper complexes include Electron Paramagnetic Resonance (EPR) spectroscopy, which is mainly applied for obtaining structural information of paramagnetic copper(II) solutions, and Nuclear Magnetic Resonance (NMR) spectroscopy, which is used for studying diamagnetic copper(I) and square-planar copper(III) complexes in solution.³⁴ $^{63/65}\text{Cu}$ NMR spectroscopy cannot be applied to most of NMR active copper complexes because of the large quadrupole moments of the metal center and NMR is limited to the active nuclei of ligands. On the other hand, Cu K-edge X-Ray Absorption Spectroscopy (XAS) has been used as an unambiguous technique for determining the oxidation state of the copper in many complexes.^{35,36} Hodgson, Solomon and coworkers reported that the distinct feature of copper(III) is a $1s \rightarrow 3d$ transition centered on 8981 eV, approximately 2 eV higher than the characteristic energy of this transition for Cu^{II} oxidation state.

I.1.1 Organometallic copper(III) complexes

The number of organometallic copper(III) complexes containing a C-Cu^{III} bond is very limited. Initially, the main strategy employed for stabilizing these complexes was the use of trifluoro- or perfluoroalkyl groups bound to the copper(III). The first crystallographically characterized organometallic copper(III) complex, [Cu^{III}(CF₃)₂(SC(S)NEt₂)], was reported in 1989 by Burton and coworkers (Scheme I.1.3, a).³⁷ They reported two synthetic strategies for obtaining [Cu^{III}(CF₃)₂(SC(S)NEt₂)], either by methathesis of [Cu^{III}Br₂(SC(S)NEt₂)] complex with trifluoromethylcadmium reagents or by chemical oxidation of complex [(CF₃)₂Cu]. In 1993, Naumann reported the synthesis of stable [(CF₃)₄Cu]⁻ (Scheme I.1.3, b).³⁸ Related organocuprate(III) complexes bearing trifluoro or difluoromethyl ligands have been also reported (Scheme I.1.3, c).³⁹



Scheme I.1.3. Stable organometallic copper(III) complexes.

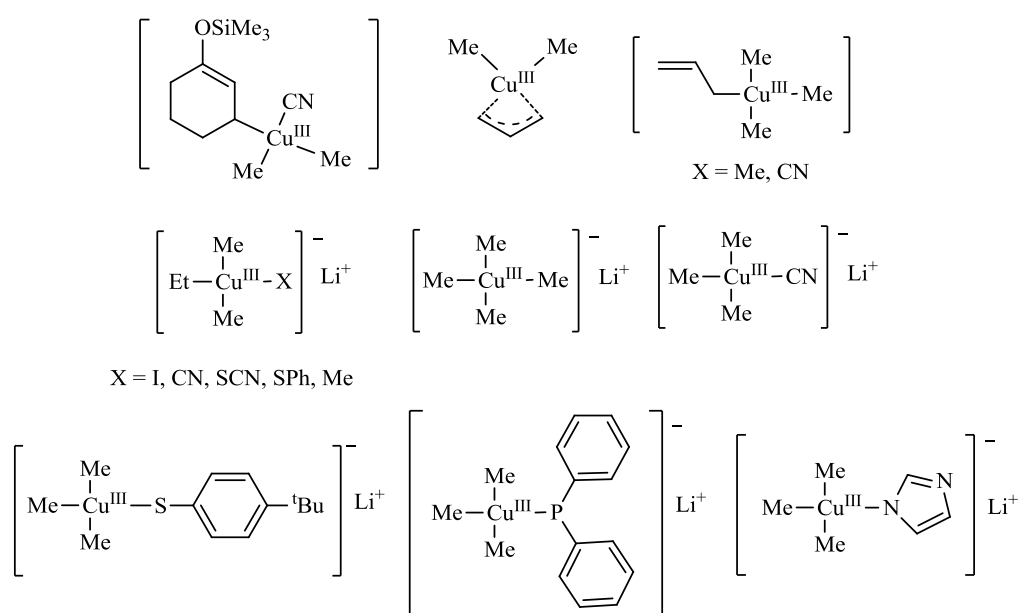
More recently, heteroatom-confused porphyrins, especially nitrogen-confused porphyrins, have been used to stabilize organometallic copper(III) complexes. In this context, Furuta and coworkers reported the formation of several organometallic copper(III) complexes in a doubly N-confused porphyrin ligand that contains strong σ donor ligands (two carbanions and one deprotonated amine) (Scheme I.1.3, d).^{40,41} Besides, N- and O-Confused-porphyrin ligands have allowed also the characterization of rare organometallic copper(II) complexes in both solution and solid state.⁴²⁻⁴⁴ Furuta and coworkers reported the interconversion between Cu^{II} and Cu^{III} complexes bearing N-confused porphyrin ligands, by one electron chemical

oxidation/reduction, which is stimulated by the accompanying protonation/deprotonation of the perimeter N atom.⁴⁵

In 2002 Ribas, Lobet, Stack and coworkers reported the synthesis and characterization of a family of triazamacrocyclic copper(III) complexes containing a $C_{\text{aryl}}\text{-Cu}^{\text{III}}$ bond (Scheme I.1.3, e).^{46,47} During the realization of this thesis, another arylcopper(III) complex based on an azacalixarene ligand was reported by Wang and coworkers (Scheme I.1.3, f).⁴⁸ Interestingly, the formation of these two organocopper(III) complexes occurs through copper(II) mediated C-H bond activation reaction (see section I.5.2).

The development of rapid injection NMR spectroscopy at very low temperature during the last decade, has allowed the characterization of several unstable tri- and tetraordinated organometallic copper(III) complexes (Scheme I.1.4). These complexes are formed in reactions of organocuprate reagents with electrophile substrates, such as alkyl and allyl halides and α,β -unsaturated ketones (see section I.2.1).⁴⁹⁻⁵¹ Among all copper(III) complexes characterized, tetraalkylcopper(III) complexes, such as $[\text{Me}_4\text{Cu}]\text{Li}$ and $[\text{EtMe}_3\text{Cu}]\text{Li}$, have been found to be stable at low temperature, despite they do not bear perfluoroalkyl groups.⁵²

Furthermore, it has been reported the synthesis, *via* ligand exchange reactions, of trialkyl copper(III) complexes bearing a fourth heteroatom ligand $[\text{EtMe}_2\text{CuX}]\text{Li}$ ($X = \text{I}, \text{CN}, \text{SCN}, \text{SPh}$) and $[\text{Me}_3\text{CuX}]$ ($X = \text{PPh}_2, \text{CN}, \text{imidazole}, p\text{-}(tert\text{-butyl})\text{thiophenolate}$).^{51,53,54} The stability of these complexes depends on the fourth ligand coordinated to the metal center, and they are less stable than tetraalkylcopper(III) complexes. Indeed, Density Functional Theory (DFT) calculations showed that the methyl anion is a strong σ -donor ligand that affords the largest stabilization energy in comparison to halides, thiolate and cyanide anions.⁵⁴

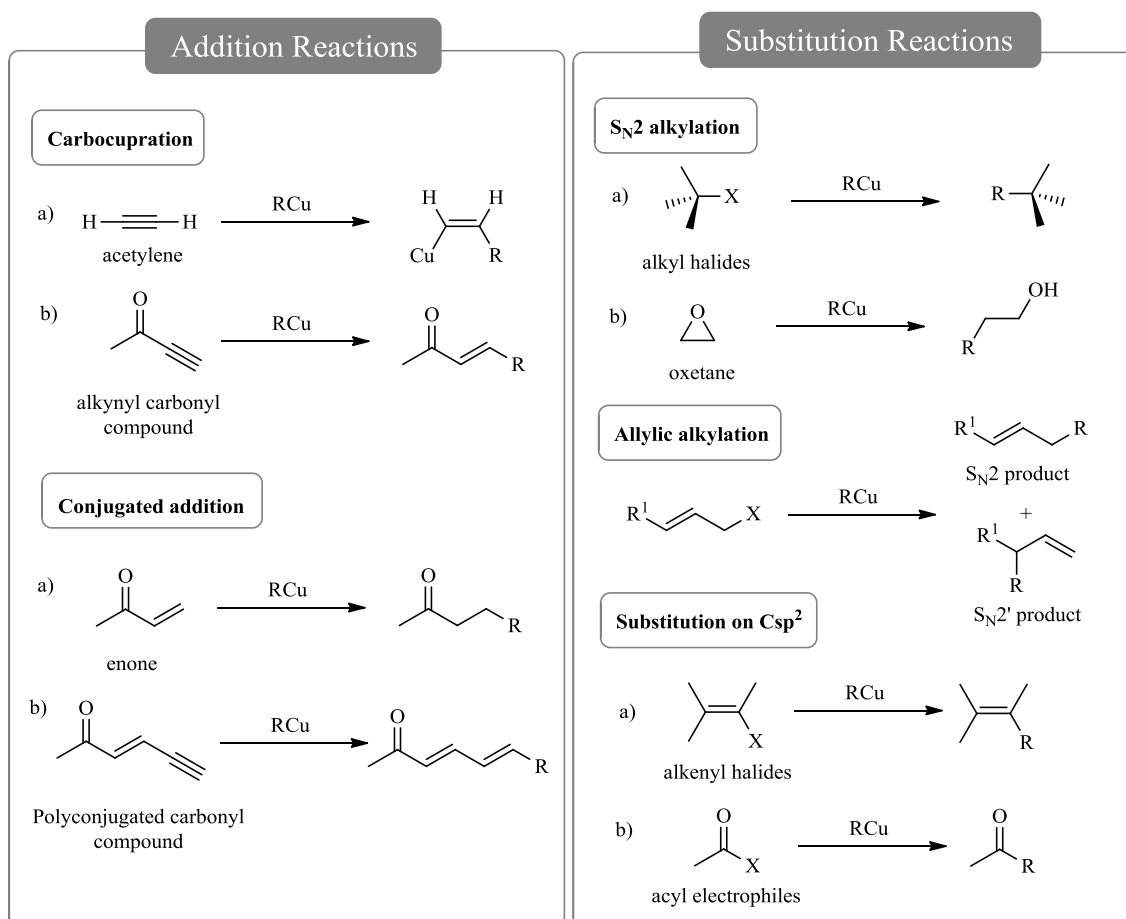


Scheme I.1.4. Copper(III) complexes detected by NMR spectroscopy at low temperature.

I.2 Nucleophilic organocuprate chemistry for C-C bond formation

In general, the organometallic chemistry of copper is almost exclusively focused on the metal oxidation state +1. Organocopper(I) compounds are widely applied in C-C bond forming processes because they are able to deliver alkyl, vinyl, alkynyl or aryl nucleophiles, which react with electrophilic carbon centers in regio- and stereoselective manner (Scheme I.2.1).⁵⁵⁻⁵⁷

Initially, organocopper reagents were usually obtained by transmetalation reaction of copper salts with organolithium or Grignard reagents. The use of less basic and nucleophilic organometallic reagents such as organo-zinc, -zirconium or -aluminium compounds increase the functional group tolerance, widening the applications of organocuprate reagents in organic synthesis. These organometallic reagents can react *in situ* with copper salts to form the corresponding organocuprate compound, which can participate in both stoichiometric and catalytic reactions with an electrophile.



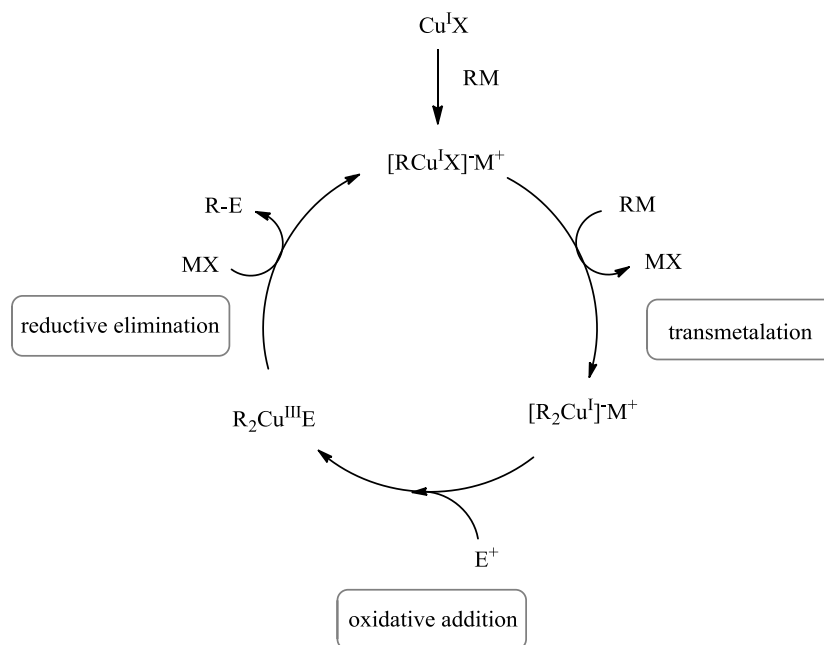
Scheme I.2.1. Classification of C-C bond forming reactions by organocopper(I) complexes. RCu corresponds to R₂CuLi, RCu(X)Li, RMgX·CuX, etc.

In order to understand the reactivity of organocuprate reagents, extensive structural studies have been performed, mainly based on lithium organocuprates. Solid state structures, obtained by X-ray crystallography, have shown the ability of lithium organocuprate compounds to form aggregates, being the dimeric structures the minimal cluster entities. However, crystal structures do not reflect the reactive conformations of these species in solution, which may also be dynamic structures. Therefore, several theoretical calculations as well as NMR investigations have focused on the comprehension of the structures of lithium organocuprates in solution.^{1,58,34} From these studies, it has been shown that small differences on solvent as well as counteranions have a big impact on the composition and aggregation state of the organocuprate reagent in solution, which is also reflected in their reactivity.⁵⁶ In general, common MeCu is polymeric in an ethereal solvent and it is unreactive, whereas Gilman reagent, R₂CuLi·LiX (X = Cl, Br, I) is a soluble and reactive dimer. Higher aggregates of Gilman cuprates have also been described. Cyano-Gilman cuprates R₂CuLi·LiCN are also widely used and they show slightly different reactivity and stability ascribed to their different aggregation properties in solution.⁵⁹

1.2.1 General mechanism of C-C bond forming reactions with organocuprates

Catalytic C-C bond forming reactions with organocuprates have been rarely studied from a mechanistic point of view, and existing experimental data are based on stoichiometric reactions. Due to the complex structures of organocuprates reagents in solution, experimental mechanistic studies have been very challenging.³⁴ Then, computational studies based on *ab initio* and DFT have been used to unravel the nature of reactive intermediates and transition states.⁵⁶ These studies supported the intermediacy of organometallic copper(III) complexes, which have been detected experimentally during the last decade thanks to the development of high resolution NMR spectroscopic methods at low temperature.

Nonetheless, it is nowadays widely accepted that both stoichiometric and catalytic reactions share the same mechanistic steps, proceeding through two electron Cu^I/Cu^{III} redox processes. The catalytic cycle proposed for reactions with organocuprates contains three key steps: transmetallation, oxidative addition by reaction with the electrophile and reductive elimination to afford C-C coupled product (Scheme 1.2.2).⁵⁶



Scheme I.2.2. Catalytic $\text{Cu}^{\text{I}}/\text{Cu}^{\text{III}}$ cycle for C-C forming-reaction with organocuprate reagents.

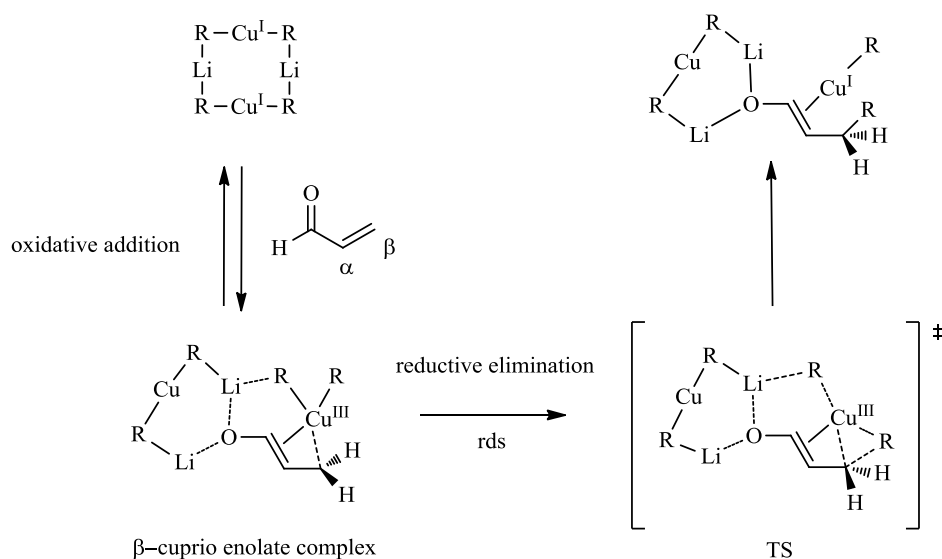
The first step consists in a transmetalation reaction of the copper(I) salt and a main-group organometallic reagent to yield either a mono- or diorganocuprate(I) reagent, the nature of which depends on the stoichiometry of the main-group organometallic reagent (RM) and its nucleophilicity. The following step in the mechanism is the nucleophilic attack of the copper(I) atom on the electrophile (E^+), which is understood as an oxidative addition because the formal oxidation state of the organocopper intermediate obtained is +3. During this step the organocopper(I) reagent loses its linear geometry, which causes a destabilization of the HOMO and changes its orbital symmetry promoting an effective back-donation interaction with the LUMO of the electrophile.⁵⁶ Finally, the reductive elimination step from organocopper(III) intermediate releases the C-C bond formed product and regenerates the copper(I) species. In stoichiometric reactions, the reductive elimination is often the rate-determining step and also determines the regio- and stereoselectivity of the reaction. On the other hand, there is little consensus about the rate-determining step in catalytic systems.

In the following sections, the mechanism of reactions with organocuprates where copper(III) intermediates have been detected (conjugate additions, $\text{S}_{\text{N}}2$ alkylations and $\text{S}_{\text{N}}2'$ allylic alkylations) will be discussed in more detail.

I.2.1.1 Conjugated additions to enones

Since Kharasch discovered in 1941 that the reaction between Grignard reagents and α,β -unsaturated ketones in the presence of copper(I) salts affords 1,4-addition products,⁶⁰ conjugate additions to enones have been widely used in synthetic chemistry.

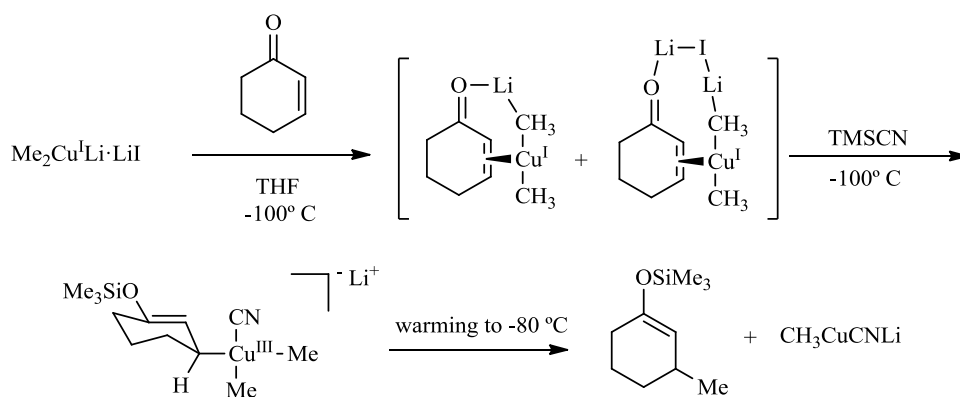
Extensive NMR experiments,^{61-63,34,61-63} kinetic measurements⁶⁴ and numerous theoretical studies⁶⁵⁻⁶⁷ have established the formation of a π -complex between the organocuprate and the α,β -unsaturated carbonyl compound, which is further stabilized by a lithium-carbonyl interaction (Scheme I.2.3). Molecular orbital analysis of enone/cuprate π -complexes indicated that there is donation/back-donation $d-\pi^*$ interaction between the 3d orbitals of the copper and the π -system of the enone. Therefore, the π -complex may be viewed as β -cuprio(III) enolate complex in which the formal oxidation state of the metal center is +3. The rate determining step is the C-C bond formation by reductive elimination. In this step, the copper(III) center recovers its d-electrons and the ligand R overlaps with the vacant orbital on the C(β) atom affording the conjugate addition product. Experimental data based on ¹³C-NMR KIE measurements agrees with a substantial bonding change at the β carbon during the RDS, concomitantly to the alkyl group transfer from the copper to the enone.⁶⁸



Scheme I.2.3. Calculated reaction pathway for conjugated addition of $(Me_2CuLi)_2$ with acrolein.

The first observation of copper(III) intermediates in conjugate addition reactions was reported in 2007 by Bertz, Ogle and coworkers by using Rapid Injection NMR spectroscopy (RI-NMR). They studied the reaction between Gilman reagent $Me_2CuLi \cdot LiX$ ($X = I, CN$) and 2-cyclohexenone in THF at very low temperature (Scheme I.2.4).⁴⁹ As characterized previously, the first intermediate formed was the π -complex between the organocuprate and the cyclic enone.⁶⁹ In the presence of trimethylsilyl cyanide, square-planar tetracoordinated copper(III)

intermediate was obtained and characterized by RI-NMR at $-100\text{ }^{\circ}\text{C}$. DFT calculations supported the proposed structure.⁷⁰ Interestingly, conjugated 1,4-addition product was obtained when the copper(III) intermediate was warmed up to $-80\text{ }^{\circ}\text{C}$. Under these reaction conditions the detection of copper(III) intermediates have been possible, even though, those are not the usual conditions applied in most conjugate addition procedures.



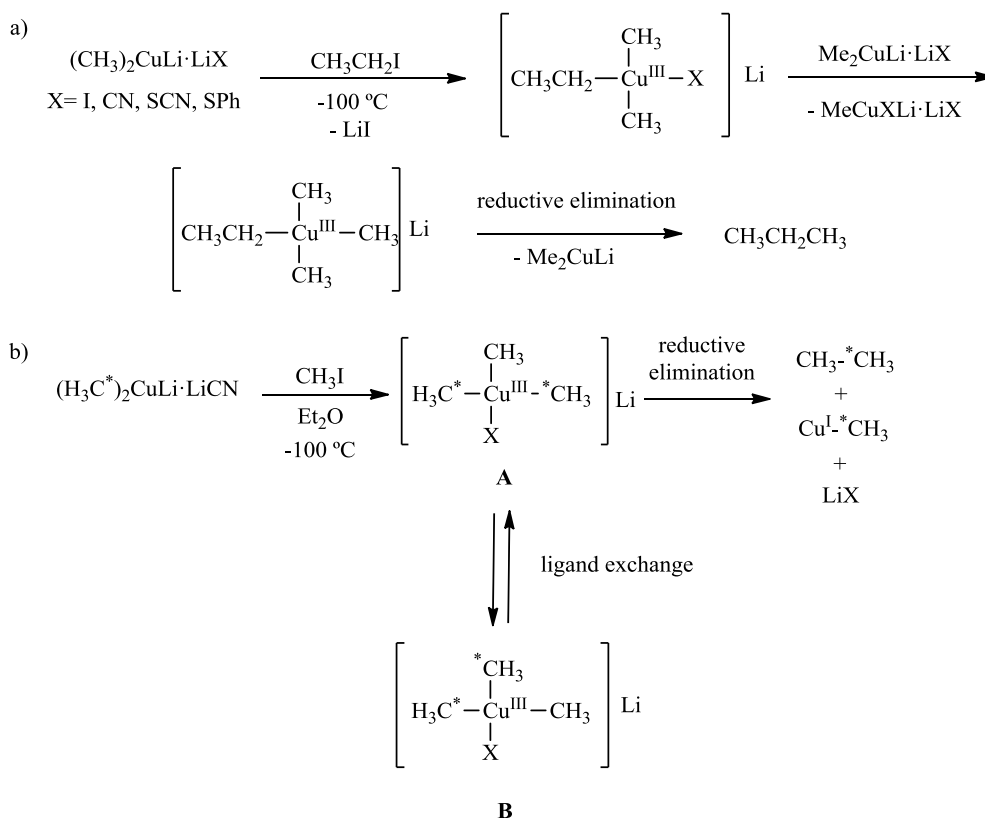
Scheme I.2.4. Observation of tetraalkyl copper(III) complex in conjugate 1,4-additions.

I.2.1.2 S_N2 alkylation reactions

Organocopper(I) reagents can participate in nucleophilic substitution S_N2 reactions of alkyl halide,⁷¹⁻⁷³ pseudohalide (tosylate),⁷⁴ epoxide or aziridine substrates. Alkyl bromides and tosylates are synthetically more useful than alkyl iodides, because the nucleophilic substitution takes place with inversion of configuration at the electrophilic carbon affording optically pure products.^{73,75,76}

The groups of Bertz and Gschwind, independently studied the S_N2 reaction of lithium organocopper reagents with alkyl substrates.^{50,51} They demonstrated that tetraordinated copper(III) complexes are intermediates in these reactions, since upon warming up these complexes, the C-C reductive elimination products are obtained (Scheme I.2.5).

During this year 2012, Koszinowski and coworkers have reported the detection of tetraalkylcuprates(III) by ESI-MS spectrometry at room temperature. These complexes are also formed by reaction of $R_2CuLi\cdot LiCN$ with alkyl halides in tetrahydrofuran. The reactivity order follows the trend $RI > RBr > RCl$ and primary alkyl iodides react faster than secondary alkyl iodides, which is consistent with a S_N2 mechanism.⁷⁷

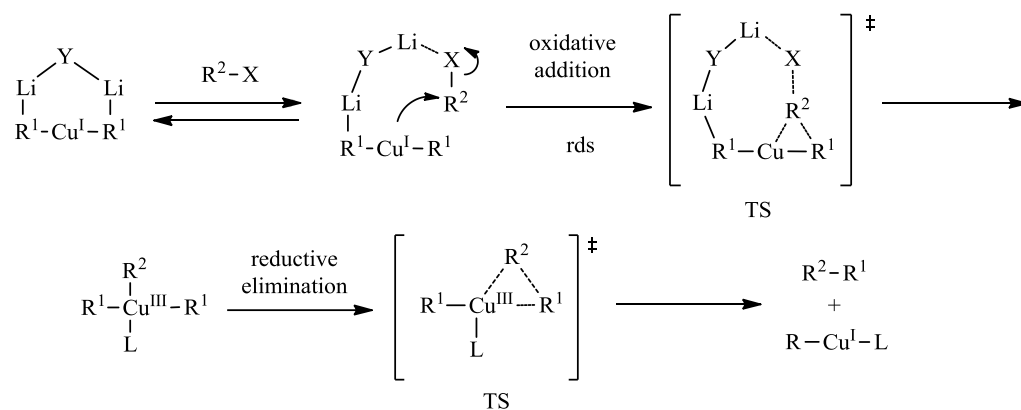


Scheme 1.2.5. Experimental detection of copper(III) complexes in $\text{S}_{\text{N}}2$ reactions by low temperature NMR spectroscopy.

Furthermore, Nakamura and Gschwind showed that ligand exchange processes occurs in copper(III) complexes at very low temperature.⁵⁴ The reaction between ^{13}C -labelled dimethylcuprate and non-labeled methyl iodide affords two isotopomers of $[\text{Me}_3\text{CuCN}]$ in the NMR spectrum (Scheme 1.2.5, b). The presence of the isotopomer that contains the unlabelled methyl group *cis* to the heteroligand (A), together with the expected isotopomer which has the unlabelled methyl group *trans* to the heteroligand (B), indicated ligand exchange processes at low temperature. ^{13}C -labelled ethane is the main product obtained by reductive elimination at temperatures above $-90\text{ }^\circ\text{C}$, which is in agreement with a *syn*-elimination from copper(III) complexes. The isotope pattern obtained in the product indicates that ligand exchange reactions are slow compared to reductive elimination at higher temperatures, which are usually applied in synthetic $\text{S}_{\text{N}}2$ reactions.

Nakamura and coworkers supported computationally the intermediacy of organometallic copper(III) intermediates in the mechanism of $\text{S}_{\text{N}}2$ reactions of alkyl halides with lithium organocuprate(I) clusters (Scheme 1.2.6).^{78,79} Organocuprate(I) reagent can interact with the electrophile displacing the leaving group in an oxidative addition step that is rate-determining. In this interaction the $3d_{z^2}$ orbital of the copper overlaps with the σ^* orbital of the C-X bond of the alkyl halide with the assistance of a lithium atom. This reaction affords a

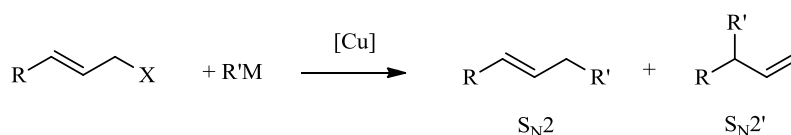
square-planar trialkylcopper(III) intermediate with a fourth ligand that depends on the reaction conditions. Reductive elimination from copper(III) complex to release the C-C coupled product is calculated to be very favorable step. The linear geometry of the organocuprate(I) R_2Cu^- during the oxidative addition situates the two groups R in *trans* position and, therefore, only the product derived from the two R and R' groups situated in *cis* position is obtained.



Scheme I.2.6. General mechanism for the S_N2 reaction with the intermediacy of organocupper complexes.

I.2.1.3 S_N2' allylic alkylations

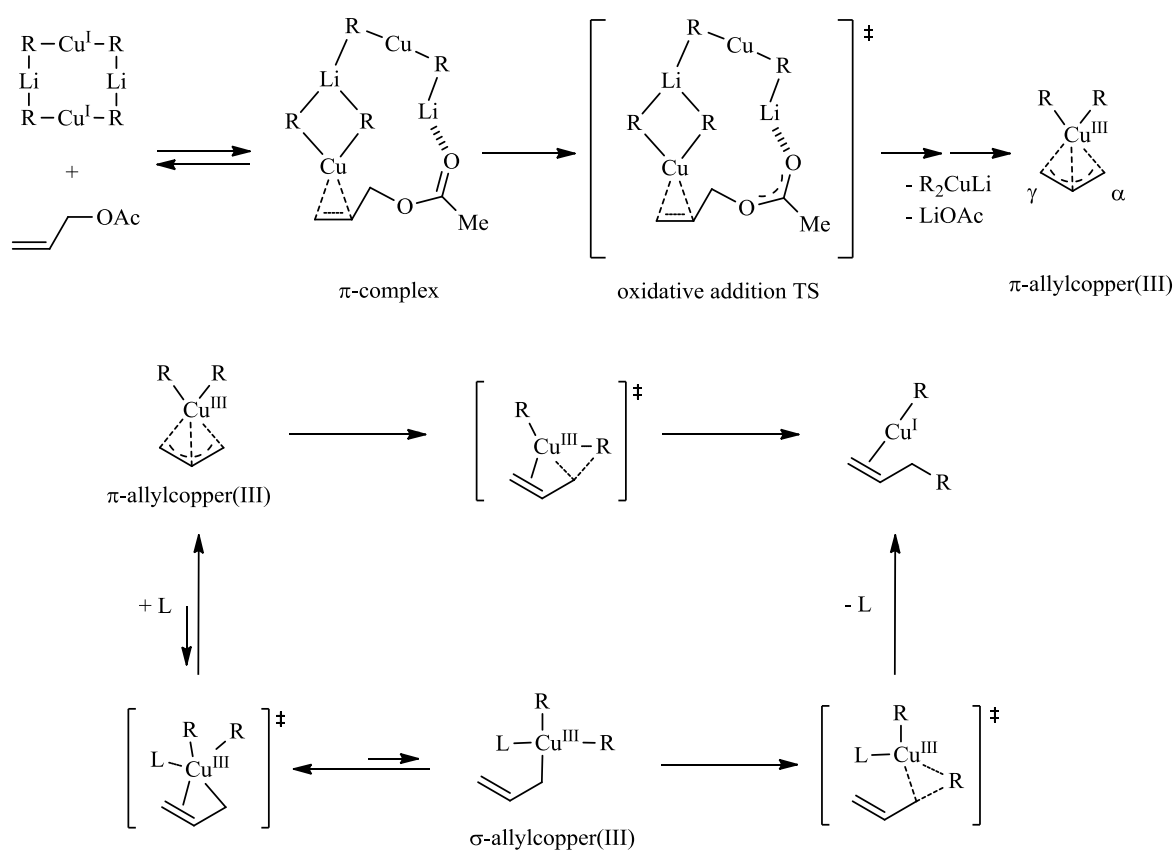
Since Crabbé reported the first conversion of allylic esters to olefins with lithium dialkylcuprates,⁸⁰ extensive work has been done in allylic alkylations with organocuprate reagents in order to control the regio- and stereoselectivity of the reaction and to increase its synthetic applications.⁸¹⁻⁸⁴ In the reaction of organocupper(I) reagents with allylic electrophiles (for instance, halides and carboxylates), the new C-C bond formation can occur either at α (S_N2 product) or in γ position (S_N2' product) of the leaving group, or at the face *anti* or *syn* to the side of the leaving group (Scheme I.2.7).



Scheme I.2.7. Allylic alkylation products with organocuprates reagents.

Allylic alkylation with organocuprates has been extensively studied from a computational point of view by Nakamura and coworkers.^{85,86} They studied the substitution reaction of homocuprate Me_2CuLi with allyl acetate in which there is no regioselectivity.⁸⁵ In

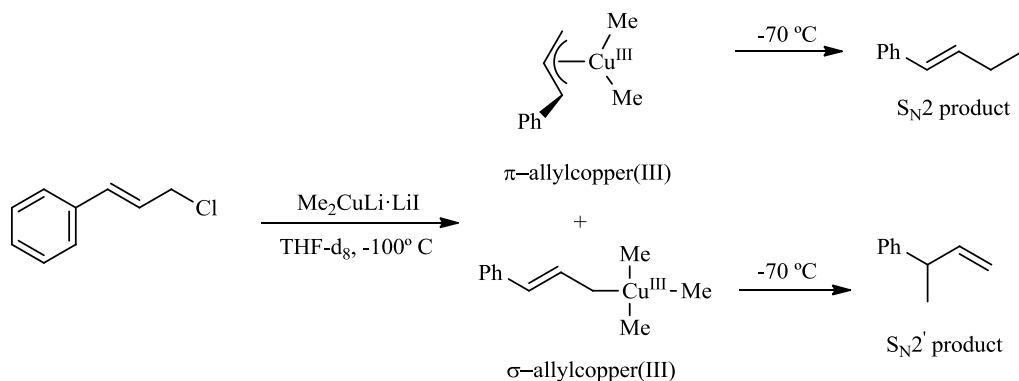
the first step, the organocuprate forms a π -complex with the olefin, which then irreversibly releases an acetate anion in an *anti* fashion with the assistance of the lithium cation, providing a symmetrical π -allylcopper(III) complex (Scheme I.2.8). In most cases, the *anti* elimination pathway of the leaving group is favored due to better overlapping between the copper $3d_{xz}$ orbital and the $C=C \pi^*/C-O \sigma^*$ mixed orbital. This π -allylcopper(III) complex is in rapid equilibrium with the σ -allylcopper(III) and both copper(III) intermediates can undergo C-C reductive elimination. However, it was calculated that reductive elimination occurs predominantly from a π -allylcopper(III) intermediate rather than from a σ -allylcopper(III) complex because of the lower energetic barrier. When the copper(III) intermediate is not symmetrical (bearing different substituent groups at the α - and/or γ -positions), the regioselectivity is determined at the reductive elimination step.⁸⁶



Scheme I.2.8. Calculated reaction pathway for substitution of allyl acetate with R_2CuLi dimer.

These theoretical results were supported by experimental data reported by Bertz and Ogle, who observed η^1 σ -allyl and η^3 π -allyl copper(III) complexes by low temperature NMR studies and studied their reactivity in allylic alkylations (Scheme I.2.9).⁸⁷ They found that the ratio of the two regioisomeric copper(III) intermediates depends in both the nature of the allyl substrate and the organocuprate(I) reagent. Moreover the ratio of the S_N2 and S_N2' products

depends on the identity of the copper(III) species in solution. For example, the addition of cinnamyl chloride to $\text{Me}_2\text{CuLi}\cdot\text{LiI}$ in THF at $-100\text{ }^\circ\text{C}$ afforded a mixture of σ - and π -allylcopper(III) complexes. It was found that σ -allylcopper(III) converted to more stable π -allylcopper(III) at $-100\text{ }^\circ\text{C}$. The ratio of the two regioisomeric copper(III) complexes is reflected in the ratio of alkene products obtained at $-70\text{ }^\circ\text{C}$. It was concluded that π -allylcopper(III) intermediates gave mainly $\text{S}_{\text{N}}2$ product whereas σ -allylcopper(III) intermediates gave mainly $\text{S}_{\text{N}}2'$ product.

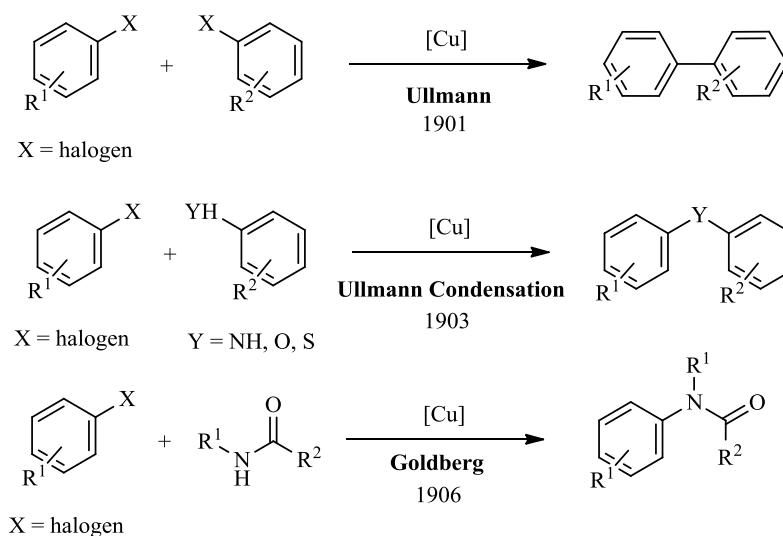


Scheme 1.2.9. Allylic alkylation reaction through detected σ - and π -allylcopper(III) intermediates.

I.3 Ullmann Condensation Reaction: C-heteroatom bond formation

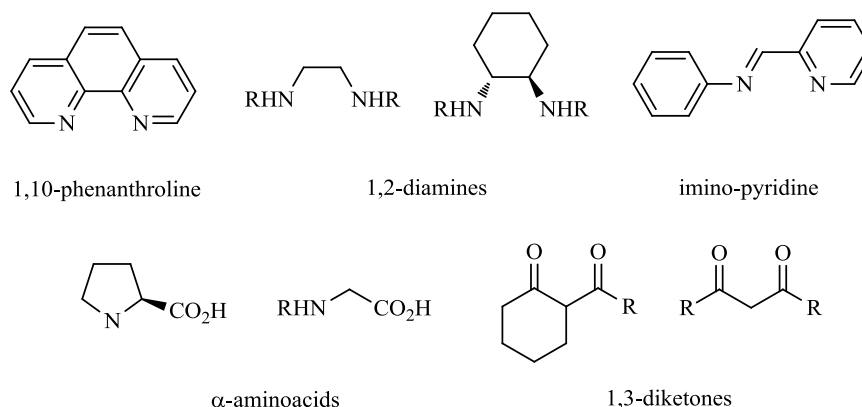
Modern copper-catalyzed cross-coupling reactions have emerged as reliable and efficient methods for the construction of C-C and C-heteroatom bonds, and now are commonly used in both industry and academic research.

These reactions were discovered in the early 1900s by Fritz Ullmann and Irma Goldberg. Ullmann reported that copper mediates biaryl coupling from aryl halides and also the coupling reaction of aryl halides with phenol or aniline,^{88,89} whereas Goldberg reported the coupling reaction between amides and aryl halides mediated by copper.⁹⁰ Nowadays, the copper-mediated reaction of aryl halides with phenols, anilines or thiophenols to form $\text{C}_{\text{aryl}}\text{-O}$, $\text{C}_{\text{aryl}}\text{-N}$, or $\text{C}_{\text{aryl}}\text{-S}$ bonds, respectively, are known as Ullmann Condensation Reactions (Scheme 1.3.1).⁹¹



Scheme I.3.1. C-C and C-heteroatom bond forming reactions mediated by copper discovered by Ullmann and Goldberg in the early 1900s.

While remarkable from a conceptual point of view, the applicability of these copper-catalyzed formal nucleophilic aromatic substitution reactions has been limited for a long time due to the requirement of highly polar solvents, high reaction temperatures (>200 °C) and long reaction times.^{92,93} However, the use of auxiliary ligands in the Ullmann Condensation reaction has allowed the formation of C-heteroatom bonds under catalytic and milder reaction conditions. The enhanced solubility and stability of copper complexes achieved by using auxiliary ligands was key to the renaissance of Ullmann-type coupling reactions. Following important earlier contributions from Ma, Hauptman and others in the late nineties,⁹⁴⁻⁹⁷ Buchwald⁹⁸⁻¹⁰⁰ and Taillefer^{101,102} pioneered at the beginning of the 21st century the use of simple auxiliary ligands in combination with bases to afford cross-coupled products at lower reaction temperatures, faster reaction rates and lower copper catalyst loadings. Since then, several auxiliary -typically bidentate- ligands have been used to promote copper-catalyzed cross-coupling reactions, for instance, phenanthrolines,⁹⁶ 1,2-diamines,¹⁰³ 1,3-diketones,^{104,105} imino-pyridines^{106,107} and α -aminoacids^{95,108,109} (Scheme I.3.2). The use of these auxiliary ligands has broadened the substrate scope of these reactions and also has driven these processes up to large-scale industrial production.^{91,110-112}



Scheme I.3.2. Some representative auxiliary ligands used in Ullmann Condensation Reactions.

Although many mechanistic pathways have been proposed for these copper-catalyzed cross-coupling reactions, experimental and computational data do not converge to a single unified mechanism. On the other hand, the great diversity of catalytic systems and nucleophiles makes difficult to include all Ullmann Condensation reactions in one single mechanism. Several key aspects are still under debate, such as the identity and oxidation state of the active copper catalyst, and the activation mode of the aryl halide. Hereafter, these mechanistic aspects will be discussed in detail in the following sections.¹¹³

I.3.1 Oxidation state of copper

Copper sources in three different oxidation states (0, 1 and 2) are found to be effective in copper-catalyzed cross-coupling reactions.⁹³ For instance, CuBr_2 , CuCl_2 , $\text{Cu}(\text{OAc})_2$, CuI , CuBr , CuCl or even copper powder have been effective catalysts in Ullmann reactions.^{94,114}

Several mechanistic studies have been reported for obtaining information about the active oxidation state of the copper catalyst. Initial work from Weingarten indicated *in situ* reduction of CuBr_2 to CuBr in the presence of phenoxide anions.⁹⁴ By means of EPR spectroscopy, Kondratov and Shein studied the interaction between Cu^{II} species and several amines.¹¹⁵ They found that Cu^{II} EPR signals decayed over time which was attributed to ligand oxidation to amide and the corresponding formation of Cu^{I} species.

In the eighties, Paine systematically studied the reaction of diphenylamine (Ph_2NH) with aryl halides catalyzed by three different oxidation states of copper to form triphenylamines.¹¹⁴ He proposed that cupric salts (CuBr_2 or $\text{Cu}(\text{acac})_2$) were first reduced to Cu^{I} by the nucleophile before catalysis occurred. When excess of Cu^{II} salts were used, the instantaneous formation of tetraphenylhydrazine (Ph_2NNPh_2) suggested the reduction of Cu^{II} to Cu^{I} along with the condensation of two $\text{Ph}_2\text{N}^{\cdot}$. Moreover, when copper-metal surfaces were used, the formation of a layer of Cu_2O of 360 Å was responsible of the coupling reaction, as deduced from

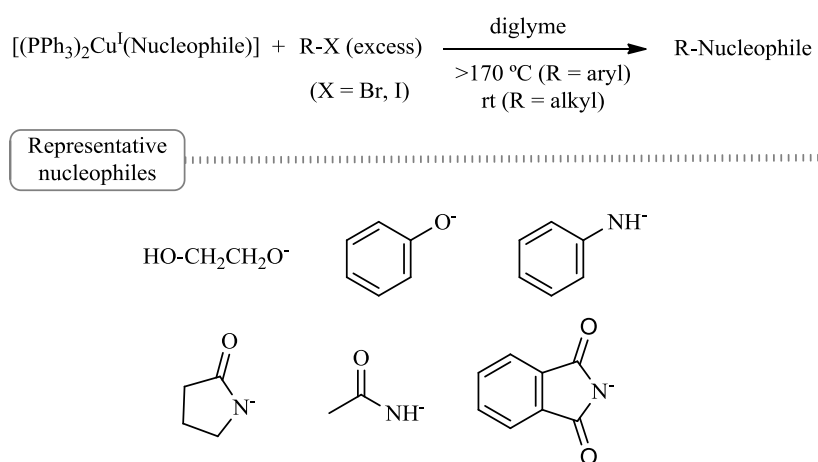
quantitative X-Ray powder diffraction. The dissolution of the Cu_2O upon coordination with Ph_2NLi was proposed to afford the active copper(I) species in solution.

Recently, Jutand and coworkers reported that electrogenerated $[\text{Cu}^0(1,10\text{-phenanthroline})]$ complex is oxidized *in situ* by the aryl iodide or aryl bromide substrate via inner sphere electron transfer mechanism, resulting in the formation of the corresponding arene and $[\text{Cu}^I(1,10\text{-phenanthroline})]^+$ complex, which is the active catalyst in the cross-coupling reaction.¹¹⁶

All experimental data collected during the past 50 years supports that copper(I) complexes are the active catalyst and, whatever starting from Cu^{II} or Cu^0 sources, copper(I) complexes are formed *in situ* by chemical reduction or oxidation processes, respectively.¹¹³

I.3.2 Studies related to the active catalyst structure

Early reports in the seventies showed that stoichiometric reactions of copper(I) complexes bearing heteroatom nucleophiles with organic halides to afford C-heteroatom coupled products. Several groups synthesized copper(I) alkoxide, phenoxide and amidate complexes and studied their reactivity towards alkyl and aryl halides to afford C-O and C-N coupled products respectively. In most cases, phosphine ligands were used in order to stabilize copper(I) nucleophile complexes (Scheme I.3.3).¹¹⁷⁻¹²⁰



Scheme I.3.3. Reactivity of preformed Cu^I -Nucleophile complexes with organic halides in C-heteroatom bond forming reactions.

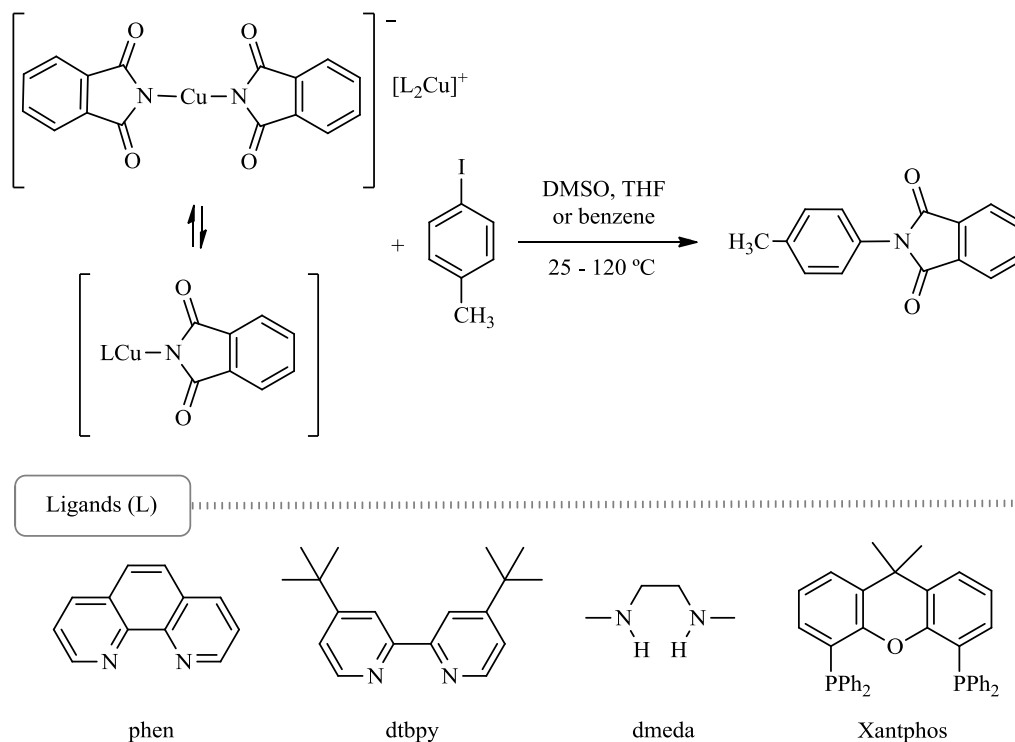
These copper(I) nucleophile complexes were proposed as intermediates in copper(I) catalyzed nucleophilic aromatic substitutions. Weingarten suggested that the formation of diaryl ether from potassium phenoxide and bromoarene in the presence of copper(I) bromide occurs through copper(I) phenoxide complexes.⁹⁴ Later on, Paine proposed the coordination of the

nucleophile to copper(I) species in the catalytic reaction of diphenylamine with aryl halides to form triphenylamines;¹¹⁴ it was found that the reaction was zero order in the amine nucleophile, indicating that copper(I) species in solution coordinate to the nucleophile in a fast and irreversible step to afford cuprous nucleophile species $[\text{Ph}_2\text{NCu}^I]$, which reacts with iodobenzene in the rate determining step.

During the past decade, the groups of Hartwig and Buchwald synthesized and characterized series of Cu^I amido¹²¹⁻¹²⁴ and Cu^I phenoxide¹²⁵ complexes bearing bidentate ligands. They showed that copper(I) nucleophile complexes are chemically and kinetically competent intermediates in the corresponding N-arylation and O-arylation coupling processes catalyzed by copper.

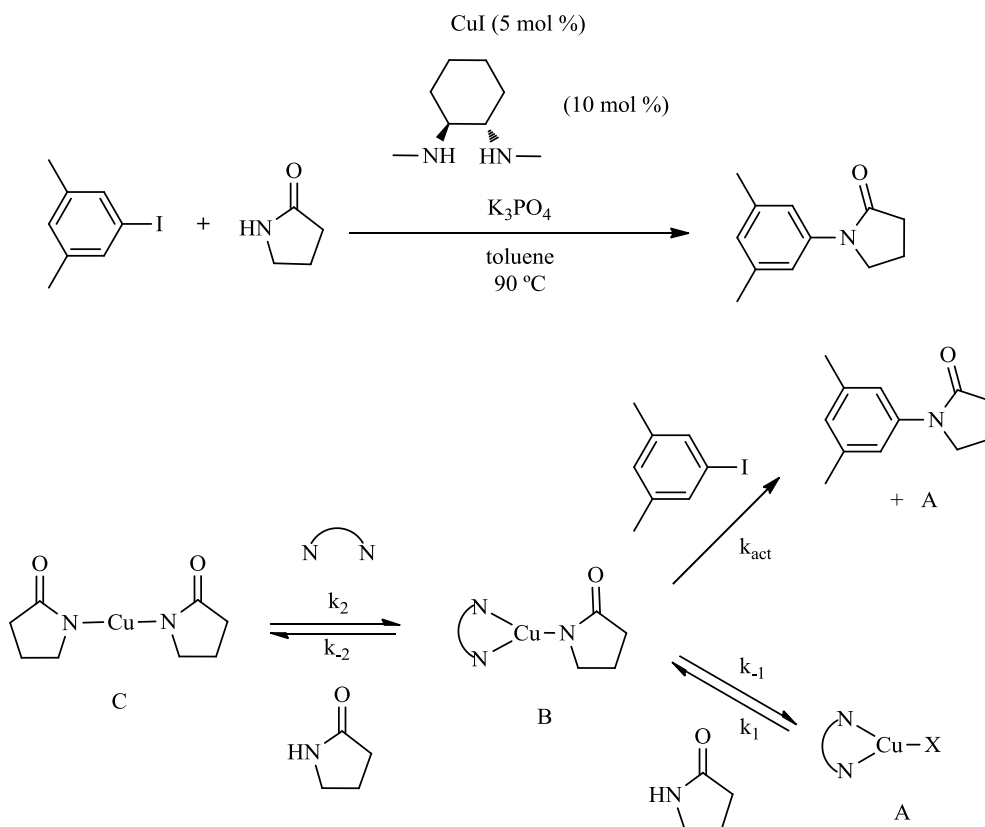
Hartwig and coworkers characterized several Cu^I imidate and Cu^I amidate complexes (i.e. phthalimidate (phth) and pyrrolidinonate (pyrr)) containing bidentate N,N and P,P donor auxiliary ligands (L), such as phenanthroline, bipyridine, diamines and diphosphines.¹²¹ Complexes in solution exist as dimeric ionic species $[\text{L}_2\text{Cu}][\text{Cu}(\text{nucleophile})_2]$ in equilibrium with neutral $[\text{LCu}(\text{nucleophile})]$ species, as determined by NMR spectroscopy and conductivity experiments (Scheme I.3.4). All complexes reacted with excess iodoarene to give C-N coupled product in high yields. The lack of reactivity of $[\text{Cu}(\text{phth})_2][\text{Bu}_4\text{N}]$ with iodobenzene indicates that the anionic moiety $[\text{Cu}(\text{nucleophile})_2]^-$ is not reactive towards aryl halides and, therefore, three-coordinated complexes $[\text{LCu}(\text{nucleophile})]$ were proposed to be the active intermediates in the cross-coupling reaction.

Related studies performed with copper(I) phenoxide complexes containing phenanthroline and cyclohexanediamine derivatives as auxiliary ligands led to similar conclusions as in the previous C-N bond forming reactions.¹²⁵ Again, the complexes in solution exist as dimeric ionic species $[\text{L}_2\text{Cu}][\text{Cu}(\text{OPh})_2]$ in equilibrium with neutral monomeric $[\text{LCu}(\text{OPh})]$ species. The three-coordinated neutral species were proposed to be the active intermediates for the formation of biaryl ethers.



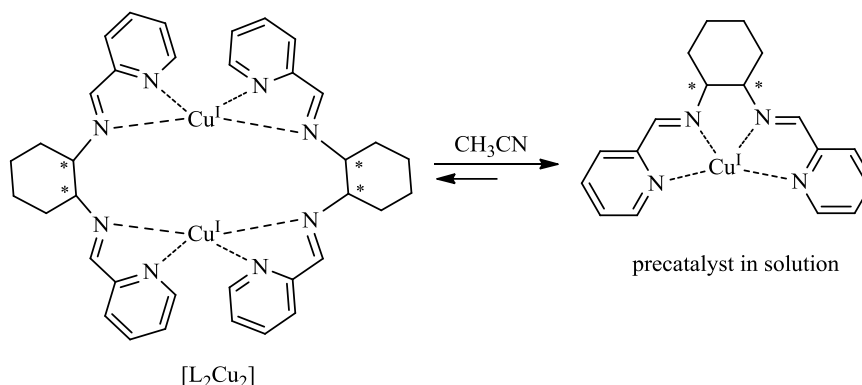
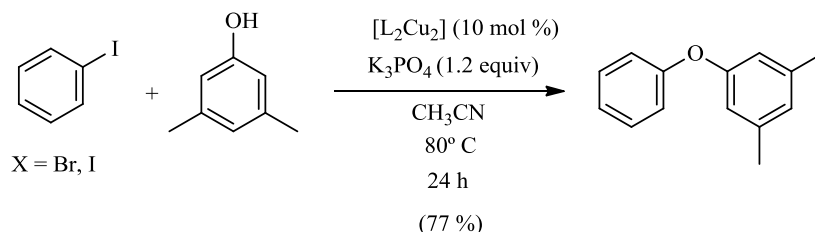
Scheme I.3.4. Reaction of Cu^I imidate complexes with aryl iodide reported by Hartwig.

By means of calorimetric methods, Buchwald and coworkers studied the kinetics of the copper(I) catalyzed N-arylation reaction between 2-pyrrolidinone and 3,5-dimethyliodobenzene using 1,2-diamines as auxiliary ligands (Scheme I.3.5).^{122,123} The dependence of the reaction rate on the amide concentration was shown to be a function of 1,2-diamine concentration: at low concentration, the reaction rate decreases upon increasing the concentration of the amide; in contrast, at high concentration, the reaction rate increases as the concentration of the amide increases. These results might be understood by the mechanism proposed in Scheme I.3.5, where several copper species exist in equilibrium before aryl iodide activation. At high concentration of diamine, the formation of multiple amide ligated complex C is prevented, thus avoiding the sequestration of Cu^I into this inactive copper species C. The synthesis of Cu^I amidate complex with *N,N*-dimethylcyclohexane-1,2-diamine ligand and their studies in stoichiometric reactions with iodoarene demonstrated that complex B was the active intermediate in the catalytic N-arylation reaction. The rate determining step was found to be the activation of the aryl iodide by the Cu^I amidate complex B. Guo calculated by DFT methods the concentration of multiple ligated species in solution and predicted that the Cu^I amidate complex [LCu(NHAc)] was the major one in the reaction mixture, supporting the experimental data reported by the Buchwald group.¹²⁶



Scheme 1.3.5. Proposed role of the chelating diamine ligand in the copper(I)-catalyzed N-arylation of amides with diamine ligands (*N,N*-dimethylcyclohexane-1,2-diamine and ethylenediamine).

Finally, Taillefer and coworkers have also done several contributions in the study of the active catalyst structure not only with bidentate ligands but also with tetradentate bis(imino-pyridine) auxiliary ligand (Scheme 1.3.6).¹²⁷ The association of copper(I) iodide and tetradentate ligand in acetonitrile led to the formation of highly insoluble dimeric complex [Cu(L)₂]₂. A very small fraction of dimeric complex is soluble in acetonitrile, thus on equilibrium displaced towards the formation of monomeric copper(I) complex. The latter complex is the active precatalyst in the biaryl ether formation reaction. Taillefer showed that in certain systems the ligand do not help to copper(I) solubilization but causes the formation of insoluble copper(I) reservoir complexes preventing any degradation process in solution.

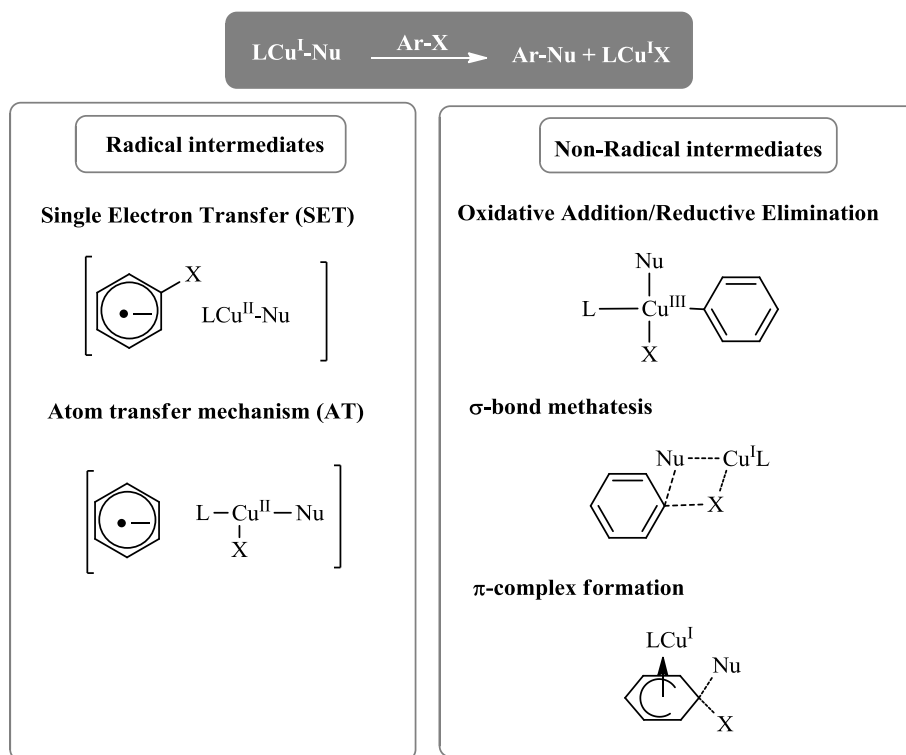


Scheme I.3.6. C-O coupling reaction of iodobenzene and 3,5-dimethylphenol with the insoluble dimeric Cu^{I} species acting as Cu^{I} -reservoirs in bis(imino-pyridine) ligand-based systems.

Taking into account these studies, most data favor the proposal that the nucleophile is coordinated to the Cu^{I} before the activation of the aryl halide takes place. The addition of auxiliary ligands to copper salts in the catalytic reactions prevents the formation of less reactive, multiply ligated cuprate structures.^{122,123,126,58} Therefore, the nature and concentration of the auxiliary ligand used in Ullmann-type condensation reactions have a big impact in the equilibrium between different Cu^{I} complexes present in solution, and in the formation of the active catalysts as well. Moreover, several efforts have been made in order to synthesize well-defined, stable and soluble copper(I) complexes that serves as efficient pre-catalyst in copper-catalyzed C-heteroatom bond formation reactions.^{128,129}

I.3.3 Studies focusing on the activation of the aryl halide

Since the activation of the aryl halide is usually rate-limiting, the detection of intermediate species after this step has been very scarce, thus most mechanistic proposals are drawn from kinetic and computational studies. The most invoked mechanism for Ullmann Condensation reactions are based on two electron redox processes via a $\text{Cu}^{\text{I}}/\text{Cu}^{\text{III}}$ catalytic cycle, and one electron redox processes through radical intermediates that may operate via $\text{Cu}^{\text{I}}/\text{Cu}^{\text{II}}$ catalytic cycle (Scheme I.3.7). Two more reaction pathways based on σ -bond metathesis and π -complex formation were also proposed but with minor experimental support.

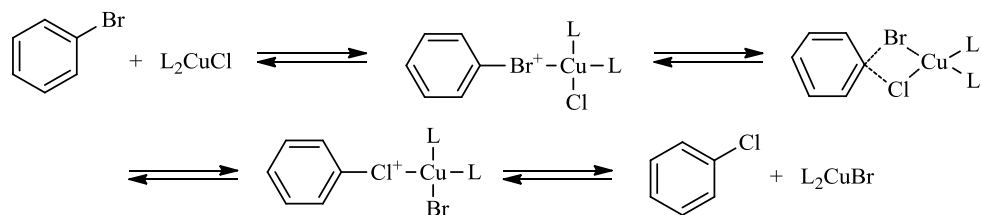


Scheme I.3.7. Radical and non-radical intermediates proposed for Ullmann Condensation Reactions.

I.3.3.1 Mechanism Involving σ -Bond Metathesis

In this mechanistic pathway the copper(I) nucleophile species activates the aryl halide via a four-centered intermediate in which the metal center forms a σ -complex with the lone electron pair of the halogen atom. The polarization of the C-X bond creates a partial positive charge on the *ipso*-carbon and facilitates the attack by the nucleophile, to give the corresponding coupling product and the copper complex, which remains with an oxidation state of +1. In early studies, in 1964 Bacon and Hill proposed this mechanism for explaining their results in the substitution reactions between aryl halides and cuprous salts (Scheme I.3.8).¹³⁰⁻

132

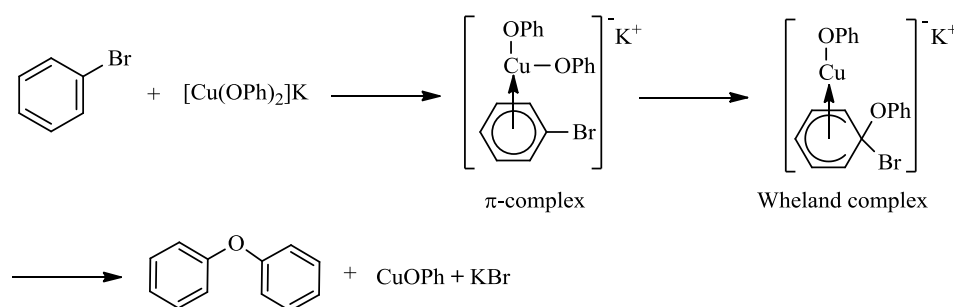


Scheme I.3.8. Bacon and Hill's proposal based on σ -bond metathesis pathway.

Very recently, a similar mechanistic proposal was evaluated computationally by Cundari for the reaction of a well-defined N-heterocycle carbene (NHC) Cu^I-nucleophile complex, [(NHC)Cu^I(NHPH)], with iodobenzene, but the higher energy barriers pointed towards an operative oxidative addition/reductive elimination Cu^I/Cu^{III} mechanism (see section I.3.3.4).¹³³

I.3.3.2 Mechanism Involving π -Complexation of Copper(I) to Aryl Halides

The first proposal of a mechanism involving nucleophilic aromatic substitution via a π -bound organocuprate species was reported in 1964 by Weingarten in the study of the copper-catalyzed coupling reaction of bromobenzene with potassium phenoxide yielding phenyl ether.⁹⁴ In this mechanism, the Cu^I-nucleophile species interacts with the π electrons of the aromatic ring in order to promote the polarization of the C-X bond. The resulting Wheland complex facilitates the substitution of the halide with the nucleophile in the ring (Scheme I.3.9), while the copper species maintains its oxidation state +1.



Scheme I.3.9. Mechanism for the coupling reaction of bromobenzene with potassium phenoxide proposed by Weingarten.

Although experimental evidences to support this hypothesis are scarce, Weingarten proposed this mechanism based on the relative reactivity order of several aryl halides ($\text{ArI} > \text{ArBr} > \text{ArCl}$).¹³⁴ The relative rates found through competition experiments followed the trend of the C-X bond strength ($\text{C-I} < \text{C-Br} < \text{C-Cl}$) as in nucleophilic aromatic substitutions, indicating that the C-X bond cleavage is involved in the rate determining step.

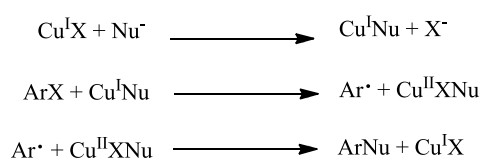
Ma and coworkers observed that α -amino acids were coupled with aryl iodides and bromides in the presence of catalytic amount of copper(I) iodide under very mild reaction conditions.⁹⁵ The structure of the α -amino acid influenced the yield of the coupled product and they suggested that an aminoacid-copper(I) complex was formed prior to the activation of the aryl halide through a π -complex intermediate. However, in a recent report, Ma proposed an alternative reaction pathway based on oxidative addition/reductive elimination steps.¹⁰⁸

I.3.3.3 One Electron Redox Processes via Cu^I/Cu^{II}: SET and AT

Some authors have supported a Cu^I/Cu^{II} catalytic cycle with the intermediacy of radical species formed via single electron transfer (SET) or an atom transfer (AT) mechanism (Scheme I.3.7). In the SET mechanism, the copper(I) complex is oxidized in one electron process by the aryl halide, yielding to the formation of a haloarene radical anion. Then, the aryl radical couples with the nucleophile and the copper(II) is reduced, regenerating the catalyst and releasing the neutral coupled product. It has also been proposed that the electron transfer is associated with the transference of the halide to the copper atom to form the aryl radical by an AT mechanism.

Hida reported in the seventies the mechanistic study of the coupling reaction of 2-aminoethanol with 1-bromoanthraquinone (AQBr) catalyzed by copper(I) bromide.^{135,136} EPR experiments showed the presence of two paramagnetic species in solution, copper(II) and 1-bromoanthraquinone radical anion, which are formed by SET from copper(I) species to 1-bromoanthraquinone (AQBr + Cu^I → AQBr^{•-} + Cu^{II}). Although haloanthraquinones are very specific substrates, the presence of the reduced product anthraquinone (AQH) together with the C-N coupled product, observed in many Ullmann condensation reactions, prompted Hida to propose SET pathway as general mechanism for the activation of aryl halides.

The atom transfer mechanism was initially supported by Kochi and coworkers more than 50 years ago.^{137,138} They studied the reactivity of free aryl radicals, obtained by decomposition of peroxides and iodonium salts, in the presence of copper salts. These aryl radicals can react with copper(II) halide salts via an atom transfer mechanism to produce the corresponding aryl halide and copper(I) species. Kochi and coworkers proposed that the Sandmeyer and Meerwein reactions proceed via radical chain mechanism in which copper has an important role as radical chain terminator (Scheme I.3.10).

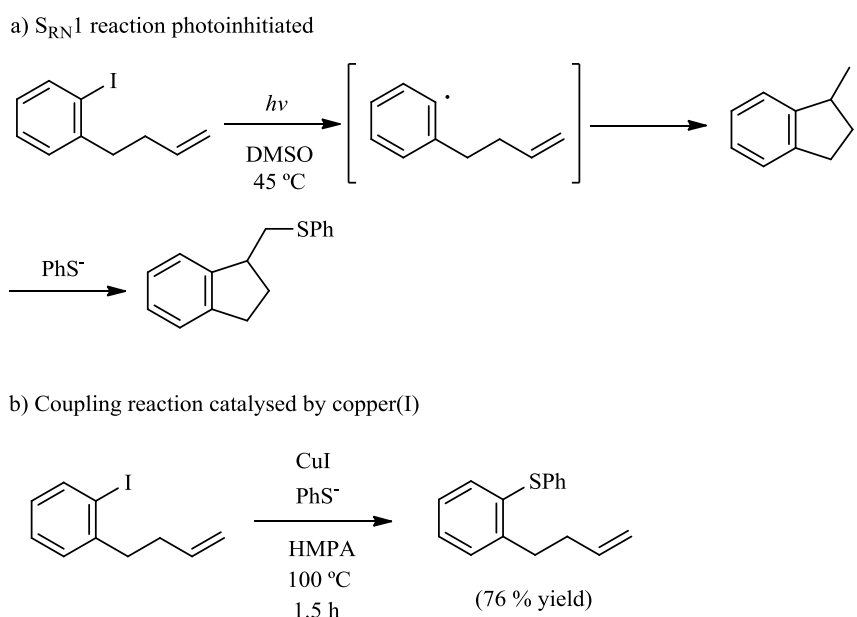


Scheme I.3.10. Kochi's proposal for ligand exchange reaction in copper(I) salts.

The use of radical trapping experiments has been reported in order to clarify the intermediacy of radical species in the reactions. However, in most cases, neither the rate nor the yield of the coupling reaction are modified by radical-scavengers, and this result have been used for arguing against free radical intermediates. On the other hand, it cannot be excluded the involvement of solvent-cage radicals with a very short half-life. In this context, Bowman and coworkers performed radical clock tests for probing the radical mechanism in the C_{aryl}-S coupling reaction.¹³⁹ They demonstrated that the photostimulated reaction of 4-(2-iodophenyl)-

1-butene with phenylthiolate proceeds via $S_{RN}1$ mechanism affording an intramolecular ring closure product (Scheme I.3.11, a). In contrast, when the reaction was repeated in the presence of catalytic copper(I) iodide, exclusively monosubstituted product was obtained indicating that a different mechanism is operating (Scheme I.3.11, b).

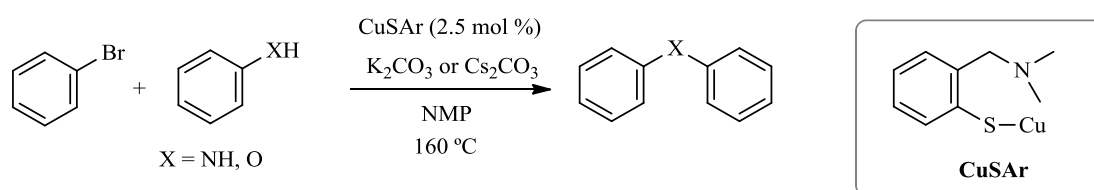
Recently, Hartwig and coworkers reported similar radical clock tests based on *o*-(allyloxy)iodobenzene substrates with nitrogen and oxygen nucleophiles in the presence of copper(I) phenanthroline complexes.^{121,124,125} The aryl radical that would be generated from *o*-(allyloxy)iodobenzene is known to undergo cyclization extremely fast to yield the 2,3-dihydrobenzofuranyl-methyl radical which can abstract hydrogen from the solvent, dimerize or could combine with the nucleophile ligand to form the C-heteroatom coupled product. In the analysis of the crude by GC/MS, no cyclization product was detected. Bowman and Hartwig interpreted the lack of cyclization products in radical clock tests as a proof against the involvement of solvent cage radicals in cross-coupling reactions. However, Van Koten and coworkers argued that these radical trapping experiments are not a reliable proof against radicals. The assumption is that intramolecular rearrangement reactions are faster than bimolecular reactions but it has not been proved that this concept is the same in the presence of transition metals.¹¹³



Scheme I.3.11. Radical clock test for the presence of aryl radicals reported by Bowman.

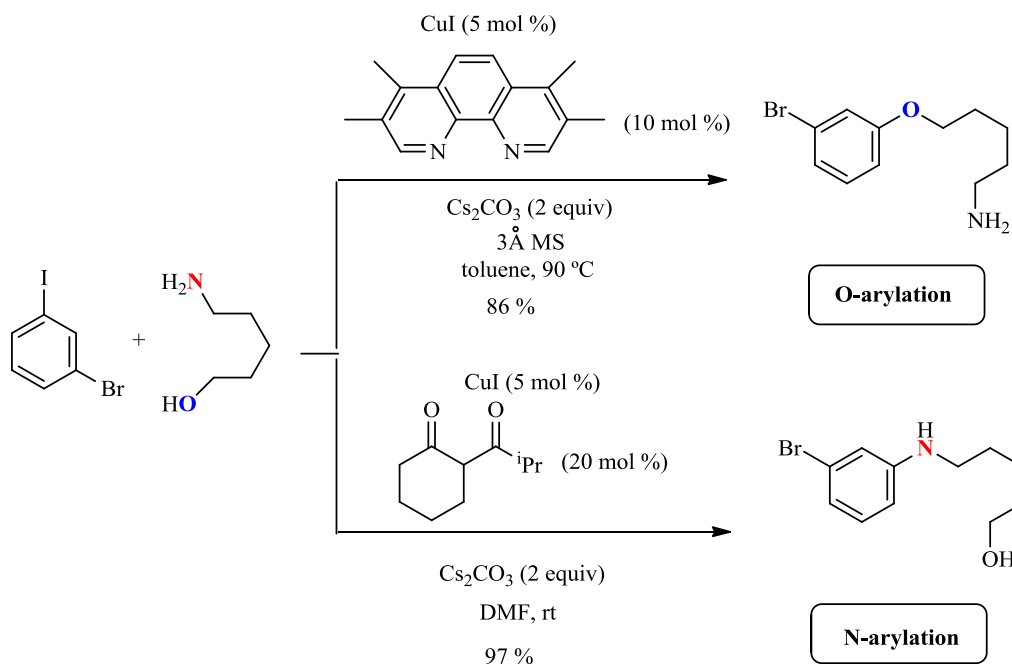
Moreover, Van Koten and co-workers reported the catalytic activity of a family of aminoarenethiolato-copper(I) complexes in the reaction of anilinic and phenolic substrates with bromobenzene derivatives (Scheme I.3.12).^{140,141} Surprisingly, in these reactions only aryl bromides were active, and almost no reactivity was found for aryl iodides or aryl chlorides.

Moreover, the authors showed that the use of radical traps slowed down or even stopped the reaction. It was also shown that certain amounts of copper(II) were present in solution when the reactivity vanished; the addition of metallic copper to the reaction mixture restored the reactivity presumably due to comproportionation with copper(II) in solution to regenerate the active Cu^{I} species. The lack of reactivity of aryl iodides was explained by the overstabilization of Cu^{I} species by the soft iodide anion, thus preventing oxidation to Cu^{II} species. These observations led the authors to propose a mechanism involving SET from the copper(I) centre to the aryl bromide. This step generates an aryl radical (kinetically protected by the back reaction with Cu^{II}) and Cu^{II} species, and in the subsequent step, the aryl radical couples with the amine moiety with a second SET that regenerates the Cu^{I} species.



Scheme I.3.12. Coupling reaction of bromobenzene with nitrogen and oxygen nucleophiles reported by Van Koten and coworkers.

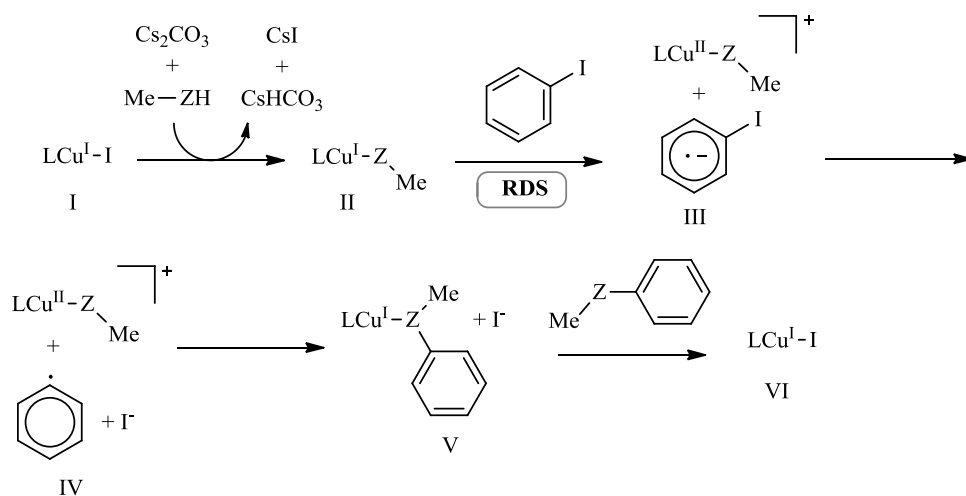
Finally, several computational studies have also supported SET and IAT mechanisms in copper-catalyzed cross-coupling reactions. In this context, Buchwald and Houk have studied ligand-directed selectivities in N- versus O-arylation of 5-amino-1-pentanol.¹⁴² Experimentally, Buchwald reported that when β -diketone ligand was used in DMF the N-arylated product was obtained with a ratio >20:1 over O-arylation. In contrast, when tetramethylphenanthroline ($\text{Me}_4\text{-phen}$) was used as ligand, the O-arylated product was obtained in a ratio 16:1 over the N-arylation (Scheme I.3.13).¹⁴³



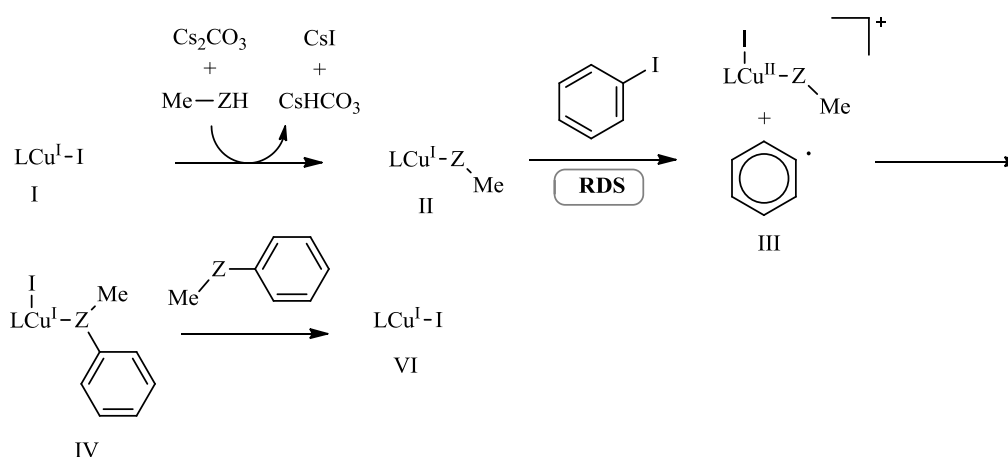
Scheme I.3.13. Chemoselective N-arylation and O-arylation of 5-amino-1-pentanol with 3-bromo-3-iodobenzene catalyzed by copper and bidentate ligands.

In the first part of the study, they calculated the energy of all possible copper(I) nucleophile complexes showing that $\text{LCu}^{\text{I}}\text{-OMe}$ complexes are more stable than $\text{LCu}^{\text{I}}\text{-NHMe}$ complexes. Secondly, they found that the ligand-directed selectivity occurred at the aryl halide activation step, which is rate-limiting. They evaluated the energy barriers for the iodobenzene activation step through four distinct scenarios: a) oxidative addition/reductive elimination, b) SET, c) IAT and d) σ -bond metathesis. The pathways showing a computed lower energy barrier were SET and IAT mechanisms and either two may occur depending on the nucleophile (Scheme I.3.4). These results indicate that β -diketone ligand promotes the SET mechanism and N-bound pathway is preferred over O-bound pathway, despite $\text{LCu}^{\text{I}}\text{-NHMe}$ complex is less stable than $\text{LCu}^{\text{I}}\text{-OMe}$. When phenanthroline is used, SET and IAT have similar barriers, and either may occur depending on the nucleophile. The Cu-catalyzed O-arylation reaction proceeds via IAT and it is lower in energy than the N-arylation, which proceeds via SET. However, very recently Fu and coworkers have proposed an alternative computational pathway for these reactions based on oxidative addition/reductive elimination pathway, using the real nucleophile 5-amino-1-pentanol, instead of MeOH and MeNH₂ as theoretical model substrates (see section I.3.3.4).¹⁴⁴

Mechanism involving Single Electron Transfer (SET)



Mechanism involving Iodine Atom Transfer (IAT)

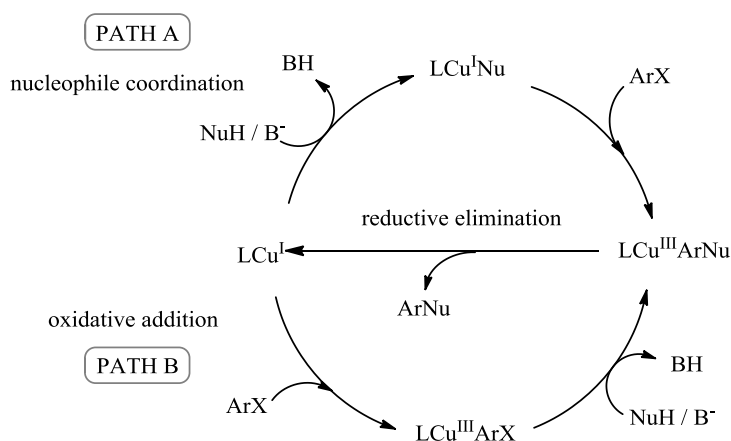


Ligand (L)	pathway	Atom Bound (Z)	ΔG I	ΔG II	ΔG III	ΔG IV	ΔG V	ΔG VI
β -diketone	SET	O	0	2.9	27.2	20.4	-33.7	-41.3
		N	0	14.8	26.2	19.4	-50.5	-48.0
Me ₄ -phen	IAT	O	0	7.2	34.0	-28.9	—	-47.1
	SET	N	0	17.0	35.1	26.1	-43.9	-52.6

Scheme I.3.14. DFT computed mechanism for the cross-coupling between aryl iodide and model MeOH and MeNH₂ nucleophiles, involving rate-limiting SET and/or IAT mechanistic pathways (tabulated AG values for each intermediate species in kcal mol⁻¹).

I.3.3.4 Oxidative Addition/Reductive elimination Cu^I/Cu^{III} pathway

Cu^I/Cu^{III} catalytic cycle based on two electron redox processes has often been proposed for Ullmann Condensation Reactions. The mechanism consists of an oxidative addition of copper(I) to C-halogen bond to form an arylcopper(III) intermediate. Then, coupling of the nucleophile and aryl moieties renders the final product through a reductive elimination step that regenerates the active copper(I) complex. With regard to the coordination of the nucleophile, two different mechanistic pathways have been proposed (Scheme I.3.15). The coordination of the base-deprotonated nucleophile to copper(I) may occur at the first step, before the activation of the aryl halide (path A). Or, on the contrary, the coordination of the nucleophile may occur after the oxidative addition step, after the formation of the arylcopper(III) intermediate. The experimental data, based mainly on the reactivity of isolated LCu^I nucleophile complexes, supports a mechanism through pathway A.

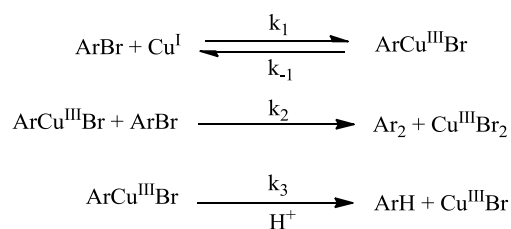


Scheme I.3.15. Proposed mechanistic pathways for the Ullmann reaction involving oxidative addition/reductive elimination steps.

Since putative arylcopper(III) intermediates species are formed after the aryl halide activation rate-limiting step, their detection has proven to be extremely challenging. Then, the proposal of Cu^I/Cu^{III} cycle is mainly supported by the lack of rate inhibition with radical-scavenging and by computational studies. Nonetheless, very early reports already proposed copper(III) species as key intermediates in Ullmann chemistry, despite their inherent instability.

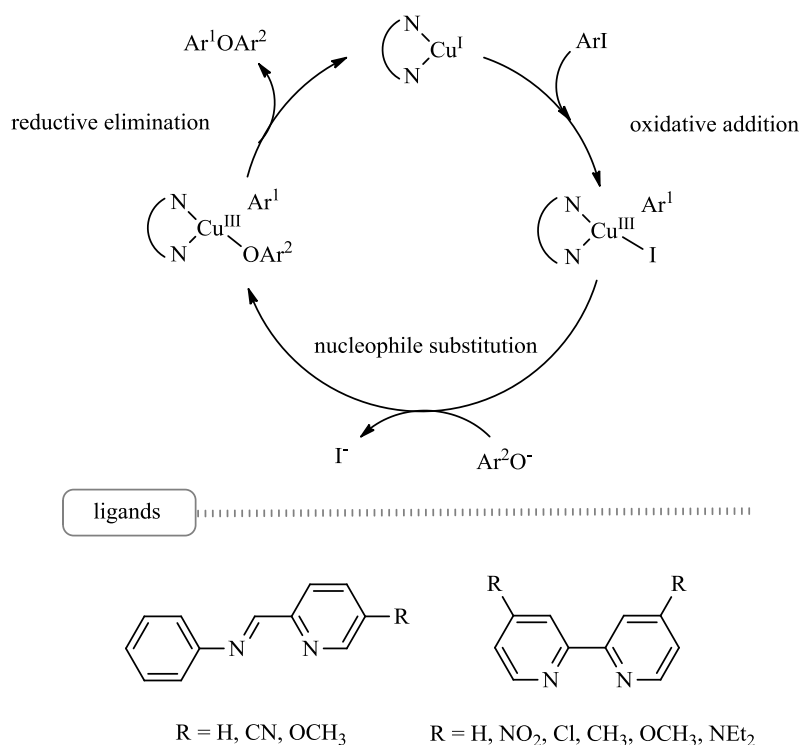
The first author to propose copper(III) was Cohen, who studied the mechanism of homocoupling reaction of *o*-bromonitrobenzene mediated by copper.^{145,146} The major product was biaryl 2,2'-dinitrobiphenyl, together with small amounts of nitrobenzene. The addition of ammonium tetrafluoroborate increased the yield of nitrobenzene, which was explained by the intermediacy of organocopper complexes that were keen to protonation. Neither the reaction rate nor the product distribution was modified by the use of radical traps, indicating that radical

intermediates are not plausible in the reaction pathway. Moreover, Cohen studied the Ullmann coupling reaction of vinyl halides, where the homocoupled products showed retention of the configuration, thus also arguing against the intermediacy of radical species.^{147,146} With these mechanistic considerations in hand, Cohen proposed that organocopper(III) species, obtained by aryl or vinyl halide oxidative addition, were key intermediates species in Ullmann reactions (Scheme I.3.16).



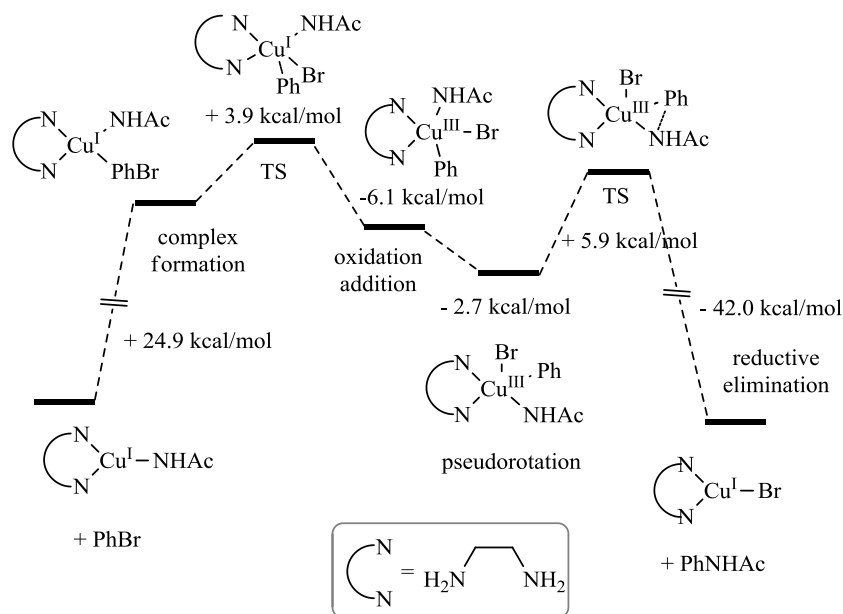
Scheme I.3.16. Proposed mechanism for the reaction of *o*-bromonitrobenzene with copper(I).

Much more recently, Taillefer and coworkers studied the copper-catalyzed arylation of phenols using several N,N-chelating ligands in order to determine the relationship between the structure of the chelates and their catalytic activity.¹⁰⁷ The results were explained using a Cu^I/Cu^{III} catalytic cycle via oxidative addition/reductive elimination steps. The most efficient ligands contained one imine- and one pyridine binding sites acting in a synergistic manner (Scheme I.3.17). By tuning the electronic properties of the pyridine moiety of the ligand, they found that the more electron donating ligands improved the catalytic activity because the oxidative addition step is more favorable, as indicated by the lower oxidation potential. In contrast, the more electron withdrawing *para*-substituents in the imine binding site favored the arylation reaction, suggesting that this binding site is related to the ligand exchange and/or reductive elimination steps, which are more favorable in electron deficient copper(III) intermediates.



Scheme I.3.17. Taillefer's mechanistic proposal for the copper-catalyzed cross-coupling reaction using N,N-bidentate ligands.

Several authors relied on computational studies for supporting the Cu^I/Cu^{III} catalytic cycle for Ullmann Condensation Reactions. Based on simple DFT computational studies, Hartwig and coworkers have supported the intermediacy of arylcopper(III) complexes in several copper-catalyzed C-N and C-O bond forming reactions as well as in Hurtley-type reactions.^{124,125,121,148} In a more detailed theoretical study, Guo calculated the oxidative addition/reductive elimination pathway in diamine ligated copper(I) amidate complexes with bromobenzene (Scheme I.3.18).¹²⁶ The oxidative addition of copper(I) complex into the C-Br bond of the aryl bromide afforded a square pyramidal pentacoordinated arylCu^{III} intermediate, where the two coupling partners are situated in *trans* position. After a pseudorotation step, in order to obtain the phenyl and amide group *cis* to each other, the reductive elimination occurs with low energetic barrier. The oxidative addition was the rate limiting step of the aryl amidation reaction catalyzed by copper(I) with overall free energy barriers among 24-35 kcal mol⁻¹, depending on the bidentate diamine ligand studied. Very recently, a related computational study for the coupling of bromobenzene with methylamine in the presence of copper/diketone ligand have been reported by Ding and coworkers and is also in favor of an oxidative addition/reductive elimination pathway.¹⁴⁹



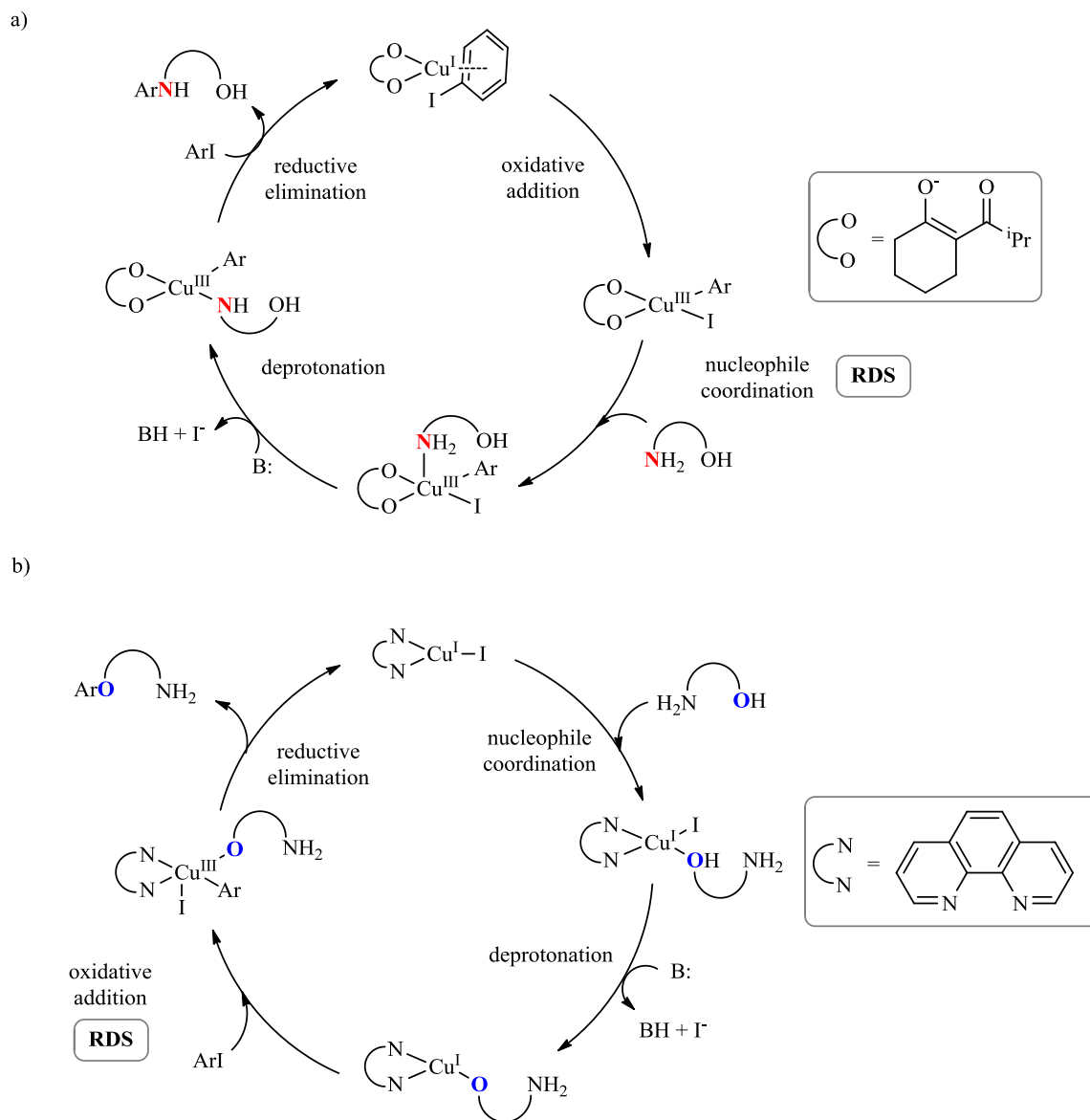
Scheme I.3.18. Energetic profile calculated for the reaction of bromobenzene and acetamide catalyzed by Cu^{I} /ethylenediamine.

Finally, Fu and coworkers have also explored computationally ligand directed N- or O-selectivities in the reaction of copper-catalyzed N- or O-arylation using $\text{NH}_2(\text{CH}_2)_5\text{OH}$ as nucleophile, and β -diketone and 1,10-phenanthroline as ligands.¹⁴⁴ Fu proposed that oxidative addition/reductive elimination pathway *via* arylcopper(III) complexes is the most favorable mechanism in this reaction, in contrast to the study of Buchwald and Houk who proposed that the most plausible mechanism for this reaction involves radical intermediates *via* $\text{Cu}^{\text{I}}/\text{Cu}^{\text{II}}$ pathway (see section I.3.3.3).

In the first part of the study, Fu and coworkers studied all possible species in equilibrium using a β -diketone ligand. They found that the activation of the aryl halide occurred before coordination of the nucleophile, so the most favorable transition state for the oxidative addition did not involve the amino alcohol nucleophile (Scheme I.3.19, a). Oxidative addition produced a tetra-coordinated Cu^{III} intermediate that binds to the nucleophile in the rate-determining step. It was calculated that the amine coordination to form a penta-coordinated Cu^{III} complex is more favorable than the coordination by the alcohol group of the nucleophile. Cesium carbonate was not a strong enough base to deprotonate the amino or alcohol group in the free substrate, thus, the removal of a proton from the coordinated amino alcohol substrate took place before the reductive elimination. A low energy barrier was calculated for the reductive elimination from penta-coordinated Cu^{III} complex to produce the final N-arylation and Cu^{I} products.

On the other hand, calculations performed with 1,10-phenanthroline ligand indicated that the coordination of the nucleophile is prior to the oxidative addition, which is the rate

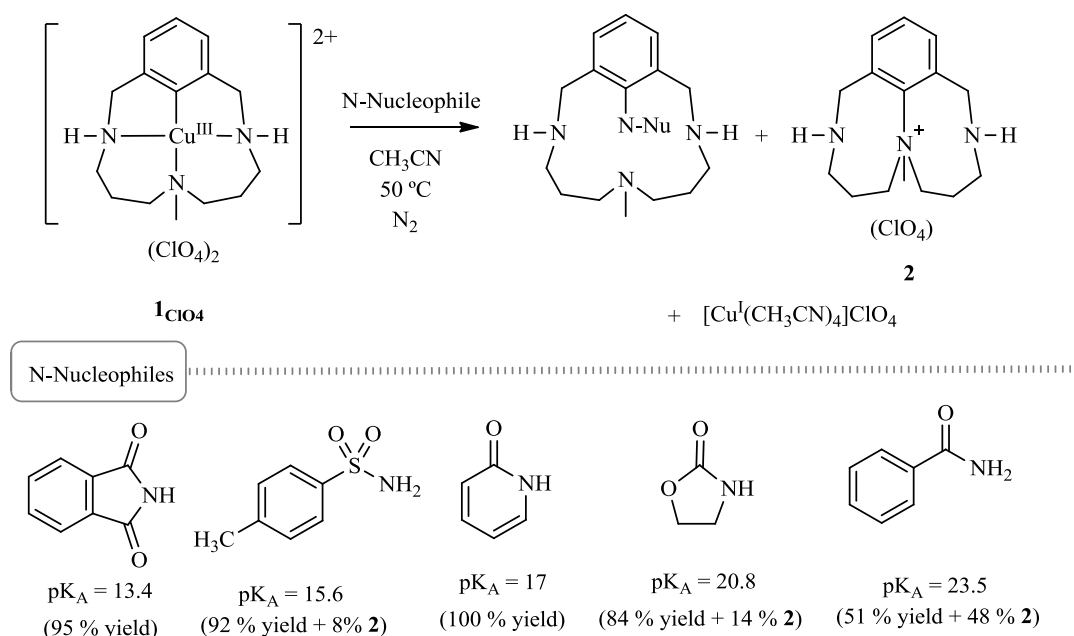
determining step (Scheme I.3.19, b). In this case, the most favorable transition state for the oxidative addition contains the copper complex coordinated to the deprotonated alcohol of the substrate. Again, the reductive elimination from a penta-coordinated arylcopper(III) is a very favorable step from a theoretical point of view and it afforded the C-O coupling product.



I.3.4 Reactivity of well-defined arylcopper(III) complexes

The detection of intermediates in C_{aryl} -heteroatom bond forming reactions catalyzed by copper after the activation of the aryl halide, which is the rate-limiting step, is very challenging due to very short-lived intermediates. Although arylcopper(III) complexes have been often proposed in these reactions, there were no experimental evidences to support the involvement of copper(III) in C_{aryl} -heteroatom bond forming reactions. A strategy for knowing the feasibility of arylcopper(III) complexes in these reactions would consist in the synthesis of stable well-defined arylcopper(III) complexes and to study their reactivity towards heteroatom nucleophiles.

A breakthrough in this field appeared during the realization of this thesis, in 2008, when Huffman and Stahl reported the involvement of an arylcopper(III) complex in C-N bond forming reactions.¹⁵⁰ They described that arylcopper(III) complex **1**_{ClO₄} react with a number of different amide type nitrogen nucleophiles in acetonitrile at 50 °C to afford the corresponding C-N coupled product (Scheme I.3.20). In reactions with less acidic nucleophiles, product **2** was also observed in the reaction mixture, that corresponds to the intramolecular C-N reductive elimination between the central tertiary amine with the aryl moiety.¹⁵¹



Scheme I.3.20. C-N bond forming reaction from well-defined aryl-copper(III) complexes.

Kinetic studies of these reactions were consistent with a simple bimolecular rate law, first-order in both **1**_{ClO₄} and nucleophile concentration. Analysis of the effect of the pK_A of the nitrogen nucleophile on the rate of the reaction revealed a reasonable Brønsted correlation with a negative slope, indicating that more acidic nucleophiles react more rapidly (Scheme I.3.1). These results implicate proton loss as a key step prior to C-N bond formation. Pyridone

resulted to have an extremely rapid rate due to its readily accessible tautomer, 2-hydroxypyridine, which may be capable of reacting without prior substrate deprotonation.

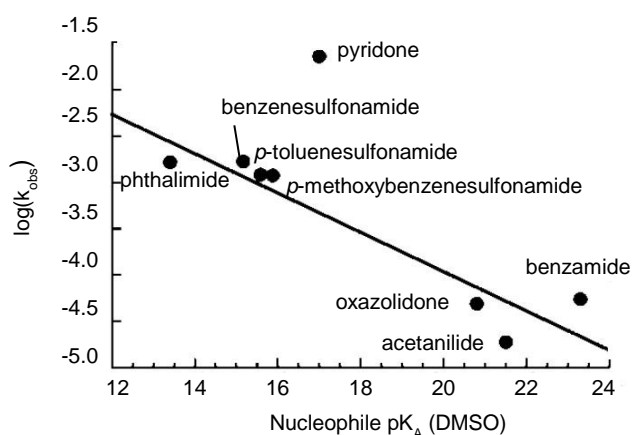
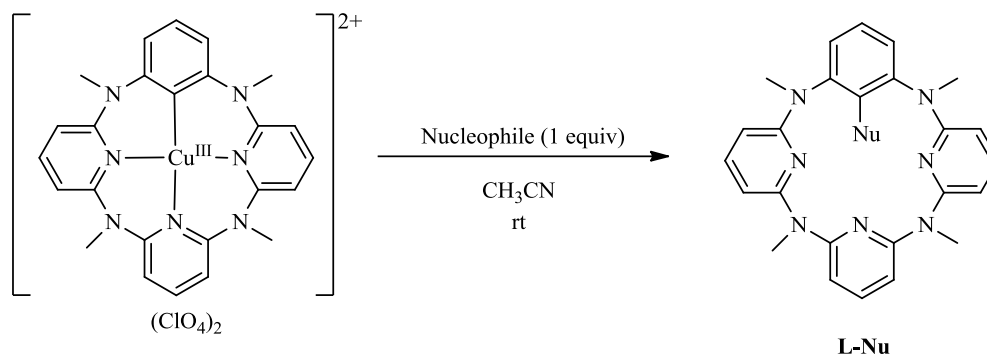


Figure I.3.1. Brønsted plot that correlates the rate of intermolecular C-N bond formation reaction with the acidity of the nitrogen nucleophile. Reaction conditions: $[1_{ClO_4}] = 0.8$ mM, $[Nucleophile] = 8.0$ mM, CH_3CN , $50^\circ C$.

In 2009, Wang and coworkers reported an arylcopper(III) complex based in a azacalix[1]arene[3]pyridine ligand and demonstrated its reactivity towards several anionic nucleophiles, such as carboxylates, halide salts (Cl, Br, I) and cyanides, to form C-heteroatom bonds under very mild reaction conditions (Scheme I.3.21).⁴⁸ More recently, Wang have reported C-O coupling reaction of this arylcopper(III) complex with several aliphatic alcohols and phenols in moderate yields in the presence of strong organic bases, such as 1,8-diazabicyclo[5.4.0]undec-7-ene (DBU), under refluxing acetonitrile during 12 h.¹⁵²



Nucleophile	% yield L-Nu	Nucleophile	% yield L-Nu
$(\text{CH}_3\text{CH}_2)_4\text{NCl}$	99	KCN	99
$(\text{CH}_3\text{CH}_2)_4\text{NBr}$	97	PhCOONa	91
$(\text{CH}_3\text{CH}_2)_4\text{NI}$	90	CH₃COONa^a	91
NaSCN	95	CH₂=CHCOONa	95

Scheme I.3.21. Stoichiometric reactions of arylCu^{III} complex described by Wang and reactivity towards several anionic nucleophiles to form C-heteroatom bonds. ^a Two equivalents were used.

From the reactivity of well-defined arylcopper(III) complexes it has been shown that C-N and C-O reductive elimination is a very favorable step that takes place under mild reactions conditions. These reactivity patterns may support the feasibility of arylcopper(III) intermediates in Ullmann Condensations Reactions.

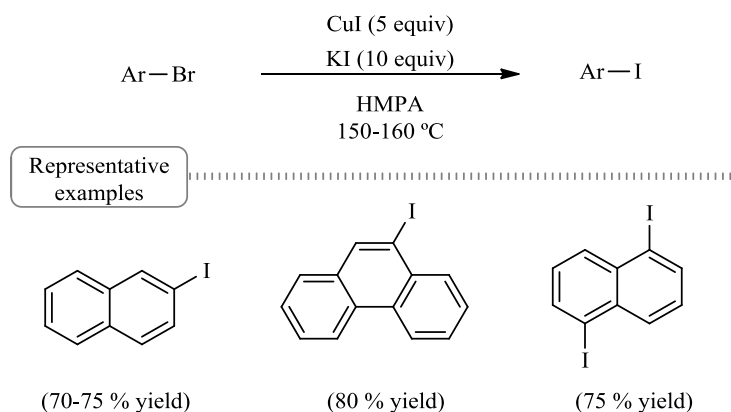
I.4 Halide Exchange reactions catalyzed by copper

Aryl halides are important synthetic targets that are present in many pharmaceuticals and agrochemicals. On the other hand, haloarenes are highly useful synthetic intermediates in Pd-based cross-coupling reactions such as Heck, Suzuki, Negishi and Stille C-C cross-coupling reactions,^{110,153} as well as Pd-catalyzed Buchwald-Hartwig C-N bond forming reactions¹⁵⁴⁻¹⁵⁶ and Cu-catalyzed Ullmann Condensation Reactions.^{110,91,113} Moreover, aryl halides are precursors for the formation of organometallic reagents and for the generation of free-radical intermediates.¹⁵⁷

The ability to exchange a given halide in an aryl group for another halide would enormously facilitate the versatility of many transition metal catalyzed cross-coupling reactions that are usually limited to less accessible aryl bromides and iodides (the typical order of

reactivity being $\text{Cl} < \text{Br} < \text{I}$). The cheaper and more accessible aryl chlorides and pseudohalides (obtained from commercially available phenols) are the less active in cross-coupling reactions. Therefore, it would be highly interesting to develop aromatic halogen exchange methods for interconverting between the different halogen derivatives.¹⁵⁷ There are limited examples on palladium-catalyzed halogen exchange reactions with aryl halides or pseudohalides.^{158,159} In contrast, several reports based on nickel catalyst have been reported, even though, they suffer from important limitations, for instance, incomplete conversion of aryl halides, biaryl products formation and the use stoichiometric amounts of metal catalyst.¹⁶⁰⁻¹⁶² Copper-catalyzed halide exchange reactions have been more successful, and during the last 20 years efficient methods under relative mild reactions conditions have been developed.^{163,103}

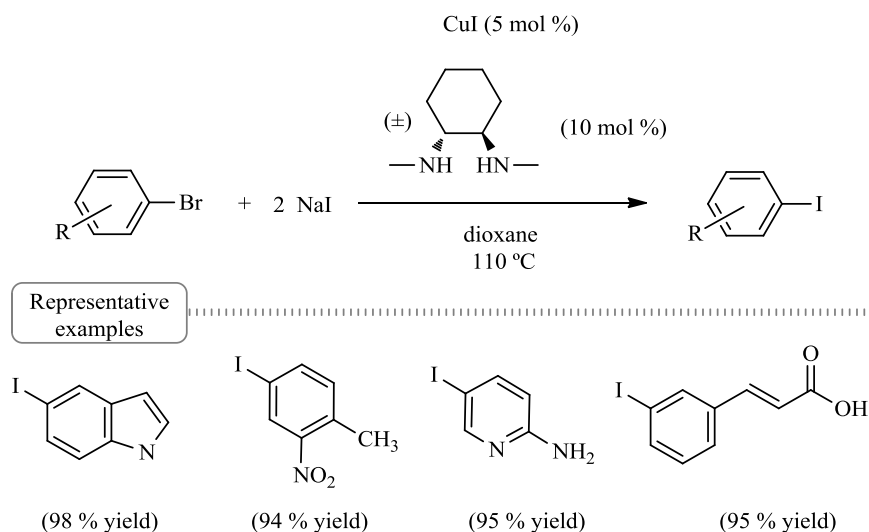
Early examples of copper-mediated halogen exchanges in aryl halides were reported by Bacon and Hill in 1964.¹³⁰ Heating aryl halides in polar solvents in the presence of stoichiometric amounts of cuprous halide, $\text{Cu}^{\text{I}}\text{X}$ ($\text{X} = \text{Cl}, \text{Br}, \text{I}$), afforded the exchanged aryl halide products. The reactivity trend is governed by the stronger energy of the aryl halide bond formed ($\text{Cl} > \text{Br} > \text{I}$). Therefore, the reaction was useful for the preparation of aryl chlorides from aryl bromides or aryl iodides and the preparation of aryl bromides from aryl iodides. In later work, Ogawa and coworkers reported preparative useful reverse halogen-exchange reactions. Aryl iodides were obtained from aryl bromides by using potassium iodide and copper(I) iodide in hexamethylphosphoramide (HMPA) at 150 °C (Scheme I.4.1).¹⁶⁴



Scheme I.4.1. Early examples of copper(I)-catalyzed bromine to iodine exchange reaction from aryl bromides.

The most significant contribution to copper-catalyzed halogen exchange reactions was made by Buchwald and Klapars in 2002.¹⁶³ They developed a methodology to synthesize a wide range of electron-rich and electron-deficient aryl iodides from the corresponding aryl bromides with an excellent functional group tolerance. This methodology have been applied for

the synthesis of complex aryl iodides molecules over the past ten years.¹⁰³ The strategy consisted of using catalytic amounts of copper(I) iodide (5 mol%), *trans*-cyclohexane-1,2-diamine (or derivatives) ligand (10 mol%) and excess sodium iodide at 110 °C in dioxane (Scheme I.4.2). In analogy to the Finkelstein reaction,¹⁶⁵ the driving force for conversion to the aryl iodide is provided by the difference in solubility of the sodium halides. The conversion to the aryl iodide is higher in solvents in which NaBr has relatively low solubility, such as dioxane or pentanol, because its precipitation displaces the equilibrium reaction.



Scheme I.4.2. Buchwald's breakthrough methodology for the conversion of aryl bromides to the corresponding iodides.

Mechanistic proposals for copper-catalyzed halogen exchange reactions are analogous to the copper-catalyzed nucleophilic substitutions described in the previous section I.3.3, even though, fewer experimental data have been obtained for these reactions.¹⁵⁷

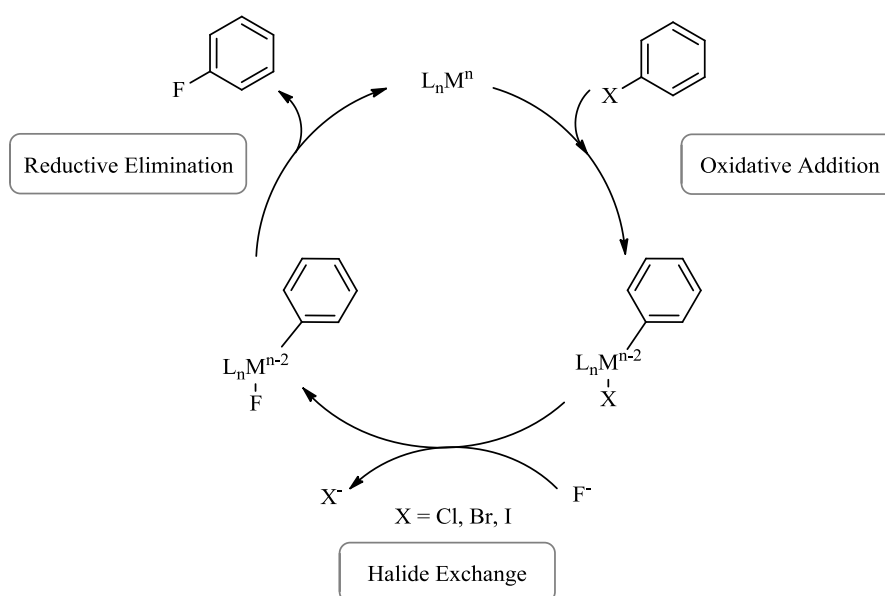
I.4.1 Fluorine insertion catalyzed by copper: a very challenging reaction

The presence of fluoroaromatic compounds in pharmaceutical and agrochemical industry have been continuously increasing during the past years due to some beneficial attributes related to fluorine atoms. The incorporation of fluorine into a drug increases metabolic chemical inertness, high thermal stability, lipophilicity, solubility and non-covalent interactions with biological targets. These attributes lead not only to increase drug efficacy, but also to lower dosing, which can reduce undesirable side effects.¹⁶⁶ Moreover, the highly demanded ¹⁸F-radiolabelling for Positron Emission Tomography (PET), an imaging technique used for

cancer diagnose and disease staging among others, has fuelled the interest in finding effective late-stage nucleophilic fluorinations by C-¹⁸F bond construction.^{167,168}

Current methods used for the preparation of fluoroarenes have several practical limitations, for instance, very harsh conditions and narrow substrate scope. A general method for the selective introduction of fluorine into an aromatic ring is the Balz-Schiemann reaction that involves diazotization of an aromatic amine in the presence of tetrafluoroboric acid.¹⁶⁹ However, this reaction produces large amounts of waste and uses potentially explosive and toxic diazonium salts at elevated temperatures. The Halex reaction is also used in industry for obtaining halogen to fluorine exchange in polyhalogenated aromatic substrates.¹⁷⁰ This transition metal-free reaction is usually conducted with potassium fluoride in dimethylformamide or dimethylsulfoxide under temperature just below the solvent boiling point and is limited to polyhalogenated aromatic substrates bearing electron-withdrawing groups.

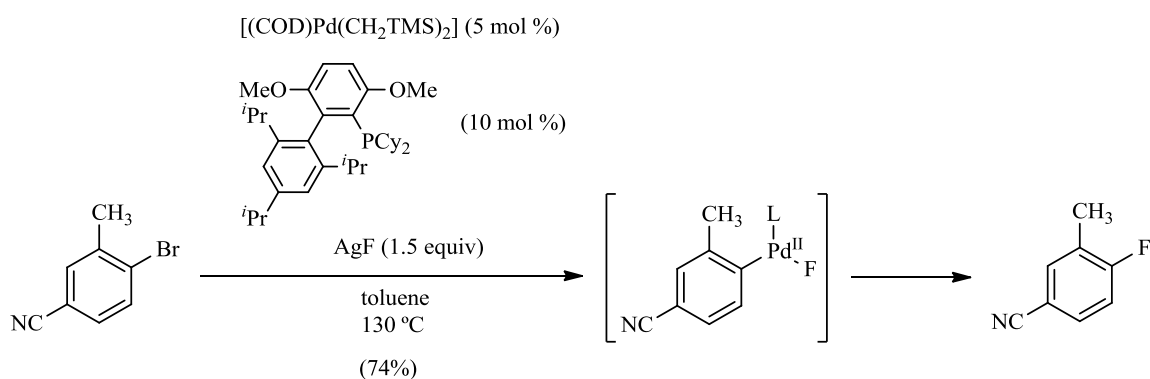
The development of aromatic fluorination reactions catalyzed by transition metal that could operate under mild reaction conditions would be highly desirable.^{171,172} This fluorination strategy can be envisioned via a three-step catalytic cycle that would involve aryl halide oxidative addition, followed by halide to fluoride exchange, and finally C_{aryl}-fluorine reductive elimination (Scheme I.4.3). Although fluorine forms the strongest single bond to carbon, C-F insertion reactions is very challenging and limited number of palladium catalysts have been identified to afford C-F aromatic bonds by reductive elimination.



Scheme I.4.3. General mechanism for transition metal catalyzed C-fluorine reductive elimination.

Several Pd^{II} fluorides complexes bearing phosphine or nitrogen dative ligands have been synthesized in order to test their ability to perform C-F reductive elimination. However, the main products obtained upon thermolysis were P-F and C-C bond forming products.¹⁷³⁻¹⁷⁵

In 2009 Buchwald and coworkers reported a breakthrough in the field, C_{aryl}-F reductive elimination was achieved from an aryl-Pd^{II} fluoride complex bearing bulky monodentated phosphine ligand.¹⁷⁶ The latter is involved in the catalytic C_{aryl}-F reductive elimination reaction of aryl triflates or bromides in the presence of AgF and palladium catalyst (Scheme I.4.4). However, this first example operating by Pd⁰/Pd^{II} catalytic cycle have been shown to be a more complex mechanism.¹⁷⁷

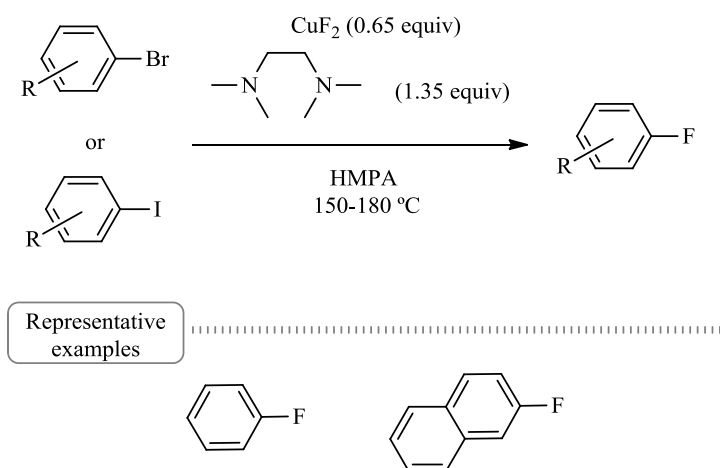


Scheme I.4.4. Palladium-catalyzed fluorination of aryl bromides using fluoride sources reported by Buchwald.

An alternative approach for C_{aryl}-F bond formation consisted in the synthesis of high oxidation state Pd^{IV} fluoride complexes with electrophilic fluorinating reagents.^{178-181,167} In this context, Ritter and coworkers have synthesized several arylPd^{IV} fluoride complexes based on N-pyridyl-sulfonyl ligands and they have demonstrated that C_{aryl}-F reductive elimination is a feasible reaction in such complexes.^{181,167} However, Sanford and coworkers synthesized several mono-σ-aryl Pd^{IV} fluoride complexes that did not afford C_{aryl}-F reductive elimination upon thermolysis. Otherwise, aromatic fluorine insertion was obtained reacting several mono-σ-aryl Pd^{IV} fluoride complexes with electrophilic fluorinating reagents in excess.¹⁷⁹

With regard to copper-catalyzed fluorination reactions, very few examples have been reported. A single example was reported in the 1990s by Vigalok and coworkers, describing copper-mediated quantitative fluorination of electron-deficient 2-bromonitrobenzene with potassium fluoride in the presence of copper(I) complex (Ph₃P)₃CuF.¹⁸² More recently, researchers at DuPont reported the formation of fluorobenzene from benzene by using HF and O₂ mediated by CuF₂.¹⁸³ Reaction interest relies on obtaining only H₂O as byproduct although very high temperatures (> 500 °C) were required, precluding a wide implementation.

A copper mediated methodology for preparing fluoroarenes from haloarenes has been recently patented by Grushin. A wide range of non-activated haloarenes can be used to exchange one or more halogen atoms by fluorine by using CuF_2 , TMEDA (*N,N,N,N*-tetramethylethylenediamine) and alkali metal fluorides under high temperature conditions (usually above 150 °C) (Scheme I.4.5).¹⁸⁴ This methodology is remarkable due to the difficulty of introducing fluorine atoms in aromatic rings, even though the harsh conditions employed and the stoichiometric loadings of CuF_2 are clear drawbacks for implementation of this methodology in late-stage functionalization of compounds.



Scheme I.4.5. Representative example of fluorination reaction mediated by CuF_2 .

I.5 Direct C-H activation through copper complexes

An alternative to standard cross-coupling reactions is C-H bond functionalization reaction which has received substantial attention because of its economic, sustainable and environmentally benign features.^{185,186} The selective transformation of ubiquitous but inert C-H bonds to other functional groups in complex molecules without previous prefunctionalization has long been a goal for many organic chemists. Initial efforts have been focused in the development of catalytic systems with second and third row transition metals, for instance, palladium, rhodium and ruthenium.¹⁸⁷⁻¹⁸⁹ Due to the cheapness and relatively low toxicity of copper, many researchers have started to develop copper-catalyzed selective C-C and C-heteroatom bond formation reactions from C-H bonds.¹⁹⁰⁻¹⁹²

First of all, we will summarize some reports that shown the feasibility of copper to participate in C-H functionalization reactions under oxidative conditions, where it has been

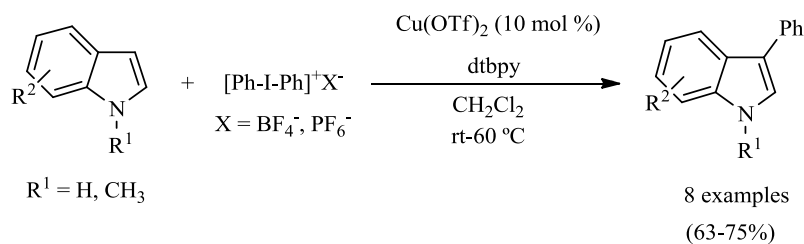
postulated the involvement of copper(III). Although the mechanistic comprehension of these reactions are very scarce, they rely on the use of sacrificial oxidants for obtaining high electrophilic Cu^{III} intermediates that may be able to activate and functionalize C-H bonds. Secondly, in this section we will focus in intramolecular C-H activation reactions mediated by copper in macrocyclic systems in which the ligand facilitates the reaction directing the copper(II) center towards the targeted C-H bond. The mechanistic understanding of the C-H bond activation mediated by copper in model systems may provide new insights into the design of new copper catalysts for effecting mild C-H bond activation reactions.

I.5.1 Electrophilic C-H functionalization reactions

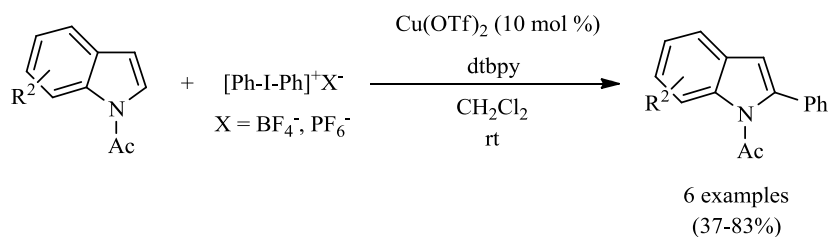
Early reports from Barton and coworkers showed the feasibility of C-H functionalization reactions with copper(I) in the presence of oxidant reagents. In 1988, they reported the arylation reaction of indoles catalyzed by copper in the presence of aryl-Bi^V reagents.¹⁹³ Barton proposed that copper(III) species were able to activate C-H bond at indole ring and promote the C-C bond formation step via reductive elimination.¹⁹³

Recently, Gaunt and coworkers reported the arylation reaction of indoles catalyzed by copper(II) using less toxic bis(aryl)iodonium salts as oxidant (Scheme I.5.1).¹⁹⁴ A substrate broad scope is obtained under very mild conditions and the reaction shows high functionality tolerance in both the indole and the aryl unit. The aryl group is transferred at position C3, but in the presence of a strong coordinating group in the nitrogen atom, such as acetyl, the arylation of indole occurs at C2 position. The mechanism of the arylation reaction is proposed to proceed via arylcopper(III) species obtained by oxidation of copper(I) (formed by *in situ* reduction of copper(II) under reaction conditions) and (bis)aryliodonium salts. These highly electrophilic arylcopper(III) intermediates promote the arylation process under mild conditions.

a) C3 arylation

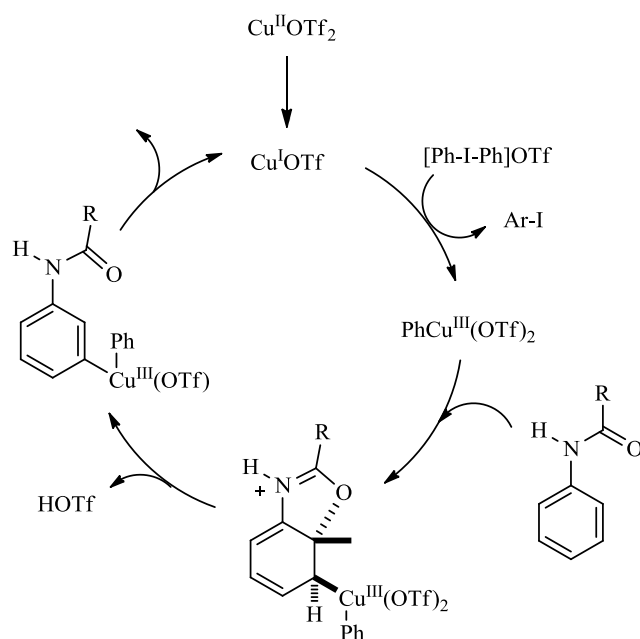
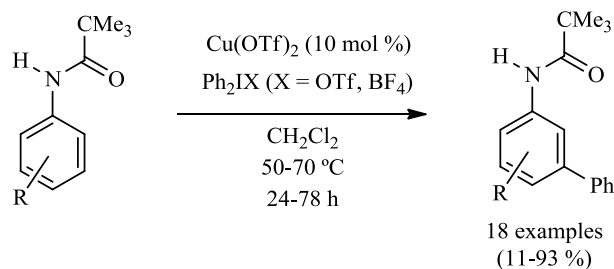


b) C2 arylation

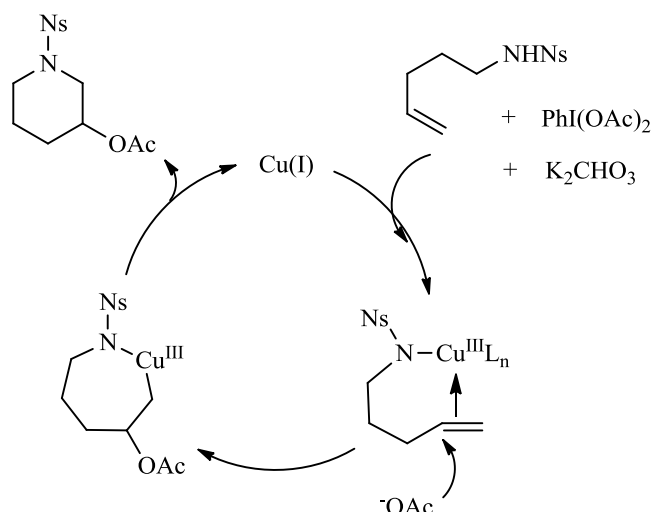
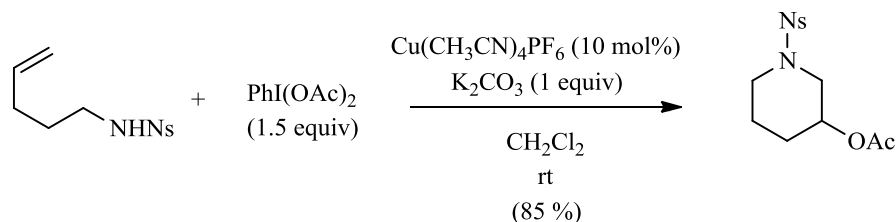


Scheme I.5.1. Indole arylation reaction catalyzed by copper with high valent iodine(III) reagents.

In 2009, using the same strategy, Phipps and Gaunt reported a breakthrough work in the field of copper-catalyzed C-H functionalization reactions. They developed the *meta*-selective electrophilic arylation reaction of pivanilide derivatives catalyzed by copper and bis(aryl)iodonium salts (Scheme I.5.2).¹⁹⁵ The importance of the reaction is that the aryl group is transferred directly to a C-H bond in *meta* position of the arene ring, a position that is difficult to functionalize by simple Friedel-Crafts reactions. The proposed mechanism consisted in a $\text{Cu}^{\text{I}}/\text{Cu}^{\text{III}}$ reaction mechanism which was studied in detail by computational methods.¹⁹⁶ Later on, it was shown that the carbonyl group plays a key role in determining the selectivity in *meta* which can be also obtained in more electronically neutral α -aryl carbonyl compounds.¹⁹⁷ In electron-rich substrates that do not bear a carbonyl group, such as aniline and phenol derivatives, the arylation reaction occurs at the *para* position. Interestingly, when the *para* position is blocked with a functional group, then, the aryl group is inserted at the *ortho* position following the selectivity patterns of Friedel Crafts reactions.¹⁹⁸

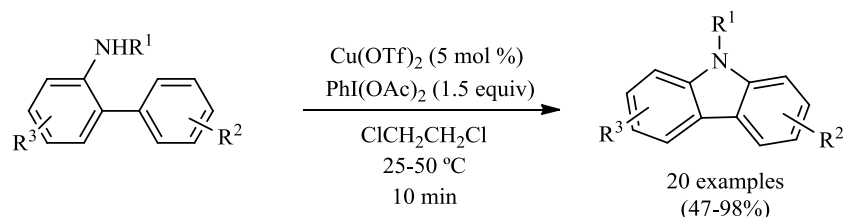
Scheme I.5.2. *Meta* arylation reaction catalyzed by copper.

Another interesting reaction, was reported by Blakey and coworkers who described an intramolecular olefin aminoacetoxylation catalyzed by copper in the presence of hypervalent iodo(III) reagent $[\text{PhI}(\text{OAc})_2]$ (Scheme I.5.3).¹⁹⁹ In most terminal olefins tested, the reaction is selective to the formation of the *endo* cyclization product affording piperidine derivatives. The authors proposed a mechanism that proceeds through electrophilic copper(III) amido species formed under oxidative conditions. Then coordination of the olefin to the copper(III) center activates the double bond for a nucleophilic attack of the acetate to the internal carbon leading to the *endo* cyclization.



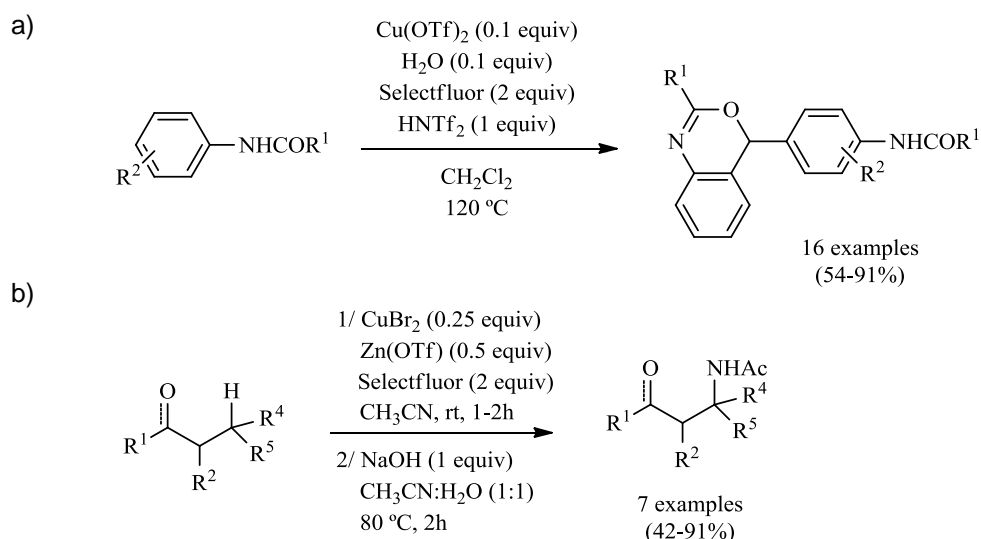
Scheme I.5.3. Intramolecular olefin aminoacetoxylation reaction catalyzed by copper in the presence of $[\text{PhI}(\text{OAc})_2]$ reported by Blakey and coworkers.

Although copper(III) species have been invoked as key intermediates in C-H functionalization reactions catalyzed by copper with high valent iodine(III) reagents, in most cases, detailed mechanistic data is still lacking.^{194,195,199-203} Nevertheless, some authors have questioned the $\text{Cu}^{\text{I}}/\text{Cu}^{\text{III}}$ catalytic cycle with high valent iodine(III) reagents. Chang and coworkers developed an intramolecular oxidative C-N bond formation for the synthesis of carbazoles catalyzed by copper and iodine(III) reagents (Scheme I.5.4).²⁰⁴ They showed that high valent hyperiodine reagents can facilitate the reactions even in the absence of copper, even though, at lower efficiency. They do not observed significant intramolecular KIE values indicating that the C-H bond cleavage may not be involved in the rds. Furthermore, the reaction rate is independent on copper concentration, suggesting that copper species do not participate in the rds. Taking into account all mechanistic data, Chang and coworkers proposed that copper species work as an activator of the iodine(III) oxidants and they described a mechanistic proposal based on the formation of aryl radicals intermediates.



Scheme I.5.4. Intramolecular oxidative C-N bond formation to synthesize carbazoles reported by Chang and coworkers.

The formation of copper(III) species have been proposed to form not only with hypervalent iodine reagents but also using electrophilic fluorinating reagents as oxidants.²⁰⁵⁻²⁰⁷ The strategy to use bystander F^+ oxidants for obtaining C-C and C-heteroatom reductive elimination from high valent transition metals has been developed, for instance, in palladium and gold complexes.¹⁴⁴ In this context, Zhang and coworkers reported the annulation of *N*-para-tolylamides catalyzed by Cu(OTf)_2 and with Selectfluor as the oxidant, for the synthesis of 4H-3,1-benzoxazines through successive intermolecular C-C and C-O bond forming reactions (Scheme I.5.5, a).²⁰⁵ Later on, Baran and coworkers developed aliphatic C-H amination reaction catalyzed by CuBr_2 in the presence of Zn(OTf)_2 as Lewis acid and Selectfluor as oxidant (Scheme I.5.5, b).²⁰⁶ In a first approach, they developed the reaction in substrates bearing hydroxyl and carbonyl moieties acting as directing functional groups. They took a step forward showing that the amination reaction was accomplished in cyclic hydrocarbons such as adamantane and cyclohexane.



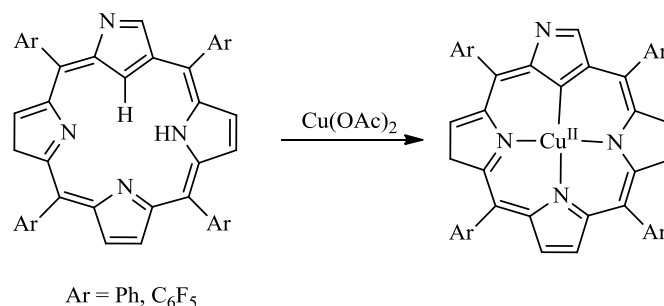
Scheme I.5.5. Examples of C-H functionalization reactions catalyzed by copper in the presence of Selectfluor as oxidant.

During the past 5 years, an increasing number of copper-catalyzed C-H functionalization reactions under oxidative conditions have appeared in the literature. Initial approach of these reports has proven the feasibility of copper to participate in C-H functionalization reactions and they represent a promising future direction in the field. Nevertheless, in order to develop more effective reactions under milder reaction conditions it is important to understand their precise mechanism.

I.5.2 Intramolecular C-H activation in macrocyclic ligands as mechanistic models

It has been well-established many mechanisms for the selective activation of C-H bonds that lead to the formation of organometallic complexes based mainly in second and third row transition metals.²⁰⁸ However, similar reactivity and detailed mechanistic studies with first row transition metals are still scarce.

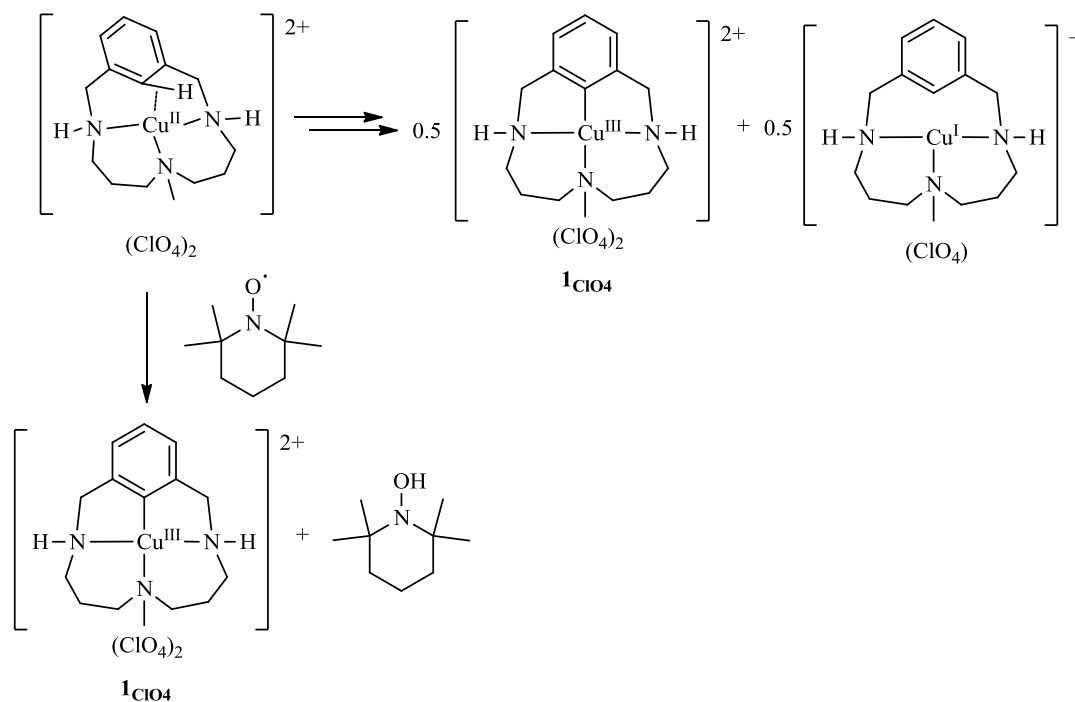
In this context, few stoichiometric intramolecular C-H bond activation reactions mediated by copper(II) salts have been reported in several macrocyclic systems. Furuta and Latos-Grażyński described the formation of several organometallic copper(II) and copper(III) complexes within heteroatom-confused porphyrins ligands.^{40-44,209,45} In these systems, copper(II) complex is formed by metalation of the C-H bond and, in many cases, subsequent oxidation lead to the copper(III) complex (Scheme I.5.6).



Scheme I.5.6. C-H metalation of N-Confused porphyrins to afford well-defined organocopper(II) species.

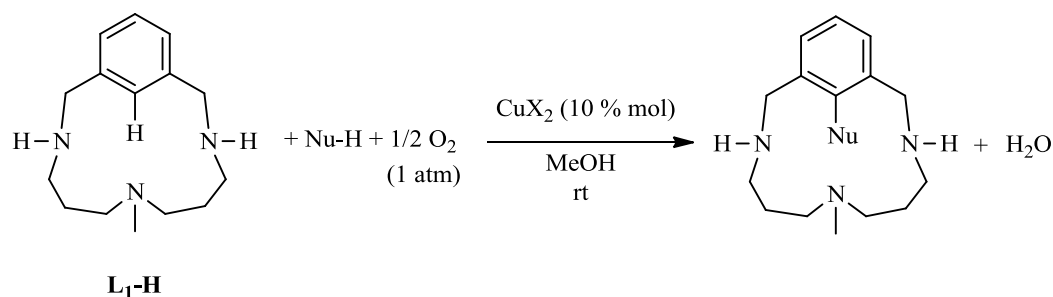
A very different approach was found in the C-H activation of macrocyclic arene ligand L₁-H (Scheme I.5.7) described by Ribas, Llobet and Stack.⁴⁶⁻⁴⁸ The reaction of copper(II) salt with ligand L₁-H affords equimolar amounts of arylcopper(III) complex **1**_{CuO4} and Cu^I species as products. They described the arene C-H interaction with copper(II) as three center-three electron C-H...Cu^{II} interaction, which was identified by pulsed-EPR spectroscopy and supported by DFT calculations.²¹⁰ Moreover, kinetic data obtained by UV-vis monitoring

supported a mechanism that involves a rate-limiting proton-coupled electron transfer (PCET) step as a key step in the C-H bond activation. Additional support for this mechanism is the reaction of copper(II) complex with 2,2,6,6-tetramethylpiperidine-1-oxyl (TEMPO) that affords quantitative formation of the arylCu^{III} complex and TEMPO-H. A similar mechanism was proposed by Wang and coworkers for the synthesis of another arylCu^{III} complex based in a calixarene ligand even though no mechanistic studies were done.⁴⁸



Scheme I.5.7. ArylCu^{III} complex formation through C-H bond activation with copper(II).

With regard to the development of more effective copper-catalyzed C-H bond functionalization reactions, it is fundamental to obtain detailed comprehension of these processes. Very recently, Stahl, Ribas and coworkers studied a copper-catalyzed C-H methoxylation and amidation reaction in macrocyclic arene substrate **L₁-H** (Scheme I.5.8).²¹¹ Reaction of **L₁-H** with oxygen or nitrogen nucleophile in the presence of 10 mol% of copper(II) salts and under O₂ atmosphere affords the corresponding C-heteroatom coupled product in moderate yields. Furthermore, by means of kinetic and spectroscopic analysis of the methoxylation reaction, employing simultaneous O₂-uptake methods and UV-Visible spectroscopy, they provided direct evidence for the involvement of an arylCu^{III}-bromide intermediate under reaction conditions. Although these studies are performed in model arene substrates, they may provide the basis for the development of more synthetically useful C-H bond functionalization reactions.



Nu-H	Cu(ClO ₄) ₂ ·6H ₂ O	CuBr ₂
MeOH (solvent)	72 %	81 %
pyridone	77 %	84 %

Scheme I.5.8. Oxidative C-H functionalization of macrocyclic arene ligand L₁-H.

I.6 References

- Krause, N. *Modern Organocopper Chemistry*; Wiley-VCH: Weinheim, **2002**.
- Cotton, F. A.; Wilkinson, G. *Advanced Inorganic Chemistry*, 5th ed.; Wiley: New York, **1988**.
- Lewis, E. A.; Tolman, W. B. *Chem. Rev.* **2004**, *114*, 1047.
- Ribas, X.; Casitas, A. In *Ideas in Chemistry and Molecular Science. Where Chemistry Meets Life*; Pignataro, B. Ed.; Wiley-VCH: Weinheim, 2010 pp. 31-57.
- Melník, M.; Kabešová, M. *J. Coord. Chem.* **2000**, *50*, 323.
- Krebs, C.; Glaser, T.; Bill, E.; Weyhermüller, T.; Meyer-Klaucke, W.; Wieghardt, K. *Angew. Chem. Int. Ed.* **1999**, *38*, 359.
- Santo, R.; Miyamoto, R.; Tanaka, R.; Nishioka, T.; Sato, K.; Toyota, K.; Obata, M.; Yano, S.; Kinoshita, I.; Ichimura, A.; Takui, T. *Angew. Chem. Int. Ed.* **2006**, *45*, 7611.
- Scholder, R.; Voelskow, U. *Z. Anorg. Allg. Chem.* **1951**, *266*, 256.
- Magee, J. S.; Wood, R. H. *Can. J. Chem.* **1965**, *43*, 1234.
- Bour, J. J.; Steggerda, J. J. *Chem. Commun.* **1967**, 85.
- Olson, D. C.; Vasilevskis, J. *Inorg. Chem.* **1971**, *10*, 463.
- Kumar, K.; Rotzinger, F. P.; Endicott, J. F. *J. Am. Chem. Soc.* **1983**, *105*, 7064.
- Meyerstein, D. *Inorg. Chem.* **1971**, *10*, 638.
- Meyerstein, D. *Inorg. Chem.* **1971**, *10*, 2244.
- Ulanski, P.; von Sonntag, C. *Eur. J. Inorg. Chem.* **2000**, 1211.
- Beck, G. *Mikrochemie ver Mikrochem. Acta.* **1950**, *35*, 169.

17. Keyworth, D. A.; Stone, K. G. *Anal. Chem.* **1955**, 27, 833.
18. Margerum, D. W.; Chellappa, K. L.; Bossu, F. P.; Burce, G. L. *J. Am. Chem. Soc.* **1975**, 97, 6894.
19. Neubecker, T. A.; Kirksey, S. T.; Chellappa, K. L.; Margerum, D. W. *Inorg. Chem.* **1979**, 18, 444.
20. Kirksey, S. T.; Margerum, D. W. *Inorg. Chem.* **1979**, 18, 966.
21. Diaddario, L. L.; Robinson, W. R.; Margerum, D. W. *Inorg. Chem.* **1983**, 22, 1021.
22. McDonald, M. R.; Scheper, W. M.; Lee, H. D.; Margerum, D. W. *Inorg. Chem.* **1995**, 34, 229.
23. Lappin, A. G.; Youngblood, M. P.; Margerum, D. W. *Inorg. Chem.* **1980**, 19, 407.
24. Anson, F. C.; Collins, T. J.; Richmond, T. G.; Santarsiero, B. D.; Toth, J. E.; Treco, B. G. R. T. *J. Am. Chem. Soc.* **1987**, 109, 2974.
25. Hanss, J.; Kruger, H.-J. *Angew Chem. Int. Ed.* **1996**, 35, 2827.
26. Hanss, J.; Beckmann, A.; Krüger, H.-J. *Eur. J. Inorg. Chem.* **1999**, 163.
27. Fritsky, I. O.; Kozlowski, H.; Kanderl, O. M.; Haukka, M.; Swiatek-Kozlowska, J.; Gumienna-Kontecka, E.; Meyer, F. *Chem. Comm.* **2006**, 4125.
28. Will, S.; Lex, J.; Vogel, E.; Schmickler, H.; Gisselbrecht, J.-P.; Hauptmann, C.; Bernard, M.; Gross, M. *Angew. Chem. Int. Ed.* **1997**, 36, 357.
29. Wasbotten, I. H.; Wondimagegn, T.; Ghosh, A. *J. Am. Chem. Soc.* **2002**, 124, 8104.
30. Brückner, C.; Briñas, R. P.; Krause Bauer, J. A. *Inorg. Chem.* **2003**, 42, 4495.
31. Ribas, X.; Dias, J.; Morgado, J.; Wurst, K.; Almeida, M.; Veciana, J.; Rovira, C. *CrystEngComm* **2002**, 4, 564.
32. Ribas, X.; Dias, J. C.; Morgado, J.; Wurst, K.; Molins, E.; Ruiz, E.; Almeida, M.; Veciana, J.; Rovira, C. *Chem. Eur. J.* **2004**, 10, 16-91.
33. Ribas, X.; Maspoch, D.; Dias, J.; Morgado, J.; Almeida, M.; Wurst, K.; Vaughan, G.; Veciana, J.; Rovira, C. *CrystEngComm* **2004**, 6, 589.
34. Gschwind, R. M. *Chem. Rev.* **2008**, 108, 3029.
35. DuBois, J. L.; Mukherjee, P.; Stack, T. D. P.; Hedman, B.; Solomon, E. I.; Hodgson, K. O. *J. Am. Chem. Soc.* **2000**, 122, 5775.
36. Sarangi, R.; DeBeer George, S.; Rudd, D. J.; Szilagy, R. K.; Ribas, X.; Rovira, C.; Almeida, M.; Hodgson, K. O.; Hedman, B.; Solomon, E. I. *J. Am. Chem. Soc.* **2007**, 129, 2316.
37. Willert-Porada, M. A.; Burton, D. J.; Baenziger, N. C. *J. Chem. Soc. Chem. Commun.* **1989**, 1633.
38. Naumann, D.; Roy, T.; Tebbe, K.-F.; Crump, W. *Angew. Chem. Int. Ed.* **1993**, 32, 1482.
39. Eujen, R.; Hoge, B.; Brauer, D. J. *J. Organomet. Chem.* **1996**, 519, 7.
40. Furuta, H.; Maeda, H.; Osuka, A. *J. Am. Chem. Soc.* **2000**, 122, 803.
41. Maeda, H.; Osuka, A.; Furuta, H. *J. Am. Chem. Soc.* **2003**, 125, 15690.
42. Chmielewski, P. J.; Latos-Grazynski, L.; Schmidt, I. *Inorg. Chem.* **2000**, 39, 5475.

43. Maeda, H.; Osuka, A.; Ishikawa, Y.; Aritome, I.; Hisaeda, Y.; Furuta, H. *Org. Lett.* **2003**, *5*, 1293.
44. Pawlicki, M.; Kanska, I.; Latos-Grazynski, L. *Inorg. Chem.* **2007**, *46*, 6575.
45. Maeda, H.; Ishikawa, Y.; Matsuda, T.; Osuka, A.; Furuta, H. *J. Am. Chem. Soc.* **2003**, *125*, 11822.
46. Ribas, X.; Jackson, D. A.; Donnadiou, B.; Mahía, J.; Parella, T.; Xifra, R.; Hedman, B.; Hodgson, K. O.; Llobet, A.; Stack, T. D. P. *Angew. Chem. Int. Ed.* **2002**, *41*, 2991.
47. Xifra, R.; Ribas, X.; Llobet, A.; Poater, A.; Duran, M.; Solà, M.; Stack, T. D. P.; Benet-Buchholz, J.; Donnadiou, B.; Mahía, J.; Parella, T. *Chem.-Eur. J.* **2005**, *11*, 5146.
48. Yao, B.; Wang, D.-X.; Huang, Z.-T.; Wang, M.-X. *Chem. Commun.* **2009**, 2899.
49. Bertz, S. H.; Cope, S.; Murphy, M.; Ogle, C. A.; Taylor, B. J. *J. Am. Chem. Soc.* **2007**, *129*, 7208.
50. Gärtner, T.; Henze, W.; Gschwind, R. M. *J. Am. Chem. Soc.* **2007**, *129*, 11362.
51. Bertz, S. H.; Cope, S.; Dorton, D.; Murphy, M.; Ogle, C. A. *Angew. Chem. Int. Ed.* **2007**, *46*, 7082.
52. Bartholomew, E. R.; Bertz, S. H.; Cope, S. K.; Murphy, M. D.; Ogle, C. A.; Thomasa, A. *Chem. Commun.* **2010**, *46*, 1253.
53. Bertz, S. H.; Murphy, M. D.; Ogle, C. A.; Thomas, A. A. *Chem. Comm.* **2010**, *46*, 1255.
54. Gärtner, T.; Yoshikai, N.; Neumeier, M.; Nakamura, E.; Gschwind, R. M. *Chem. Comm.* **2010**, *46*, 4625.
55. Normant, J. F. *Synthesis* **1972**, 63.
56. Yoshikai, N.; Nakamura, E. *Chem. Rev.* **2012**, DOI: dx.doi.org/10.1021/cr200241f.
57. Krause, N.; Gerold, A. *Angew. Chem. Int. Ed.* **1997**, *36*, 186.
58. Nakamura, E.; Mori, S. *Angew. Chem. Int. Ed.* **2000**, *39*, 3750.
59. Krause, N. *Angew. Chem. Int. Ed.* **1999**, *38*, 79.
60. Kharasch, M. S.; Tawney, P. O. *J. Am. Chem. Soc.* **1941**, *63*, 2308.
61. Bertz, S. H.; Smith, R. A. J. *J. Am. Chem. Soc.* **1989**, *111*, 8276.
62. Hallnemo, G.; Olsson, T.; Ullenius, C. *J. Organomet. Chem.* **1985**, *282*, 133.
63. Krause, N.; Wagner, R.; Gerold, A. *J. Am. Chem. Soc.* **1994**, *116*, 381.
64. Krauss, S. R.; Smith, S. G. *J. Am. Chem. Soc.* **1981**, *103*, 141.
65. Nakamura, E.; Mori, S.; Morokuma, K. *J. Am. Chem. Soc.* **1997**, *119*, 4900.
66. Snyder, J. P. *J. Am. Chem. Soc.* **1995**, *117*, 11025.
67. Yamanaka, M.; Nakamura, E. *Organometallics* **2001**, *20*, 5675.
68. Frantz, D. E.; Singleton, D. A.; Snyder, J. P. *J. Am. Chem. Soc.* **1997**, *119*, 3383.
69. Bertz, S. H.; Carlin, C. M.; Deadwyler, D. A.; Murphy, M. D.; Craig A. Ogle, C. A.; Seagle, P. H. *J. Am. Chem. Soc.* **2002**, *124*, 13650.
70. Hu, H.; Snyder, J. P. *J. Am. Chem. Soc.* **2007**, *129*, 7210.
71. Corey, E. J.; Posner, G. H. *J. Am. Chem. Soc.* **1967**, *89*, 3911.
72. Corey, E. J.; Posner, G. H. *J. Am. Chem. Soc.* **1968**, *90*, 5615.

73. Whitesides, G. M.; Fischer, J. W. F.; San Filippo, J. J.; Bashe, R. W.; House, H. O. *J. Am. Chem. Soc.* **1969**, *91*, 4871.
74. Johnson, C. R.; Dutra, G. A. *J. Am. Chem. Soc.* **1973**, *95*, 7777.
75. Lipshutz, B. H.; Wilhelm, R. S. *J. Am. Chem. Soc.* **1982**, *104*, 4698.
76. Johnson, C. R.; Dutra, G. A. *J. Am. Chem. Soc.* **1973**, *95*, 7783.
77. Putau, A.; Brand, H.; Koszinowski, K. *J. Am. Chem. Soc.* **2012**, *134*, 613.
78. Nakamura, E.; Mori, S. *J. Am. Chem. Soc.* **1998**, *120*, 8273.
79. Mori, S.; Nakamura, E.; Morokuma, K. *J. Am. Chem. Soc.* **2000**, *122*, 7294.
80. Rona, P.; Tökes, L.; Tremble, J.; Crabbé, P. *J. Chem. Soc., Chem. Commun.* **1969**, 43.
81. Goering, H. L.; Singleton, V. D. *J. Am. Chem. Soc.* **1976**, *98*, 7854.
82. Tseng, C. C.; Paisley, S. D.; Goering, H. L. *J. Org. Chem.* **1986**, *51*, 2884.
83. Tseng, C. C.; Yen, S.-J.; Goering, H. L. *J. Org. Chem.* **1986**, *51*, 2892.
84. Nakamura, E.; Sekiya, K.; Arai, M.; Aoki, S. *J. Am. Chem. Soc.* **1989**, *111*, 3093.
85. Yamanaka, M.; Kato, S.; Nakamura, E. *J. Am. Chem. Soc.* **2004**, *126*, 6287.
86. Yoshikai, N.; Zhang, S.-L.; Nakamura, E. *J. Am. Chem. Soc.* **2008**, *130*, 12862.
87. Bartholomew, E. R.; Bertz, S. H.; Cope, S.; Murphy, M.; Ogle, C. A. *J. Am. Chem. Soc.* **2008**, *130*, 11244.
88. Ullmann, F.; Bielecki, J. *Chem. Ber.* **1901**, *34*, 2174.
89. Ullmann, F. *Ber. Dtsch. Chem. Ges.* **1903**, *36*, 2389.
90. Goldberg, I. *Ber. Dtsch. Chem. Ges.* **1906**, *39*, 1691.
91. Ley, S. V.; Thomas, A. W. *Angew. Chem. Int. Ed.* **2003**, *42*, 5400.
92. Fanta, P. E. *Synthesis* **1974**, 9.
93. Lindley, J. *Tetrahedron* **1984**, *40*, 1433.
94. Weingarten, H. *J. Am. Chem. Soc.* **1964**, *29*, 3624.
95. Ma, D.; Zhang, Y.; Yao, J.; Wu, S.; Tao, F. *J. Am. Chem. Soc.* **1998**, *120*, 12459.
96. Goodbrand, H. B.; Hu, N.-X.-. *J. Org. Chem.* **1999**, *64*, 670.
97. Fagan, P. J.; Hauptman, E.; Shapiro, R.; Casalnuovo, A. *J. Am. Chem. Soc.* **2000**, *122*, 5043.
98. Klapars, A.; Antilla, J. C.; Huang, X.; Buchwald, S. L. *J. Am. Chem. Soc.* **2001**, *123*, 7727.
99. Klapars, A.; Huang, X.; Buchwald, S. L. *J. Am. Chem. Soc.* **2002**, *124*, 7421.
100. Buchwald, S. L.; Klapars, A.; Antilla, J. C.; Job, G. E.; Wolter, M.; Kwong, F. Y.; Nordmann, G.; Hennessy, E. J. *Patent WO 02/085838 A1*, **2001**.
101. Taillefer, M.; Cristau, H.-J.; Cellier, P. P.; Spindler, J.-F.; Ouali, A. *Patent Fr 2840303-WO 03101966 (Pr. Nb. Fr 2002 06717)*, **2002**.
102. Taillefer, M.; Cristau, H.-J.; Cellier, P. P.; Spindler, J.-F. *Patent Fr 2833947-WO 0353225 (Pr. Nb. Fr. 01 16547)*, **2001**.
103. Surry, D. S.; Buchwald, S. L. *Chem. Sci.* **2010**, *1*, 13.
104. Shafir, A.; Buchwald, S. L. *J. Am. Chem. Soc.* **2006**, *128*, 8742.

105. de Lange, B.; Lambers-Verstappen, M. H.; Schmieder-van de Vondervoort, L.; Sereinig, N.; de Rijk, R.; de Vries, A. H. M.; de Vries, J. G. *Synlett* **2006**, 3105.
106. Cristau, H.-J.; Cellier, P. P.; Spindler, J.-F.; Taillefer, M. *Chem. Eur. J.* **2004**, *10*, 5607.
107. Ouali, A.; Spindler, J.-F.; Jutand, A.; Taillefer, M. *Adv. Synth. Catal.* **2007**, *349*, 1906.
108. Ma, D.; Cai, Q. *Acc. Chem. Res.* **2008**, *41*, 1450.
109. Ma, D.; Cai, Q.; Zhang, H. *Org. Lett.* **2003**, *5*, 2453.
110. Beletskaya, I. P.; Cheprakov, A. V. *Coord. Chem. Rev.* **2004**, *248*, 2337.
111. Evano, G.; Blanchard, N.; Toumi, M. *Chem. Rev.* **2008**, *108*, 3054.
112. Monnier, F.; Taillefer, M. *Angew. Chem. Int. Ed.* **2009**, *48*, 6954.
113. Sperotto, E.; Klink, G. P. M. v.; Koten, G. v.; Vries, J. G. d. *Dalton Trans.* **2010**, *39*, 10338.
114. Paine, A. J. *J. Am. Chem. Soc.* **1987**, *109*, 1496.
115. Kondratov, S. A.; Shein, S. M. *Zh. Org. Khim.* **1979**, *15*, 2160.
116. Mansour, M.; Giacomazzi, R.; Ouali, A.; Taillefer, M.; Jutand, A. *Chem. Comm.* **2008**, 6051.
117. Kawaki, T.; Hashimoto, H. *Bull. Chem. Soc. Jpn.* **1972**, *45*, 1499.
118. Whitesides, G. M.; Sadowski, J. S.; Lilburn, J. *J. Am. Chem. Soc.* **1974**, *96*, 2829.
119. Kubota, M.; Yamamoto, A. *Bull. Chem. Soc. Jpn.* **1978**, *51*, 2909.
120. Yamamoto, T.; Ehara, Y.; Kubota, M.; Yamamoto, A. *Bull. Chem. Soc. Jpn.* **1980**, *53*, 1299.
121. Tye, J. W.; Weng, Z.; Johns, A. M.; Incarvito, C. D.; Hartwig, J. F. *J. Am. Chem. Soc.* **2008**, *130*, 9971.
122. Strieter, E. R., Blackmond, D. G., Buchwald, S. L. *J. Am. Chem. Soc.* **2005**, *127*, 4120.
123. Strieter, E. R.; Bhayana, B.; Buchwald, S. L. *J. Am. Chem. Soc.* **2009**, *131*, 78.
124. Giri, R.; Hartwig, J. F. *J. Am. Chem. Soc.* **2010**, *132*, 15860.
125. Tye, J. W.; Weng, Z.; Giri, G.; Hartwig, J. F. *Angew. Chem. Int. Ed.* **2010**, *49*, 2185.
126. Zhang, S.-L.; Liu, L.; Fu, Y.; Guo, Q.-X. *Organometallics* **2007**, *26*, 4546.
127. Ouali, A.; Taillefer, M.; Spindler, J.-F.; Jutand, A. *Organometallics* **2007**, *26*, 65.
128. Haldón, E.; Alvarez, E.; Nicasio, M. C.; Pérez, P. J. *Organometallics* **2009**, *28*, 3815.
129. Gujadhur, R. K.; Bates, C. G.; Venkataraman, D. *Org. Lett.* **2001**, *3*, 4315.
130. Bacon, R. G. R.; Hill, H. A. O. *J. Chem. Soc.* **1964**, 1097.
131. Bacon, R. G. R.; Hill, H. A. O. *J. Chem. Soc.* **1964**, 1108.
132. Bacon, R. G. R.; Hill, H. A. O. *J. Chem. Soc.* **1964**, 1112.
133. Delp, S. A.; Goj, L. A.; Pouy, M. J.; Munro-Leighton, C.; Lee, J. P.; Gunnoe, T. B.; Cundari, T. R.; Petersen, J. L. *Organometallics* **2011**, *30*, 55.
134. Weingarten, H. *J. Org. Chem.* **1964**, *29*, 977.
135. Arai, S.; Hida, M.; Yamagishi, T. *Bull. Chem. Soc. Jpn.* **1978**, *51*, 277.
136. Arai, S.; Yamagishi, T.; Ototake, S.; Hida, M. *Bull. Chem. Soc. Jpn.* **1977**, *50*, 547.
137. Kochi, J. K. *J. Am. Chem. Soc.* **1957**, *79*, 2942.

138. Kochi, J. K.; Subramanian, R. V. *J. Am. Chem. Soc.* **1965**, *87*, 1508.
139. Bowman, W. R.; Heaney, H.; Smith, P. H. G. *Tetrahedron Lett.* **1984**, *25*, 5821.
140. Sperotto, E.; van Klink, G. P. M.; de Vries, J. G.; van Koten, G. *Tetrahedron* **2010**, *66*, 9009.
141. Sperotto, E.; van Klink, G. P. M.; de Vries, J. G.; van Koten, G. *Tetrahedron* **2010**, *66*, 3478.
142. Jones, G. O.; Liu, P.; Houk, K. N.; Buchwald, S. L. *J. Am. Chem. Soc.* **2010**, *132*, 6205.
143. Shafir, A.; Lichtor, P. A.; Buchwald, S. L. *J. Am. Chem. Soc.* **2007**, *129*, 3490.
144. Engle, K. M.; Mei, T.-S.; Wang, X.; Yu, J.-Q. *Angew. Chem. Int. Ed.* **2011**, *50*, 1478.
145. Cohen, T.; Cristea, I. *J. Am. Chem. Soc.* **1976**, *98*, 748.
146. Cohen, T.; Cristea, I. *J. Org. Chem.* **1975**, *40*, 3649.
147. Cohen, T.; Poeth, T. *J. Am. Chem. Soc.* **1972**, *94*, 4363.
148. Huang, Z.; Hartwig, J. F. *Angew. Chem. Int. Ed.* **2012**, *51*, 1028.
149. Zhang, Y.; Ding, Y. *Organometallics* **2011**, *30*, 633.
150. Huffman, L. M.; Stahl, S. S. *J. Am. Chem. Soc.* **2008**, *130*, 9196.
151. Huffman, L. M.; Stahl, S. S. *Dalton Trans.* **2011**, *40*, 8959.
152. Wang, Z.-L.; Zhao, L.; Wang, M.-X. *Org. Lett.* **2011**, *13*, 6560.
153. Henry, P. M. *In Handbook of Organopalladium Chemistry for Organic Synthesis*, Negishi, E. Ed.; Wiley & Sons: New York, **2002**.
154. Wolfe, J. P.; Wagaw, S.; Marcoux, J.-F.; Buchwald, S. L. *Acc. Chem. Res.* **1998**, *31*, 805.
155. Hartwig, J. F. *Acc. Chem. Res.* **1998**, *31*, 852.
156. Hartwig, J. F. *Acc. Chem. Res.* **2008**, *41*, 1534.
157. Sheppard, T. D. *Org. Biomol. Chem.* **2010**, *7*, 1043.
158. Thathagar, M. B.; Rothenberg, G. *Org. Biomol. Chem.* **2006**, *4*, 111.
159. Shen, X.; Hyde, A. M.; Buchwald, S. L. *J. Am. Chem. Soc.* **2010**, *132*, 14076.
160. Cramer, R.; Coulson, D. R. *J. Org. Chem.* **1975**, *40*, 2267.
161. Tsou, T. T.; Kochi, J. K. *J. Org. Chem.* **1980**, *45*, 1930.
162. Takagi, K.; Hayama, N.; Inokawa, S. *Bull. Chem. Soc. Jpn.* **1980**, *53*, 3691.
163. Klapars, A.; Buchwald, S. L. *J. Am. Chem. Soc.* **2002**, *124*, 14844.
164. Suzuki, M.; Uehara, A.; Endo, K. *Inorg. Chim. Acta* **1986**, *123*, L9-L10.
165. Finkelstein, H. *Ber. Dtsch. Chem. Ges.* **1910**, *43*, 1528-1532.
166. Müller, K.; Faeh, C.; Diederich, F. *Science* **2007**, *317*, 1881.
167. Lee, E.; Kamlet, A. S.; Powers, D. C.; Neumann, C. N.; Boursalian, G. B.; Furuya, T.; Choi, D. C.; Hooker, J. M.; Ritter, T. *Science* **2011**, *334*, 639.
168. Gouverneur, V. *Nat. Chem.* **2012**, *4*, 152.
169. Balz, G.; Schiemann, G. *Chem. Ber.* **1927**, *60*, 1186.
170. Langlois, B.; Gilbert, L.; Forat, G. *Ind. Chem. Lib.* **1996**, *8*, 244.
171. Furuya, T.; Kamlet, A. S.; Ritter, T. *Nature* **2011**, *473*, 470.

172. Hollingworth, C.; Gouverneur, V. *Chem. Comm.* **2012**, 48, DOI: 10.1039/C2CC16158C
173. Grushin, V. V. *Chem. Eur. J.* **2002**, 8, 1006.
174. Ball, N. D.; Kampf, J. W.; Sanford, S. S. *Dalton Trans.* **2009**, 39, 632.
175. Grushin, V. V. *Acc. Chem. Res.* **2010**, 43, 160.
176. Watson, D. A.; Su, M.; Teverovskiy, G.; Zhang, Y.; García-Fortanet, J.; Kinzel, T.; Buchwald, S. L. *Science* **2009**, 325, 1661.
177. Maimone, T. J.; Milner, P. J.; Kinzel, T.; Zhang, Y.; Takase, M. K.; Buchwald, S. L. *J. Am. Chem. Soc.* **2011**, 133, 18106.
178. Hull, K. L.; Anani, W. Q.; Sanford, M. S. *J. Am. Chem. Soc.* **2006**, 128 7134.
179. Ball, N. D.; Sanford, M. S. *J. Am. Chem. Soc.* **2009**, 131, 3796.
180. Furuya, T.; Ritter, T. *J. Am. Chem. Soc.* **2008**, 130, 10060.
181. Furuya, T.; Benitez, D.; Tkatchouk, E.; Strom, A. E.; Tang, P.; Goddard-III, W. A.; Ritter, T. *J. Am. Chem. Soc.* **2010**, 132, 3793.
182. Antipin, I. S.; Vigalok, A. I.; Konovalov, A. I. *Zh. Org. Khim.* **1991**, 27, 1577.
183. Subramanian, M. A.; Manzer, L. E. *Science* **2002**, 297, 1665.
184. Grushin, V. V., **2007**; p. US Patent 7.202.388.
185. Labinger, J. A.; Bercaw, J. E. *Nature* **2001**, 417, 507.
186. Godula, K.; Sames, D. *Science* **2006**, 312, 67.
187. Colby, D. A.; Bergman, R. G.; Ellman, J. A. *Chem. Rev.* **2010**, 110, 624.
188. Mkhaliid, I. A. I.; Barnard, J. H.; Marder, T. B.; Murphy, J. M.; Hartwig, J. F. *Chem. Rev.* **2010**, 110, 890.
189. Lyons, T. W.; Sanford, M. S. *Chem. Rev.* **2010**, 110, 1147.
190. Zhang, M. *Appl. Organometal. Chem.* **2010**, 24, 269.
191. Díaz-Requejo, M. M.; Pérez, P. J. *Chem. Rev.* **2008**, 108, 3379.
192. Wendlandt, A. E.; Suess, A. M.; Stahl, S. S. *Angew. Chem. Int. Ed.* **2011**, 50, 11062.
193. Barton, D. H. R.; Finet, J.-P.; Khamisi, J. *Tetrahedron Lett.* **1988**, 29, 1115.
194. Phipps, R. J.; Grimster, N. P.; Gaunt, M. J. *J. Am. Chem. Soc.* **2008**, 130, 8172-8174.
195. Phipps, R. J.; Gaunt, M. J. *Science* **2009**, 323, 1593.
196. Chen, B.; Hou, X.-L.; Li, Y.-X.; Wu, Y.-D. *J. Am. Chem. Soc.* **2011**, 133, 7668.
197. Duong, H. A.; Gilligan, R. E.; Cooke, M. L.; Phipps, R. J.; Gaunt, M. J. *Angew. Chem. Int. Ed.* **2011**, 50, 463.
198. Ciana, C.-L.; Phipps, R. J.; Brandt, J. R.; Meyer, F.-M.; Gaunt, M. J. *Angew. Chem. Int. Ed.* **2011**, 50, 458.
199. Mancheno, D. E.; Thornton, A. R.; Stoll, A. H.; Kong, A.; Blakey, S. B. *Org. Lett.* **2010**, 12, 4110.
200. Seayad, J.; Seayad, A. M.; Chai, C. L. L. *Org. Lett.* **2010**, 12, 1412.
201. Xu, J.; Fu, Y.; Luo, D.-F.; Jiang, Y.-Y.; Xiao, B.; Liu, Z.-J.; Gong, T.-J.; Liu, L. *J. Am. Chem. Soc.* **2011**, 133, 15300.

202. Harvey, J. S.; Simonovich, S. P.; Jamison, C. R.; MacMillan, D. W. C. *J. Am. Chem. Soc.* **2011**, *133*, 13782.
203. Bigot, A.; Williamson, A. E.; Gaunt, M. J. *J. Am. Chem. Soc.* **2011**, *133*, 13778.
204. Hwan Cho, S. H.; Yoon, J.; Chang, S. *J. Am. Chem. Soc.* **2011**, *133*, 5996.
205. Xiong, T.; Li, Y.; Bi, X.; Lv, Y.; Zhang, Q. *Angew. Chem. Int. Ed.* **2011**, *50*, 7140.
206. Michaudel, Q.; Thevenet, D.; Baran, P. S. *J. Am. Chem. Soc.* **2012**, *134*, 2547.
207. Zhuang Jin; Bo Xu; Gerald B. Hammond. *Tetrahedron Lett.* **2011**, *52*, 1956.
208. Crabtree, R. H. *Chem. Rev.* **1995**, *95*, 987.
209. Furuta, H.; Ishizuka, T.; Osuka, A.; Uwatoko, Y.; Ishikawa, Y. *Angew. Chem. Int. Ed.* **2001**, *40*, 2323.
210. Ribas, X.; Calle, C.; Poater, A.; Casitas, A.; Gómez, L.; Xifra, R.; Parella, T.; Benet-Buchholz, J.; Schweiger, A.; Mitrikas, G.; Solà, M.; Llobet, A.; Stack, T. D. P. *J. Am. Chem. Soc.* **2010**, *132*, 12299.
211. King, A. E.; Huffman, L. M.; Casitas, A.; Costas, M.; Ribas, X.; Stahl, S. S. *J. Am. Chem. Soc.* **2010**, *132*, 12068.



CHAPTER II.
Main Objectives

II. Main Objectives

Copper(III) complexes have been proposed as intermediates in many organic transformations, as presented in the introductory chapter. The detection of Cu^{III} under reaction conditions is a challenging goal and, nowadays, Cu^{III} has only been detected in C-C bond forming reactions with organocuprates. Therefore, extensively computational studies have been done in order to support the involvement of copper(III) in most reactions. On the other hand, an alternative approach for supporting these intermediates in organic transformations is the synthesis of stable organometallic copper(III) complexes for studying of their reactivity.

II.1. Aims of the thesis

In this context, the aim of this thesis is to explore the reactivity of well-defined organometallic arylcopper(III) complexes, since they have been proposed to be involved in Ullmann Condensation Reactions through a Cu^I/Cu^{III} catalytic cycle. Our target is to study the feasibility of arylcopper(III) complexes to participate in C-heteroatom bond forming reactions. Furthermore, we are interested in studying the fundamental two electron redox steps proposed in these reactions by means of isolated copper complexes. The results obtained will provide a better understanding of Ullmann Condensation reactions, from a mechanistic point of view, and the key-experimental parameters that will allow the development of new efficient and low-cost strategies in these copper-catalyzed reactions.

II.2. Objectives of the thesis

For this purpose we have focused in a family of well-defined arylCu^{III} complexes based in triazamacrocyclic ligands. Our research group has experience in copper-mediated aromatic C-H activation within these macrocyclic ligands that drive to the formation of arylCu^{III} complexes (Figure II.1).¹

¹ Ribas, X. Ph.D. Dissertation, Universitat de Girona, Girona, 2001.

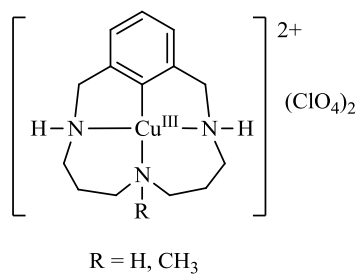


Figure II.1. ArylCu^{III} complexes that constituted the starting point of the thesis.

Therefore, based on these precedents, the general objectives of this thesis are summarized hereafter in three main aspects:

- To study the fundamental redox chemistry of well-defined arylCu^{III} complexes.
- To study the ability of isolated arylCu^{III} complexes to undergo aryl functionalization, thus to explore their reactivity in front of different nucleophiles (mainly N- and O-Nucleophiles).
- To unravel the fundamental mechanistic aspects of this reactivity and their relevance in Ullmann Condensation reactions.



CHAPTER III.
Results and Discussion

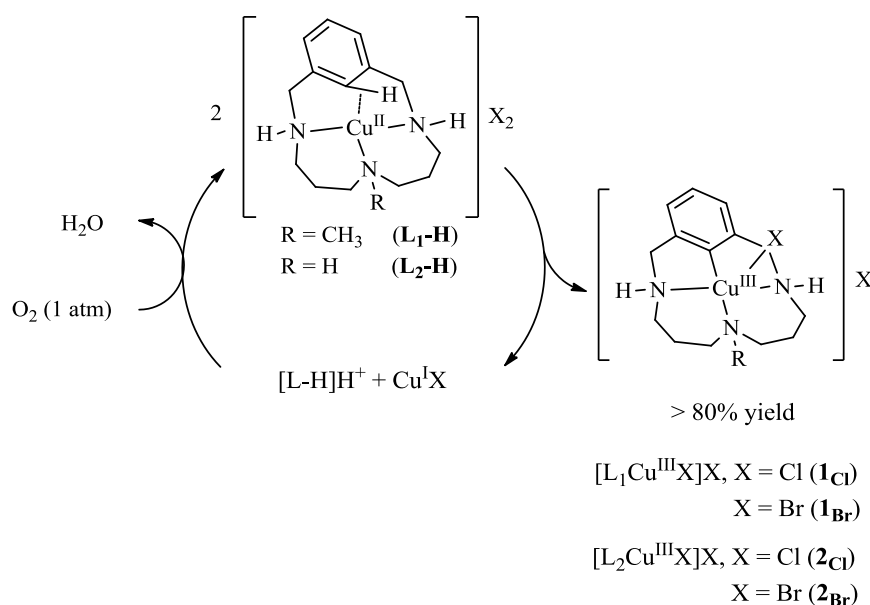
III.1 Direct Observation of Cu^I/Cu^{III} redox steps relevant to Ullmann-type coupling reactions

This section mainly corresponds to the contents of the paper by Casitas *et al.* *Chem. Sci.* **2010**, *1*, 326-330, which is found in chapter IV of this thesis.

III.1.1 Synthesis of arylCu^{III}-halide complexes

ArylCu^{III}-halide complexes **1_x** and **2_x** (X = Cl, Br, I) have been prepared based in a previous family of complexes using triazamacrocyclic ligands first described by Ribas, Llobet, Stack and coworkers (see section I.5.2).^{1,2}

Reaction of CuCl₂ or CuBr₂ as copper(II) sources with an small excess of ligand **L₁-H** or **L₂-H** (1.1 equiv) in acetonitrile affords equimolar amounts of arylcopper(III)-halide complex (**1_{Cl}**, **1_{Br}**, **2_{Cl}** and **2_{Br}**), and [L-H]H⁺ and Cu^I salt. Unfortunately, the maximum 50% disproportionation yield is an experimental drawback for the synthesis of arylCu^{III}-halide complexes in bulk quantities for further exploration of their chemistry. In order to address this inconvenience, we developed a new strategy to improve the synthesis of arylCu^{III}-halide complexes, based on the use of O₂ as an external sacrificial oxidant (Scheme III.1.1).³

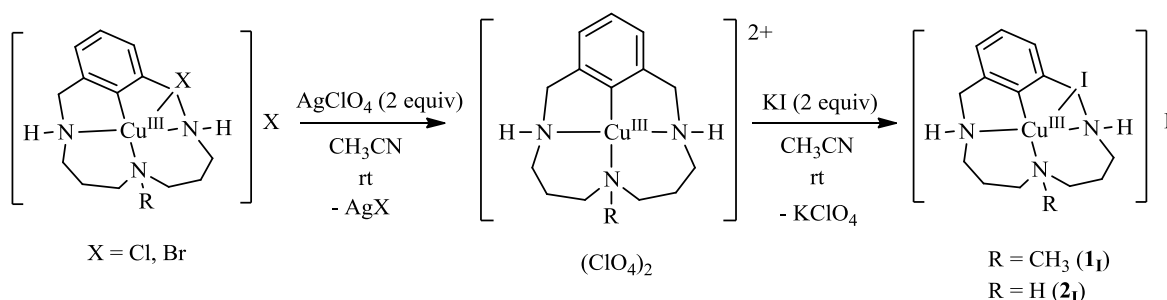


Scheme III.1.1. Synthesis of arylCu^{III}-X complexes using O₂ as external oxidant.

When the reaction is carried out in acetone, which is a non-coordinating solvent, and under oxygen atmosphere (1 atm) the yield of arylcopper(III) chloride and bromide complexes

is increased up to 80%. In solvents that do not stabilize Cu^{I} oxidation state, aerobic oxidation of copper(I) feeds back copper(II) into the solution to start the disproportionation reaction. Moreover, complexes $\mathbf{1}_x$ and $\mathbf{2}_x$ are very insoluble in acetone and they can be isolated as solids by centrifugation of the final suspension.

The corresponding arylcopper(III) iodide complexes $\mathbf{1}_\text{I}$ and $\mathbf{2}_\text{I}$ are synthesized from complexes $\mathbf{1}_\text{Cl}$ and $\mathbf{2}_\text{Cl}$ respectively by anion exchange, using 2 equivalents of AgClO_4 and then 2 equivalents of KI in acetonitrile at room temperature (Scheme III.1.2). Complexes $\mathbf{1}_\text{I}$ and $\mathbf{2}_\text{I}$ are isolated in high yields (84-95%) by crystallization from acetonitrile solutions after slow diffusion of diethyl ether.



Scheme III.1.2. Synthesis of arylcopper(III)-iodide complexes by anion exchange reactions.

III.1.2 Characterization of aryl- Cu^{III} -halide complexes

Well-defined aryl Cu^{III} -X (X = Cl, Br, I) complexes $\mathbf{1}_x$ and $\mathbf{2}_x$ have been characterized by means of NMR and UV-Vis spectroscopy, ESI-MS spectrometry, Cyclic Voltammetry and X-Ray diffraction analysis.

III.1.2.1 Solid state structures

Crystalline material suitable for single crystal X-Ray diffraction analysis was obtained for all complexes except for $\mathbf{2}_\text{Br}$ by means of slow diffusion of diethyl ether over solutions of the complexes in CH_3CN or DMF. The solid state structure of complexes $\mathbf{1}_\text{Cl}$, $\mathbf{1}_\text{Br}$, $\mathbf{1}_\text{I}$, $\mathbf{2}_\text{Cl}$ and $\mathbf{2}_\text{I}$ was determined by single crystal X-ray diffraction. A list of selected bond distances and angles are described in Table III.1.1, and Figure III.1.1 shows the ellipsoid diagrams for all five complexes. Crystal structures show each copper center in a pentacoordinated, square-pyramidal geometry, where the halide anion is coordinated to the axial position, whereas the aryl moiety and the three amine N atoms are found coplanar with the copper center. Taking into account Cu-C bond distances, along with the charge balance and the diamagnetic behaviour exhibited by all aryl Cu^{III} -halide complexes, the metal center is best described as copper(III) in all complexes.

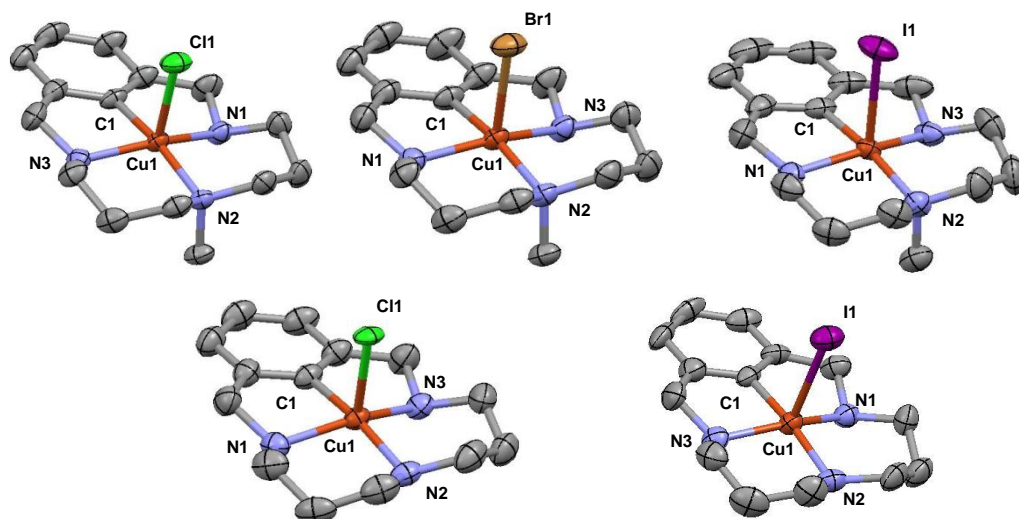


Figure III.1.1. Crystal structures of complexes **1_{Cl}**, **1_{Br}**, **1_I**, **2_{Cl}** and **2_I**. Ellipsoid representation at 50% probability of their molecular cation [LCu^{III}X]⁺ (hydrogen atoms have been omitted for clarity).

Table III.1.1. Selected bond lengths [Å] and angles [°] for complexes **1_{Cl}**, **1_{Br}**, **1_I**, **2_{Cl}** and **2_I**.

	1_{Cl}	1_{Br}	1_I	2_{Cl}	2_I
Cu-X (X= Cl, Br, I)	2.455 (16)	2.6999 (5)	2.9001 (4)	2.4675 (10)	2.8122 (13)
N1-Cu	1.972 (3)	1.974 (2)	1.972 (2)	1.986 (5)	1.997 (7)
N2-Cu	2.037 (3)	2.034 (2)	2.017 (2)	1.999 (3)	1.996 (6)
N3-Cu	1.971 (3)	1.974 (2)	1.968 (2)	1.974 (4)	1.988 (7)
C1-Cu	1.908 (3)	1.914 (3)	1.905 (3)	1.898 (3)	1.911 (7)
C1-Cu-N1	82.58 (11)	81.69 (12)	81.92 (12)	81.64 (17)	81.5 (3)
C1-Cu-N3	81.78 (12)	82.53 (12)	82.65 (15)	82.25 (16)	81.6 (3)
N1-Cu-N2	95.06 (9)	96.98 (10)	96.46 (10)	96.70 (15)	97.4 (3)
N2-Cu-N3	96.89 (9)	95.17 (9)	95.74 (10)	95.37 (15)	95.2 (3)
C1-Cu-N2	169.39 (10)	169.44 (11)	170.01 (11)	170.06 (15)	169.7 (3)
N1-Cu-N3	155.70 (11)	155.78 (10)	156.78 (11)	152.64 (17)	152.1 (2)

III.1.2.2 NMR characterization

The full set of all complexes 1_x and 2_x have been fully characterized by NMR spectroscopy. The structure observed in their crystal structures is apparently retained in solution (DMSO- D_6 or CD_3CN solvents). The Cu^{III} central coordination allows the formation of two 5-member and two 6-member rings that fix each proton in a different environment. That is reflected in the assignment of all proton atoms of the molecule by means of bidimensional NMR experiments such as COSY, NOESY, HSQC and HMBC. A remarkable issue of some of these complexes is that four-bond distance coupling between C_{ipso} and N- CH_3 group is clearly seen in the HMBC experiment. The latter observation is very rare and is a demonstration that in solution these molecules retain the same conformation as in the crystal structure, thus allowing this long distance carbon-proton coupling to be observed in the HMBC experiment.

III.1.2.3 UV-Visible spectroscopy

Electronic spectra for arylcopper(III)-halide complexes exhibit halide-to-metal charge transfer bands in the 360-640 nm range and the energies of these bands vary systematically with the identity of the halide (Figure III.1.2). Aryl Cu^{III} -Cl compounds (1_{Cl} , 2_{Cl}) show two bands centered at 369 and 521 nm, aryl Cu^{III} -Br compounds (1_{Br} , 2_{Br}) at 399 and 550 nm, and aryl Cu^{III} -I compounds (1_I , 2_I) at 422 and 635 nm (Table III.1.2). The red-shift observed in the bands upon changing from Cl^- to Br^- to I^- is in agreement with the respective ligand-field strength of the halide ligands ($Cl^- > Br^- > I^-$), indicating that the bands correspond to ligand-to-metal charge transfer (LMCT) electronic transitions. Furthermore, these bands are not observed in the previously reported $[L_1Cu^{III}](ClO_4)_2$ (1_{ClO_4}) and $[L_2Cu^{III}](ClO_4)_2$ (2_{ClO_4}) complexes, supporting again the electronic interaction of halide and copper orbitals.²

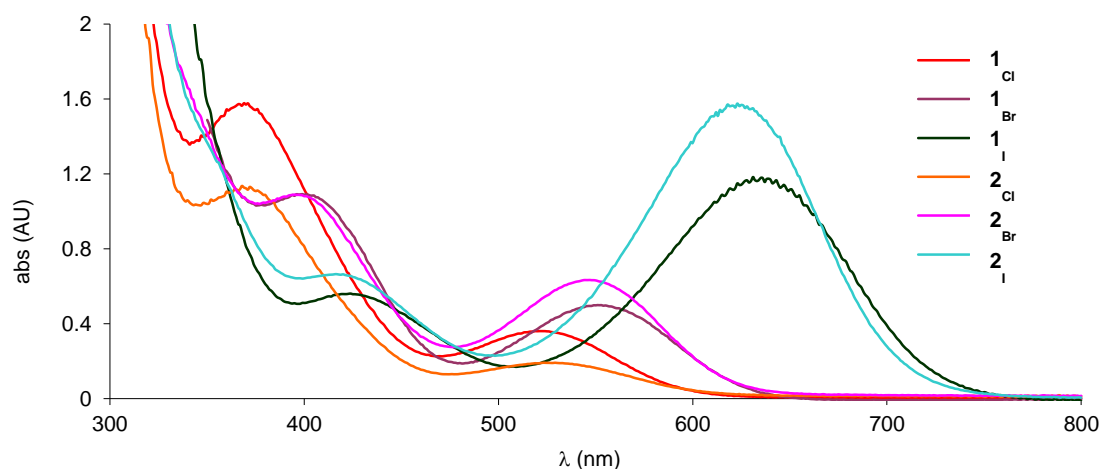


Figure III.1.2. UV-Vis spectra of aryl Cu^{III} -halide complexes 1_x and 2_x . Conditions: 0.8 mM in CH_3CN at 25 °C.

Table III.1.2. UV-Vis characterization of complexes **1_x** and **2_x**. Conditions: 0.8 mM in CH₃CN at 25 °C.

1_x	λ_1 (nm)	ϵ_1 (M ⁻¹ cm ⁻¹)	λ_2 (nm)	ϵ_2 (M ⁻¹ cm ⁻¹)	2_x	λ_1 (nm)	ϵ_1 (M ⁻¹ cm ⁻¹)	λ_2 (nm)	ϵ_2 (M ⁻¹ cm ⁻¹)
Cl	369	1409	524	238	Cl	369	1972	521	451
Br	399	1365	550	624	Br	395	1362	545	793
I	422	697	635	1473	I	417	831	621	1955

III.1.2.4 Electronic properties determined by Cyclic Voltammetry

Electronic properties of complexes **1_x** and **2_x** in CH₃CN were studied by Cyclic Voltammetry in order to evaluate the effect of halide coordination on their $E_{1/2}$ redox potentials compared to complexes **1_{ClO4}** and **2_{ClO4}**, in which the counteranion is non-coordinated.²

Cyclic Voltammetry measurements of arylCu^{III}-X complexes show chemically reversible $1e^-$ processes associated with the Cu^{III}/Cu^{II} redox couple (Figure III.1.3 and Table III.1.3). Xifra *et al.* described that the Cu^{III}/Cu^{II} redox couple depends on both the electronic nature of the central macrocyclic amine and the substituents in *para* position in the aromatic ring.² We can summarize that arylCu^{III}-X complexes bearing **L₂**, with a secondary amine *trans* to the aryl moiety, exhibit $E_{1/2}$ values 40–70 mV lower than the corresponding complexes bearing **L₁**, with a tertiary amine in the *trans* position to the aryl group. These results show that copper(III) oxidation state is more stabilized with secondary amines, due to their higher σ -donating capacity, in comparison to tertiary amines.^{4,5}

Furthermore, the Cu^{III}/Cu^{II} $E_{1/2}$ values of arylCu^{III}-X complexes follow the trend $E_{1/2}^{Cl} < E_{1/2}^{Br} < E_{1/2}^I$ indicating that redox potentials also depend on the nature of the halide coordinated to the axial position. Compared to **1_{ClO4}** and **2_{ClO4}**, the redox potentials for Cu^{III}/Cu^{II} of halide complexes **1_x** and **2_x** are substantially lower (up to 250 mV). These results indicate that halides in the apical position stabilize the Cu^{III} oxidation state, presumably because of their anionic nature, and this stabilization is enhanced upon change from I to Br and Cl because of the increasing donating capability of the halide.

Finally, in comparison to Cu^{III}/Cu^{II} redox potentials (measured in CH₃CN) of other copper(III) complexes described in the literature, arylCu^{III}-halide complexes **1_x** and **2_x** are among the most stabilized. Only three square planar copper(III) complexes bearing strong σ -donor amido groups in combination with thiolate or alkoxide groups showed a Cu^{III}/Cu^{II} redox potential lower than -0.8 V (vs. Fc/Fc⁺).⁶

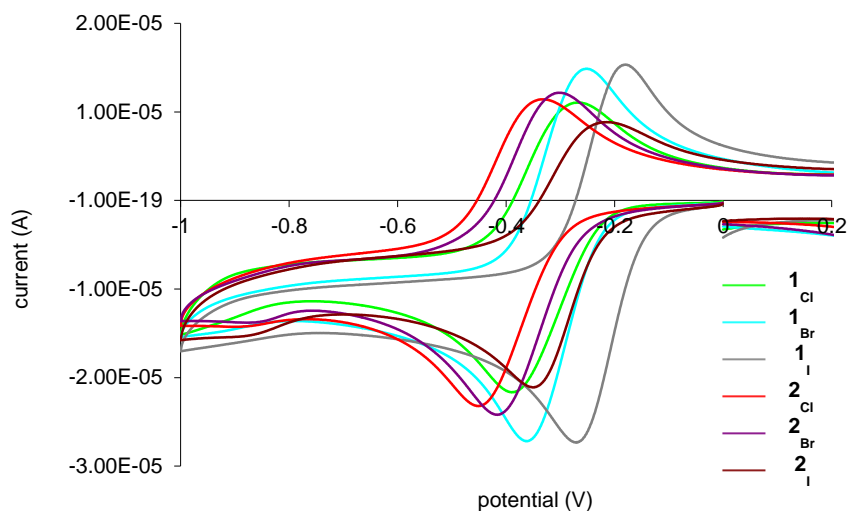


Figure III.1.3. Cyclic voltammetry of arylCu^{III}-halide complexes **1_x** and **2_x**. Conditions: 1 mM, scan rate = 0.2 V/s, [TBAP] = 0.1 M, CH₃CN, 15 °C, using SSCE as the reference electrode and Fc/Fc⁺ as internal reference.

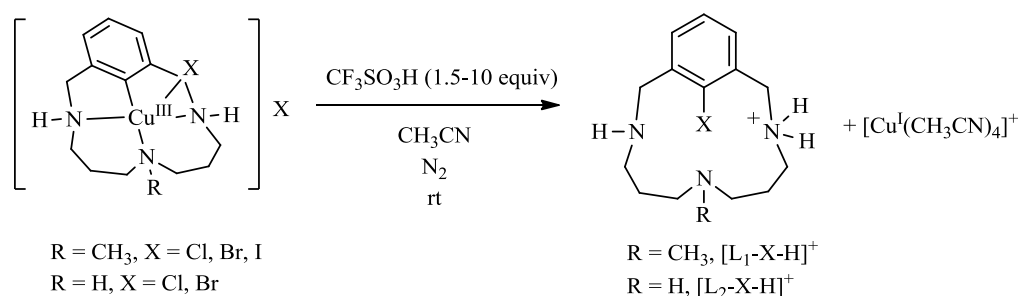
Table III.1.3. Electrochemical parameters (versus SSCE) of complexes **1_x** and **2_x**. Conditions: 1 mM, scan rate = 0.2 V/s, [TBAP] = 0.1 M, CH₃CN, 15 °C, using SSCE as the reference electrode and Fc/Fc⁺ as internal reference.

	$E_{1/2}$ (V) (vs. Fc/Fc ⁺)	E_{pc} (V)	E_{pa} (V)	ΔE (V)	I_{pa}/I_{pc}
1_{Cl}	-0.33 (-0.72)	-0.40	-0.26	0.14	0.7
1_{Br}	-0.31 (-0.69)	-0.37	-0.24	0.13	0.8
1_I	-0.23 (-0.62)	-0.28	-0.17	0.11	0.6
2_{Cl}	-0.40 (-0.79)	-0.46	-0.33	0.13	0.7
2_{Br}	-0.36 (-0.75)	-0.42	-0.30	0.12	0.7
2_I	-0.29 (-0.68)	-0.36	-0.21	0.15	0.9

III.1.3 Acid triggered C-halogen bond formation from well-defined arylCu^{III}-halide complexes

C_{aryl}-halogen reductive elimination from well-defined aryl-metal-halide species has been seldom observed, and examples are restricted to selected Pd^{II}, Pd^{IV} and Pt^{IV} complexes.^{7,8,9} The isolation and characterization of arylCu^{III}-halide complexes **1_x** and **2_x** prompted us to study their ability to undergo intramolecular C_{aryl}-halogen reductive elimination, which has no precedents in the literature.

ArylCu^{III}-halide complexes are very stable in solution and C-halogen reductive elimination is not observed upon heating. On the other hand, the reaction is triggered by the addition of different acid sources (CF₃SO₃H, HClO₄, H₂SO₄ and HNO₃). Reaction of arylCu^{III}-halide complexes **1_x** and **2_x** with 1.5-10 equivalents of triflic acid affords quantitative formation of protonated halogenated macrocyclic ligands [L₁-X-H]⁺ and [L₂-X-H]⁺ (X = Cl, Br) and [Cu^I(CH₃CN)₄]⁺ at room temperature (Scheme III.1.3). When iodides complexes are used, the reductive elimination becomes slower and that allows side reactions to compete, thus decreasing the aryl-iodide yields. In the case of complex **1_I**, 85% yield (calculated by ¹H-NMR) of coupling product [L₁-I-H]⁺ is obtained, but no halide coupling product is observed with complex **2_I**.



Scheme III.1.3. C-halogen reductive elimination from arylCu^{III} complexes in acidic media.

III.1.3.1 Kinetic analysis

Detailed kinetic data for C_{aryl}-halogen reductive elimination reactions was obtained by monitoring the reaction of complexes **1_{Cl}**, **1_{Br}** and **2_{Cl}** with triflic acid by UV-Vis spectroscopy. However, no kinetic experiments were done for complexes **2_{Br}** and **2_I** due to extremely slow reaction at room temperature. The kinetic profiles of the decay of the arylCu^{III}-X LMCT bands exhibited first-order behavior (Figure III.1.4). Rate constants of C-halogen reductive elimination measured for these complexes at 10 °C follows the trend **1_{Cl}** > **2_{Cl}** > **1_{Br}**. The faster rate of C-Cl reductive elimination from **1_{Cl}** relative to **2_{Cl}** is consistent with the higher reduction potential of **1_{Cl}** relative to **2_{Cl}**. However, **1_{Br}** exhibits the slowest reductive elimination rate of the three

complexes, despite having the highest reduction potential. In addition, complexes **1_I** and **2_I**, which have the highest reduction potential, showed qualitatively the slowest rates of C-I reductive elimination. All data together indicate that the C-X reductive elimination rates do not correlate with the reduction potentials of the arylCu^{III}-X complexes across the halide series.

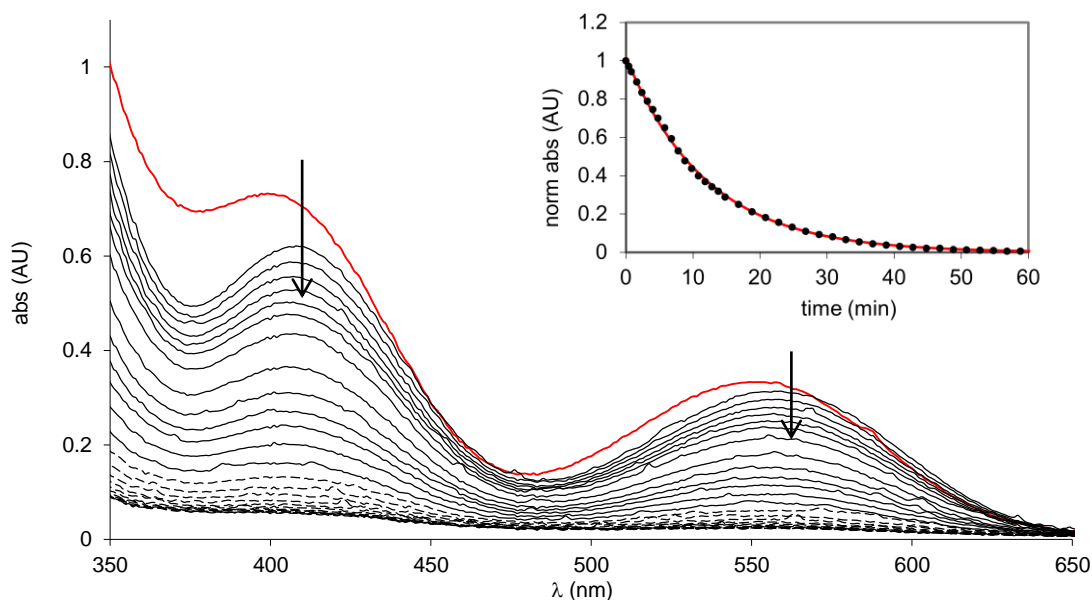


Figure III.1.4. UV-Vis spectrum of complex **1_{Br}** (0.5 mM) (top spectrum). Kinetic decay of complex adding 1.5 equiv of CF₃SO₃H at 15° C (inset shows the kinetic profile at 420 nm).

Furthermore, the activation parameters obtained from Eyring analyses (Table III.1.4) reveal that the reductive elimination reactions exhibit a relatively large enthalpy of activation (21.5–23.2 kcal/mol), consistent with significant Cu–X bond cleavage in the transition state. These observations suggest that the trends in the rates of C–X reductive elimination are controlled by the relative carbon-halogen bond strengths: C–Cl > C–Br > C–I. But the differences in the rate constants translate into small differences in terms of free activation energies between different halides, suggesting that other parameters need to be considered. A different trend has been observed for aryl carbon-halogen reductive elimination from Pd^{II} complexes, for which the relative rates $k_{\text{C-Br}} > k_{\text{C-I}} > k_{\text{C-Cl}}$ were measured.⁷

Table III.1.4. Activation parameters calculated monitoring the reaction by UV-Visible at different temperatures for complexes **1_{Cl}**, **1_{Br}**, **2_{Cl}** and k_{obs} at 15 °C.

	T range (K)	ΔH^\ddagger (kcal mol ⁻¹)	ΔS^\ddagger (cal mol ⁻¹ K ⁻¹)	k_{obs} (s ⁻¹) (T = 15 °C)
1_{Cl}	253-283	23.2 ± 0.5	18.1 ± 2.0	7.12 (± 0.06) × 10 ⁻²
1_{Br}	278-298	21.5 ± 0.7	3.3 ± 2.3	4.08 (± 0.05) × 10 ⁻⁴
2_{Cl}	278-298	22.8 ± 0.5	11.9 ± 1.9	5.05 (± 0.05) × 10 ⁻³

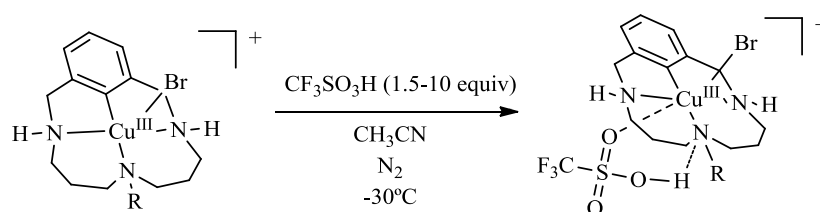
III.1.3.2 Characterization of intermediates in the reductive elimination reaction

Electrochemical data was obtained after addition of CF₃SO₃H in order to understand the role of the acid in the C-halogen bond forming reaction. When 4.5 equivalents of CF₃SO₃H were added to the complex solution, electronic absorption spectra of acidified solutions of complexes **1_{Cl}**, **1_{Br}** and **2_{Cl}** show a 5 nm, 9 nm and 8 nm red-shift in the UV-Visible bands, respectively, consistent with formation of intermediates. Cyclic Voltammetry experiments were performed under these acidified conditions, with complexes **1_{Cl}**, **1_{Br}**, **2_{Cl}** and **2_{Br}** in previously deoxygenated CH₃CN at -10 °C. In these conditions, cyclic voltammetry spectra significantly changed with regard to neutral conditions. The electrochemically and chemically quasireversible Cu^{III}/Cu^{II} waves of initial complexes changed to irreversible waves, so E_{1/2} of protonated species could not be measured. However, the comparison between reduction peaks of both species shows an anodic shift in acidic media, which means that the Cu^{III} oxidation state is less stable, and that there is an increase in the thermodynamic driving force towards metal ion reduction, that is most likely released *via* reductive elimination to give the C-halogen coupled product.

In order to obtain structural information about intermediates species after acid addition, we performed NMR experiments at low temperature. ¹H-NMR data of reactions of complexes **1_{Br}** and **2_{Cl}** in acidic media in CD₃CN at -30 °C are also consistent with the formation of intermediate species before the C-halogen bond forming step.

When 1.5 equivalents of CF₃SO₃H are added to a solution of complex **1_{Br}**, signals assigned to N-CH₃ and vicinal protons pointing towards the opposite face of the bromide side of the molecule are modified, whereas neither signals corresponding to proton atoms oriented towards the other face of the molecule nor aromatic signals are affected (Figure III.1.5, a and b). We may conclude that the overall compound scaffold with two 5-member and two 6-member rings mediated by Cu^{III} central coordination is retained. Moreover, these shifts suggest that CF₃SO₃H approaches the molecule opposite to the bromide side and the protonation affects to

the central amine which contains the methyl group (Scheme III.1.4). The strong *trans* effect of the aryl ligand, as visualized in the larger Cu-N2 bond distances of all compounds, is also in agreement with a preferential protonation to the central amine. Thus, a weakening of the Cu^{III}-NCH₃ bond might explain an overall higher electron density on the NCH₃ moiety as observed in an upper-field shift in the ¹H-NMR. We postulate that weakening of the Cu-N2 bond, in combination with the changes that occur in the red-ox potentials upon protonation are enough to disrupt the stability of the complex and to onset the intramolecular aryl-X coupling by reductive elimination.



Scheme III.1.4. Proposed interaction of triflic acid with complex **1_{Br}** determined by low temperature NMR experiments.

The same NMR study in complex **2_{Cl}** shows that, despite the retained structure in acidic media, all proton signals of the molecule are shifted in contrast to complex **1_{Br}**, but this shifts are larger in amine and aliphatic chain protons (Figure III.1.5, a and c). A possible interpretation is that due to the lack of *trans* effect in the Cu-N2 bond, the protonation of the central amine is not so specific and it may occur at the lateral amine. Therefore, the NMR spectra results from an average shifts of different triflic acid/arylCu^{III}-Br adducts in solution.

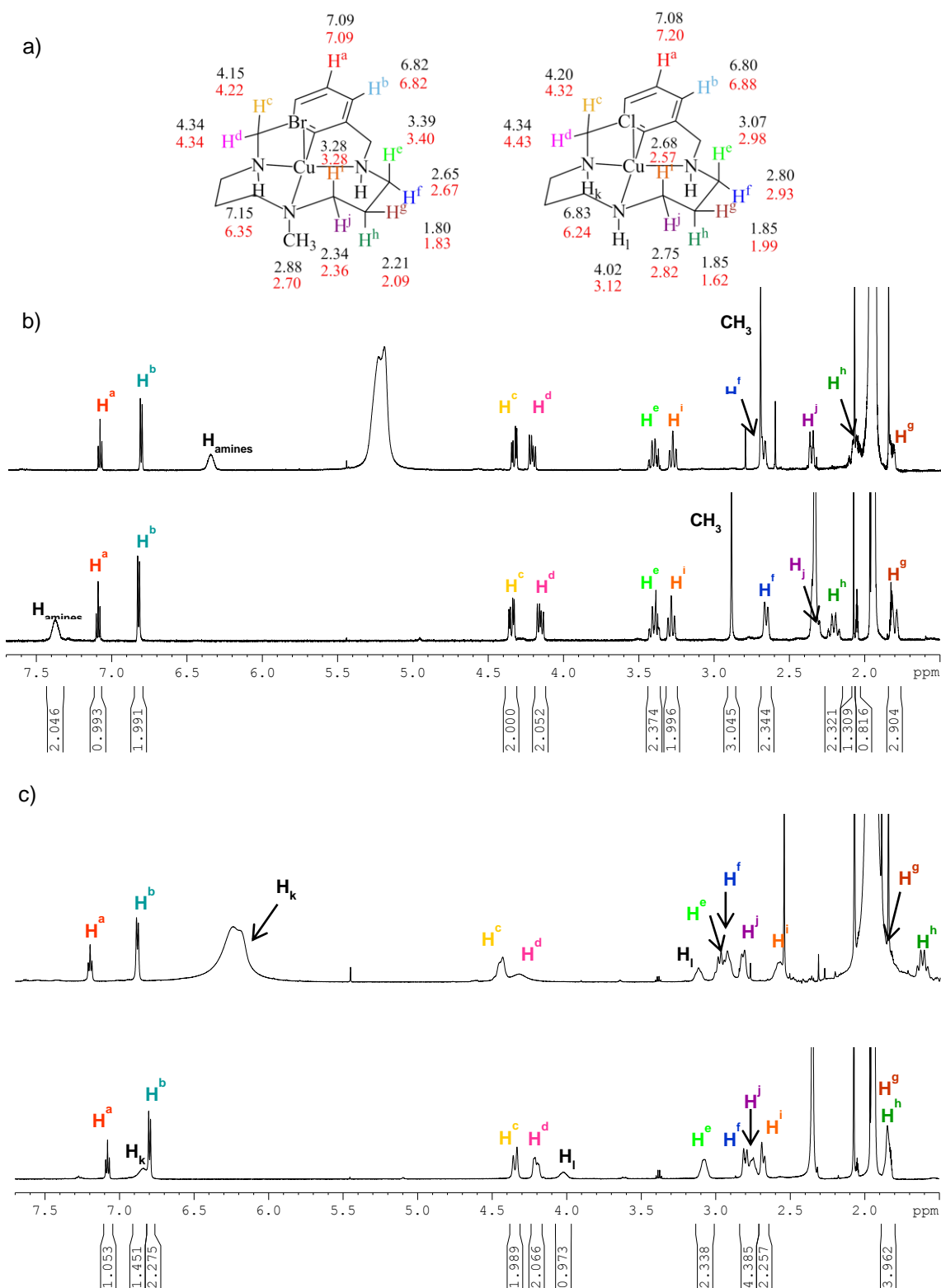


Figure III.1.5. a) Characterization of complexes **1_{Br}** and **2_{Cl}** by 1D and 2D NMR studies at -30 °C in CD₃CN before (black numbers) and after addition of 1.5 equivalents of CF₃SO₃H (red numbers). b) ¹H-NMR spectra of **1_{Br}** at -30 °C in CD₃CN (lower spectrum) and in acidic media (upper spectrum). c) ¹H-NMR spectra of **2_{Cl}** at -30 °C in CD₃CN (lower spectrum) and in acidic media (upper spectrum).

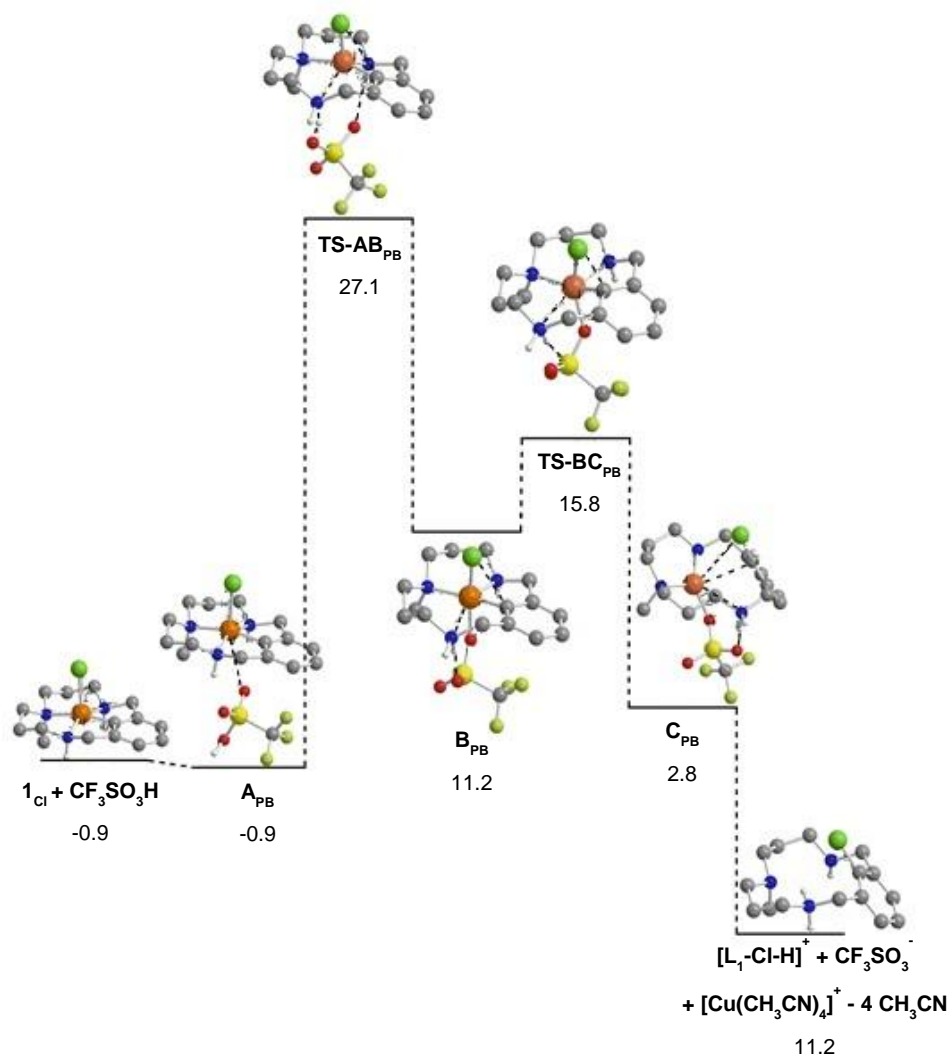
III.1.3.3 Computational studies on C-Cl reductive elimination triggered by triflic acid

In collaboration with Dr. Albert Poater and Prof. Miquel Solà from Institut de Química Computacional at Universitat de Girona, we studied computationally the mechanism of acid-triggered C_{aryl}-Cl reductive elimination in arylcopper(III)-chloride complex **1_{Cl}**.^{10,17}

First of all, we evaluated the formation of an adduct between triflic acid molecule and **1_{Cl}**, based on our first hypothesis from the experimental data obtained (see section III.1.3.2). It was found that this intermediate is stabilized with regard to the reactants by 0.9 kcal/mol. Secondly we studied the mechanistic pathway taking into account that protonation step may occur either at central tertiary amine or at lateral secondary amine. The examination of both pathways showed that protonation step of the amine is rate determining and both mechanisms only differ by 2.2 kcal/mol. Besides, a proper axial coordination of the triflate anion to the copper(III) complex is found to be a key factor for affording a lower energetic barrier once the amine protonation is achieved. Then, reductive elimination from protonated copper(III) complex has a very low energy barrier and downhill release of [Cu^I(CH₃CN)₄]⁺ and protonated [L₁-Cl-H]⁺ accounts for the experimentally observed product formation.

On the other hand, we have studied the mechanistic pathway considering an acetonitrile molecule in the coordination sphere of arylcopper(III)-chloride complex. The coordination of an axial acetonitrile molecule blocked the entrance of the triflic acid at the opposite face of the chloride atom; consequently, the protonation of the Cu^{III} complex occurred at the secondary amine by lateral approach. However, the addition of an acetonitrile molecule does not influence the stabilization of the transition state.

After evaluating all computational data we proposed that the most plausible mechanism for C-Cl reductive elimination in complex **1_{Cl}** corresponds to protonation at the secondary amine with previous formation of an adduct between triflic acid molecule and the copper(III) complex (Scheme III.1.5). The protonation of the secondary amine enlarges the corresponding Cu^{III}-NH distance, shortening the Cu-Cl bond and widening the NH-Cu-Cl angle to 129°. This complex reorganization places the chloride and the aryl moiety in the proper *cis* position for undergoing reductive elimination, which has a very small energetic barrier. However the energetic barrier of 28 kcal/mol of the calculated mechanism is higher in energy than the experimental value of 23.2 ± 0.5 kcal/mol. Altogether, experimental and theoretical data suggest that distinct competitive pathways may be operative at the same time, all of them having the protonation step as rate-limiting.



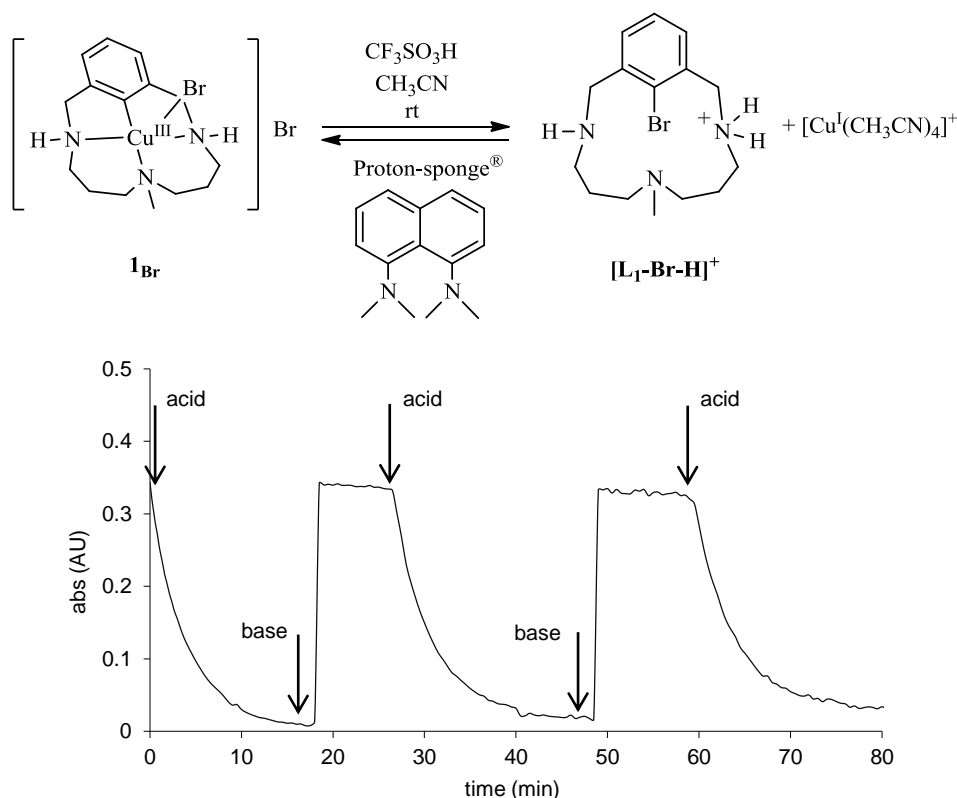
Scheme III.1.5. DFT mechanism calculated for the acid-triggered C_{aryl} -Chloride reductive elimination from complex 1_{Cl} (energy values in kcal/mol).

III.1.4 Reversible oxidative addition of aryl halides to copper(I)

Oxidative addition of haloarenes to low-oxidation state metal ions is a commonly observed reaction, and mechanistic studies have been performed with a large number of complexes, generally limited to bromo- and iodoarene substrates.¹¹ However, aryl-halide oxidative addition to copper(I) to form an $\text{arylCu}^{\text{III}}$ -halide complex has been proposed in many mechanistic studies of Ullmann Condensation Reactions, despite there are no precedents in the literature for the direct observation of this reaction.

The study of the reaction of copper(I) with ligands $\text{L}_1\text{-X}$ has led to the first experimental observation of the oxidative addition of an C_{aryl} -halogen bond to copper. Ligand $\text{L}_1\text{-X}$ ($\text{X} = \text{Cl}, \text{Br}, \text{I}$) reacts with $[\text{Cu}^{\text{I}}(\text{CH}_3\text{CN})_4](\text{PF}_6)$ in acetonitrile to form quantitatively $\text{arylCu}^{\text{III}}\text{-X}$ complex at room temperature. The reaction is exceedingly fast at $-40\text{ }^\circ\text{C}$ and neither kinetics data nor activation parameters could be obtained with conventional spectroscopic monitoring.

Remarkably, intramolecular C-halogen bond formation by reductive elimination is a reversible, pH dependent reaction. Indeed, once reductive elimination of arylCu^{III}-Br upon addition of acid is finished, and full formation of protonated coupling products **[L-Br-H]⁺** and Cu^I salts is achieved, the addition of Proton-sponge[®] as a non-coordinating strong base to deprotonate the amine causes the instantaneous reversal oxidative addition reaction, and repeated cycles are possible without significant decomposition of **1_{Br}** (Scheme III.1.6). Triflic acid destabilizes the arylCu^{III}-X species and also stabilizes the Cu^I/aryl-X state since the amine protonation precludes the Cu^I coordination in close proximity to the inner-macrocyclic aromatic C-halogen bond.



Scheme III.1.6. Reversible reductive elimination/oxidative addition under pH control (starting concentration of **1_{Br}** is 0.5 mM, addition of 1.5 equivalents of CF₃SO₃H and 2 equivalents of Proton-sponge[®] and CF₃SO₃H in the subsequent additions –see arrows-; CH₃CN, 24 °C).

III.1.5 Catalytic intramolecular C–N reductive elimination reaction

After having demonstrated the **L₁-X** oxidative addition to copper(I), and taking into account the previous study by Huffman and Stahl in C–N bond forming reaction in arylCu^{III} complex **1_{C104}** (see section I.3.4),¹² we further explored catalytic C–N bond forming reactions with nitrogen nucleophiles in ligand **L₁-X**.

Reaction of **L₁-Br** with 2-hydroxypyridine (pyridone) as nitrogen nucleophile in the presence of catalytic amounts of copper(I) (3.3 mol %), in acetonitrile solution and at room temperature, yielded quantitative formation of the C-N coupling product **L₁-Nu-HBr**, as determined by ¹H-NMR (Figure III.1.6, a). Interestingly, by means of ¹H NMR and UV-Vis spectroscopy arylCu^{III}-bromide complex **1_{Br}** was detected as intermediate in the C-N bond forming reaction (Figure III.1.6, b and Figure III.1.7). Integration of the NMR signals associated with **1_{Br}** indicates that the arylCu^{III} complex accounts for essentially all of the copper present in solution during the first 60-70 min of the reaction. The observation of a steady-state concentration of arylCu^{III}-halide complex in catalytic reaction, until the consumption of initial substrate **L₁-Br** implies that the arylcopper(III)-bromide **1_{Br}** complex is involved in the rate-determining step. Therefore, we propose a mechanism consisting in a fast oxidative addition of the aromatic C-halogen bond to Cu^I, to form the arylCu^{III}-halide complex, followed by ligand exchange in the presence of excess of nitrogen nucleophile and final C-N reductive elimination step to afford the coupled product.

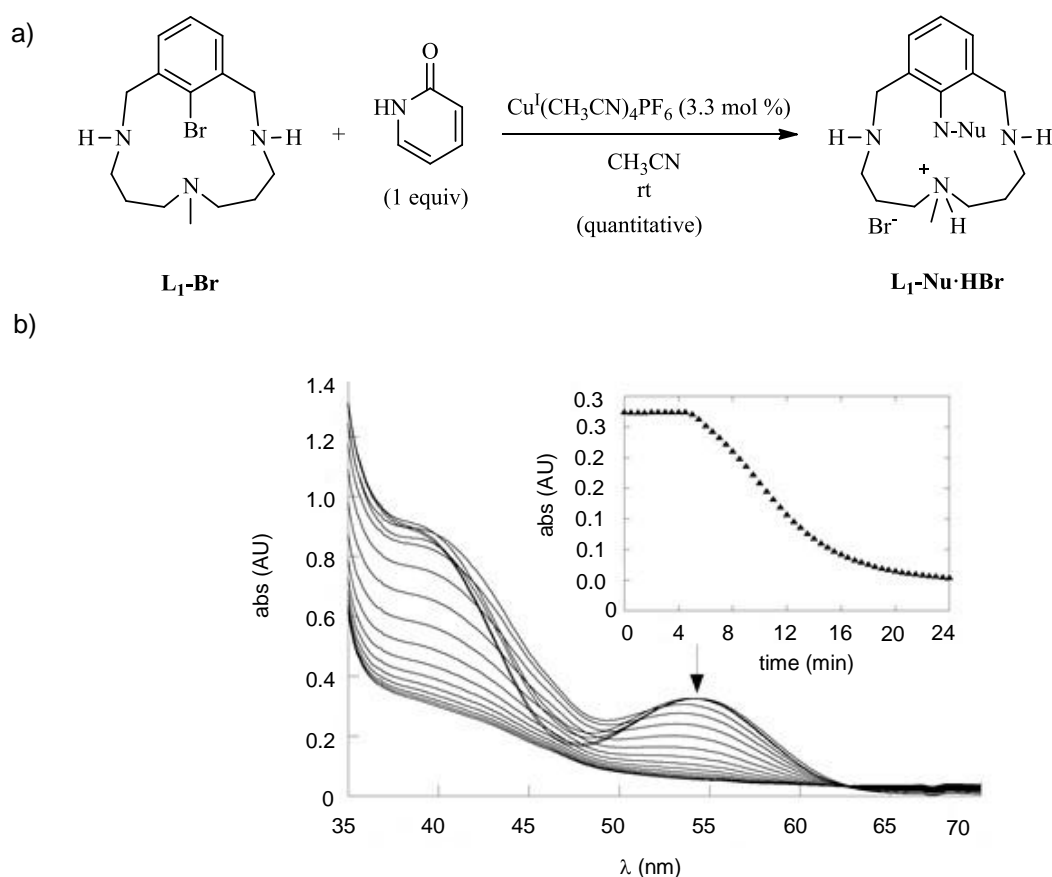


Figure III.1.6. a) Copper-catalyzed C–N bond forming reaction for the conversion of **L₁-Br** and pyridone into **L₁-Nu-HBr** at 25 °C. b) UV-Vis spectroscopy analysis and the time-dependent progression of the absorbance at 542 nm (inset). Conditions: [**L₁-Br**] = 9 mM, [pyridone] = 10 mM, [Cu^I(CH₃CN)₄PF₆] = 0.3 mM, CD₃CN, 15 °C.

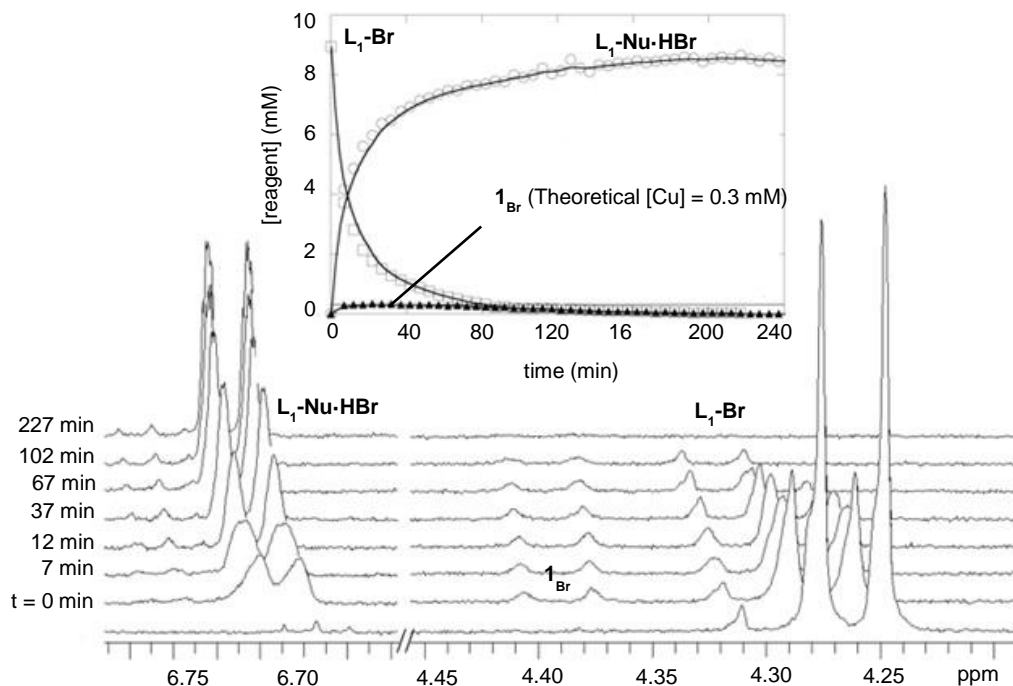


Figure III.1.7. ^1H NMR spectroscopic analysis of the C-N bond forming reaction of model substrate $\text{L}_1\text{-Br}$ with pyridine in the presence of catalytic amounts of copper; for clarity only selected regions of the NMR spectrum are shown. Conditions: $[\text{L}_1\text{-Br}] = 9 \text{ mM}$, $[\text{pyridone}] = 10 \text{ mM}$, $[\text{Cu}^{\text{I}}(\text{CH}_3\text{CN})_4\text{PF}_6] = 0.3 \text{ mM}$, CD_3CN , $15 \text{ }^\circ\text{C}$.

This is the first experimental evidence consistent with the involvement of an $\text{arylCu}^{\text{III}}$ intermediate in a catalytic C-N cross-coupling reaction. In macrocyclic model substrate $\text{L}_1\text{-X}$ the activation barrier for oxidative addition is very low probably because of the directed orientation of the C-halogen bond to the Cu^{I} ion upon binding inside the macrocyclic ligand and the high stabilization of copper(III) owing to the donor properties of the secondary amine groups. This scenario is different to most of Ullmann Condensation mechanisms, where the activation of the C-halogen bond by copper is the rate-determining step and, thus, no intermediates have been observed. Moreover, in copper(I) complexes having bidentate nitrogen ligands the coordination of the nucleophile proceeds prior to the activation of the aryl halide (see section I.3.2). However, the mechanism of Ullmann Condensation Reactions may vary depending on the identity of the substrates, auxiliary ligands and/or the reaction conditions. For example, reactions involving nucleophiles that coordinate less readily to copper, or catalysts bearing tri- or tetradentate ligands, may disfavor pre-coordination of the nucleophile to copper(I), and activation of the aryl halide may occur before nucleophile coordination.

In conclusion, by using macrocyclic ligands we have demonstrated the feasibility of copper to participate in catalytic C-N bond forming reaction at room temperature, through oxidative addition/reductive elimination $\text{Cu}^{\text{I}}/\text{Cu}^{\text{III}}$ redox processes that may have an involvement in more synthetically useful C-heteroatom bond forming reactions.

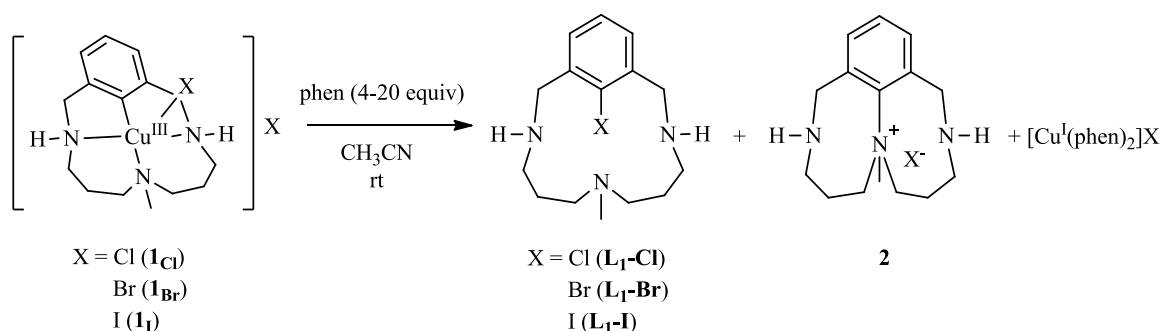
III.2 Nucleophilic aryl fluorination and aryl halide exchange mediated by a Cu^I/Cu^{III} catalytic cycle

This section mainly corresponds to the contents of paper by Casitas *et al.* *J. Am. Chem. Soc.* **2011**, *133*, 19386–19392, which is found in chapter V of this thesis.

III.2.1 C-Halogen Reductive Elimination Triggered by External Ligands

Experimental data discussed in the previous section shows that copper in oxidation state +3 is highly stabilized when bound to macrocyclic ligand **L₁-X**, and that reaction of the ligand with Cu^I proceeds via a very favorable oxidative addition step. In addition, we speculated about the existence of a reactant-displaced equilibrium between arylCu^{III}-X complexes and corresponding aryl-X...Cu^I species in solution. Therefore, we reasoned that the presence of external ligands with high affinity towards copper(I), i.e. 1,10-phenanthroline (phen), could displace the Cu^{III}/Cu^I equilibrium towards reductive elimination products.

Reaction of arylCu^{III}-X complexes **1_x** with several equivalents of phen in acetonitrile at 25 °C (Scheme III.2.1 and Table III.2.1) afforded quantitative formation of **L₁-X** ligands (X = Cl, Br, I) and [Cu^I(phen)₂]⁺. Reactions were faster for Cl > Br > I, indicating that the aryl-X bond strength governed the carbon-halogen bond forming reaction triggered by entrapping Cu^I through binding with 1,10-phenanthroline. Reaction with complex **1_I** was slower and minor amounts of intramolecular aryl-amine reductive elimination product **2** were also obtained as a side-product,^{12,13} which was minimized by increasing the number of equivalents of phen in the reaction.



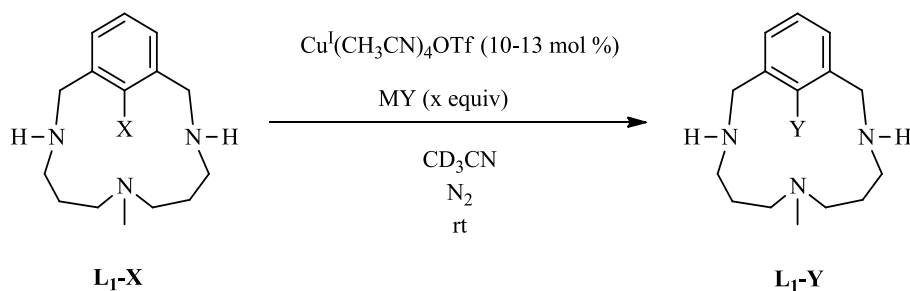
Scheme III.2.1. C-halogen reductive elimination promoted by the addition of 1,10-phenanthroline to **1_x** complexes at room temperature.

Table III.2.1. Stoichiometric C-X bond formation from 1_x triggered by 1,10-phenanthroline as a chelating ligand for Cu^I . ^a $^1\text{H-NMR}$ yield using 1,3,5-trimethoxybenzene as internal standard in CD_3CN . ^b Intramolecular C-N reductive elimination product **2** yield in parenthesis.

	equiv phen	% yield of $\text{L}_1\text{-X}^a$
1_{Cl}	4	98
	6	99
1_{Br}	6	77
	15	96
	20	97
1_{I}	6	86 (10) ^b
	15	88 (12) ^b
	20	95 (5) ^b

III.2.2 Halide Exchange in Aryl-X Model Substrates (X = Cl, Br, I)

The demonstration of the existence of a reductive elimination/oxidative addition $\text{Cu}^{\text{III}}/\text{Cu}^I$ equilibrium in $\text{arylCu}^{\text{III}}\text{-X}$ complexes opened the door to explore copper-catalyzed halide exchange reactions in our model aryl halide system. We reasoned that halide exchange reaction in ligand $\text{L}_1\text{-X}$ could be possible in the presence of catalytic amounts of copper(I) and excess of the halide salt MY (Scheme III.2.2). The proposed mechanism consisted in an initial oxidative addition to form $\text{arylCu}^{\text{III}}\text{-X}$ complex, followed by subsequent halide exchange and C-halogen reductive elimination for finally obtaining the aryl halide exchanged product $\text{L}_1\text{-Y}$.



Scheme III.2.2. Ligand exchange reactions catalyzed by copper(I) in aryl halide model substrates $\text{L}_1\text{-X}$.

First of all, we studied the exchange starting with the aryl iodide ligand, which was converted to the corresponding aryl chloride and aryl bromide ligands. In these reactions, a stronger C-halogen bond is formed and, therefore, the exchange reaction is thermodynamically favored (Table III.2.2). Aryl iodide (**L₁-I**) exchange to afford aryl chloride (**L₁-Cl**) and aryl bromide (**L₁-Br**) in acetonitrile at 25 °C is achieved in the presence of a catalytic amount of [Cu^I(CH₃CN)₄]OTf and excess of Bu₄NCl and Bu₄NBr as halide sources, respectively (Table III.2.3), entry 1 and 2). A control experiment indicates that the halide exchange reaction is catalyzed by copper(I) as in its absence no halide exchanged product is obtained under reaction conditions. In similar conditions the halide exchange of aryl bromide ligand **L₁-Br** towards **L₁-Cl** is also obtained quantitatively at room temperature (Table III.2.3, entry 4).

The exchange reaction of **L₁-I** to **L₁-Cl** was monitored by ¹H-NMR spectroscopy at 25 °C in CD₃CN. In first place, the addition of Cu^I to a solution containing both **L₁-I** and excess of Bu₄NCl affords complex arylCu^{III}-chloride **1_{Cl}**. Gradual formation of product **L₁-Cl** was accompanied by the disappearance of initial ligand **L₁-I** as monitored by ¹H-NMR, whereas **1_{Cl}** complex concentration is maintained in small steady-state amounts until full consumption of **L₁-I** (Figure III.2.1). These observations agree with the proposal involving arylCu^{III}-Y intermediate as resting state, and the C_{aryl}-Y reductive elimination as the rate-limiting step. Indeed, the exchange of I to Br using Bu₄NBr salt afforded the **L₁-Br** product in 87% yield. A 13 mol% content of **1_{Br}** complex as resting state remained in the final crude mixture (determined by ¹H-NMR) and accounted for the mass balance of the macrocyclic ligand.

Table III.2.2. Bond dissociation energies of aryl halides.¹⁴

Bond	Dissociation energy (kJ mol ⁻¹)
Ph-F	533
Ph-Cl	407
Ph-Br	346
Ph-I	280

Then, we studied the reversible halide exchange reactions towards heavier halides, or in other words, towards the formation of a weaker C-halogen bond. First of all, we explored the conversion of aryl bromide and aryl chloride towards the more reactive aryl iodide ligand. Conversion from **L₁-Br** to **L₁-I** was achieved in good yields by using 12 mol% of Cu^I salt and an excess of soluble NaI in CH₃CN at room temperature. The reaction is accompanied by the precipitation of the halide exchanged salt NaBr from the crude. In this case, yields reach a top

limit of 84% because the final reaction mixture contains a 12% mol content of the corresponding arylCu^{III}-I complex **1_I** (Table III.2.3, entry 3). Nevertheless, halide exchange is clean since only **L₁-I** product and a small quantity of remaining starting material (**L₁-Br**, <5%) are detected by ¹H NMR in the final reaction mixture after reaction optimization.

Table III.2.3. Summary of halide exchange reactions yields catalyzed by copper(I) at 25 °C in ligand **L₁-X** (X = Cl, Br, I). ^a ¹H-NMR yield using 1,3,5-trimethoxybenzene as internal standard in CD₃CN. Yield of intramolecular C-N product **2** is indicated in parenthesis. Conditions: [**L₁-Br**] = 7.5-9 mM, [Cu(CH₃CH)₄OTf] = 0.9-1 mM. ^b Reaction using acetone-d₆ as solvent at 40 °C.

entry	L₁-X	halide salt (equiv)	time (h)	% yield L₁-Y^a
1	L₁-I	Bu ₄ NCl (5)	1.5	96
2		Bu ₄ NBr (10)	40	87
3	L₁-Br	NaI (20)	36	84
4		Bu ₄ NCl (10)	2	99
5	L₁-Cl	NaI (10)	24	56 (17)
6		NaI (10)	24 ^b	57 (2)
7		NaBr (10)	24	37

Copper-catalyzed halide exchange from **L₁-Cl** to **L₁-I** using excess of soluble NaI in acetonitrile is extremely slow at room temperature and after 96 h only 36% yield of the desired product is obtained. When the reaction is carried out at 40 °C the yield of **L₁-I** product is increased up to 56% (Table III.2.3, entry 5). However, at this temperature a competing intramolecular side-reaction involving aryl-amine coupling occurs, affording also a 17% yield of product **2**. The change of CD₃CN solvent by acetone-d₆ affords **L₁-I** in similar yield (57%) but the contribution of the side reaction is reduced, and **2** is obtained in only a 2% yield (Table III.2.3, entry 6). Finally, the low conversion of **L₁-Cl** to **L₁-Br** using excess of NaBr may be attributed to the low solubility of the initial halide salt in acetonitrile (Table III.2.3, entry 7).

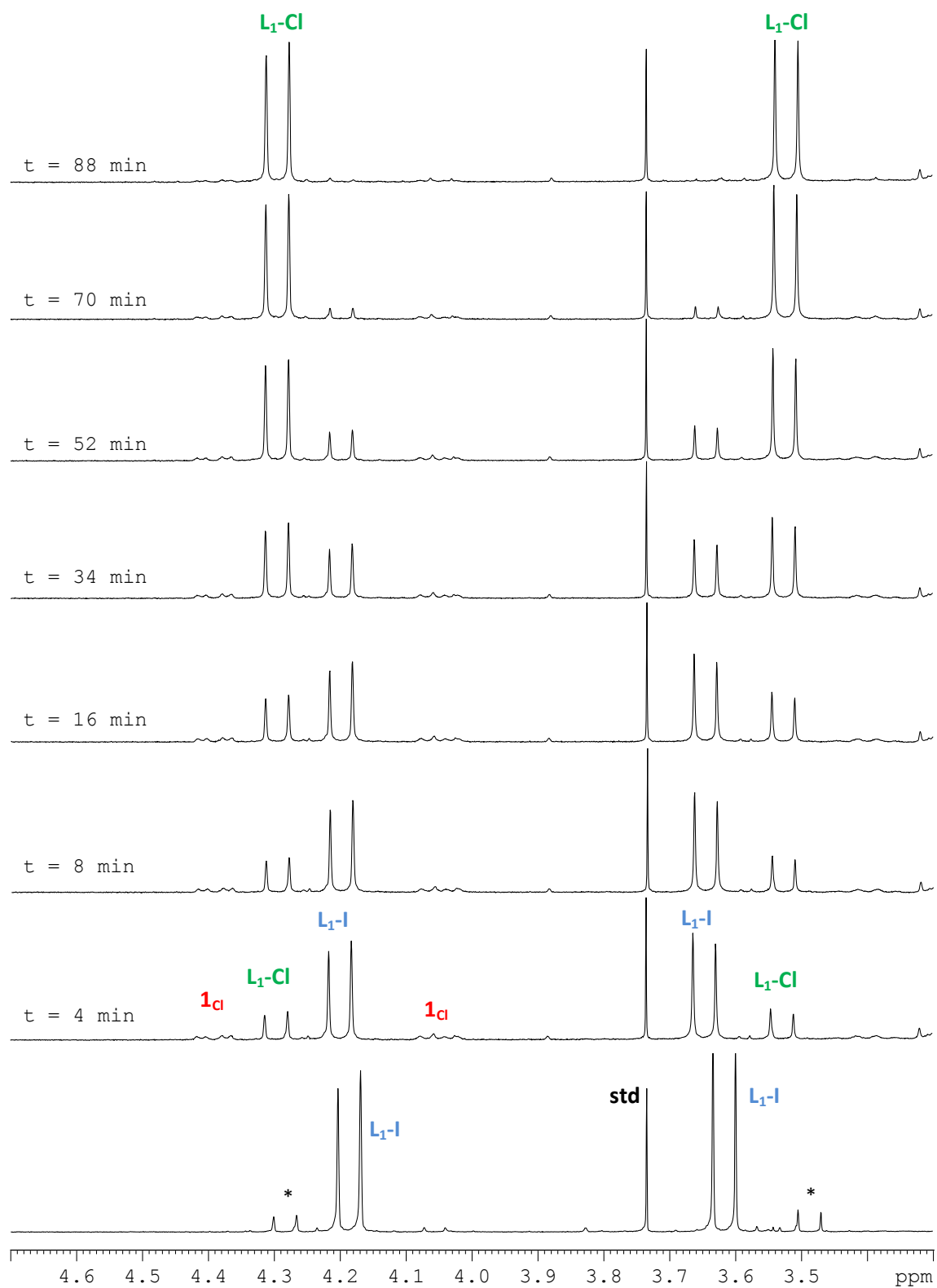
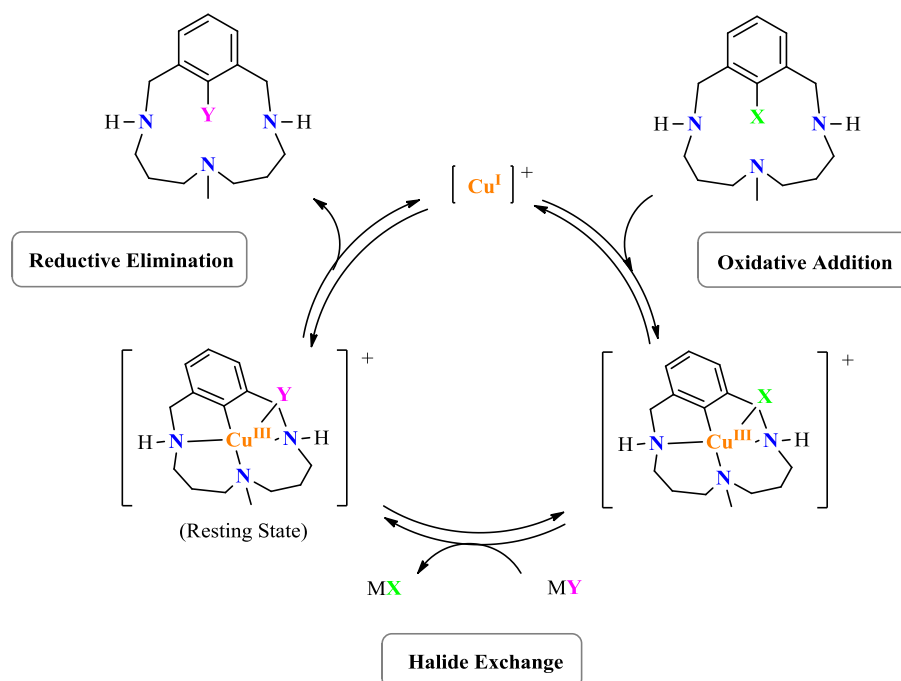


Figure III.2.1. $^1\text{H-NMR}$ spectra acquired during the catalytic timecourse of the exchange from $\text{L}_1\text{-I}$ to $\text{L}_1\text{-Cl}$ (selected NMR range shown for clarity purposes). Conditions: $[\text{L}_1\text{-I}] = 9$ mM, $[\text{Cu}(\text{CH}_3\text{CN})_4\text{OTf}] = 1$ mM, $[\text{Bu}_4\text{NCl}] = 90$ mM (10 equiv). Peaks with * indicates 5 % of $\text{L}_1\text{-Br}$ present in initial ligand $\text{L}_1\text{-I}$.

The proposed mechanism for copper catalytic halide exchange reactions in our model aryl halide ligands is depicted in Scheme III.2.3. The rate determining step is the C-halogen reductive elimination. Catalytic halide exchange for a given model aryl halide can be performed by exchanging both towards heavier and also lighter halides. Copper-catalyzed halide exchange reactions are favored towards the product with the strongest C-halogen bond (C-Cl > C-Br > C-I) when both halide salts (MX and MY) are soluble in the reaction mixture. In this case, transformation from L_1-I and L_1-Br towards lighter aryl halides is obtained rapidly and in high yields. On the other hand, the precipitation of the sodium salts out of the CH_3CN solution is key to understand the catalytic cycle turnover towards heavier halide products and overcome the reversibility of the aryl halide oxidative addition step. Therefore, no halide exchange reaction is observed in the exchange of aryl chloride towards aryl bromide or aryl iodide by using Bu_4NBr or Bu_4NI respectively.

The existence of a thermodynamic equilibrium between two aromatic halides, for instance aryl bromide and aryl iodide, finds precedent in the literature. Buchwald and coworkers, showed that the copper-catalyzed halide exchange reaction in aryl halides is an equilibrium reaction whose position is influenced by the solubility difference among the different halide salts.¹⁵ Later on, Taillefer and coworkers demonstrated that starting either with an equimolar mixture of bromobenzene and potassium iodide, or an equimolar mixture of iodobenzene and potassium bromide, the final mixture in DMF, using $Cu^I/1,10$ -phenanthroline as catalyst, was composed of about 20 % of bromobenzene and 80% of iodobenzene.¹⁶ The precipitation of KBr is key role and it is reminiscent to the reactivity found in our model systems L_1-X .



Scheme III.2.3. Mechanism of copper(I)-catalyzed halide exchange reactions through aryl $Cu^{III}-X$ complexes as intermediates (X = I, Br, Cl).

III.2.2.1 DFT calculations on C-Cl reductive elimination reaction

In collaboration with Mercè Canta from Departament de Química and Prof. Miquel Solà from Institut de Química Computacional at Universitat de Girona, we studied computationally the C-Cl reductive elimination step from arylCu^{III}-Cl complex **1_{Cl}**. Figure III.2.2 shows the energetic profile obtained by DFT calculations.¹⁷ C-Cl reductive elimination from complex **1_{Cl}** has a high activation barrier of 26.9 kcal/mol. Moreover, reductive elimination products **L₁-Cl** and copper(I) are 24.7 kcal/mol higher in energy than arylCu(III)-chloride complex **1_{Cl}** supporting the downhill reversal oxidative addition reaction towards arylCu^{III}-Cl complex as observed experimentally (see section III.2.1).

This result rationalizes the experimental observation of **1_{Cl}** stability in solution, and it is in agreement with the theoretical results for triflic acid triggered reductive elimination. The computed barrier for the C-Cl bond forming pathway triggered by triflic acid from complex **1_{Cl}** is 28 kcal/mol (see section III.1.3.3). The rate-determining step corresponds to protonation of one of the amines of the ligand, which causes the enlargement of a Cu-N bond. In this case, C-Cl reductive elimination from a tetracoordinated arylCu^{III} complex is only 4.6 kcal/mol, which is much lower in comparison to the 26.9 kcal/mol needed for C-Cl reductive elimination from a more strained pentacoordinated **1_{Cl}** complex. This suggests that the presence of an acid molecule leads to the formation of an unstable arylCu^{III} intermediate from which reductive elimination is very favorable. Moreover, protonated ligand **[L₁-X-H]⁺** and **[Cu^I(CH₃CN)_{4]⁺}** products are more stable than initial arylCu^{III}-Cl complex **1_{Cl}**.

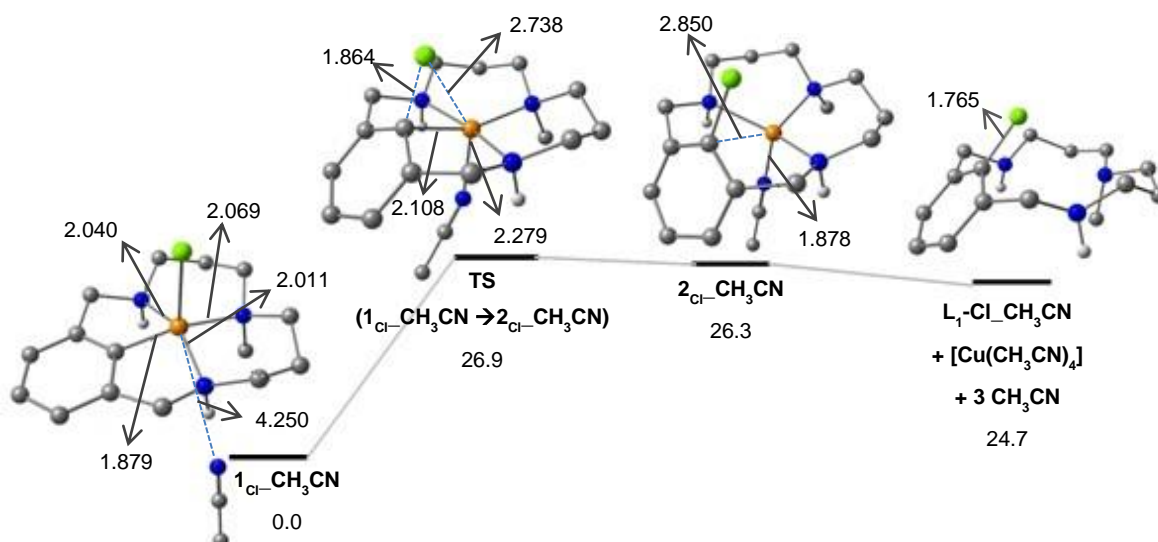
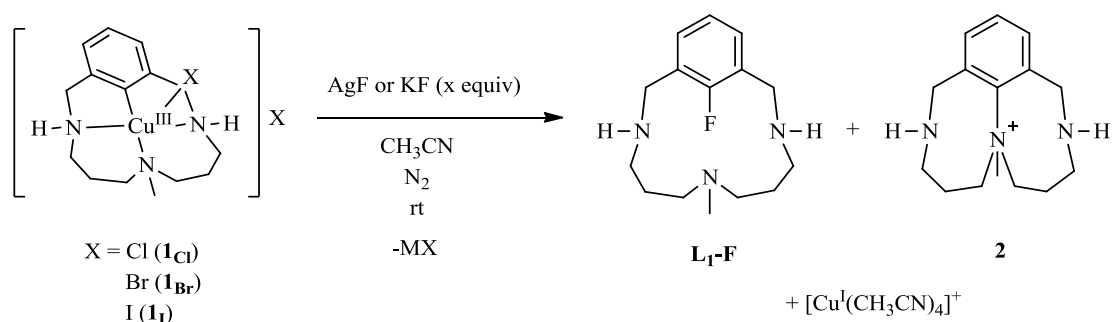


Figure III.2.2. DFT reaction pathway for the C-Cl reductive elimination from complex **1_{Cl}** (energy values in kcal/mol).

III.2.3 Stoichiometric C-F bond forming reactions

Due to the lack of organometallic copper(III) fluoride complexes in the literature, we were interested in the synthesis of arylCu^{III}-fluoride complexes for studying their ability to undergo carbon-fluorine reductive elimination. The applied strategy for synthesizing arylCu^{III}-fluoride complexes consisted in ligand exchange reaction from arylCu^{III}-halide complexes **1_x** (X = Cl, Br, I) by using nucleophilic fluoride sources, such as AgF and KF. However, the reaction of complexes **1_x** with several equivalents of KF or AgF in acetonitrile does not lead to the formation of arylCu^{III}-fluoride complexes; on the contrary, we obtained the formation of aryl fluorides **L₁-F** as the major product (C-F bond detected by ¹⁹F-NMR at -122.5 ppm in DMSO-d₆), together with intramolecular C-N reductive elimination product **2** (Scheme III.2.4).



Scheme III.2.4. Room temperature nucleophilic fluorination of **1_x** with MF salts (M= Ag, K) to afford **L₁-F** and Cu^I (compound **2** is also obtained in minor quantities).

Reaction of complexes **1_x** with 5 equivalents of AgF in acetonitrile at room temperature afforded aryl fluoride **L₁-F** ligand in moderate yields (74-84 %) (Table III.2.4, entries 1, 5 and 7). In the reaction of complex **1_{Cl}**, the addition of 8 the equivalents of AgF improved the yield of **L₁-F** to 91 % (Table III.2.4, entry 2). We observed that the optimization of AgF equivalents added is key to obtain **L₁-F** in good yields; for example, in the reaction of complex **1_{Cl}**, the use of 12 equivalents of AgF causes a decrease to 77% yield (Table III.2.4, entry 3).

Otherwise, we showed that aryl fluoride ligand **L₁-F** can be also obtained using KF as nucleophilic fluoride source. However, the reaction of complexes **1_{Cl}** and **1_{Br}** with 5 equiv of KF afforded the desired product only in low yields, together with intramolecular C-N reductive elimination product **2** and ligand **L₁-H** as side-products (Table III.2.4, entry 4 and 6). In this case, protonolysis of arylCu^{III} complex to afford **L₁-F** side-product may be due to the presence of traces of water in the reaction mixture.

Table III.2.4. Stoichiometric C-F bond formation through arylCu^{III}-X complexes with several equivalents of MF (M = Ag, K) at 25 °C in CH₃CN under N₂. ^a NMR yields using 1,3,5-trimethoxybenzene as an internal standard in dms_o-d₆ after extractions of copper with NH₄OH/MgSO₄. ^b Reactions with KF also afforded a 33% (entry 4) and 27% (entry 6) yield of **L₁-H** product.

Entry	complex	MF (equiv)	solvent	time (h)	% yield L₁-F ^a	% yield 2
1	1_{Cl}	AgF (5)	CH ₃ CN	8	74	23
2		AgF (8)	CH ₃ CN	8	91	8
3		AgF (12)	CH ₃ CN	8	77	22
4		KF (5) ^b	CH ₃ CN:dms _o -d ₆ (8:1)	24	31	36
5	1_{Br}	AgF (5)	CH ₃ CN	4	84	14
6		KF (5) ^b	CH ₃ CN:dms _o -d ₆ (8:1)	100	23	47
7	1_I	AgF (5)	CH ₃ CN	3	76	22

¹H-NMR monitoring of the reaction of arylCu^{III}-Br complex **1_{Br}** with 2 equivalents of silver fluoride in acetonitrile at 35 °C, showed that proton signals corresponding to complex **1_{Br}** decrease over time while signals attributed to aryl fluoride **L₁-F** increase without the detection of any arylCu^{III}-fluoride intermediate (Figure III.2.3). Therefore, ligand exchange reaction is proposed to be the rate limiting step. Several equivalents of silver fluoride are needed in order to displace the halide coordinated to the Cu^{III}, which may be facilitated by the precipitation of the formed AgCl or AgBr from the crude.

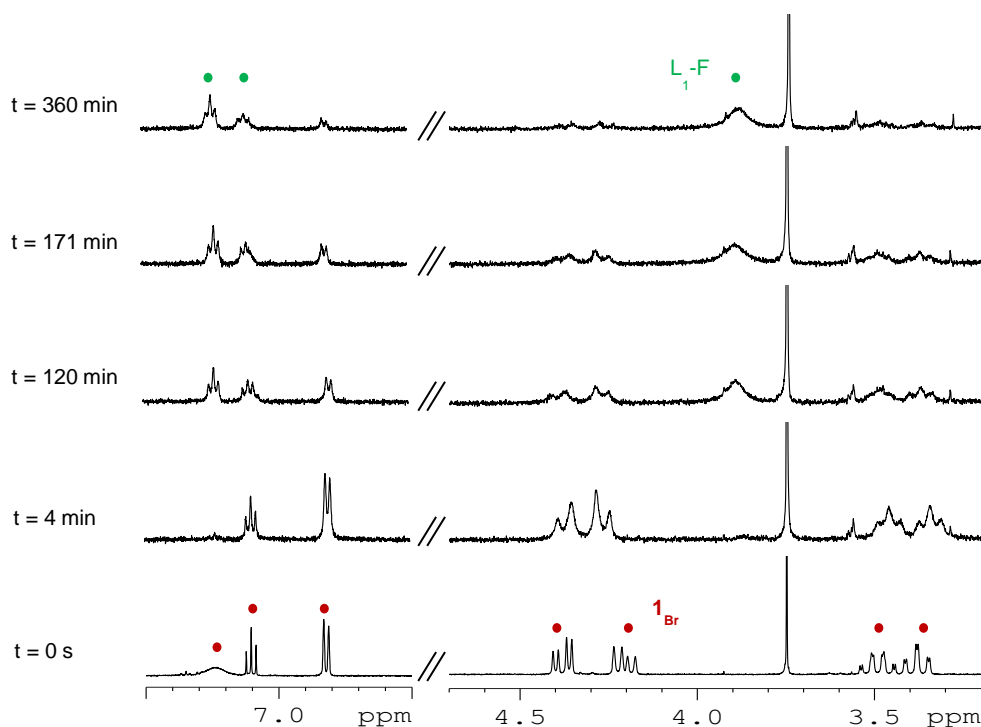


Figure III.2.3. $^1\text{H-NMR}$ monitoring of the reaction of $\mathbf{1}_{\text{Br}}$ (red dots) with 2 equiv of AgF to afford $\text{L}_1\text{-F}$ (green dots). Conditions: $[\mathbf{1}_{\text{Br}}] = 2.34 \text{ mM}$, CD_3CN at $35 \text{ }^\circ\text{C}$. For clarity only selected regions of the NMR spectrum are shown.

III.2.3.1 DFT calculations on C-F reductive elimination reaction

In collaboration with Mercè Canta from Departament de Química and Prof. Miquel Solà from Institut de Química Computacional at Universitat de Girona, we performed DFT calculations with the aim to support theoretically the feasibility of C-F reductive elimination reaction from a putative $\text{arylCu}^{\text{III}}$ -fluoride complex.¹⁷

The computed molecular structure of pentacoordinated cationic $\text{arylCu}^{\text{III}}$ -fluoride complex $\mathbf{1}_{\text{F}}$ resembles those of the previously crystallographically characterized $\text{arylCu}^{\text{III}}$ -halide complexes. In a square pyramidal geometry the copper center is bound to the fluoride anion situated in the axial position (Figure III.2.4). Besides, we have considered an acetonitrile molecule that is weakly coordinated to the copper center in the empty axial coordination site. The reductive elimination reaction to form the aryl fluoride $\text{L}_1\text{-F}$ product and Cu^{I} salt has an energetic barrier of only 16 kcal/mol. Reaction products are computed to be 4.1 kcal/mol below the initial complex $\text{arylCu}^{\text{III}}$ -fluoride complex. This result is in agreement with a fast and irreversible C-F reductive elimination step in acetonitrile solvent.

This energetic profile is different to the reaction pathway calculated for C-Cl reductive elimination from $\text{arylCu}^{\text{III}}$ -chloride complex $\mathbf{1}_{\text{Cl}}$ (see section III.2.2.1). C-Cl reductive elimination has an activation barrier 11 kcal/mol higher in energy than in C-F reductive elimination. Moreover, C-Cl reductive elimination products are higher in energy than $\text{arylCu}^{\text{III}}$ -

chloride complex, in contrast to C-F reductive elimination products, which are more stable than initial arylCu^{III}-fluoride complex, due to the formation of very strong C-halogen bond. Both theoretical reaction pathways support the experimental data obtained in arylCu^{III}-halide complexes.

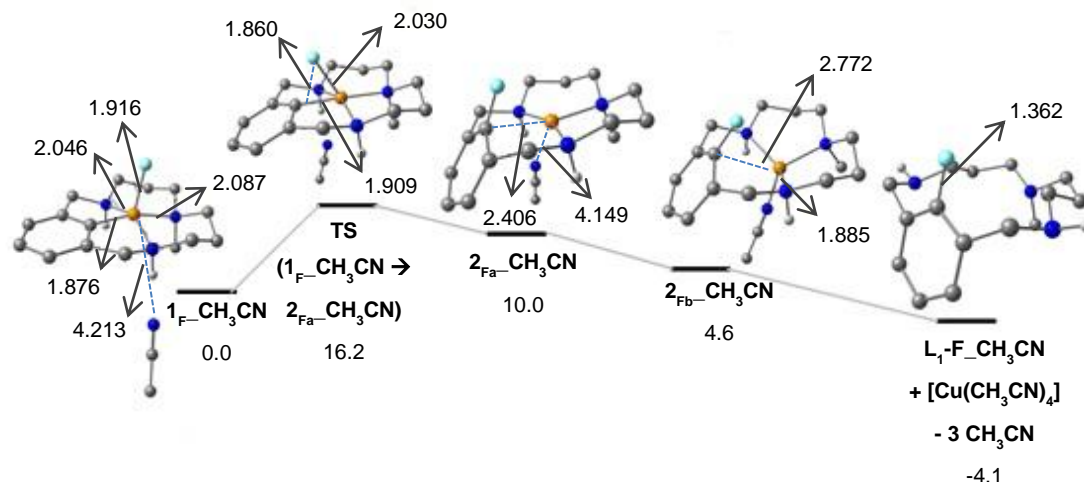
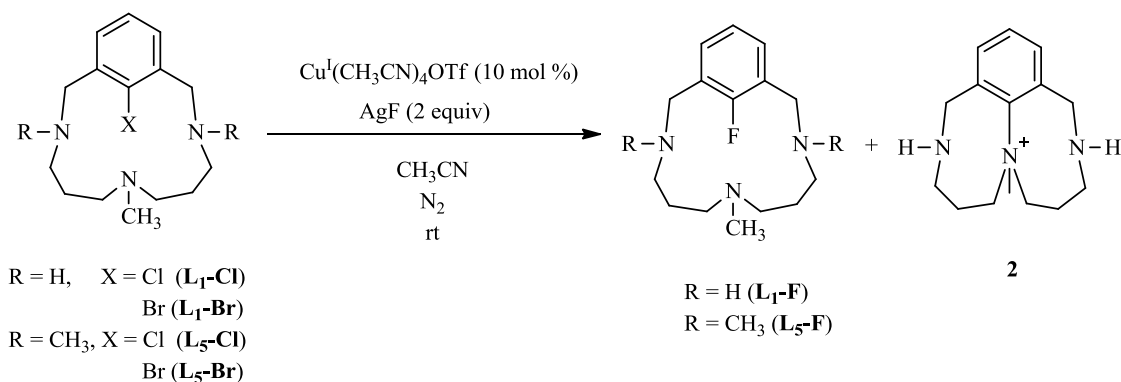


Figure III.2.4. Reaction pathway calculated by DFT methods for carbon-fluorine reductive elimination from putative arylCu^{III}-fluoride complex (energy values in kcal/mol).

III.2.4 Catalytic C-F bond forming reactions

After demonstrating that carbon-fluorine reductive elimination occurs in well-defined arylcopper(III)-halide complexes **1_x**, we wanted to study fluorination exchange reactions catalyzed by Cu^I in macrocyclic ligands **L₁-X** (X = Cl, Br) using silver fluoride (Scheme III.2.5). Direct addition of 2 equiv of AgF to a solution of ligand **L₁-Cl** and 10 mol % of [Cu(CH₃CN)₄]OTf afforded only 40 % of the aryl fluoride ligand **L₁-F**. On the other hand, the dropwise addition of a solution of AgF in acetonitrile improved the yield to approximately 71-76% of aryl fluoride **L₁-F** and 20% of the intramolecular C-N reductive elimination side-product **2** (Table III.2.5, entry 1 and 2). We tested other fluorides sources, for instance, Bu₄NF, Me₄NF or CsF, but they were completely inefficient.



Scheme III.2.5. Catalytic fluorination of aryl-X (X = Cl, Br) substrates at room temperature.

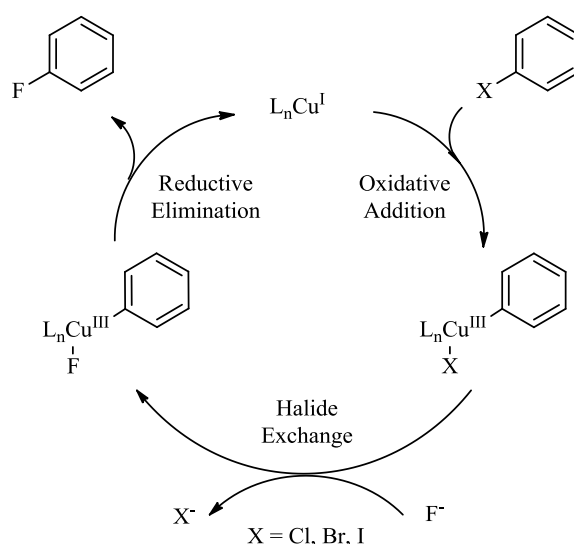
Table III.2.5. Catalytic Reactions Cu^I-catalyzed C-F bond formation through the reaction of L₁-X and L₅-X (X = Cl, Br) substrates with 2 equivalents of AgF at 298 K (CH₃CN as solvent, under N₂ and excluding light). ^a ¹H-NMR yields using 1,3,5-trimethoxybenzene as internal standard in dms_o-d₆ after extractions of copper with NH₄OH/MgSO₄. ^b Reactions also afforded 4% (entry 1) and 8% (entry 2) yield of another non-identified product. ^c CH₃CN:acetone (1:3) as solvent.

Entry	L-X	[Cu(CH ₃ CN) ₄ OTf] (mM)	time (h)	% yield L-F ^a	% yield 2
1	L ₁ -Cl	10	6	76 ^b	20
2	L ₁ -Br	10	4	71 ^b	21
3	L ₅ -Cl	10	12	98 ^c	-
4		5	24	98 ^c	-
5	L ₅ -Br	10	24	97 ^c	-

We hypothesized that arylcopper(III)-halide intermediates may decompose under reaction conditions due to the high basicity of fluoride anions.^{18,19,20} Secondary amines of the macrocyclic ligand may be keen to deprotonation triggering the formation of side-products such as the intramolecular C-N coupling product **2** (see section III.4). For this reason, we studied the catalytic fluoride insertion in the structurally related macrocyclic ligands L₅-X (X = Cl, Br) as substrates, bearing three tertiary amines (Scheme III.2.5). However, copper-catalyzed C-F bond forming reactions at L₅-X substrates failed when reactions were performed in acetonitrile. Ligand L₅-X contains tertiary amines that have lower σ donor capacity than secondary amines, overenhancing the stability of Cu^I complex.^{2,5} Therefore, L₅-X oxidative addition is precluded in CH₃CN. Otherwise, when fluorination reaction was carried out in less coordinating solvent as

the mixture acetone:acetonitrile (3:1), quantitative formation of the desired aryl fluoride product **L₅-F** was achieved (Table III.2.5, entry 3 and 5). Moreover, the loading of Cu^I catalyst can be lowered to the half, albeit longer reaction times are required (Table III.2.5, entry 4).

The proposed mechanism for fluoride exchange reactions in macrocyclic ligands **L₁-X** and **L₅-X** can be also accommodated by invoking the mechanistic proposal involving a Cu^I/Cu^{III} catalytic cycle. Aryl-X oxidative addition at Cu^I to form arylCu^{III}-X species, subsequent X⁻ to F⁻ exchange to form a putative arylCu^{III}-fluoride complex and final C-F reductive elimination affords aryl fluorides products (Scheme III.2.6). However, in contrast to the halide-exchange catalysis (Scheme III.2.3), the rate determining step is the halide exchange step since only arylCu^{III}-X (X = Cl, Br) complexes can be detected spectroscopically during the reaction, but no evidence of arylCu^{III}-F was observed. This is supported by the very low energy found by DFT calculations for the C_{aryl}-F reductive elimination step (Figure III.2.4).

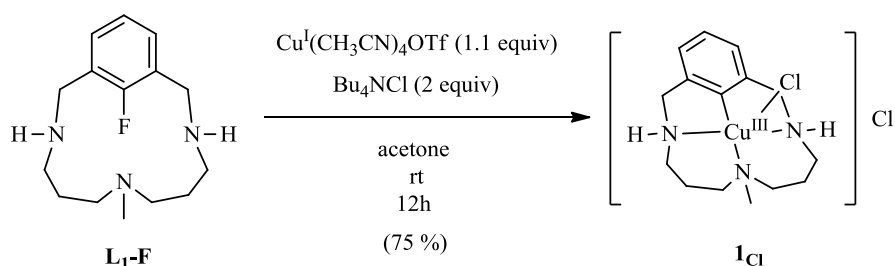


Scheme III.2.6. Catalytic cycle proposed for halogen to fluorine exchange in aryl halide substrates mediated by a Cu^I/Cu^{III} system.

III.2.5 Defluorination of Aryl Fluoride to Afford Aryl Chloride

Due to the difficulty of preparing aryl fluoride compounds, several research groups have focused in the development of strategies to activate carbon-fluorine bonds by the intermediacy of transition metals.^{21,22} The interest relies on polyfluorinated compounds since the selective activation of one of the C-F bonds can lead to derivatization of aromatic fluoroarenes. Catalytic C-F activation reactions are based mainly in hydrodefluorination and cross-coupling of fluoroarenes. In this field, mainly nickel and palladium catalyzed C-C bond forming reactions from polyfluorinated aryl compounds have been described.²²

In this context, we studied the viability of activating the C-F bond in our model system, even though, all previous results suggested that the C-F bond forming reaction is very favored for macrocyclic ligand **L₁-F**. Reaction of ligand **L₁-F** and equimolar amounts of copper(I) triflate in acetonitrile at room temperature does not undergo oxidative addition reaction. However, the combination of **L₁-F** with 1.1 equivalents of copper(I) triflate, with the subsequent addition of 2 equivalents of Bu₄NCl in acetone yielded 75 % of complex **1_{Cl}** (Scheme III.2.7). Complete halogen exchange reaction product **L₁Cl** is obtained by adding 1,10-phenanthroline in the reaction mixture. We reasoned that acetone may lower the energy barrier corresponding to the reversible aryl-F oxidative addition step to afford arylCu^{III}-F which is rapidly converted to arylCu^{III}-Cl complex in the presence of chloride anions. Moreover, the low solubility of **1_{Cl}** in acetone displaces all equilibria towards its formation. Therefore, we have developed both nucleophilic fluorination and defluorination reaction depending on the experimental conditions, and evidences have been presented to support a Cu^I/Cu^{III} pathway.



Scheme III.2.7. Defluorination of **L₁-F** mediated by Cu^I at room temperature to afford **1_{Cl}**.

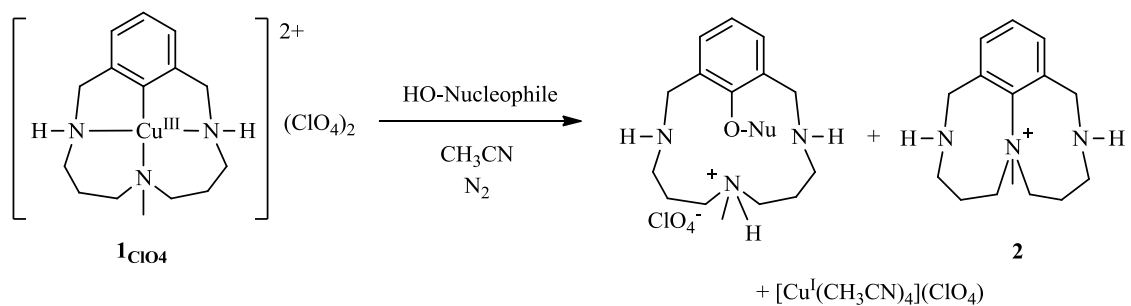
III.3 Observation and mechanistic study of facile C–O bond formation between a well-defined arylcopper(III) complex and oxygen nucleophiles

This section corresponds mainly to the contents of the paper by Huffman, Casitas *et al.* *Chem. Eur. J.* **2011**, *17*, 10643-10650, which is found in chapter VI of this thesis. This work was done in collaboration with the group of Prof. Stahl at the University of Wisconsin-Madison.

As disclosed in the introductory chapter (see section I.3.3.4), the intermediacy of arylCu^{III}-Nucleophile species have been widely invoked in Ullmann Condensation reactions. In this section, the reactivity of the isolated arylCu^{III} species with HO-nucleophiles is discussed and compared with the previous data with NH-nucleophiles (see section I.3.4). A general mechanism for both oxygen and nitrogen nucleophiles will be proposed.

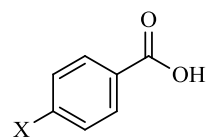
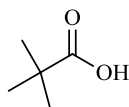
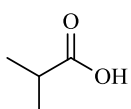
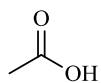
III.3.1 Stoichiometric Carbon-Oxygen bond forming reactions

Complex **1**_{ClO₄} was tested in stoichiometric reactions with several OH-nucleophiles, i.e. carboxylic acids, phenols and aliphatic alcohols (Scheme III.3.1). The reaction of several aliphatic and aromatic carboxylic acids with arylcopper(III) complex **1**_{ClO₄} affords quantitatively the corresponding aryl esters in acetonitrile at 25 °C in less than 10 minutes (Table III.3.1, entry 1 and 2). The reaction of **1**_{ClO₄} with different *para*-substituted phenols also yielded quantitative formation of the corresponding biaryl ethers in acetonitrile but at higher temperature (50 °C) indicating that phenols are less reactive than carboxylic acids (Table III.3.1, entry 3). Whereas acidic aliphatic alcohols such as 2,2,2-trifluoroethanol and 2,2,2-tribromoethanol react in good yield (Table III.3.1, entry 4 and 5), other aliphatic alcohols with a higher pK_A, such as cyclohexanol or *tert*-butanol failed to react (Table III.3.1, entry 6 and 7). In the latter cases, initial complex **1**_{ClO₄} was partially recovered from the crude, and the rest of the complex was isolated as the intramolecular C-N coupling product **2**.

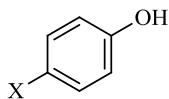


HO-Nucleophiles

carboxylic acids
(T = 25°C)

X = H, CH₃, OCH₃, CF₃, NO₂

phenols
(T = 50°C)

X = H, CH₃, OCH₃, CF₃, NO₂

Alcohols
(T = 50°C)

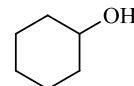
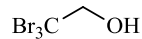
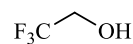
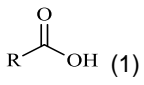
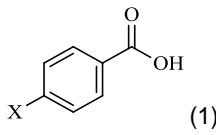
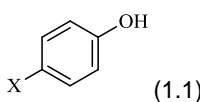
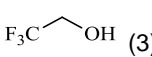
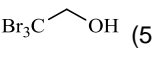
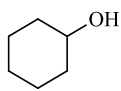
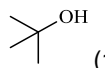
Scheme III.3.1. Reaction of aryCu^{III} complex **1**_{ClO₄} with oxygen nucleophiles.

Table III.3.1. C-O bond forming reaction of complex 1_{ClO_4} with oxygen nucleophiles. ^a $^1\text{H-NMR}$ yield using 1,3,5-trimethoxybenzene as internal standard in CD_3CN . Intramolecular C-N coupling product **2** in parenthesis. ^b $[1_{\text{ClO}_4}] = 2.2 \text{ mM}$, at $24 \text{ }^\circ\text{C}$. ^c $[1_{\text{ClO}_4}] = 12 \text{ mM}$, $50 \text{ }^\circ\text{C}$.

Entry	HO-Nucleophile (equiv)	pK _A	% yield ^a
1	 (1) R = CH ₃ , isopropyl, <i>t</i> -butyl	12.6-12.9	100 ^b
2	 (1) X = H, CH ₃ , OCH ₃ , CF ₃ , NO ₂	9.1-11.4	100 ^b
3	 (1.1) X = H, CH ₃ , OCH ₃ , CF ₃ , NO ₂	10.8-19.1	100 ^c
4	 (3)	23.5	75 ^c
5	 (5)	-	85 ^c
6	 (5)	-	0 (47) ^c
7	 (10)	32.2	0 (52) ^c

III.3.2 Kinetic analysis of C-O bond forming reaction

In this section we analyse the kinetic data obtained by NMR and UV-Vis experiments in the reaction of arylcopper(III) complex 1_{ClO_4} with carboxylic acids and phenols. NMR data was obtained by monitoring the decay of signals corresponding to 1_{ClO_4} and the formation of the corresponding C-O coupling product using an internal standard. Kinetic studies by UV-Vis spectroscopy were based on monitoring the decay of the characteristic band of 1_{ClO_4} at 450 nm after the addition of the corresponding HO-nucleophile.

III.3.2.1 Carboxylic acids

First of all, we studied the effect of the pK_A of carboxylic acids on the rate of the reaction. The positive slope found in the Brønsted plot (Figure III.3.1) indicates that less acidic carboxylic acids react more rapidly, which is the opposite trend observed with amide and sulfonamide substrates (see section I.3.4).¹² Then, we observed different kinetic behavior depending on the concentration of substrate. At low carboxylic acid concentration (5-10 equiv) the reaction exhibits exponential time courses and zero order dependence on carboxylic acid concentration (Figure III.3.2). In contrast, at relative high carboxylic acid concentration (10-15 equiv) there are non-exponential time courses and inhibition in the reaction rates. The inhibitory effect at high carboxylic acid concentration was attributed to the formation of acid carboxylic/carboxylate dimers.²³

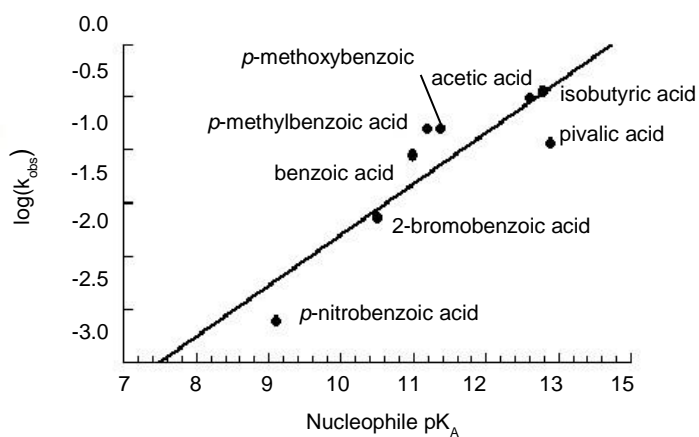


Figure III.3.1. Brønsted plot for the reaction of 1_{ClO_4} complex with carboxylic acids. Conditions: $[1_{ClO_4}] = 0.8$ mM, $[HO-Nu] = 8$ mM, CH_3CN , 15 °C.

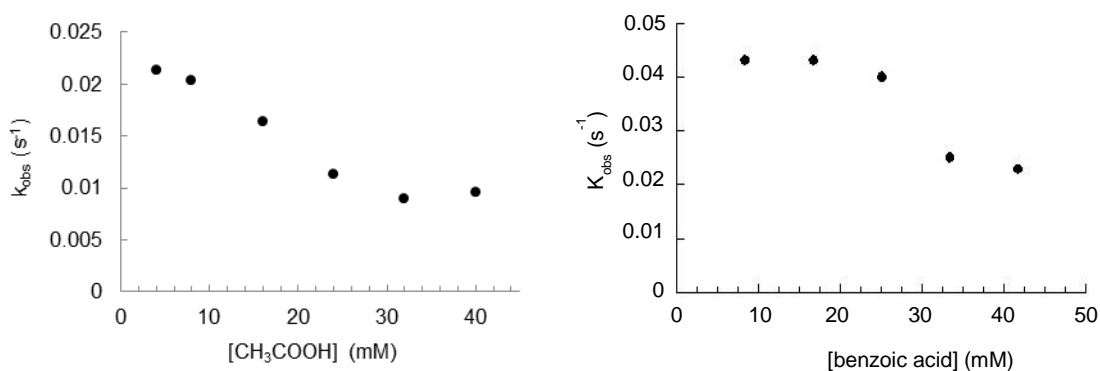


Figure III.3.2 Nucleophile concentration dependence on the reaction rate of 1_{ClO_4} complex with acetic acid (a) and benzoic acid (b). Conditions: $[1_{ClO_4}] = 0.55$ mM, $[HO-Nu] = 0.8$ mM to 40 mM at 5 °C for acetic acid and 15 °C for benzoic acid.

III.3.2.2 Phenols

The wide range of pK_A of the *para*-substituted phenols chosen for this study, from 10.8 to 19.1 (values in DMSO), is reflected in the different kinetic behavior observed among the several phenols. Less acidic phenols, such as *p*-methoxy and *p*-fluorophenol, with a pK_A of 19.1 and 18.0 respectively, exhibited first order dependence of the rate on phenol concentration (Figure III.3.3, a). In contrast, the reaction of complex 1_{ClO_4} with more acidic *p*-trifluoromethyl- and *p*-cyanophenol, with a pK_A of 15.3 and 13.2 respectively, exhibited a saturation dependence on phenol concentration (Figure III.3.3, b). Finally, *p*-nitrophenol that has the lowest pK_A , 10.8, showed a kinetic behavior similar to carboxylic acids: zero order dependence of rate on the phenol concentration (5-10 equiv) and inhibition of the rate at higher phenol concentration (Figure III.3.3, c).

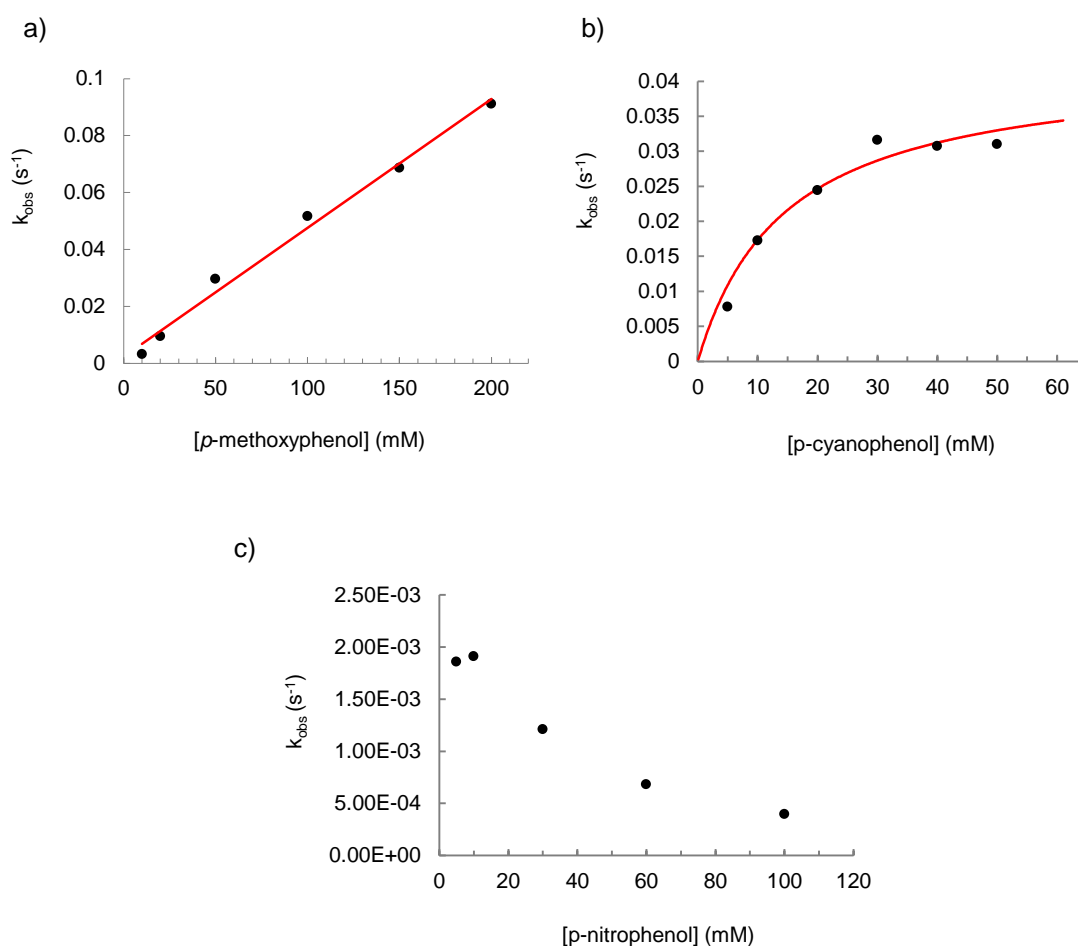


Figure III.3.3. Nucleophile concentration dependence of the reaction rate with several *para*-substituted phenols: a) *p*-methoxyphenol b) *p*-cyanophenol and c) *p*-nitrophenol. Conditions: $[1_{ClO_4}] = 1$ mM, CH_3CN at 25 °C except for the reaction of *p*-nitrophenol, which was performed at 15 °C.

The effect of phenol pK_A was evaluated by comparing the reaction rates obtained when the reaction was carried out in the presence of 10 equivalents of nucleophile (under these conditions reaction is first order in nucleophile concentration). The Brønsted plot showed a negative slope, with the exception of *para*-nitrophenol. Then, the general trend is that more acidic phenols react faster, similarly to nitrogen nucleophiles (Figure I.3.1), but this represents an opposite behavior in comparison to carboxylic acids. From these studies we can conclude that the deprotonation of the nucleophile has an important role in the mechanism of the C-O and C-N bond forming reactions.

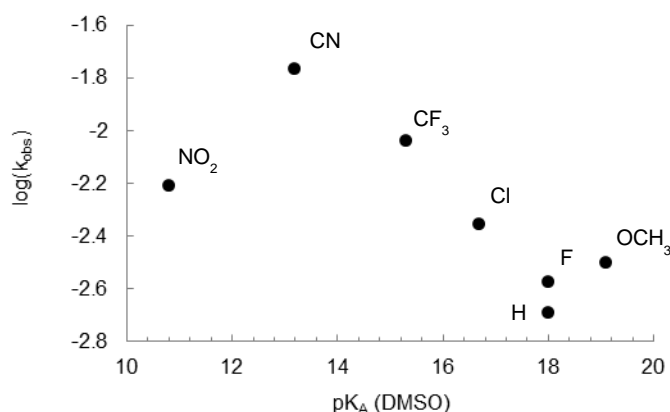


Figure III.3.4. Plot of $\log(k_{obs})$ versus $pK_{A(DMSO)}$ (Brønsted plot) with the several *para*-substituted phenols. Conditions: $[1_{ClO_4}] = 1 \text{ mM}$, $[HO-Nu] = 10 \text{ mM}$, CH_3CN , $25 \text{ }^\circ\text{C}$.

III.3.3 Efforts to identify arylCu^{III}-nucleophile adducts

The zero-order kinetic dependence on oxygen nucleophile concentration in some specific substrates and conditions (at low concentration for carboxylic acids and *p*-nitrophenol, and at high concentration for *p*-cyanophenol and *p*-trifluoromethylphenol), suggests the implication of a ground-state adduct between the nucleophile and the arylcopper(III) complex 1_{ClO_4} . Extensive NMR studies at low temperature under zero-order kinetics conditions were performed, even though no adduct intermediate was observed. Otherwise, low temperature UV-Vis spectroscopy experiments showed small spectroscopic changes in the spectra, which were attributed to coordination of oxygen nucleophile (HONu) to the copper(III) center of complex 1_{ClO_4} .

Titration of complex 1_{ClO_4} with several equivalents of acetic acid at $-30 \text{ }^\circ\text{C}$ in acetonitrile resulted in a noticeable change in the UV-Vis spectrum (Figure III.3.5, a). In this case, ongoing C-O coupling reaction was observed during the course of the experiment and, therefore, the spectra reflected a combination of reactions. Similar experiments using benzoic acid as oxygen nucleophile led to the observation of isosbestic points at 430 nm and 710 nm consistent with clean formation of new species (, b), without contamination of the following C-O bond forming

reaction. Titration of complex $\mathbf{1}_{\text{ClO}_4}$ with *p*-cyanophenol also afforded changes in the spectra (Figure III.3.5, c). Besides, a plot of volume-corrected absorbance at 550 nm versus *p*-cyanophenol concentration exhibits a saturation curve that resembles the saturation kinetic profile for formation of the corresponding Aryl-OAr product (Figure III.3.6). In contrast, when *p*-methoxyphenol was added to a solution of arylCu^{III} complex no changes in the spectra were observed what is consistent with the fact that the reaction with this nucleophile never deviates from a first-order kinetic dependence (Figure III.3.5, d) and no adduct species is formed.

Considering UV-Vis titration experiments at low temperature we suggest the formation of a ground-state interaction between arylCu^{III} complex and more acidic nucleophiles. However, it must be recognized that spectral changes are small and are not observed in the NMR spectra.

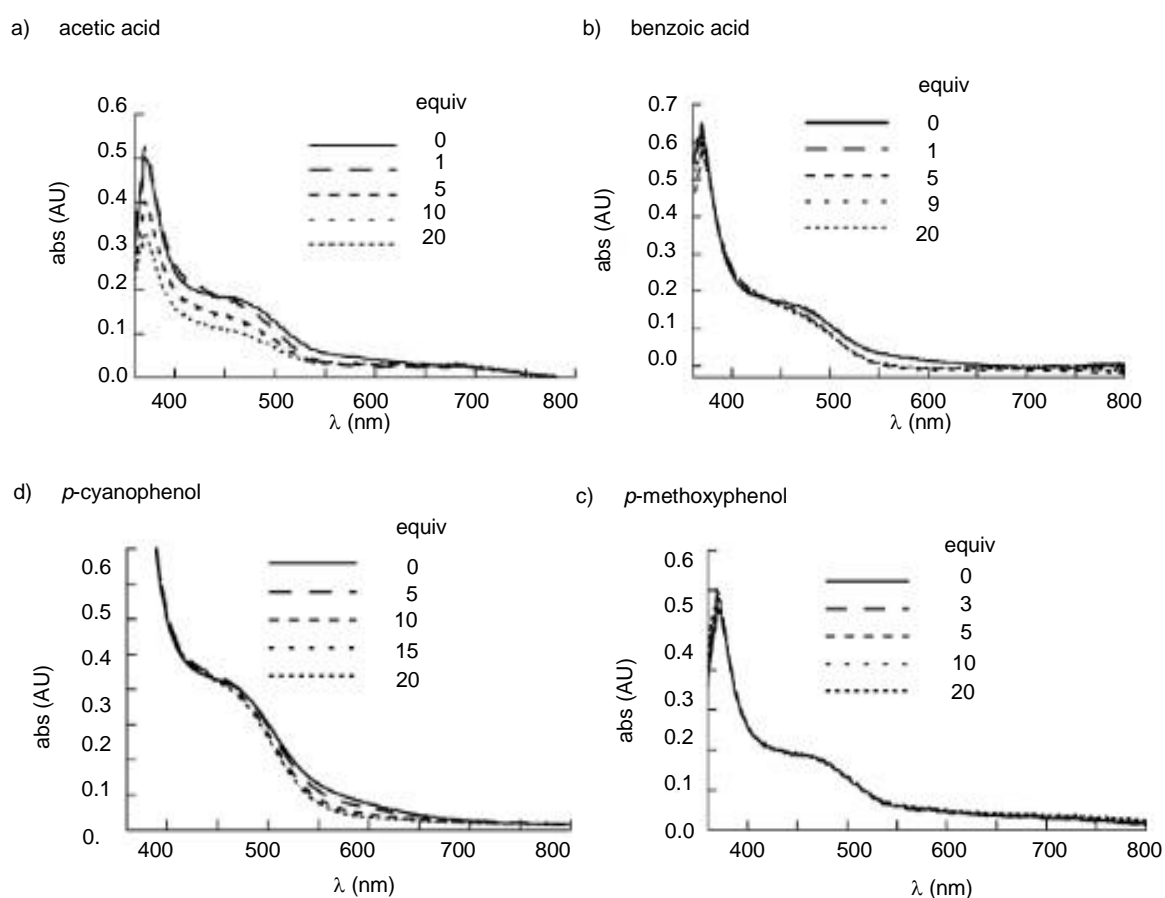


Figure III.3.5. Volume corrected UV-Vis spectra of the titration of a) acetic acid, b) benzoic acid, c) *p*-cyanophenol and d) *p*-methoxyphenol nucleophiles into an acetonitrile solution of $\mathbf{1}_{\text{ClO}_4}$. Conditions for acetic, benzoic acid and *p*-methoxyphenol: $[\mathbf{1}_{\text{ClO}_4}] = 0.8 \text{ mM}$, $[\text{HO-Nu}] = 0.8\text{--}16 \text{ mM}$, $-30 \text{ }^\circ\text{C}$. Conditions for *p*-cyanophenol: $[\mathbf{1}_{\text{ClO}_4}] = 1.5 \text{ mM}$, $[\text{HO-Nu}] = 1.5 \text{ mM}\text{--}75 \text{ mM}$, $0 \text{ }^\circ\text{C}$.

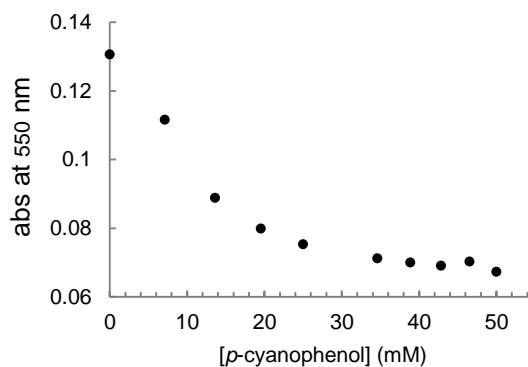


Figure III.3.6. Plot of absorbance (volume corrected) versus [p-cyanophenol] at 550 nm for the titration of p-cyanophenol into a cooled solution of $\mathbf{1}_{\text{ClO}_4}$ at 0 °C. Conditions: $[\mathbf{1}_{\text{ClO}_4}]_{\text{initial}} = 1.5$ mM, 1 cm path length.

III.3.4 Mechanistic proposal

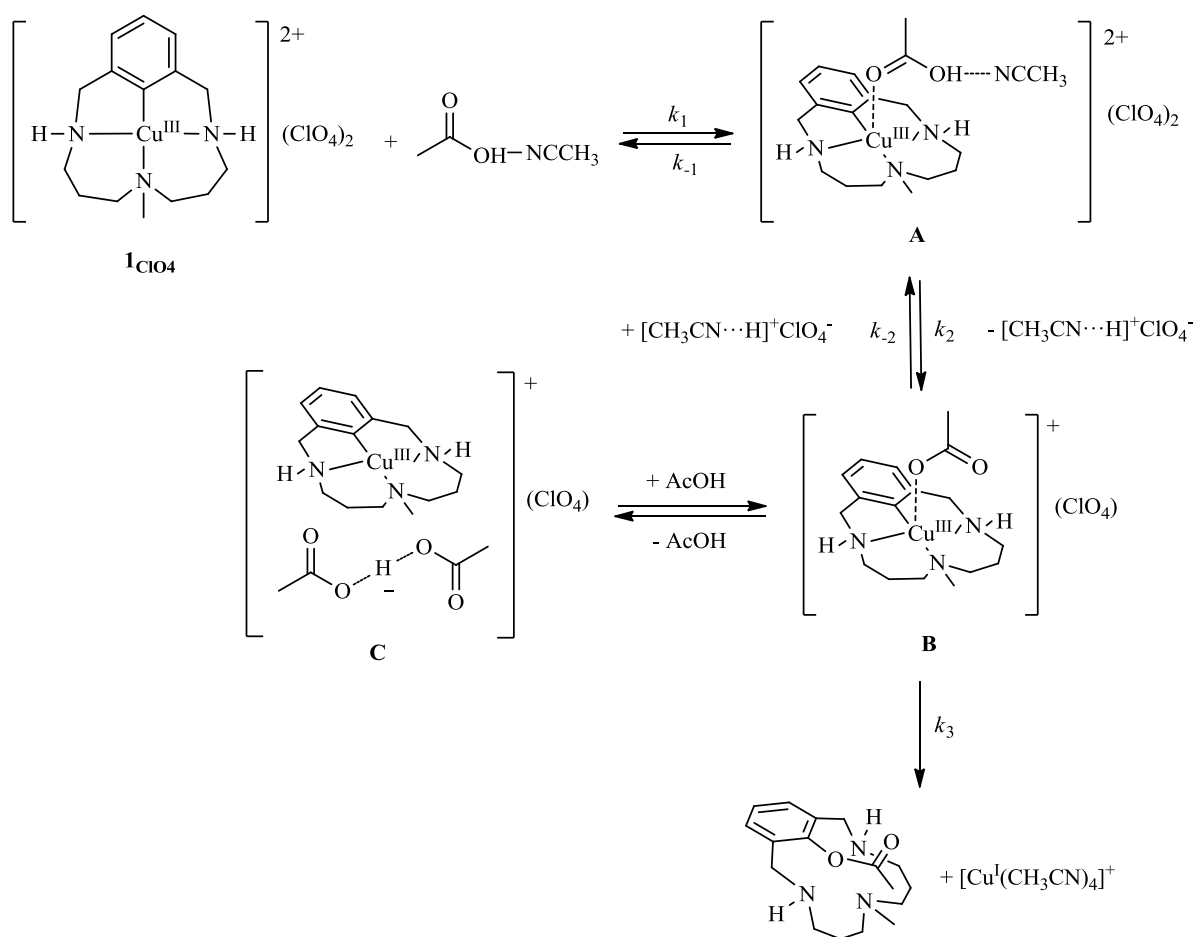
Accordingly to all kinetic data obtained in stoichiometric C-N¹⁵⁰ and C-O bond forming reactions from arylcopper(III) complexes, we propose a general mechanism for all nitrogen and oxygen nucleophiles studied within this system (Scheme III.3.2). In the first step, there is a preequilibrium formation of an arylCu^{III}-nucleophile adduct **A**, stabilized by hydrogen bonding between the O-H group and CH₃CN. Then, deprotonation of the coordinated nucleophile follows, and finally C-heteroatom reductive elimination takes place, resulting in the formation of the coupling product and copper(I).

The ability of more acidic nucleophiles to coordinate more effectively to the copper(III) complex is rationalized by their capability to undergo hydrogen bonding to an acetonitrile solvent molecule. This interaction will enhance the anionic character of the HO-Nuc, thereby making it a better ligand.^{24,25} This type of weak Cu^{III}/HO-Nuc interaction rationalizes the small spectroscopic changes observed upon nucleophile binding. Formation of adduct **A** as the resting state species in solution would account for the zero-order kinetic dependence on carboxylic acid concentration (at low concentration), because loss of a proton from adduct **A** followed by C-O reductive elimination will be unaffected by excess carboxylic acid in solution. The inhibitory behavior observed might arise from dissociation of the coordinated nucleophile to form carboxylic acid/carboxylate hydrogen-bonded dimers, which are reported to be strong.²³

With regard to phenols, their different kinetic behavior observed may be explained by the relative propensity of the different phenols to form the ground-state adduct **A**. While *p*-nitrophenol is sufficiently acidic to form **A** at low concentrations, *p*-cyanophenol and *p*-trifluoromethylphenol only favors formation of adduct **A** at high concentrations. In these cases, the reaction exhibits a zero-order kinetic dependence on nucleophile concentration (saturation).

The differences in the Brønsted plot among the different nucleophiles may be rationalized by a change in the rate-limiting step for different nucleophiles. In the case of more acidic nucleophiles (carboxylic acids or *p*-nitrophenol) the rate-limiting step is the C-O reductive elimination. In contrast, the rate-limiting step for less acidic nucleophiles is the deprotonation of the nucleophile, which is favored in nucleophiles with lower pK_A as indicates the negative slope in the Brønsted plot.

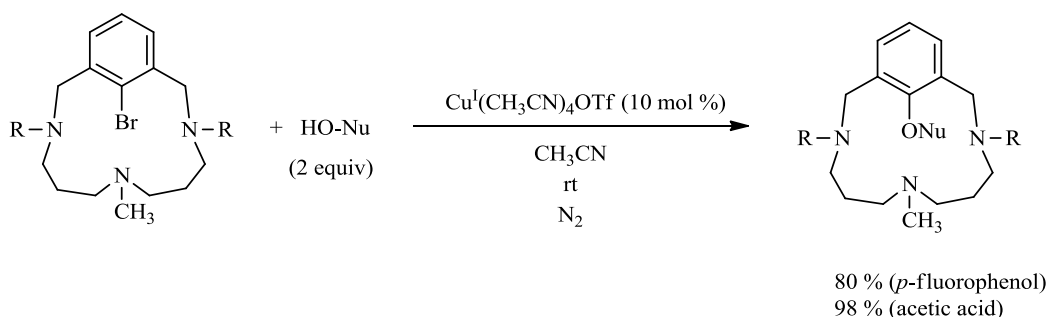
Finally, we have also observed that the addition of acetates to the reaction of complex 1_{ClO_4} with acetic acid increase the rate of the C-O bond forming reaction. This is in line with our mechanistic proposal since acetate may play a similar base role than acetonitrile, and it may promote the deprotonation of the adduct **A** between $\text{arylCu}^{\text{III}}$ with the acetic acid in more effective manner than the acetonitrile, as acetate is more basic.



Scheme III.3.2. Proposed mechanism for the reaction of $\text{aryl-Cu}^{\text{III}}$ complex 1_{ClO_4} with HO-Nu (acetic acid used in the depicted proposal).

III.3.5 Catalytic C-O bond forming reaction

Finally, we studied the catalytic C-O bond forming reaction between aryl bromide substrate **L₁-Br** and oxygen nucleophiles catalyzed by copper(I) (Scheme III.3.3). Reaction of **L₁-Br** with 2 equivalents of *p*-fluorophenol in the presence of 10 mol % of [Cu(CH₃CN)₄]OTf in acetonitrile at room temperature yielded 80 % of the corresponding biaryl ether coupling product after 24h. Similar reaction was obtained between ligand **L₁-Br** and acetic acid as oxygen nucleophile, affording quantitative formation of the corresponding aryl ester. The inhibitory effect observed in the stoichiometric reactions of **1_{ClO4}** with carboxylic acids is also observed in the catalytic reaction. When the acetic acid was added slowly to the reaction mixture via syringe pump, the reaction proceeds about two-fold faster in comparison to the acid addition at once at the beginning of the reaction. The spectroscopic observation of arylcopper(III)-bromide complex **1_{Br}** as the resting state of the catalytic C-O coupling reaction indicated that the ligand exchange step is rate-determining as also observed in the previous catalytic C-N bond forming reaction (see section III.1.5). The copper catalyzed C-O bond forming reactions within this model substrate are the first examples of Ullmann Condensation reactions undergoing an initial aryl-halide oxidative addition to form arylCu^{III}-X, followed by halide to HO-nucleophile exchange and final reductive elimination, thus supporting path B of Scheme I.3.15 of the introduction chapter.



Scheme III.3.3. Catalytic C-O bond forming reaction in macrocyclic model substrate **L₁-Br**.

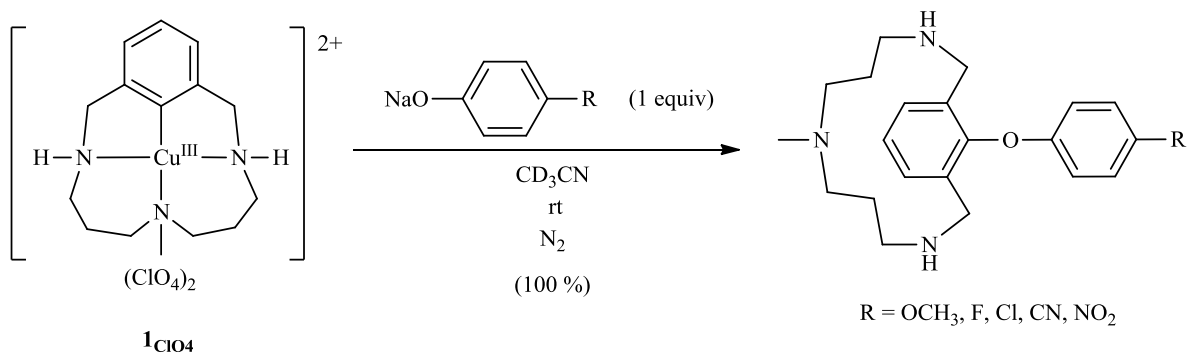
III.4 Aryl-O reductive elimination from reaction of well-defined aryl-copper(III) species with phenolates: the importance of ligand reactivity

This section corresponds mainly to the contents of the paper by Casitas *et al.*, *Dalton Trans.* **2011**, *40*, 8796-8799, which is found in chapter VII of this thesis.

Amine functional groups situated in the macrocyclic ligand of arylcopper(III) complex are involved not only in the stabilization of copper in high oxidation state, but also in their reactivity. This is attributed to the strong sigma donor nature of the amine coordinating atoms. Previous results we have shown that amine groups are involved in the mechanism of acid triggered carbon-halide reductive elimination as well as C-N and C-O bond forming reactions. On the other hand, the non-innocent ligand reactivity might also be reflected by the deprotonation of the coordinated secondary amines, as it has been seldom reported.²⁶ In this section we explore the reactivity of arylCu^{III} complex with non-coordinating bases, such as Proton-sponge[®], as well as with several *para*-substituted phenolates, with the aim of investigating the pH influence on the outcome of cross-coupling reactions in the context of arylCu^{III} reactivity.

III.4.1 Stoichiometric reactions with phenolates

Complex [L₁Cu^{III}](ClO₄)₂ (**1**_{ClO₄}) reacts with 1 equivalent of sodium *para*-substituted phenolates (OCH₃, Cl, F, CN and NO₂) in acetonitrile under N₂ atmosphere at room temperature (Scheme III.4.1) to afford quantitatively the corresponding C-O coupling product biaryl ether, as determined by ¹H-NMR spectra of the crude mixtures using 1,3,5-trimethoxybenzene as internal standard. Products were characterized by NMR spectroscopy and ESI-MS spectrometry of reaction mixtures. In comparison with the corresponding *para*-substituted phenols, phenolates react faster under milder reaction conditions.



Scheme III.4.1. Reaction of complex 1_{CuO_4} with sodium *para*-substituted phenolates to afford biaryl ether and Cu^{I} coupling products.

III.4.2 Kinetic analysis of stoichiometric reactions with phenolates

The reaction of complex 1_{CuO_4} with equimolar amounts of several sodium phenolates was monitored by UV-Vis spectroscopy. Phenolate addition caused the instantaneous formation of a deep-violet species **3** ($\lambda_{\text{max}} = 545 \text{ nm}$, $\epsilon = 2040 \text{ M}^{-1} \text{ cm}^{-1}$)²⁷, which is not formed in the reaction of complex 1_{CuO_4} with phenols (Figure III.4.1). The decay of intermediate **3** is accompanied with the formation of the C-O coupling product without accumulation of any additional intermediate species. In addition, UV-Vis spectroscopic features of **3** are the same irrespective of the nature of *para*-substituted phenolate substrate. This result indicates that the band at 545 nm does not correspond to the coordination of the phenolate to the copper(III) complex. We suspected that the formation of intermediate **3** was caused by the deprotonation of a secondary amine of the arylCu^{III} complex in the presence of phenolates.

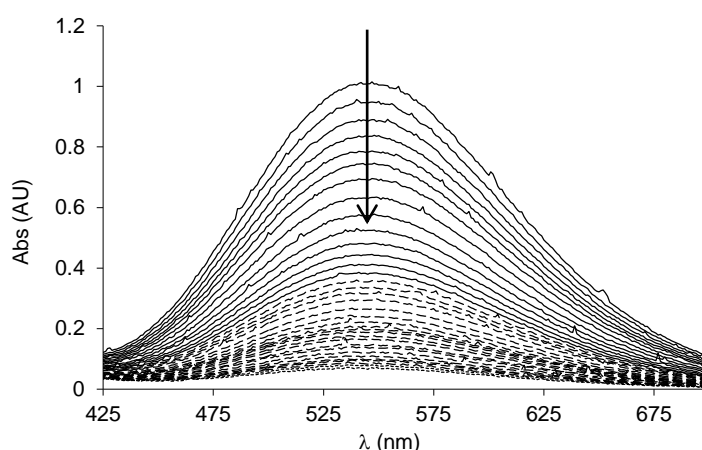


Figure III.4.1. Reaction of complex 1_{CuO_4} with 1 equiv of sodium *p*-fluorophenolate in CH_3CN to form complex **3**. Conditions: $[1_{\text{CuO}_4}] = 0.6 \text{ mM}$, $[4\text{-fluorophenolate}] = 0.6 \text{ mM}$ at $-10 \text{ }^\circ\text{C}$.

On the other hand, the relative reaction rates, measured by the decay of spectral features corresponding to intermediate **3**, correlate with the electronic nature of the phenolate (Figure III.4.2). Faster reaction rates are obtained with more electron-withdrawing substituents in the phenolate ring in analogy to phenol substrates. However, after several attempts, no kinetics parameters of the C-O coupling reaction between arylcopper(III) complex and *para*-substituted phenolates could be obtained under *pseudo*-first order conditions due to precipitation in the reaction crude, presumably because of the formation of multiple ligated Cu(I)-phenolate species. In order to compare the reaction rate of complex **1**_{ClO₄} with *para*-substituted phenolates and the corresponding phenols, we monitored the decay of arylcopper(III) complex with both substrates at the same temperature using only 1 equivalent of reactant. In the case of phenolates we followed the decay of the band at 545 nm corresponding to intermediate **3**, whereas for monitoring the reaction with phenols the band of complex **1**_{ClO₄} at 450 nm was followed (Figure III.4.3). From these experiments it is clearly shown that phenolates react faster than the corresponding phenols.

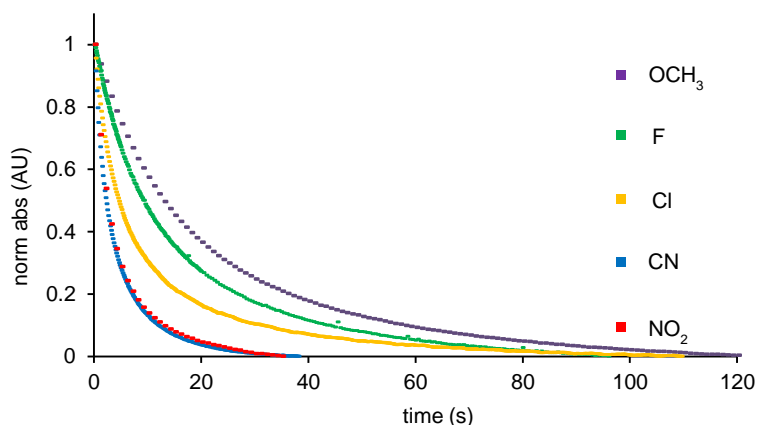


Figure III.4.2. UV-Vis decay of intermediate **3** formed after reaction of complex **1**_{ClO₄} with 1 equiv of *para*-substituted phenolate (R = OCH₃, F, Cl, CN, NO₂). Conditions: [**1**_{ClO₄}] = 0.6 mM in CH₃CN at 10 °C.

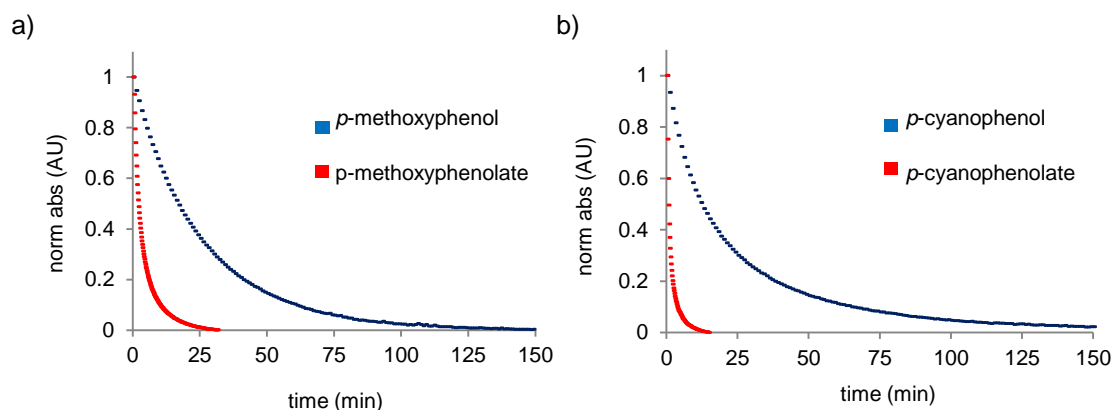
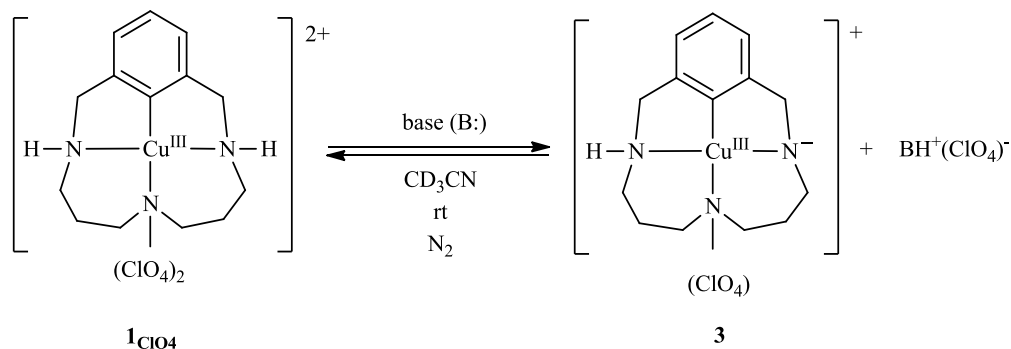


Figure III.4.3. Decay profile for reactions of complex 1_{ClO_4} with 1 equivalent of a) *p*-methoxyphenol at 450 nm and sodium *p*-methoxyphenolate at 550 nm, b) *p*-cyanophenol at 450 nm and sodium *p*-cyanophenolate at 550 nm. Conditions: $[1_{\text{ClO}_4}] = 1.2 \text{ mM}$, $25 \text{ }^\circ\text{C}$, N_2 atmosphere.

III.4.3 Reactivity of arylcopper(III) complex with bases

We reasoned that complex 1_{ClO_4} suffers deprotonation of one of the secondary amines of the macrocyclic ligand when the nucleophile has also basic properties (Scheme III.4.2). Thus, deprotonated oxygen nucleophiles, such as phenolates and carboxylates, as well as basic amines, for instance triethylamine and Proton-sponge[®], lead to the formation of arylCu^{III} complex **3**. We observed that reaction of complex 1_{ClO_4} with Proton-sponge[®] is an acid-base equilibrium and full formation of intermediate **3** is obtained after adding 5-7 equivalents of base (Figure III.4.4). Therefore, the intense violet chromophore may be assigned to LMCT transitions from the amido group to the Cu^{III} center. Indeed, similar UV-Vis spectroscopic features have been described by Margerum and co-workers to arise after amine deprotonation in Cu^{III}-peptide complexes.²⁸



Scheme III.4.2. Amine deprotonation equilibrium in complex 1_{ClO_4} after addition of base.

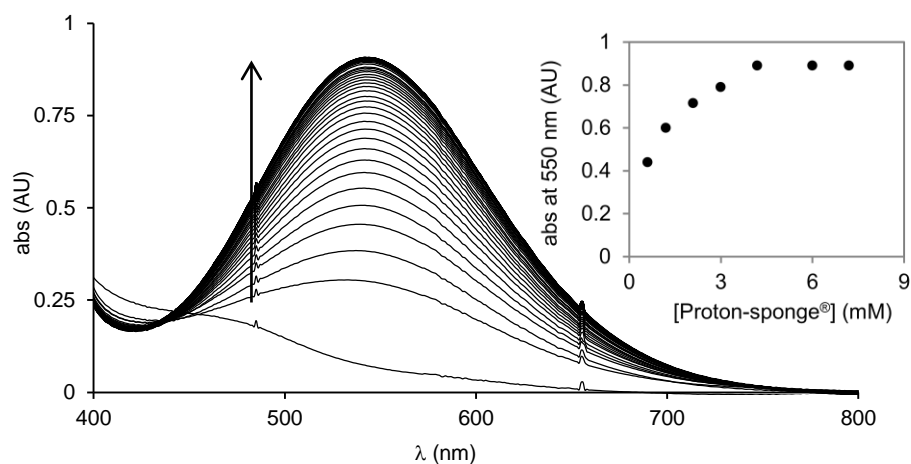
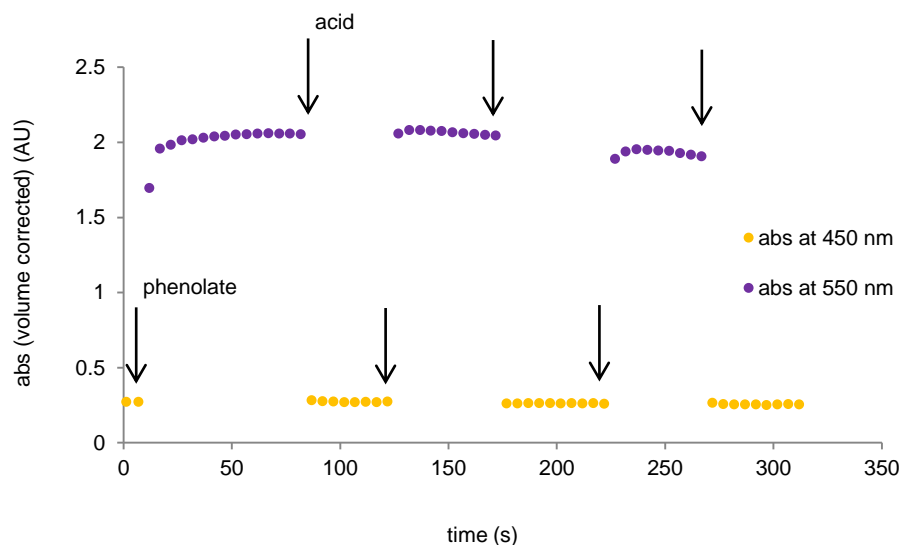


Figure III.4.4. Formation of intermediate **3** upon addition of 7 equiv of Proton-sponge to complex 1_{ClO_4} monitored by UV-Vis spectroscopy. Inset plot corresponds to the maximum absorbance at 550 nm for reaction of complex 1_{ClO_4} with several equiv of Proton-sponge[®]. Conditions: $[1_{\text{ClO}_4}] = 0.6 \text{ mM}$, $[\text{Proton-sponge}^{\text{®}}] = 0.6\text{-}7.2 \text{ mM}$ (1-12 equiv) in CH_3CN at $-30 \text{ }^\circ\text{C}$.

The reversible acid-base ligand reactivity has been demonstrated by subsequent addition of sodium *p*-fluorophenolate and triflic acid at $-30 \text{ }^\circ\text{C}$ to a solution of complex 1_{ClO_4} in acetonitrile. The addition of phenolate causes the instantaneous formation of intermediate **3**, and subsequent addition of triflic acid restores complex 1_{ClO_4} . The phenolate/acid cycle can be repeated several times with minor decomposition of copper(III) complex caused by ongoing formation of the $\text{C}_{\text{aryl}}\text{-O}$ coupling product.



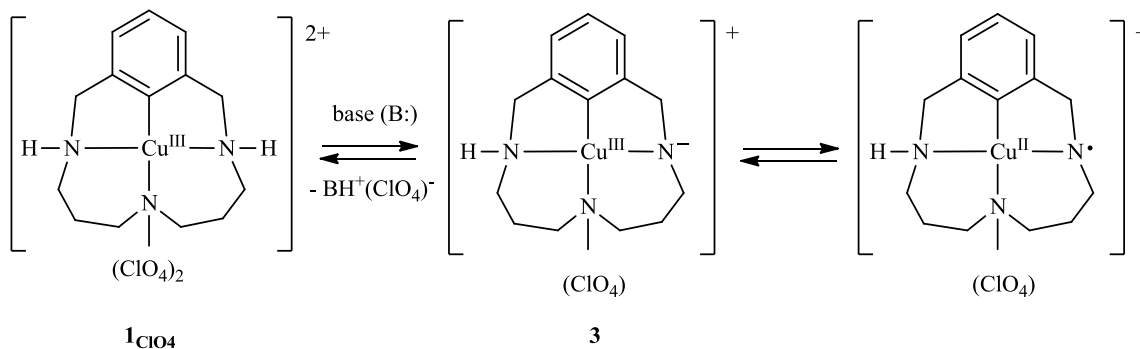
Scheme III.4.3. UV-Vis monitoring of the consecutive additions of 1 equiv of sodium *p*-fluorophenolate and triflic acid to a solution of 1_{ClO_4} . $[1_{\text{ClO}_4}]_{\text{initial}} = 1 \text{ mM}$, in CH_3CN at $-30 \text{ }^\circ\text{C}$.

III.4.4 Low Temperature NMR studies of intermediates

Complex **3** was characterized by NMR spectroscopy at low temperature and is calculated to be formed in approximately 90% respect to initial complex **1**_{ClO₄} by relative integration of the NMR signals with regards to an internal standard. The reaction of arylcopper(III) complex **1**_{ClO₄} with either sodium *para*-fluorophenolate or Proton-sponge[®] caused the same changes in the ¹H-NMR spectrum indicating the formation of the same intermediate **3**, as proposed on the basis of UV-Vis experiments. Signals corresponding to protons nearby the deprotonated secondary amine group showed a broadening (benzylic CH₂ at 4.25 ppm; α-CH₂ at 2.95 ppm), whereas the rest of signals remained unmodified. Furthermore, NMR signals of intermediate **3** formed by addition of excess of Proton-sponge are temperature dependent. Slight shifts and further broadening are observed in the ¹H-NMR spectra upon gradual warming up to 20 °C and the initial spectrum is recovered when the solution is cooled back to low temperature again. Bidimensional correlations also indicated the disappearance of ¹³C peaks corresponding to the affected CH₂ moieties in **3**. The temperature dependence of selected NMR signals of intermediate **3** may be understood as the coordinated secondary amine deprotonation at the macrocyclic Cu^{III} complex, which allows for different conformations (flipping) that give rise to a severe broadening effect of the alpha-CH₂ signals.

III.4.5 EPR experiments: detection of a Cu^{II} complex

The existence of amide/aminyl radical equilibrium in some metal complexes²⁹ prompted us to study complex **3** by EPR spectroscopy, since aminyl radical Cu^{II} complex should show characteristic signals in the EPR spectra (Scheme III.4.4). However, EPR spectroscopy measurements revealed the presence of active copper(II) complex without any radical centered at the nitrogen of the ligand. They are present in solution at very low concentration, being the major species diamagnetic Cu^{III} amide complex.



Scheme III.4.4. Initial amine/aminyl radical equilibrium hypothesis in arylCu^{III} complex **3**.

The reaction of complex **1**_{C104} with stoichiometric sodium phenolates and also with excess of Proton-sponge[®] as base was studied extensively by cw and pulse-EPR spectroscopy. Reaction samples of **1**_{C104} (44 mM) and 4 equivalents of Proton-sponge[®] were mixed under N₂ at 0 °C, stirred for a few seconds and immediately frozen in an EPR tube. X-band (9.4 GHz) and Q-band (34.6 GHz) measurements were performed at T = 120 K (Figure III.4.5). The EPR spectra in both mw frequencies can be satisfactorily simulated with the following spin Hamiltonian parameters: $g_x = 2.0384$, $g_y = 2.0215$, $g_z = 2.1147$; $A_x = 124$ MHz, $A_y = 447$ MHz, $A_z = 134$ MHz. Although g and A tensors are typical for $S = \frac{1}{2}$ Cu^{II} species, the orientation of the tensors was unusual: the large hyperfine value 447 MHz is along g_y and not g_z , as is the case for most common Cu^{II} EPR signals. However, this behavior can be rarely found in the literature.^{30,31,32}

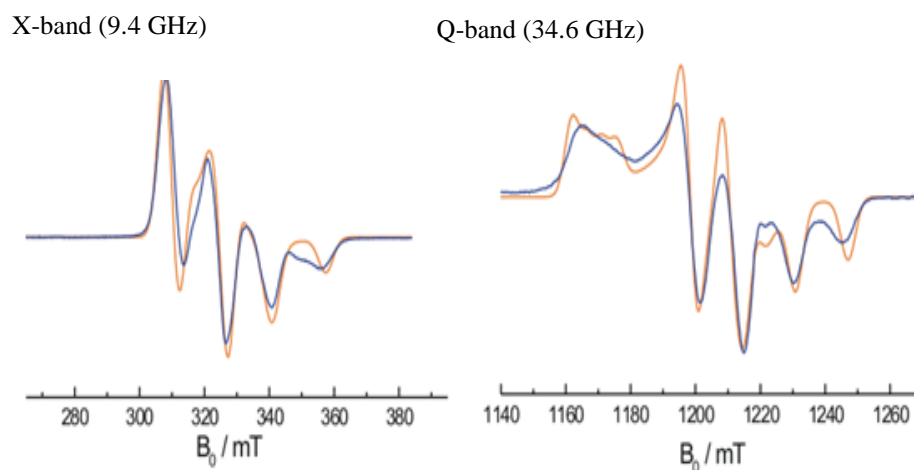
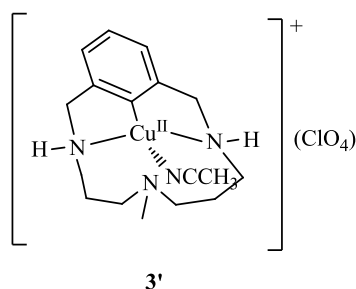


Figure III.4.5. X- and Q-band EPR spectra of **3'** in frozen acetonitrile solution (T=120 K). Blue traces: experiment; red traces: simulation.

Some insight about the atoms surrounding the Cu^{II} ions could be obtained by ENDOR and HYSCORE spectroscopy. The ENDOR study showed two strongly-coupled nitrogen atoms, with $A = 12$ MHz and $A = 46$ MHz hyperfine coupling constants, respectively. Additionally, HYSCORE spectra allowed for the detection of a third weakly ($A = 4$ MHz) coupled N atom. The latter findings could be tentatively rationalized with a Cu^{II} coordination sphere consisting of two strongly bound amine moieties, as well as a third weakly coordinated N belonging to a CH₃CN molecule. Since a tetrahedral geometry is deduced from spin Hamiltonian parameters, and the macrocyclic ligand appears unable of adapting to this geometry, while keeping the four N atoms bound to the metal, an external CH₃CN ligand is proposed to be bound to the metal center, leaving one of the macrocyclic secondary amine groups as non-coordinated (Scheme I.4.5). Moreover, spectra also showed the existence of two weakly coupled protons, one at $A_1 = 6$ MHz and another one at $A_2 = 14$ MHz with modest anisotropy (agreement between ENDOR

and HYSORE). An additional proton coupling with considerable anisotropy is found, with a short $\text{Cu}^{\text{II}} \cdots \text{H}$ distance of 2.34 Å (assuming a 100% spin density at Cu^{II}).

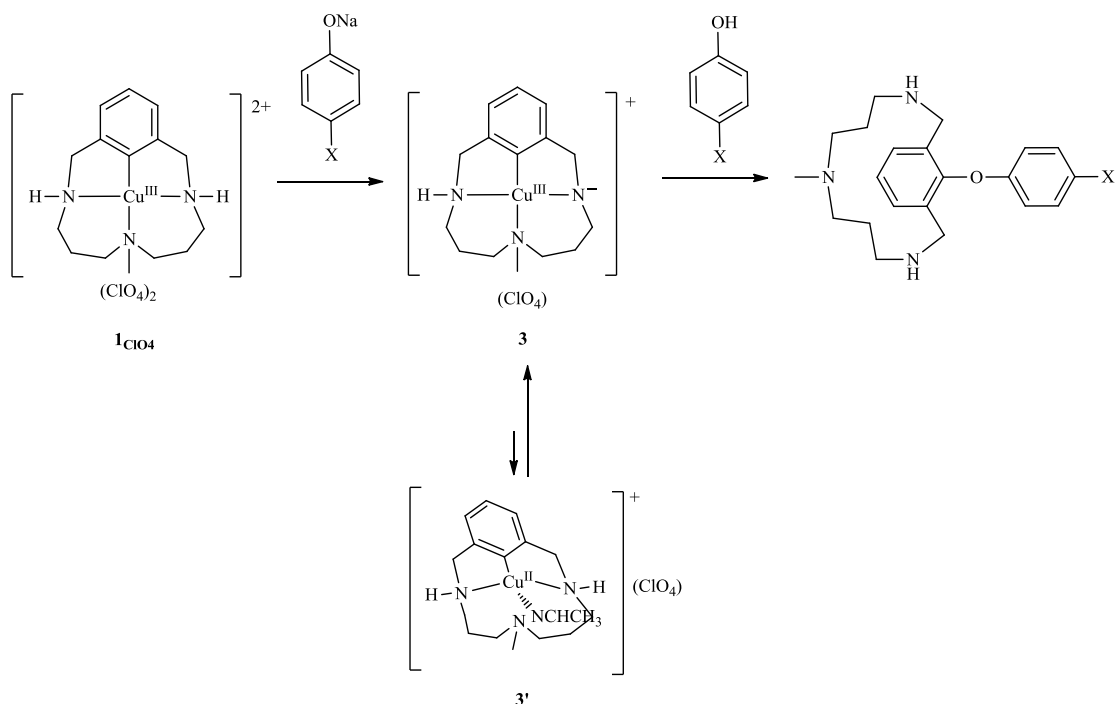


Scheme III.4.5. Proposed structure of characterized copper(II) complex by EPR experiments.

Reliable quantification could be performed by EPR spectroscopy in systems with $S = \frac{1}{2}$, by double integration of signals with regard to a well-characterized Cu(II) complex, i.e. $\text{Cu}(\text{acac})_2$. We noticed that copper(II) EPR active species are only present in solution approximately in 2% respect to the starting arylcopper(III) $\mathbf{1}_{\text{ClO}_4}$ complex at 5 mM concentration, but these percentage increases up to 6 % after 30 minutes. When initial $\mathbf{1}_{\text{ClO}_4}$ concentration was increased up to 44 mM, the formation of copper(II) complex $\mathbf{3}'$ accounts for an initial 11 %, and 30 % after 10 minutes. However, C-O coupling reactions between arylcopper(III) complex and phenolates are carried out at 0.6-2.5 mM, suggesting that the concentration of active EPR copper(II) complexes under reaction conditions is negligible. The formation of copper(II) complex $\mathbf{3}'$ is still unclear, but may correspond to one electron and one proton transfer processes.

III.4.6 Mechanistic proposal

The mechanism proposed for the reaction of arylcopper(III) complex $\mathbf{1}_{\text{ClO}_4}$ with several phenolates consisted in the initial deprotonation of the amine group of the complex to form intermediate $\mathbf{3}$ and the corresponding phenol (Scheme III.4.6). The facile formation of the C-O coupling product by the reaction of intermediate $\mathbf{3}$ and phenol indicates that deprotonated amine assists the O-H cleavage of the oxygen nucleophile, before reductive elimination. Furthermore, the more acidic is the nucleophile, the faster is the reaction. Since EPR signals disappear at the end of the C-O bond forming reaction, we propose an equilibrium between $\mathbf{3}$ and $\mathbf{3}'$. Although we propose this mechanism as the main reaction pathway for the C-O coupling product, we cannot discard the involvement of copper(II) complex $\mathbf{3}'$ in a competitive mechanism.



Scheme III.4.6. Proposed mechanism for the reactivity of arylcopper(III) complex with sodium *para*-substituted phenolates.

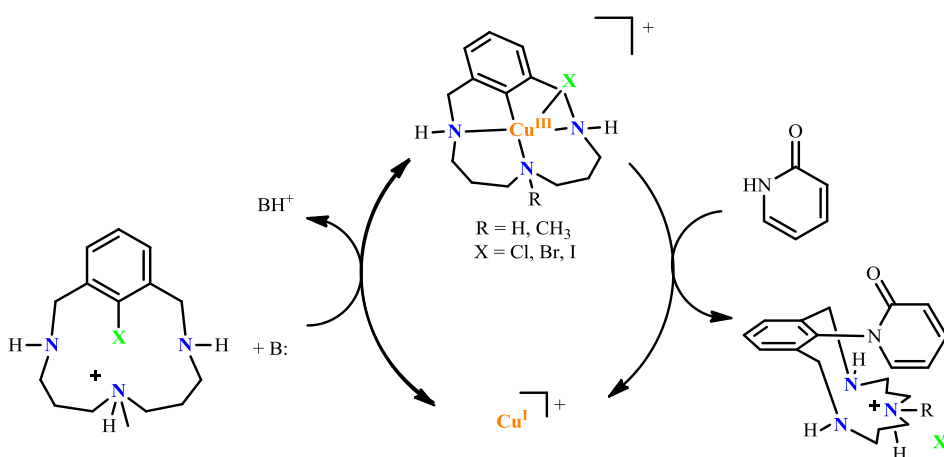
III.5 References

- Ribas, X.; Jackson, D. A.; Donnadieu, B.; Mahía, J.; Parella, T.; Xifra, R.; Hedman, B.; Hodgson, K. O.; Llobet, A.; Stack, T. D. P. *Angew. Chem. Int. Ed.* **2002**, *41*, 2991.
- Xifra, R.; Ribas, X.; Llobet, A.; Poater, A.; Duran, M.; Solà, M.; Stack, T. D. P.; Benet-Buchholz, J.; Donnadieu, B.; Mahía, J.; Parella, T. *Chem.-Eur. J.* **2005**, *11*, 5146.
- This part of the work has been published in another publication not included in this thesis, but commented here for its relevance at this point. See reference: King, A. E.; Huffman, L. M.; Casitas, A.; Costas, M.; Ribas, X.; Stahl, S. S. *J. Am. Chem. Soc.* **2010**, *132*, 12068.
- Bernhardt, P. V. *J. Am. Chem. Soc.* **1997**, *119*, 771.
- Golub, G.; Cohen, H.; Paoletti, P.; Bencini, A.; Messori, L.; Bertini, I.; Meyerstein, D. *J. Am. Chem. Soc.* **1995**, *117*, 8353.
- Hanss, J.; Beckmann, A.; Krüger, H.-J. *Eur. J. Inorg. Chem.* **1999**, 163.
- Roy, A. H.; Hartwig, J. F. *J. Am. Chem. Soc.* **2003**, *125*, 13944.
- Whitfield, S. R.; S. Sanford, M. S. *J. Am. Chem. Soc.* **2007**, *129*, 15142.
- Vigalok, A. I. *Chem. Eur. J.* **2008**, *14*, 5102.

10. This part of the work has been published in another publication not included in this thesis, but commented here for its relevance at this point. See reference: Casitas, A.; Poater, A.; Solà, M.; Stahl, S. S.; Costas, M.; Ribas, X. *Dalton Trans.*, **2010**, 39, 10458.
11. Hartwig, J. F. *Organotransition Metal Chemistry: From Bonding to Catalysis*, University Science Books, Sausalito, **2009**.
12. Huffman, L. M.; Stahl, S. S. *J. Am. Chem. Soc.* **2008**, 130, 9196.
13. Huffman, L. M.; Stahl, S. S. *Dalton Trans.* **2011**, 40, 8959.
14. Sheppard, T. D. *Org. Biomol. Chem.* **2010**, 7, 1043.
15. Klapars, A.; Huang, X.; Buchwald, S. L. *J. Am. Chem. Soc.* **2002**, 124, 7421.
16. Cristau, H.-J.; Ouali, A.; Spindler, J.-F.; Taillefer, M. *Chem Eur. J.* **2005**, 11, 2483.
17. DFT calculations were performed with the Gaussian03 Package, using B3LYP functional and the standard 6-31G(d) basis set. Solvent effects have estimated in single-point calculations on the gas-phase optimized structures, based on polarizable continuous solvation model (PCM) and considering CH₃CN as solvent.
18. Furuya, T.; Kamlet, A. S.; Ritter, T. *Nature* **2011**, 473, 470.
19. Grushin, V. V. *Angew. Chem. Int. Ed.* **1998**, 37, 994.
20. Grushin, V. V. *Acc. Chem. Res.* **2010**, 43, 160.
21. Amii, H.; Uneyama, K. *Chem. Rev.* **2009**, 109, 2119.
22. Sun, A. D.; Love, J. A. *Dalton Trans.* **2010**, 39, 10362.
23. Giui, P.; Bertolasi, B.; Ferretti, V.; Gilli, G. *J. Am. Chem. Soc.* **1994**, 116, 909.
24. Del Bene, J. E. *J. Am. Chem. Soc.* **1993**, 115, 1610.
25. Legon, A. C.; Millen, D. J.; North, H. M. *J. Phys. Chem.* **1987**, 91, 5210-5213.
26. Crabtree, R. H. *Science* **2010**, 330, 455.
27. Absorption coefficient calculated considering full formation of complex **3**.
28. Neubecker, T. A.; Kirksey, S. T.; Chellappa, K. L.; Margerum, D. W. *Inorg. Chem.* **1979**, 18, 444.
29. Büttner, T.; Geier, J.; Frison, G.; Harmer, J.; Calle, C.; Schweiger, A.; Schönberg, H.; Grützmacher, H. *Science* **2005**, 307, 235.
30. Roberts, J. E.; Brown, T. G.; Hoffman, B. M.; Peisach, J. *J. Am. Chem. Soc.* **1980**, 102, 825.
31. Romero, A.; Hoitink, C. W.; Nar, H.; Huber, R.; Messerschmidt, A.; Canters, G. W. *J. Mol. Biol.* **1993**, 229, 1007.
32. George, S. D.; Basumallick, L.; Szilagy, R. K.; Randall, D. W.; Hill, M. G.; Nersissian, A. M.; Valentine, J. S.; Hedman, B.; Hodgson, K. O.; Solomon, E. I. *J. Am. Chem. Soc.* **2003**, 125, 11314.

CHAPTER IV.

Direct observation of Cu^I/Cu^{III} redox steps relevant to Ullmann-type coupling reactions



This chapter corresponds to the following publication:

Alicia Casitas, Amanda E. King, Teodor Parella, Miquel Costas, Shannon S. Stahl*, Xavi Ribas*

Chem. Sci. **2010**, *1*, 326-330

For this publication A. C. synthesized and characterized arylcopper(III)-halide complexes. Besides A. C. developed C-halide reductive elimination and oxidative addition reactions in Cu^{III} complexes. Finally, A. C. was involved in argumentations and discussions, and wrote the manuscript draft with X.R.; A. C. contribution is approximately 75 %.

Direct observation of Cu^I/Cu^{III} redox steps relevant to Ullmann-type coupling reactions†

Alicia Casitas,^a Amanda E. King,^b Teodor Parella,^c Miquel Costas,^a Shannon S. Stahl^{*b} and Xavi Ribas^{*a}

Received 31st March 2010, Accepted 15th April 2010

DOI: 10.1039/c0sc00245c

A series of aryl–copper(III)–halide complexes have been synthesized and characterized by NMR and UV-visible spectroscopy, cyclic voltammetry and X-ray crystallography. These complexes closely resemble elusive intermediates often invoked in catalytic reactions, such as Ullmann–Goldberg cross-coupling reactions, and their preparation has enabled direct observation and preliminary characterization of aryl halide reductive elimination from Cu^{III} and oxidative addition to Cu^I centers. *In situ* spectroscopic studies (¹H NMR, UV-visible) of a Cu-catalyzed C–N coupling reaction provides definitive evidence for the involvement of an aryl–copper(III)–halide intermediate in the catalytic mechanism. These results provide the first direct observation of the Cu^I/Cu^{III} redox steps relevant to Ullmann-type coupling reactions.

Introduction

Ullmann and Goldberg cross-coupling reactions of aryl halides for carbon–carbon and carbon–heteroatom bond formation were discovered more than 100 years ago,¹ and were among the earliest uses of catalysis in organic chemical synthesis. These classic copper-catalyzed methods have experienced a renaissance in recent years.² The recent advances, particularly in carbon–heteroatom coupling, have widespread utility in organic synthesis and medicinal chemistry, and they address important limitations of related palladium-catalyzed methods, associated with substrate scope, functional group compatibility and catalyst cost and toxicity.³ The reactions typically use a copper(I) catalyst in combination with an auxiliary ligand and a Brønsted base, and a variety of nitrogen-, oxygen-, sulfur- and carbon-based nucleophiles serve as effective coupling partners.⁴ A number of different mechanisms have been postulated for these reactions, but the most widely invoked is a Cu^I/Cu^{III} catalytic cycle initiated by oxidative addition of a haloarene to Cu^I to form an aryl–Cu^{III}–X intermediate.^{2a,5–7} Despite the prominence of this mechanistic proposal, observation of aryl halide oxidative addition (or reductive elimination) at copper lacks any direct precedent. Here we report the synthesis and full characterization of a series of aryl–Cu^{III}–X (X = Cl, Br, I) complexes. These species undergo an acid-triggered C–X reductive elimination reaction to afford

aryl–X products. The reverse reaction, aryl–X oxidative addition to Cu^I to regenerate aryl–Cu^{III}–X, proceeds rapidly in the absence of an acid source. The latter reaction is shown to be compatible with catalytic C–N coupling when the aryl–X reagent is combined with a nitrogen nucleophile in the presence of catalytic quantities of Cu^I. *In situ* spectroscopic studies (¹H NMR, UV-visible) provide experimental evidence for the involvement of an aryl–copper(III)–halide intermediate in the catalytic mechanism. These results represent the first direct observation of the Cu^I/Cu^{III} redox steps relevant to Ullmann-type coupling reactions.

Results and discussion

Synthesis and characterization of aryl–Cu^{III}–X complexes

The synthesis of aryl–Cu^{III}–X (X = Cl, Br) species was achieved by a modification of a previously reported aromatic C–H activation reaction mediated by Cu^{II} salts.⁸ By using CuCl₂ or CuBr₂ as the Cu^{II} source, the triazamacrocyclic ligands H₂Me33m (**L**₁) and H33m (**L**₂) react *via* disproportionation of Cu^{II} to afford 0.5 equiv of Cu^IX and the protonated ligand, and 0.5 equiv of aryl–Cu^{III}–X species **1**_X and **2**_X (X = Cl, Br; Fig. 1a). The corresponding [aryl–Cu^{III}–I] compounds **1**_I and **2**_I were obtained by anion exchange from [aryl–Cu^{III}](ClO₄)₂ with KI. All aryl–Cu^{III}–X species are stable and have been fully characterized spectroscopically and crystallographically. The crystal structures of compounds **1**_X and **2**_X show that each copper center is penta-coordinate with a square-pyramidal geometry, in which the halide anion is coordinated in the axial position and the aryl moiety and three amine N atoms are coplanar with the copper center (see selected crystal structures in Fig. 1b). The short Cu–C bond distances (1.90(1) Å) are very similar to those in previously reported [aryl–Cu^{III}]²⁺ compounds with the same ligands.⁸ This observation, together with the charge balance and diamagnetic behaviour of the complexes, suggest the metal center is best described as Cu^{III} in all cases.

Electronic spectra for [aryl–Cu^{III}–X]X species exhibit halide-to-metal charge transfer bands in the 360–640 nm range, and the energies of these bands vary systematically with the identity of

^aDepartament de Química, Universitat de Girona, Campus de Montilivi, 17071 Girona, Catalonia, Spain. E-mail: xavi.ribas@udg.edu; Fax: +34-972418150; Tel: +34-972419842

^bDepartment of Chemistry, University of Wisconsin-Madison, 1101 University Avenue, Madison, WI, 53706, USA. E-mail: stahl@chem.wisc.edu; Fax: +1-608-262-6143; Tel: +1-608-265-6288

^cServei de RMN, Facultat de Ciències, Universitat Autònoma de Barcelona, Campus UAB, Bellaterra, E-08193, Catalonia, Spain

† Electronic supplementary information (ESI) available: Full experimental details for the synthesis, spectroscopic, and crystallographic characterization of **1**_X and **2**_X. Synthesis of reductive elimination **L**₁–X and **L**₂–X products. NMR and UV-vis monitoring of catalytic coupling of **L**₁–Br with pyridone. Crystal data for **1**_{Cl}, **1**_{Br}, **1**_I, **2**_{Cl} and **2**_I. CCDC reference numbers 735508–735512. For ESI and crystallographic data in CIF or other electronic format see DOI: 10.1039/c0sc00245c

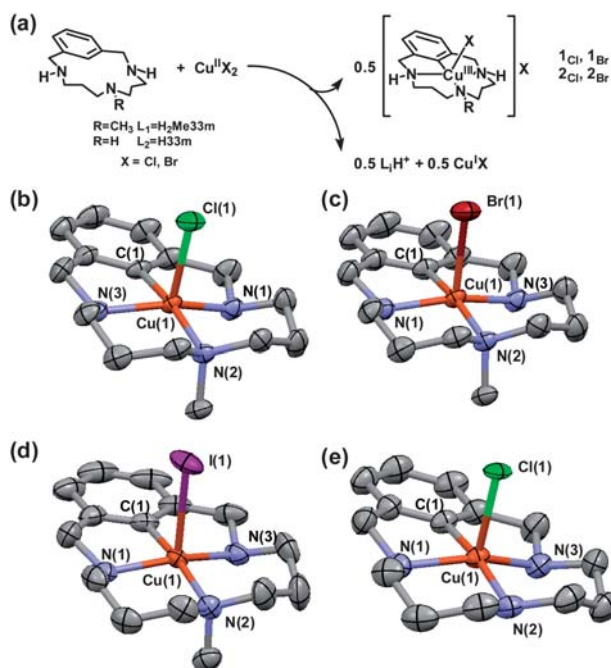


Fig. 1 (a) Synthesis of [aryl-Cu^{III}-X]X complexes. Their X-ray structures are depicted in (b) **1_{Cl}**, (c) **1_{Br}**, (d) **1_I** and (e) **2_{Cl}**. The ellipsoid representation is at 50% probability. The hydrogen atoms and respective second halide counteranion are omitted for clarity. Selected bond lengths [Å] for **1_{Cl}**: Cu(1)–C(1) 1.908(3), Cu(1)–Cl(1) 2.455(2), Cu(1)–N(1) 1.972(3), Cu(1)–N(2) 2.037(3), Cu(1)–N(3) 1.971(3); for **1_{Br}**: Cu(1)–C(1) 1.914(3), Cu(1)–Br(1) 2.600(1), Cu(1)–N(1) 1.974(3), Cu(1)–N(2) 2.034(2), Cu(1)–N(3) 1.974(2); for **1_I**: Cu(1)–C(1) 1.905(3), Cu(1)–I(1) 2.900(1), Cu(1)–N(1) 1.972(2), Cu(1)–N(2) 2.017(2), Cu(1)–N(3) 1.968(2); for **2_{Cl}**: Cu(1)–C(1) 1.898(3), Cu(1)–Cl(1) 2.468(1), Cu(1)–N(1) 1.986(5), Cu(1)–N(2) 1.999(3), Cu(1)–N(3) 1.974(4).

the halide. The aryl-Cu^{III}-Cl compounds (**1_{Cl}**, **2_{Cl}**) show two bands centred at 369 and 521 nm, the aryl-Cu^{III}-Br compounds (**1_{Br}**, **2_{Br}**) at 399 and 550 nm, and the aryl-Cu^{III}-I compounds (**1_I**, **2_I**) at 422 and 635 nm. The red-shift observed in the bands upon changing from Cl⁻ to Br⁻ to I⁻ is in agreement with the ligand-field strength of the halide ligands (Cl⁻ > Br⁻ > I⁻), indicating that the bands correspond to ligand-to-metal charge transfer (LMCT) electronic transitions.

The diamagnetic character of all aryl-Cu^{III}-X species permitted their characterization by NMR spectroscopy. Diagnostic ¹H NMR peaks are evident in the 4–5 ppm range corresponding to the benzylic protons, and the ¹³C NMR spectrum exhibits a distinctive low field resonance for the C_{ipso}-Cu^{III} at about 180 ppm.⁸ Indeed, NOESY (Nuclear Overhauser Effect Spectroscopy) and HMBC (Heteronuclear Multiple Bond Correlation) experiments reveal that the rigid structure found in the solid state is retained in solution (see ESI[†]).

Cyclic voltammetry (CV) measurements of the aryl-Cu^{III}-X species show chemically reversible 1e⁻ processes associated with the Cu^{III}/Cu^{II} redox couple. The Cu^{III}/Cu^{II} E_{1/2} values for these complexes follow the trend E_{1/2}^{Cl} < E_{1/2}^{Br} < E_{1/2}^I, and the compounds bearing L₂, with a secondary amine *trans* to the aryl ligand, exhibit E_{1/2} values 40–70 mV lower than the corresponding complexes bearing L₁, with a tertiary amine in the *trans* position (see ESI[†]). Overall, the redox potentials for Cu^{III}/Cu^{II}

are substantially lower (up to 250 mV) than those measured previously for the corresponding perchlorate or triflate salts,⁸ indicating that halide coordination stabilizes the Cu^{III} oxidation state.

Aryl-X reductive elimination

The isolation of complexes **1_X** and **2_X** (X = Cl, Br, I) provides an unprecedented opportunity to study the reactivity of aryl-Cu^{III}-halide species related to those believed to be key intermediates in Ullmann–Goldberg cross-coupling reactions. Initial studies revealed that these complexes are remarkably stable in solution, even upon warming acetonitrile solutions at 70 °C for days (monitored by ¹H NMR spectroscopy). Addition of one equivalent of Proton Sponge® as a Brønsted base did not affect the stability of the aryl-Cu^{III}-halide compounds. On the contrary, the addition of a Brønsted acid (CF₃SO₃H, 1.5–10 equiv) at room temperature triggered quantitative aryl-X reductive elimination to form the halide-substituted triazamacrocycles, obtained as the protonated derivatives [L-X-H]⁺ (X = Cl, Br, I), and [Cu^I(CH₃CN)₄]⁺ (Fig. 2a).

The reactions of **1_{Cl}**, **1_{Br}** and **2_{Cl}** were investigated in more detail by UV-visible spectroscopy. The kinetic profiles of the decay of the aryl-Cu^{III}-X LMCT bands exhibited first-order behaviour, with rates following the trend: **1_{Cl}** > **2_{Cl}** > **1_{Br}** (Fig. 2b–c). Activation parameters obtained from Eyring analyses (Fig. 2c) reveal that the reductive elimination reactions exhibit a relatively large enthalpy of activation (21.5–23.2 kcal mol⁻¹), consistent with significant Cu–X bond cleavage in the transition state. The reactions of **2_{Br}**, **1_I** and **2_I** were much slower, and systematic kinetic studies of these complexes were not performed. The aryl-Cu^{III}-I compound **1_I** undergoes reductive elimination to afford (L₁-I-H)⁺ in slightly lower yields (85%). The reaction of **2_I** requires extended reaction time (days), is complicated by side-reactions and (L₂-I-H)⁺ is not observed. The faster rate of C–Cl reductive elimination from **1_{Cl}** relative to **2_{Cl}** is consistent with the higher reduction potential of **1_{Cl}** relative to **2_{Cl}**. In contrast, **1_{Br}** exhibits the slowest reductive elimination rate of the three complexes, despite having the highest reduction potential (Fig. 2c). The latter observation is amplified by the even-slower qualitative rates of C–I reductive elimination from **1_I** and **2_I**, which have the highest reduction potentials of the six aryl-Cu^{III}-X compounds (E_{1/2} = –230 and –290 mV, respectively). Thus, the C–X reductive elimination rates do not correlate with the reduction potentials of the aryl-Cu^{III}-X species across the halide series. Rather, these observations suggest that the trends in the rates of C–X reductive elimination are controlled by the relative carbon–halogen bond strengths: C–Cl > C–Br > C–I. A different trend has been observed for aryl carbon–halogen reductive elimination from Pd^{II} complexes, for which the relative rates k_{C–Br} > k_{C–I} > k_{C–Cl} were measured.⁹

The mechanistic origin of the H⁺-triggered aryl-X reductive elimination event is not fully understood; however, electrochemical data indicate that CF₃SO₃H destabilizes the aryl-Cu^{III}-X species. Cyclic voltammetry studies of **1_{Cl}**, **1_{Br}** and **2_{Cl}** in acetonitrile reveal that the Cu^{III}/Cu^{II} reduction potential increases by 70–170 mV when CF₃SO₃H is present in solution (see ESI[†]). In addition, electronic absorption spectra of acidified solutions of these complexes show a 5 nm, 9 nm and 8 nm

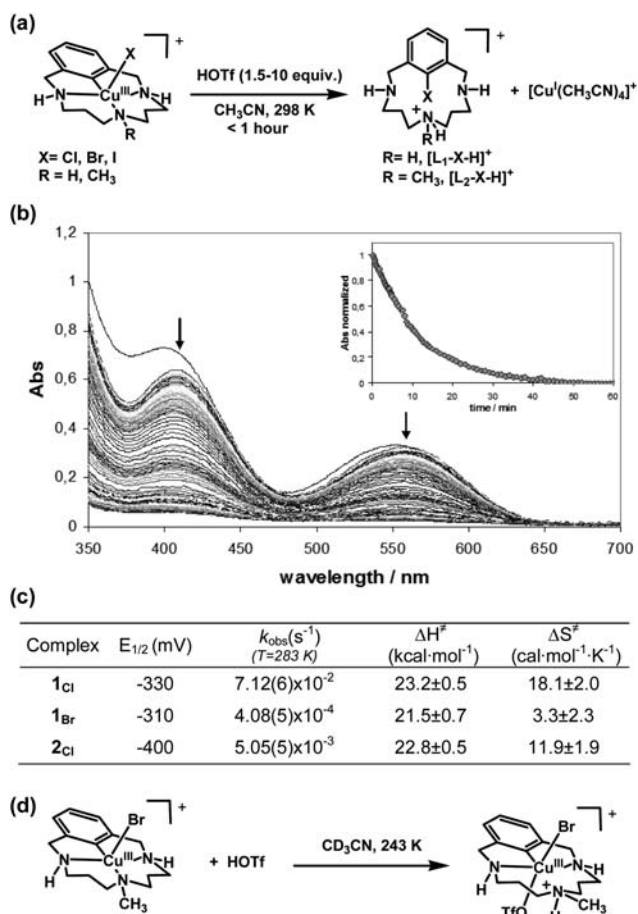


Fig. 2 (a) Acid-triggered quantitative aryl-X reductive elimination from aryl-Cu^{III}-X at room temperature (counteranions omitted for clarity). (b) UV-vis monitoring of reductive elimination of complex [L₁C-Cu^{III}-Br]Br (**1_{Br}**) upon addition of 1.5 equiv. of acid ([**1_{Br}**] = 0.5 mM, [CF₃SO₃H] = 0.75 mM, CH₃CN, 288 K). Inset shows decay profile at 420 nm (circles = experimental data, solid line = first-order theoretical fit). (c) Electrochemical (vs. SSCE, [complex] = 1 mM, scan rate = 0.2 V s⁻¹, TBAPF₆ 0.1 M, CH₃CN, 263 K) and kinetic data associated with aryl halide reductive elimination from aryl-Cu^{III}-X species ([complex] = 0.5 mM, [CF₃SO₃H] = 0.75 mM, CH₃CN, 253–283 K for **1_{Cl}**, 278–298 K for **1_{Br}** and **2_{Cl}**). (d) Proposed interaction of triflic acid with **1_{Br}** through weak axial coordination of the triflate anion to the Cu^{III} center with concomitant protonation of the central amine.

red-shift in the UV-visible bands, respectively, consistent with formation of new species. Our current hypothesis is that CF₃SO₃H protonates the central amine of the macrocyclic ligand, thereby destabilizing the Cu^{III} oxidation state and facilitating C–X bond formation (Fig. 2d). The strong *trans* effect of the aryl ligand, as visualized in the larger Cu^{III}–N(2) bond distances of all compounds, also is in agreement with a preferential protonation to the central amine. Preliminary experimental support for this hypothesis is available from ¹H NMR spectroscopic studies of **1_{Br}**. Triflic acid (1.5 equiv) was added to a solution of **1_{Br}** in CD₃CN at –30 °C. No aryl-Br reductive elimination was observed under these conditions; however, resonances corresponding to the N–CH₃ group and the C–H protons of the adjacent methylene group undergo a noticeable upfield shift, while the other resonances remain essentially

unchanged (see ESI[†]). We suspect that weak axial coordination of the triflate anion to the Cu^{III} center, approaching from the face opposite to the halide, facilitates the protonation of the central amine (Fig. 2d).

Reversible oxidative addition of aryl halides to Cu^I

The protonated aryl halides obtained from the reductive elimination reaction depicted in Fig. 2a are stable in the presence of Cu^I. Upon purification, however, the neutral aryl halide derivatives **L₁-X** and **L₂-X** (X = Cl, Br) react very rapidly with [Cu^I(CH₃CN)₄]⁺ in acetonitrile to afford the corresponding oxidative addition products **1_X** and **2_X** (X = Cl and Br) in quantitative yields based on ¹H NMR and UV-visible spectroscopic analysis (Fig. 3). The reactions are complete in less than 5 s, even at –40 °C in CH₃CN. *In situ* interconversion between the two redox states, Cu^I/L-X-H⁺ and aryl-Cu^{III}-X, was demonstrated *via* sequential addition of triflic acid and Proton Sponge® (as a non-coordinating base) to an acetonitrile solution of **1_{Br}**. Repeated cycles were possible without significant decomposition of **1_{Br}** (Fig. 3b). The electrochemical data described above together with the present results reveal that triflic acid destabilizes the aryl-Cu^{III}-X species and also stabilizes the Cu^I/aryl-X state. This unprecedented interconversion between Cu^I/aryl-X and aryl-Cu^{III}-X will provide the basis for future studies to gain fundamental mechanistic insights into these important processes.

Reversible aryl halide oxidative addition to Cu^I is directly relevant to catalytic transformations. For example, Cohen and coworkers have provided kinetic evidence that the Ullmann coupling of *o*-bromonitrobenzene proceeds *via* reversible oxidative addition of aryl bromide to Cu^I in the first step of the mechanism.¹⁰ Copper(I) salts are also known to catalyze halogen exchange reactions with aryl halide substrates. In a noteworthy example reported recently by Buchwald and coworkers, Cu^I

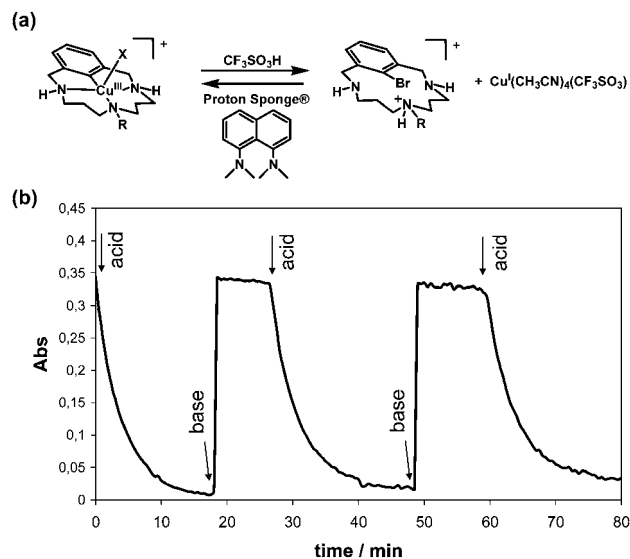


Fig. 3 (a) Reversible reductive elimination/oxidative addition induced by the presence of acid or base. (b) Monitoring of **1_{Br}** by UV-visible spectroscopy at 400 nm upon successive acid and base additions (initial conditions: [**1_{Br}**] = 0.3 mM, addition of 2 equiv. of triflic acid and Proton Sponge® in the respective additions, CH₃CN, 297 K).

catalyzes the conversion of aryl bromides into aryl iodides in the presence of NaI.¹¹

Catalytic C–N bond formation

The reactions of $[\text{Cu}^{\text{I}}(\text{CH}_3\text{CN})_4]^+$ with $\text{L}_1\text{-X}$ and $\text{L}_2\text{-X}$ ($\text{X} = \text{Cl}, \text{Br}$) provide the first observations of aryl-halide oxidative additions to Cu^{I} to form well-defined aryl- Cu^{III} species. In order to probe the relevance of these observations to Ullmann–Goldberg cross-coupling reactions, we combined $\text{L}_1\text{-Br}$ and pyridone, as a nitrogen nucleophile, in acetonitrile with 3.3 mol % of $[\text{Cu}^{\text{I}}(\text{CH}_3\text{CN})_4]\text{PF}_6$ (Fig. 4a). The solution turned from colourless to pale red immediately upon adding Cu^{I} , and the colour persisted for approximately 60–70 min before fading. *In situ* analysis of the catalytic reaction mixture by ^1H NMR spectroscopy (CD_3CN , 288 K) revealed nearly quantitative conversion of $\text{L}_1\text{-Br}$ and pyridone into the HBr adduct of the C–N cross-

coupling product, $3\cdot\text{HBr}$ (Fig. 4b). A steady-state concentration of aryl- $\text{Cu}^{\text{III}}\text{-Br}$ complex I_{Br} was also evident in the ^1H NMR spectra. Integration of the resonances associated with I_{Br} indicates that the aryl- Cu^{III} species accounts for essentially all of the Cu present in solution during the first 60–70 min of the reaction, and it disappears only after consumption of $\text{L}_1\text{-Br}$ (Fig. 4b). The presence of an aryl- Cu^{III} species under catalytic conditions is supported further by UV-visible spectroscopic data (Fig. 4c): charge-transfer bands associated with I_{Br} persist during the first 60–70 min of the reaction and then begin to decay as the reaction depletes the substrates. Observation of an aryl- Cu^{III} species under catalytic conditions is consistent with the rapid formation of I_{Br} , as described above, and implicates the involvement of the aryl- Cu^{III} species in the turnover-limiting step of this catalytic reaction.¹²

Relationship to Ullmann-type coupling reactions

The relationship between the results described here and traditional Ullmann and Goldberg coupling reactions warrants further discussion. Many features of the mechanism of Ullmann–Goldberg reactions remain poorly understood. Recent studies by the groups of Buchwald and Hartwig provide valuable insights into the identity and comparative reactivity of Cu^{I} species that exist under the catalytic reaction conditions.^{6,7} No aryl- Cu^{III} species were observed in these studies, however, presumably because C–N coupling from the aryl- Cu^{III} intermediate is much more rapid than aryl halide oxidative addition to Cu^{I} . The ability to observe the $\text{Cu}^{\text{I}}/\text{Cu}^{\text{III}}$ redox steps in the present study can be attributed to the influence of the macrocyclic substrate on the relative stability and reactivity of the Cu^{I} and Cu^{III} species. The preorganized nature of the macrocyclic ligand is expected to lower the activation barrier for aryl-X oxidative addition to Cu^{I} and stabilize the high-valent aryl- Cu^{III} species. Such factors combine to invert the relative rates of two key redox steps with respect to previously studied Ullmann–Goldberg-type coupling reactions, and, for the first time, an aryl- Cu^{III} intermediate has been observed under catalytic reaction conditions.

The aforementioned studies by Buchwald and Hartwig have provided evidence that, in reactions with bidentate nitrogen ligands, amide substrates react with Cu^{I} to form Cu^{I} -amidate intermediates prior to oxidative addition of the aryl halide. An alternative mechanistic possibility, as discussed in a recent review by Monnier and Taillefer,^{2c} involves oxidative addition of the aryl halide, followed by reaction of the nucleophile with the aryl- Cu^{III} intermediate. The results of the present study, together with previous observations of stoichiometric C–N coupling reactions,¹² conform to the latter mechanism. It seems reasonable to expect that the mechanism of Ullmann–Goldberg-type coupling reactions will vary, depending on the identity of the substrates, ancillary ligand and/or the reaction conditions. Reactions involving nucleophiles that coordinate less readily to copper, or catalysts that feature higher-coordinate (*e.g.*, tri- or tetradentate) ancillary ligands may disfavor pre-coordination of the nucleophile to Cu^{I} . In such cases, the reaction may proceed *via* a mechanism in which reaction of the aryl halide with Cu^{I} precedes that of the nucleophile. These issues will be important to address in future studies of Ullmann-type coupling reactions.

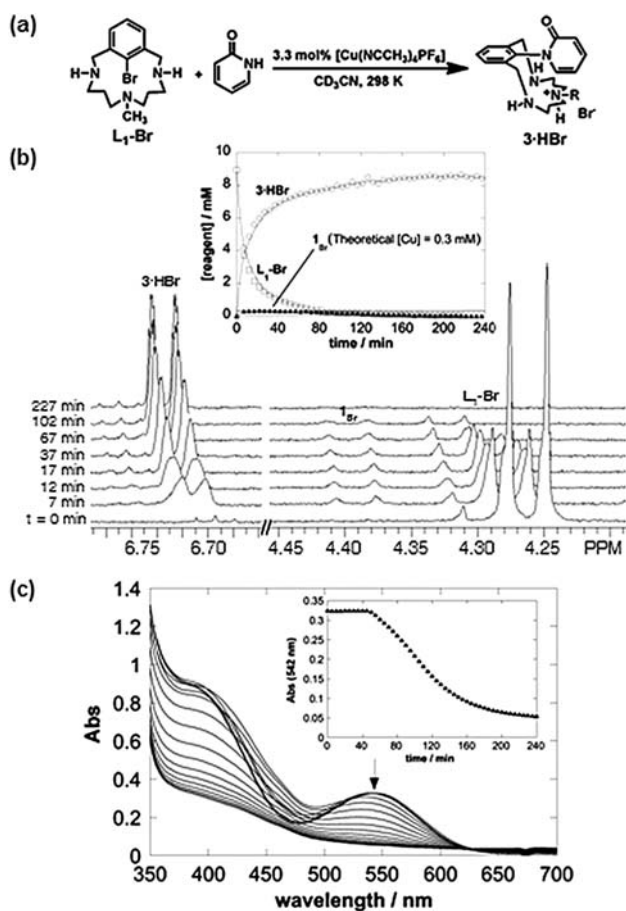


Fig. 4 (a) Copper-catalyzed catalytic C–N bond forming reaction for the conversion of $\text{L}_1\text{-Br}$ and pyridone into $3\cdot\text{HBr}$ at room temperature. (b) ^1H NMR spectroscopic analysis of the Cu-catalyzed amination reaction: the catalytic resting state, aryl- $\text{Cu}^{\text{III}}\text{-Br}$ (I_{Br}), is evident in the spectra obtained prior to $t \sim 120$ min (for clarity only selected regions of the NMR spectrum are shown; full spectra are available in the ESI.† Conditions: $[\text{L}_1\text{-Br}] = 9$ mM, $[\text{pyridone}] = 10$ mM, $[\text{Cu}^{\text{I}}(\text{CH}_3\text{CN})_4]\text{PF}_6 = 0.3$ mM, CD_3CN , 288 K). (c) Analysis of the catalytic reaction by UV-visible spectroscopy and the time-dependent progression of the absorbance at 542 nm (inset). Immediately upon mixing, the charge-transfer bands associated with I_{Br} are observed, and these features persist until most of the reaction is complete (same experimental conditions as in (b)).

Conclusions

In summary, a series of aryl–Cu^{III}-halide species have been isolated and fully characterized, and these complexes have been shown to undergo H⁺-triggered reductive elimination of aryl halides.¹³ Investigation of the reactivity of the resulting aryl halides with Cu^I has led to two key results: (1) the first observation of aryl halide oxidative addition to Cu^I resulting in formation of an aryl–Cu^{III}-X species and (2) the first experimental evidence consistent with the involvement of an aryl–Cu^{III} intermediate in a catalytic C–N cross-coupling reaction. These observations provide cogent support to the oft-invoked, but heretofore unobserved, redox steps in Ullmann–Goldberg cross-coupling reactions. The two-electron redox reactivity of the Cu^I/Cu^{III} pair is thought to be involved in a wide range of synthetically important reactions mediated by copper.^{8,14} Further mechanistic insights into critical catalytic reaction steps such as the ones described here can provide a foundation for major advances in the application of non-precious-metal catalysts to chemical synthesis.

Acknowledgements

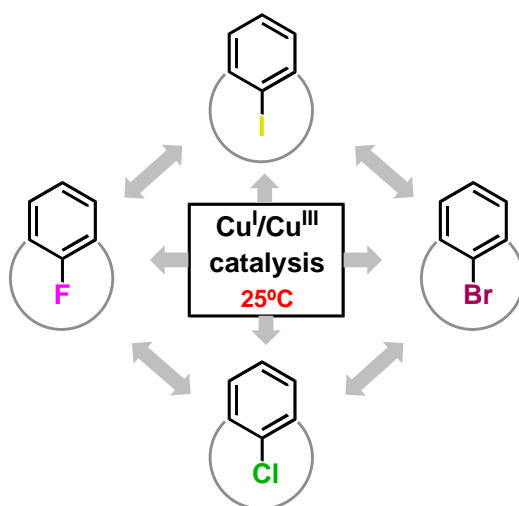
We acknowledge financial support from the MICINN of Spain (CTQ2009–08464/BQU to M.C., CTQ2009–08328 to T.P.) and the US DOE (DE-FG02-05ER15690 to S.S.S.). AC thanks MICINN for a PhD grant. MC thanks ICREA-Academia. We also thank STR's from UdG for NMR, ESI-MS and XRD technical support.

Notes and references

- (a) F. Ullmann and J. Bielecki, *Ber. Dtsch. Chem. Ges.*, 1901, **34**, 2174–2185; (b) F. Ullmann, *Ber. Dtsch. Chem. Ges.*, 1903, **36**, 2382; (c) I. Goldberg, *Ber. Dtsch. Chem. Ges.*, 1906, **39**, 1691–1962.
- (a) I. P. Beletskaya and A. V. Cheprakov, *Coord. Chem. Rev.*, 2004, **248**, 2337–2364; (b) S. V. Ley and A. W. Thomas, *Angew. Chem., Int. Ed.*, 2003, **42**, 5400–5449; (c) F. Monnier and M. Taillefer, *Angew. Chem., Int. Ed.*, 2009, **48**, 6954–6971.
- (a) J. F. Hartwig, *Acc. Chem. Res.*, 2008, **41**, 1534–1544; (b) D. S. Surry and S. L. Buchwald, *Angew. Chem., Int. Ed.*, 2008, **47**, 6338–6361.
- (a) A. A. Kelkar, N. M. Patil and R. V. Chaudhari, *Tetrahedron Lett.*, 2002, **43**, 7143–7146; (b) D. Ma and Q. Cai, *Acc. Chem. Res.*, 2008, **41**, 1450–1460; (c) A. Klapars, X. H. Huang and S. L. Buchwald, *J. Am. Chem. Soc.*, 2002, **124**, 7421–7428; (d) J. F. Marcoux, S. Doye and S. L. Buchwald, *J. Am. Chem. Soc.*, 1997, **119**, 10539–10540; (e) M. Wolter, G. Nordmann, G. E. Job and S. L. Buchwald, *Org. Lett.*, 2002, **4**, 973–976; (f) C. G. Bates, R. K. Gujadhur and D. Venkataraman, *Org. Lett.*, 2002, **4**, 2803–2806; (g) R. K. Gujadhur, C. G. Bates and D. Venkataraman, *Org. Lett.*, 2001, **3**, 4315–4317.
- (a) T. Cohen, J. Wood and A. G. Dietz, *Tetrahedron Lett.*, 1974, **15**, 3555–3558; (b) A. J. Paine, *J. Am. Chem. Soc.*, 1987, **109**, 1496–1502.
- E. R. Strieter, B. Bhayana and S. L. Buchwald, *J. Am. Chem. Soc.*, 2009, **131**, 78–88.
- J. W. Tye, Z. Weng, A. M. Johns, C. D. Incarvito and J. F. Hartwig, *J. Am. Chem. Soc.*, 2008, **130**, 9971–9983.
- (a) X. Ribas, D. A. Jackson, B. Donnadieu, J. Mahía, T. Parella, R. Xifra, B. Hedman, K. O. Hodgson, A. Llobet and T. D. P. Stack, *Angew. Chem., Int. Ed.*, 2002, **41**, 2991–2994; (b) R. Xifra, X. Ribas, A. Llobet, A. Poater, M. Duran, M. Solà, T. D. P. Stack, J. Benet-Buchholz, B. Donnadieu, J. Mahía and T. Parella, *Chem.–Eur. J.*, 2005, **11**, 5146–5156.
- A. H. Roy and J. F. Hartwig, *J. Am. Chem. Soc.*, 2003, **125**, 13944–13945.
- T. Cohen and I. Cristea, *J. Am. Chem. Soc.*, 1976, **98**, 748–753.
- A. Klapars and S. L. Buchwald, *J. Am. Chem. Soc.*, 2002, **124**, 14844–14845.
- L. M. Huffman and S. S. Stahl, *J. Am. Chem. Soc.*, 2008, **130**, 9196–9197.
- B. Yao, D.-X. Wang, Z.-T. Huang and M.-X. Wang, *Chem. Commun.*, 2009, 2899–2901.
- (a) S. H. Bertz, S. Cope, M. Murphy, C. A. Ogle and B. J. Taylor, *J. Am. Chem. Soc.*, 2007, **129**, 7208–7209; (b) H. Hu and J. P. Snyder, *J. Am. Chem. Soc.*, 2007, **129**, 7210–7211; (c) T. Gartner, W. Henze and R. M. Gschwind, *J. Am. Chem. Soc.*, 2007, **129**, 11362–11363; (d) S. H. Bertz, S. Cope, D. Dorton, M. Murphy and C. A. Ogle, *Angew. Chem., Int. Ed.*, 2007, **46**, 7082–7085; (e) X. Ribas, R. Xifra, T. Parella, A. Poater, M. Solà and A. Llobet, *Angew. Chem., Int. Ed.*, 2006, **45**, 2941–2944; (f) R. J. Phipps and M. J. Gaunt, *Science*, 2009, **323**, 1593–1597.

CHAPTER V.

Nucleophilic aryl fluorination and aryl halide exchange mediated by a $\text{Cu}^{\text{I}}/\text{Cu}^{\text{III}}$ catalytic cycle



This chapter corresponds to the following publication:

Alicia Casitas, Mercè Canta, Miquel Solà, Miquel Costas, Xavi Ribas*

J. Am. Chem. Soc. **2011**, 133, 19386–19392

For this publication A. C. performed all experiments. Besides she wrote the manuscript draft and was involved in argumentations and discussions. A. C. has contributed in approximately 80 %.

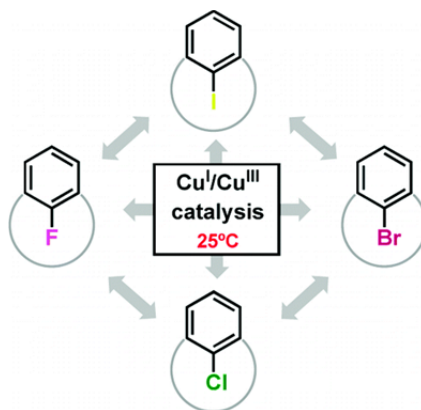
Casitas, A., Canta, M., Solà, M., Costas, M., Ribas, X. "Nucleophilic aryl fluorination and aryl halide exchange mediated by a Cu^I/Cu^{III} catalytic cycle". Journal of the American chemical society. Vol. 133, issue 48 (December 7, 2011) : p. 19386-19392

Copyright © 2011 American Chemical Society

<http://pubs.acs.org/doi/abs/10.1021/ja2058567>

DOI: <http://dx.doi.org/10.1021/ja2058567>

Publication Date (Web): October 25, 2011



Abstract

Copper-catalyzed halide exchange reactions under very mild reaction conditions are described for the first time using a family of model aryl halide substrates. All combinations of halide exchange (I, Br, Cl, F) are observed using catalytic amounts of Cu^I. Strikingly, quantitative fluorination of aryl–X substrates is also achieved catalytically at room temperature, using common F[–] sources, via the intermediacy of aryl–Cu^{III}–X species. Experimental and computational data support a redox Cu^I/Cu^{III} catalytic cycle involving aryl–X oxidative addition at the Cu^I center, followed by halide exchange and reductive elimination steps. Additionally, defluorination of the aryl–F model system can be also achieved with Cu^I at room temperature operating under a Cu^I/Cu^{III} redox pair.

Citing Articles

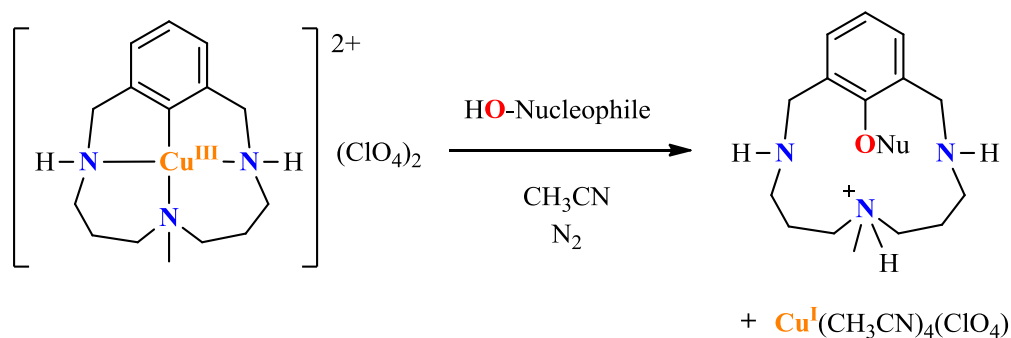
[View all 3 citing articles](#)

Citation data is made available by participants in [CrossRef's](#) Cited-by Linking service. For a more comprehensive list of citations to this article, users are encouraged to perform a search in [SciFinder](#).

This article has been cited by 1 ACS Journal articles

CHAPTER VI.

Observation and mechanistic study of facile C–O bond formation between a well-defined aryl-copper(III) complex and oxygen nucleophiles



This chapter corresponds to the following publication:

Lauren M. Huffman, Alicia Casitas, Marc Font, Mercè Canta, Miquel Costas, Xavi Ribas,*
Shannon S. Stahl*

Chem. Eur. J. **2011**, *17*, 10643-10650

For this publication A. C. studied the reactivity of arylCu^{III} complex with phenols and aliphatic alcohols. She developed copper-catalyzed C–O bond forming reaction in model aryl halide substrates. Besides A. C. wrote the manuscript draft with L.M.H. and was involved in argumentations and discussions. A. C. has contributed in approximately 40 %.

Huffman, L.M., Casitas, A., Font, M., Canta, M., Costas, M., Ribas, X., Stahl, Sh.S.
"Observation and mechanistic study of facile C—O bond formation between a well-defined aryl–Copper(III) complex and oxygen nucleophiles. *Chemistry: a European journal*. Vol. 17, issue 38 (September 12, 2011) : p. 10643–10650

Copyright © 2011 WILEY-VCH Verlag GmbH & Co. KGaA, Weinheim

Article first published online: 16 AUG 2011

<http://onlinelibrary.wiley.com/doi/10.1002/chem.201100608/abstract>

DOI: <http://dx.doi.org/10.1002/chem.201100608>

Abstract

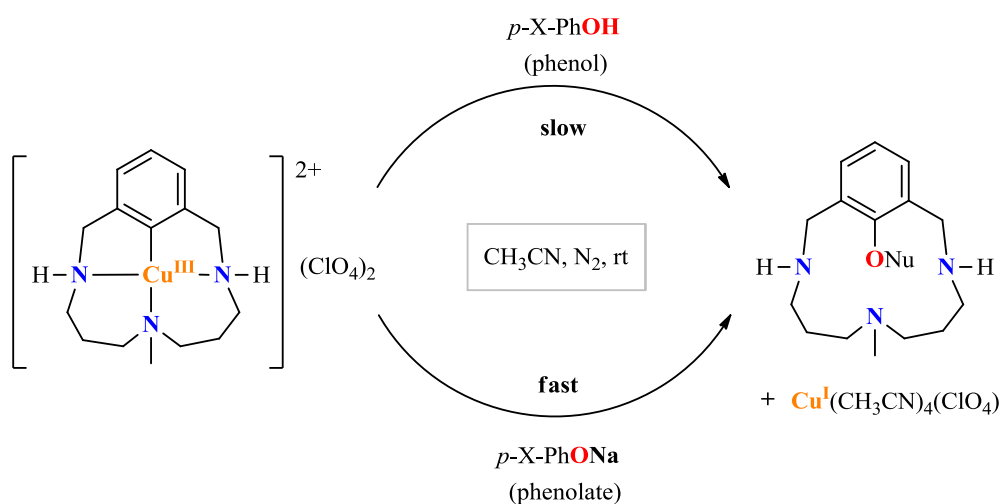
A well-defined macrocyclic aryl–Cu^{III} complex (**2**) reacts readily with a variety of oxygen nucleophiles, including carboxylic acids, phenols and alcohols, under mild conditions to form the corresponding aryl esters, biaryl ethers and alkyl aryl ethers. The relationship between these reactions and catalytic C—O coupling methods is demonstrated by the reaction of the macrocyclic aryl–Br species with acetic acid and *p*-fluorophenol in the presence of 10 mol % Cu^I. An aryl–Cu^{III}–Br species **2**_{Br} was observed as an intermediate in the catalytic reaction. Investigation of the stoichiometric C—O bond-forming reactions revealed nucleophile-dependent changes in the mechanism. The reaction of **2** with carboxylic acids revealed a positive correlation between the log(*k*_{obs}) and the p*K*_a of the nucleophile (less-acidic nucleophiles react more rapidly), whereas a negative correlation was observed with most phenols (more-acidic phenols react more rapidly). The latter trend resembles previous observations with nitrogen nucleophiles. With carboxylic acids and acidic phenols, UV-visible spectroscopic data support the formation of a ground-state adduct between **2** and the oxygen nucleophile. Collectively, kinetic and spectroscopic data support a unified mechanism for aryl–O coupling from the Cu^{III} complex, consisting of nucleophile coordination to the Cu^{III} center, deprotonation of the coordinated nucleophile, and C—O (or C—N) reductive elimination from Cu^{III}.

Keywords:

- C—O bond formation;
- copper;
- homogeneous catalysis;
- reductive elimination

CHAPTER VII.

Aryl-O reductive elimination from reaction of well-defined aryl-copper(III) species with phenolates: the importance of ligand reactivity



This chapter corresponds to the following publication:

Alicia Casitas, Nikolaos Ioannidis, George Mitrikas, Miquel Costas, Xavi Ribas*
Dalton Trans., **2011**, 40, 8796-8799

For this publication A. C. performed all experiments and she prepared the samples for EPR experiments. Besides she wrote the manuscript draft and was involved in argumentations and discussions. A. C. has contributed in approximately 80%.

Cite this: *Dalton Trans.*, 2011, **40**, 8796

www.rsc.org/dalton

PAPER

Aryl–O reductive elimination from reaction of well-defined aryl–Cu^{III} species with phenolates: the importance of ligand reactivity†

Alicia Casitas,^a Nikolaos Ioannidis,^b George Mitrikas,^{*b} Miquel Costas^a and Xavi Ribas^{*a}

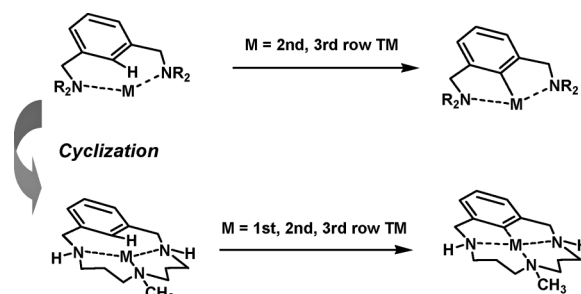
Received 14th March 2011, Accepted 12th April 2011

DOI: 10.1039/c1dt10428d

Well-defined aryl–Cu^{III} species undergo rapid reductive elimination upon reaction with phenolates (PhO[−]), to form aryl–OPh cross-coupling products. Kinetic studies show that the reaction follows a different mechanistic pathway compared to the reaction with phenols. The pH active cyclized pincer-like ligand undergoes an initial amine deprotonation that triggers a faster reactivity at room temperature. A mechanistic proposal for the enhanced reactivity and the role of EPR-detected Cu^I species will be discussed in detail.

Fundamental mechanistic knowledge of the relevant redox steps in Cu-catalyzed Ullmann-type aryl–heteroatom cross-coupling chemistry is still scarce.^{1–4} These classic reactions have gained renewed interest due to cost and toxicity benefits in comparison to Pd-based methodologies for the synthesis of key intermediates in the pharmaceutical industry.^{5,6} Focusing in the copper-based cross-coupling reactions to form aryl–O bonds,⁷ we have recently reported a detailed mechanistic investigation on the reactivity of well-defined aryl–Cu^{III} species system with HO-nucleophiles (HO-Nuc). These reactions afford corresponding aryl–O-Nuc products under mild conditions, *via* a reductive elimination path.⁸ The aryl–Cu^{III} species (complex **2**) under study has been synthesized by copper(II) metallation at the aromatic ring of the triazamacrocyclic ligand (**1**) *via* a disproportionation pathway.^{9,10} Interestingly, ligand **1** can be considered as a cyclized evolution of typical NCN-pincer-like complexes, that are usually prepared by metallation with 2nd and 3rd row transition metals, more prone to direct C–H activation.¹¹ The cyclized ligand **1** thus shows the ability of coordinating a first row transition metal ion such as Cu or Ni in close proximity to the aromatic C–H bond. This feature enables easy C–H bond cleavage under very mild conditions (Scheme 1).⁹

Furthermore, increasing interest is devoted to reactivity with multifunctional ligands that are not mere spectators, but on the contrary, that respond to effects such as changes in pH.¹² In this paper we show a diverse reactivity of the cyclized pincer-like complex **2**, in response to the nucleophile Brønsted base nature; the reaction of **2** with different *para*-substituted sodium phenolate (*p*X-PhONa) substrates substantially differs from that



Scheme 1

with the corresponding phenols, despite both type of reactions afford the same biaryl ether products.⁸ Unlike reactions with phenols, for which reaction intermediates are not observed, and are kinetically described as simple bimolecular **2**/HO-Nuc reactions, the reaction of **2** with phenolates involves formation of a purple intermediate solution and a notable enhancement of aryl–OPh formation reaction rates. The chemical nature of the reaction intermediates, as well as the pH-non-innocence role of the ligand is discussed.

The reaction of **2** with equimolar amounts of several sodium phenolates was monitored by UV-vis spectroscopy. Phenolate addition caused the instantaneous formation of a deep-violet species **3** ($\lambda_{\text{max}} = 545 \text{ nm}$, $\epsilon = 2040 \text{ M}^{-1} \text{ cm}^{-1}$). Compound **3** decayed without accumulation of any additional intermediate species, affording the corresponding aryl–O biaryl ethers in quantitative yields (Fig. 1 and Table 1), as ascertained by ¹H NMR, UV-vis and ESI-MS. The formation of the violet species **3** is not observed for the reaction of **2** with the corresponding phenols.⁸ In addition, species **3** decays faster than complex **2**, upon reaction with phenol substrates (Fig. 2), under analogous experimental conditions. The latter observations suggest that the two reactions occur through distinct mechanistic pathways, albeit for the obtention of the same biaryl ether and Cu^I final products. When a series of *p*X-PhONa were employed as nucleophiles, relative reaction rates correlate

^aDepartament de Química, Universitat de Girona, Campus de Montilivi, 17071, Girona, Catalonia, Spain. E-mail: xavi.ribas@udg.edu; Fax: +34-972418150; Tel: 972-418262

^bInstitute of Materials Science, NCSR “Demokritos”, 15310, Athens, Greece. E-mail: mitrikas@ims.demokritos.gr; Fax: + (30-210-6503381); Tel: + (30-210-6503304)

† Electronic supplementary information (ESI) available: Experimental details. See DOI: 10.1039/c1dt10428d

Table 1 Reactivity of complex **2** with 1 equiv. of *p*-X-phenolate substrates (X = OCH₃, Cl, F, CN and NO₂) to afford the corresponding biaryl ethers ([**2**] = 1.2 mM, 25 °C, N₂ atmosphere). The reactivity of **2** with three corresponding phenols is included for comparison

Substrate	Time (min)	Aryl–O product yield (%)
<i>p</i> -OCH ₃ -phenolate	10	100
<i>p</i> -OCH ₃ -phenol	100	100
<i>p</i> -F-phenolate	25	100
<i>p</i> -F-phenol	200	100
<i>p</i> -CN-phenolate	15	100
<i>p</i> -CN-phenol	125	100
<i>p</i> -NO ₂ -phenolate	—	100 ^a
<i>p</i> -Cl-phenolate	—	100 ^a

^a [**2**] = 0.6 mM, T = 10 °C.

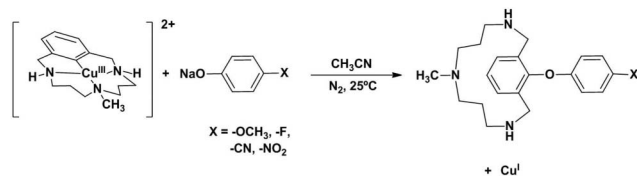


Fig. 1 Reaction of **2** with a family of *para*-substituted phenolates (Na salt) to afford the corresponding biaryl ether coupling products and Cu^I.

with the electronic nature of X, and electron withdrawing groups provide the fastest reaction rates (see Fig. S4†).

Mechanistically, the aryl–O coupling reaction between **2** and phenols consists of a reductive elimination from a transient, spectroscopically and kinetically detected aryl–Cu^{III}–(phenol) species (*i.e.* for *p*CN-phenol) to afford corresponding biaryl ethers and Cu^I.⁸ On the contrary, the distinct formation of the violet species **3** upon reaction of **2** with *p*X-PhONa, as well as the substantially faster reaction rates observed, prompted us to undertake a detailed study in order to gain more insight into the mechanistic pathway. The first question to resolve was the identity of species **3**. UV-vis analysis show that the UV-vis spectroscopic features of **3**, prepared by reaction with 1 equiv. *p*X-PhONa (X = OCH₃, Cl, F, CN and NO₂), are the same, irrespective of the nature of *p*X-PhONa. On the other hand, the addition of bases such as Et₃N or Proton Sponge[®] also caused the formation of **3**, albeit up to 5–7 equiv. of the base were necessary for full formation of **3** (see Supp Info†). Furthermore, the reaction of **2** with Proton Sponge[®] followed by the addition of 1 equiv. of *p*F-phenol renders exactly the same decay profile, monitored at λ = 555 nm, to the one observed for the reaction with 1 equiv. of *p*F-PhONa (Fig. 2a). Altogether, the data suggest that complex **2** suffers a deprotonation of one of the secondary amines (Scheme 2). In this regard, the intense violet chromophore may tentatively be assigned to LMCT transitions from the amido N to the Cu^{III} center. Indeed, similar UV-vis spectroscopic features have been described by Margerum and co-workers to arise after amine deprotonation in Cu^{III}–peptide complexes.^{13–15}

In order to prove the reversibility of this reaction we conducted a UV-vis experiment to monitor the spectrum upon subsequent addition of *p*F-phenolate and triflic acid (Fig. 3). The experiment was performed at –30 °C to minimize evolution of **3** towards the formation of the aryl–O product. The addition of *p*F-PhONa causes the instantaneous formation of species **3**, and subsequent addition of triflic acid restores complex **2**. The phenolate/acid

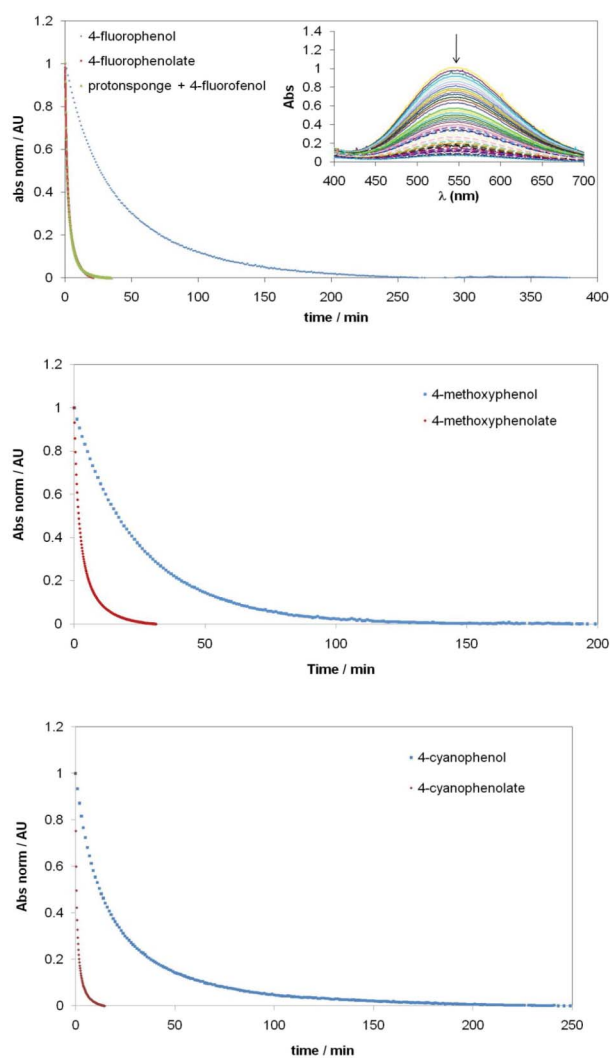
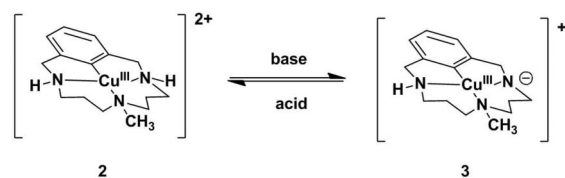


Fig. 2 Decay profiles (abs normalized vs. time) for the 550 nm band for the reaction of equimolar amounts of **2** and different *p*X-PhONa (and corresponding phenols): (a) 1 equiv. *p*F-PhONa; 1 equiv. *p*F-PhOH (inset: 550 nm band decay); 3 equiv. Proton Sponge[®] + 1 equiv. *p*F-PhOH; (b) 1 equiv. *p*MeO-PhONa; 1 equiv. *p*MeO-PhOH; and (c) 1 equiv. *p*CN-PhONa; 1 equiv. *p*CN-PhOH. (Conditions: [**2**] = 1.2 mM, 25 °C, N₂ atmosphere.)



Scheme 2

cycle can be repeated several times, and only a minor loss of 6% for complex **2** (at 450 nm) is observed after 3 cycles. Similarly, the recovery of complex **3** after three cycles is up to 94%. The minor decomposition observed may be caused by ongoing formation of the aryl–O coupling product.

The equimolar reaction of **2** and sodium *p*F-phenolate to form **3** was monitored by ¹H NMR at –30 °C (Supp. Info†). The addition of 1 equiv. of *p*F-PhONa caused important changes in

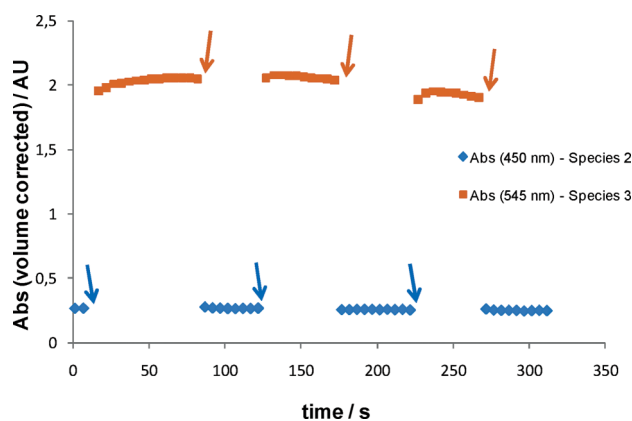


Fig. 3 UV-vis monitoring of the consecutive additions of 1 equiv. of *p*F-PhONa and triflic acid to a solution of **2**. Blue arrows indicate addition of phenolate; orange arrows indicate addition of triflic acid. $[2]_{\text{initial}} = 1 \text{ mM}$, $-30 \text{ }^\circ\text{C}$.

the spectrum with respect to that of the diamagnetic Cu^{III} species **2**: signals corresponding to protons nearby the deprotonated secondary amine group showed a broadening (benzylic CH_2 at 4.25 ppm; $\alpha\text{-CH}_2$ at 2.95 ppm), whereas the rest of the signals remained unmodified. Similarly, when species **3** was generated with a base (6 equiv. of Proton Sponge[®] at $-30 \text{ }^\circ\text{C}$), the same signals were affected (Supp. Info[†]). Indeed, the same signals suffered slight up-field shifts and further broadening upon gradual warming up to $20 \text{ }^\circ\text{C}$, but the initial spectrum was recovered if the solution was cooled back to low temperature. Bi-dimensional correlations indicated also the disappearance of ^{13}C peaks corresponding to the affected CH_2 moieties in **3**. A reasonable explanation to these observations is that amine deprotonation allows for different conformations (flipping) at the deprotonated amine, giving rise to a severe broadening effect of the $\alpha\text{-CH}_2$ signals.

A low temperature ^1H NMR experiment corresponding to the reaction of **2** with *p*F-PhONa also showed that species **3** is not stable and gradual fading of the signals assigned to **3** was observed, along with the growth of signals corresponding to *p*F-OPh-aryl coupling product (Fig. S10[†]). No accumulation of other intermediate species was observed along this transformation. Signals corresponding to **3** account for $\sim 90\%$ of complex mass balance, and thus we suspected that another NMR silent copper-containing species, namely **3'**, could be present.

The chemical nature of species **3'** is unclear. We conducted an extensive cw and pulse-EPR study to shed some light into its chemical nature. Reaction samples of **2** (44 mM) and 4 equiv. of Proton Sponge[®] were mixed under N_2 at $0 \text{ }^\circ\text{C}$, stirred for a few seconds and immediately frozen in an EPR tube. X-band (9.4 GHz) and Q-band (34.6 GHz) measurements were performed at $T = 120 \text{ K}$ (see Fig. 4). The EPR spectra in both mw frequencies can be satisfactorily simulated with the following spin Hamiltonian parameters: $g_x = 2.0384$, $g_y = 2.0215$, $g_z = 2.1147$; $A_x = 124 \text{ MHz}$, $A_y = 447 \text{ MHz}$, $A_z = 134 \text{ MHz}$. Although g and A tensors are typical for $S = \frac{1}{2}$ Cu^{II} species, the orientation of the tensors is unusual: the large hyperfine value 447 MHz is along g_y and not g_z , as is the case for most common Cu^{II} EPR signals. However, this behavior can be rarely found in the literature.¹⁶ For instance, wild-type *stellacyanin*, a blue copper protein, shows a roughly axial hyperfine tensor A , but the largest hyperfine splitting (hfs) is along

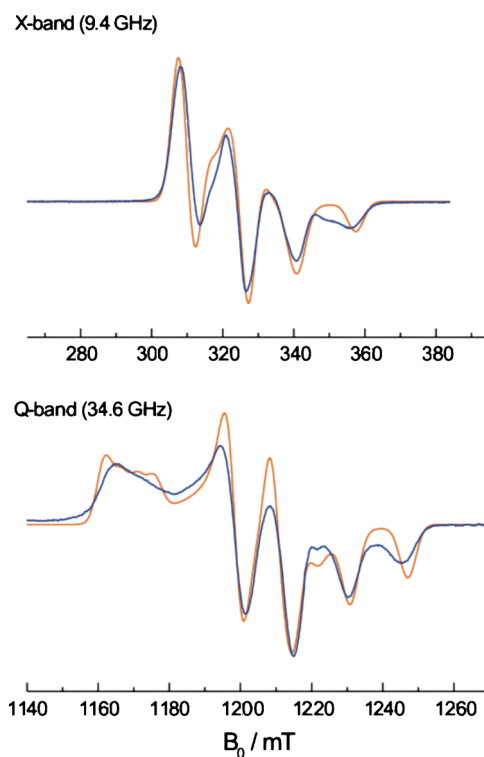


Fig. 4 X- and Q-band EPR spectra of **3** in frozen acetonitrile solution ($T = 120 \text{ K}$). Blue traces: experiment; orange traces: simulation. For simulation parameters see text.

the minimum g value, that is assigned to a tetrahedral or nearly tetrahedral geometry for Cu^{II} .^{17–19}

Some insight about the atoms surrounding the Cu^{II} ions could be obtained by ENDOR and HYSCORE spectra (see Supp. Info[†]). The ENDOR study showed two strongly-coupled nitrogen atoms, with $A = 12 \text{ MHz}$ and $A = 46 \text{ MHz}$ hyperfine coupling constants, respectively. Additionally, HYSCORE spectra allowed for the detection of a third weakly ($A = 4 \text{ MHz}$) coupled N atom. The latter findings could be tentatively rationalized with a Cu^{II} coordination sphere consisting of two strongly bound amine moieties, as well as a third weakly coordinated N belonging to a CH_3CN molecule. Since a tetrahedral geometry is deduced from spin Hamiltonian parameters, and the macrocyclic ligand appears incapable of adapting to this geometry, while keeping the four N atoms bound to the metal, an external CH_3CN ligand is proposed to be bound to the metal center, leaving one of the macrocyclic secondary amine groups as non-coordinated. Moreover, spectra also showed the existence of two weakly coupled protons, one at $A_1 = 6 \text{ MHz}$ and another one at $A_2 = 14 \text{ MHz}$ with modest anisotropy (agreement between ENDOR and HYSCORE). An additional proton coupling with considerable anisotropy is found, with a short $\text{Cu}^{\text{II}} \cdots \text{H}$ distance of 2.34 \AA (assuming a 100% spin density at Cu^{II}).

Despite the uncertainty on the nature of **3'**, since it is a $S = \frac{1}{2}$ system, we could perform a reliable quantification by comparison with the signal of a well-characterized $\text{Cu}^{\text{II}}(\text{acac})_2$ complex (see Supp. Info[†]). We noticed that the formation of the EPR active species **3'** is only about the 2% of the starting copper content for base treatment of low concentration of **2**, whereas it increases up to 11% for higher concentrations of **2**.

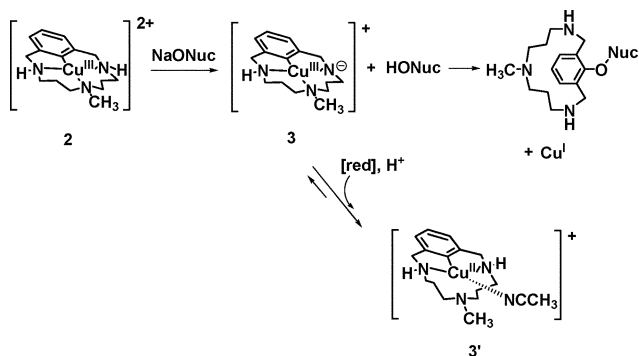


Fig. 5 Proposed mechanism for the reactivity of aryl-Cu^{III} species **2** with *pX*-phenolates (sodium salt).

Given the above reported data, we can tentatively propose the mechanism depicted in Fig. 5 for the equimolar reaction of **2** with *pX*-PhONa. The first step consists of the deprotonation of one secondary amine by the basic phenolate to yield **3** and the corresponding phenol. At this point, deprotonated Cu^{III} complex **3** interacts with *in situ* formed phenol substrate and undergoes reductive elimination to form the final aryl-O and Cu^I products. This reaction is much faster than that of complex **2** with phenols. The proposal of a reductive elimination step is consistent with several examples in the literature of reactions between well-defined aryl-Cu^{III} species and N- and O-nucleophiles,^{8,20,21} as well as with aryl-halide reductive elimination examples at well-defined aryl-Cu^{III}-halides.²² Furthermore, reductive elimination at aryl-Cu^{III} species is also proposed in mechanistic studies on Ullmann-like coupling reactions.^{4,7,23,24}

In addition, in a side reaction (2–11%), **3** can undergo 1e⁻ reduction to form an aryl-Cu^{II}N₃ species **3'** with a tetrahedral coordination geometry. The origin of the e⁻ could not be ascertained, but possible sources could be Cu^I, PhOH and PhO⁻ species, all of them present in the reaction mixture. Whatever its origin, since aryl-ONuc products are obtained in quantitative yield, we conclude that **3'** is also consumed in the reaction, and that side reactivity of **3** to form **3'** must be reversible.


Summarizing, we have demonstrated that the reactivity of well-defined aryl-Cu^{III} species in front of phenol-type nucleophiles differs substantially from the reactivity with corresponding phenolates, and a significant enhancement is found to produce the same aryl-O coupling product. Mechanistic studies show that easy deprotonation of coordinated secondary amines is responsible of the intense LMCT band at 545 nm; indeed, this pH-dependent reactivity of the pincer-like coordinated ligand somewhat enhances its reactivity. The origin of such enhancement is not clearly understood, and is currently been studied computationally. A parallel reaction path for deprotonated species **3** affords minor quantities of an EPR-active species **3'**. The present observations of a substantial enhancement in the cross-coupling reactivity observed upon ligand deprotonation suggests that this might be

a strategy to take into account in the design of more efficient Cu^{III}-mediated C–heteroatom bond-forming reactions.

We thank S. S. Stahl and L. M. Huffman for fruitful discussions. We also thank T. Parella for help on the NMR analysis. We acknowledge financial support from the MICINN of Spain (CTQ2009-08464/BQU to M.C. and CTQ2008-03077/BQU to M.S.), the DIUE of Catalonia (2009SGR637). A.C. thanks MICINN for a PhD grant. M.C. and X.R. thank Generalitat de Catalunya for ICREA Academia Awards and 2009 SGR637. We also thank STR-UdG for NMR and ESI-MS technical support.

Notes and references

- 1 I. Goldberg, *Ber. Dtsch. Chem. Ges.*, 1906, **39**, 1691–1696.
- 2 F. Ullmann, *Ber. Dtsch. Chem. Ges.*, 1903, **36**, 2389.
- 3 F. Ullmann and J. Bielecki, *Chem. Ber.*, 1901, **34**, 2174.
- 4 E. Sperotto, G. P. M. v. Klink, G. v. Koten and J. G. d. Vries, *Dalton Trans.*, 2010, **39**, 10338–10351.
- 5 I. P. Beletskaya and A. V. Cheprakov, *Coord. Chem. Rev.*, 2004, **248**, 2337–2364.
- 6 G. Evano, N. Blanchard and M. Toumi, *Chem. Rev.*, 2008, **108**, 3054–3131.
- 7 F. Monnier and M. Taillefer, *Angew. Chem., Int. Ed.*, 2009, **48**, 6954–6971.
- 8 L. M. Huffman, A. Casitas, M. Font, M. Canta, M. Costas, X. Ribas and S. S. Stahl, *Chem. Eur. J.*, 2011, DOI: 10.1002/chem.201100608.
- 9 X. Ribas, C. Calle, A. Poater, A. Casitas, L. Gómez, R. Xifra, T. Parella, J. Benet-Buchholz, A. Schweiger, G. Mitrikas, M. Solà, A. Llobet and T. D. P. Stack, *J. Am. Chem. Soc.*, 2010, **132**, 12299–12306.
- 10 X. Ribas, D. A. Jackson, B. Donnadieu, J. Mahia, T. Parella, R. Xifra, B. Hedman, K. O. Hodgson, A. Llobet and T. D. P. Stack, *Angew. Chem., Int. Ed.*, 2002, **41**, 2991–2994.
- 11 M. Albrecht and G. van Koten, *Angew. Chem., Int. Ed.*, 2001, **40**, 3750–3781.
- 12 R. H. Crabtree, *Science*, 2010, **330**, 455–456.
- 13 T. A. Neubecker, S. T. Kirksey, K. L. Chellappa and D. W. Margerum, *Inorg. Chem.*, 1979, **18**, 444–448.
- 14 S. T. Kirksey and D. W. Margerum, *Inorg. Chem.*, 1979, **18**, 966–970.
- 15 The same violet species **3** is obtained by reaction of **2** with sodium acetate, no deprotonation is achieved by treating aryl-Cu^{III}-halide species with base due to the enhanced stability (see ref. 8); furthermore, the addition of one equiv. of Cl⁻ to **3** forms quenches immediately its violet color and forms aryl-Cu^{II}-Cl (see ref. 22).
- 16 C. P. Keijzers, G. F. M. Paulussen and E. D. Boer, *Mol. Phys.*, 1975, **29**, 973–1006.
- 17 J. E. Roberts, T. G. Brown, B. M. Hoffman and J. Peisach, *J. Am. Chem. Soc.*, 1980, **102**, 825–829.
- 18 A. Romero, C. W. Hoytink, H. Nar, R. Huber, A. Messerschmidt and G. W. Canters, *J. Mol. Biol.*, 1993, **229**, 1007–1021.
- 19 S. D. George, L. Basumallick, R. K. Szilagyi, D. W. Randall, M. G. Hill, A. M. Nersissian, J. S. Valentine, B. Hedman, K. O. Hodgson and E. I. Solomon, *J. Am. Chem. Soc.*, 2003, **125**, 11314–11328.
- 20 L. M. Huffman and S. S. Stahl, *J. Am. Chem. Soc.*, 2008, **130**, 9196–9197.
- 21 A. E. King, L. M. Huffman, A. Casitas, M. Costas, X. Ribas and S. S. Stahl, *J. Am. Chem. Soc.*, 2010, **132**, 12068–12073.
- 22 A. Casitas, A. E. King, T. Parella, M. Costas, S. S. Stahl and X. Ribas, *Chem. Sci.*, 2010, **1**, 326–330.
- 23 H.-Z. Yu, Y.-Y. Jiang, Y. Fu and L. Liu, *J. Am. Chem. Soc.*, 2010, **132**, 18078–18091.
- 24 G. O. Jones, P. Liu, K. N. Houk and S. L. Buchwald, *J. Am. Chem. Soc.*, 2010, **132**, 6205–6213.



CHAPTER VIII.
General Discussion

VIII.1. General Discussion

ArylCu^{III}-halide complexes **1_x** and **2_x** have been synthesized based in a previous family of complexes using triazamacrocyclic ligands **L₁-H** and **L₂-H** that stabilized copper in high oxidation state (Figure VIII.1). These complexes are obtained through a C-H bond activation reaction with copper(II) salts that disproportionate to yield arylCu^{III}-halide complex and **[LH-H]⁺** and Cu^I products. In non-coordinating solvents and under oxygen atmosphere, the Cu^I can be oxidized to Cu^{II} in order to resume the disproportionation reaction and to increase the final yield of arylCu^{III}-halide complexes above 80%. These complexes have been characterized by means of NMR and UV-Vis spectroscopy, ESI-MS spectrometry, Cyclic Voltammetry and X-Ray diffraction analysis, and constitute the first well-defined and isolated aryl-Cu^{III}-halide described in the literature. Pentacoordinated Cu^{III} complex adopts a square pyramidal geometry where the halogen is bound to the metal center in the axial position.

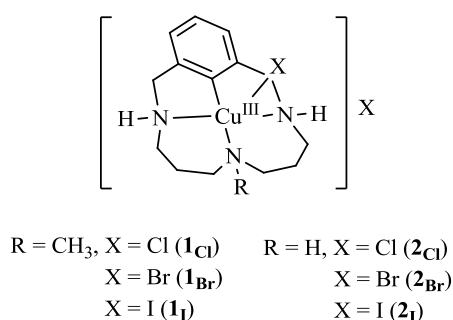


Figure VIII.1. Family of arylCu^{III}-halide complexes synthesized within triazamacrocyclic ligands.

These arylCu^{III}-halide complexes **1_x** and **2_x** undergo C_{aryl}-halogen reductive elimination upon addition of a proton source such as triflic acid to form **[L-X-H]⁺** and Cu^I products. Kinetic analysis of the decay of the arylCu^{III}-X LMCT bands showed first-order behavior. Rate constants measured follow the relative C-halogen strength, being faster for the formation of stronger C-halogen bond (Cl > Br > I). Based in experimental and computational data, we propose the initial formation of an adduct between the triflic acid and the arylCu^{III}-halide complex. In the next step, the protonation and subsequent decoordination of an amine of the complex causes the formation of a tetracoordinated Cu^{III} intermediate from which C-halogen reductive elimination has a very low energetic barrier. Calculated energy barriers from reaction pathways considering protonation at secondary and tertiary amines indicated that protonation is rate-limiting and both pathways are plausible since they only differ in 2.2 kcal/mol.

After the formation of **[L-X-H]⁺** and Cu^I products from acid triggered C-halogen reductive elimination reaction from **1_x** and **2_x**, the addition of base promotes the reversible

oxidative addition reaction to form again arylCu^{III}-halide complexes. The relevance of these findings sits on the uniqueness of this system to prove the two-electron Cu^I/Cu^{III} redox chemistry of the oxidative addition and reductive elimination fundamental steps.

We have studied copper-catalyzed C-N bond forming reaction for the conversion of aryl bromide substrate **L₁-Br** and pyridone into **L₁-Nu-HBr** at room temperature. By means of ¹H-NMR and UV-Vis spectroscopy arylCu^{III}-bromide complex **1_{Br}** has been detected in a steady-state concentration until the consumption of initial substrate **L₁-Br**. This result implies that **1_{Br}** complex is involved in the rate-determining step of the reaction. Therefore, we propose a mechanism involving a very facile oxidative addition to form arylCu^{III}-bromide complex **1_{Br}**, followed by ligand exchange in the presence of excess of nitrogen nucleophile and C-N reductive elimination. This is the first example of a catalytic Ullmann-type coupling where an arylCu^{III}-halide intermediate has been identified.

We have also developed C_{aryl}-halogen reductive elimination from **1_X** complexes by using external ligands such as 1,10-phenanthroline. This result suggests the existence of a reactant-displaced between arylCu^{III}-halide complexes and the corresponding aryl-X...Cu^I species in solution. In this context, we have developed copper-catalyzed halide exchange reactions in aryl halide model substrates **L₁-X** (X = Cl, Br, I), towards both lighter and heavier halides, in the presence of excess of halide salt (MY) at room temperature. The reaction mechanism is based in a Cu^I/Cu^{III} catalytic cycle that involves oxidative addition, halide exchange and C-halogen reductive elimination steps. Although the rate-limiting reductive elimination step is favored towards the formation of a stronger C-halogen bond, the halide exchange towards weaker C-halogen bond can be accomplished by taking advantage of the precipitation of the exchanged halide salt. This chemistry affords new mechanistic insight in halide exchange reactions, and adds to the previously copper-catalyzed reactions developed by Buchwald in 2002.¹

We have developed stoichiometric C_{aryl}-F bond forming reactions from arylCu^{III}-halide complexes by using excess of AgF as nucleophilic fluoride source in acetonitrile at room temperature. Moreover, catalytic fluorination reactions have also been developed in model aryl halide substrates **L₁-X** (X = Cl, Br) in the presence of AgF and catalytic amounts of copper(I). Exquisite care of the experimental conditions is crucial to obtain moderate yields, and special attention has been paid on the slow AgF addition due to the high basicity of fluoride anions. Under experimental conditions, arylCu^{III}-fluoride complex has not been detected because halide exchange step is rate-determining, even though computational studies have supported a very low activation barrier for the reductive elimination pathway from a putative arylCu^{III}-fluoride complex. Quantitative copper-catalyzed nucleophilic fluorination has also been obtained in aryl halide models **L₅-X** (X = Cl, Br), which contains all tertiary amines. In this case, reactions were carried out in a mixture acetone:acetonitrile (3:1) at 25 °C. Based in a Cu^I/Cu^{III} catalytic cycle, the presence of less σ-donating tertiary amines, in comparison to secondary amines of ligand **L₁-X**, precludes **L₅-X** oxidative addition to Cu^I in coordinating solvents such as acetonitrile. The

pioneering nucleophilic fluorination catalyzed by copper described here is unprecedented, and may open the door to develop new copper-catalyzed nucleophilic fluorination methodologies for usual aryl halide substrates. Until now, only Pd-based methodologies had been very recently reported by Buchwald and Ritter.^{2,3}

Furthermore, careful choice of the experimental conditions allowed us to develop defluorination reaction of ligand **L₁-F** mediated by equimolar amounts of copper(I) triflate in acetone at room temperature, in the presence of chloride anions. The arylCu^{III} complex formed by oxidative addition in non-coordinating solvent is trapped by chloride anions to form the more stable arylCu^{III}-Cl complex **1_{Cl}**, which precipitates from the solution displacing the reaction. Usually, aryl fluoride activation had been reported with Ni and Pd catalysts,⁴ but no example was known for a copper-mediated process.

On the context of Ullmann cross-couplings, we have explored the reactivity of arylCu^{III} complex **1_{ClO₄}** with external heteroatom nucleophiles. We have focused in C-O bond forming reactions using oxygen nucleophiles (carboxylic acids, phenols and aliphatic alcohols) and the results obtained have been compared with the previous stoichiometric C-N bond forming reactions described by Huffman and Stahl.⁵ The reaction between **1_{ClO₄}** with carboxylic acids affords quantitative formation of the C-O coupled product at room temperature in less than 10 minutes. Complex **1_{ClO₄}** reacts quantitatively with phenols and in moderate yields with acidic aliphatic alcohols but at higher temperature (50 °C).


Mechanistic studies have shown that the cleavage of the O-H bond of the nucleophile, reflected by the pK_A, has an important role in the reaction mechanism. Furthermore, we have observed zero order dependence of the reaction rate on carboxylic acid concentration whereas at high carboxylic acid concentration there is an inhibitory effect. In contrast, the more acidic phenols react faster with the exception of *p*-nitrophenol that showed a similar behavior as carboxylic acids. Besides, first-order dependence on phenol concentration is observed with *p*-methoxyphenol in comparison to saturation dependence with *p*-cyanophenol and inhibition with *p*-nitrophenol. Taking into account the experimental data we propose a mechanism that consists in the formation of an arylCu^{III}/HO-Nu adduct (detected by UV-vis spectroscopy), deprotonation and reductive elimination steps. A pK_A dependent change in the rate-determining step has been proposed based on all experimental data.

Moreover, copper-catalyzed C-O bond forming reactions between model aryl halide substrate **L₁-Br** and oxygen nucleophiles (acetic acid and *p*-fluorophenol) have been developed. ArylCu^{III}-bromide complex **1_{Br}** is observed as the resting state of the reaction by *in situ* UV-Vis spectroscopy. Therefore, the rate-determining step is the ligand exchange in the arylCu^{III}-halide complex. Altogether, C-O bond forming reactions catalyzed by copper in **L₁-X** model substrates demonstrate the feasibility of these couplings through a Cu^I/Cu^{III} redox cycle, that occur at very mild conditions.

Finally, we have explored the reaction between arylCu^{III} complex **1**_{ClO₄} with deprotonated oxygen nucleophiles, i.e. phenolates, to form the corresponding C-O coupling products. We have observed that coordinated secondary amines in **1**_{ClO₄} are prone to deprotonation when the nucleophile has also basic properties. Therefore, species **3** have been characterized by UV-vis and NMR spectroscopy under reaction conditions, which are also obtained with a non-coordinating base such as Proton-sponge[®]. The reaction rate with phenolate substrates is faster in comparison to phenols, supporting that amines of the ligand in complex **1**_{ClO₄} are involved in the C-O bond forming pathway. Moreover, we have detected paramagnetic copper(II) complex **3'** by EPR spectroscopy, in very low concentration, which is in equilibrium with complex **3**. We support a mechanism that involves species **3** in the C-O coupling reaction, even though we cannot discard the involvement of species **3'** in a competitive mechanism.

VIII.2. References

1. Klapars, A.; Huang, X. H.; Buchwald, S. L. *J. Am. Chem. Soc.* **2002**, *124*, 7421.
2. Watson, D. A.; Su, M.; Teverovskiy, G.; Zhang, Y.; García-Fortanet, J.; Kinzel, T.; Buchwald, S. L. *Science* **2009**, *325*, 1661.
3. Furuya, T.; Benitez, D.; Tkatchouk, E.; Strom, A. E.; Tang, P.; Goddard-III, W. A.; Ritter, T. *J. Am. Chem. Soc.* **2010**, *132*, 3793.
4. Sun, A. D.; Love, J. A. *Dalton Trans.* **2010**, *39*, 10362.
5. Huffman, L. M.; Stahl, S. S. *J. Am. Chem. Soc.* **2008**, *130*, 9196.



CHAPTER IX.
General Conclusions

IX. General Conclusions

- We have synthesized a family of arylCu^{III}-halide complexes, **1_X** and **2_X** (X = Cl, Br, I), based on triazamacrocyclic ligands **L₁-H** and **L₂-H** that allow the stabilization of copper in high oxidation state. Pentacoordinated Cu^{III} complex adopts a square-pyramidal geometry where the halogen is bound to the metal center in the axial position.
- ArylCu^{III}-halide complexes undergo C_{aryl}-halogen reductive elimination upon addition of a proton source such as triflic acid. Rate constants measured showed that the formation of a stronger C-halogen bond is faster. Computational studies considering protonation to both tertiary and secondary amine have shown that protonation step is rate-limiting. Decoordination of the protonated amine leads to the formation of a tetracoordinated Cu^{III} intermediate from which reductive elimination has a very low energetic barrier.
- Oxidative addition of Cu^I to aryl halide model systems **L₁-X** (X = Cl, Br, I) is a very favorable reaction that affords quantitative formation of the corresponding arylCu^{III}-halide complex. Computational DFT studies have shown that this reaction is energetically downhill, with an insignificant energy barrier.
- We have explored copper-catalyzed halide exchange reactions in aryl halide model substrates **L₁-X** (X = Cl, Br, I) in the presence of excess of halide salt (MY) at room temperature. The halide exchange reactions towards heavier and lighter halides are achieved in moderate to high yields. The experimental observations agree with reaction mechanism involving an oxidative addition of Cu^I to the aryl halide substrate **L₁-X** to afford arylCu^{III}-X complex; then, halide exchange step followed by reductive elimination releases the aryl halide product **L₁-Y**. Reductive elimination is the rate-limiting step, which is favored towards the formation of a stronger C-halogen bond. Nevertheless, the halide catalytic exchange towards heavier halides can be obtained by taking advantage of the precipitation of the exchanged halide salt.
- Stoichiometric nucleophilic C_{aryl}-F bond forming reaction from arylCu^{III}-halide complexes has been accomplished by using silver fluoride at room temperature. Catalytic fluorination reactions have also been developed in model aryl halide substrates **L₁-X** (X = Cl, Br) in the presence of AgF and catalytic amounts of Cu^I. In these reactions, halide exchange step is rate-determining, precluding the detection of arylCu^{III}-fluoride complex. Computational studies have supported a reductive elimination pathway from a putative arylCu^{III}-fluoride complex, which has a low activation barrier.

- Catalytic fluorination has been accomplished in good to quantitative yields for a set of model aryl halide substrates L_1-X and L_5-X ($X = Cl, Br$), in the presence of AgF and catalytic amounts of copper at room temperature. Exquisite care of the experimental conditions are crucial to obtain quantitative transformation, and special attention has been paid on the slow AgF addition, the change of solvent from acetonitrile to acetonitrile:acetone mixture, and methylation of secondary amines of L_1-X to L_5-X substrate.
- We have developed stoichiometric defluorination reaction of ligand L_1-F mediated by a Cu^I/Cu^{III} pathway in acetone at room temperature. The solvent choice and entrapment of the $arylCu^{III}$ intermediate with chloride anions to form the high stable $arylCu^{III}-Cl$ 1_{Cl} are key to explain the defluorination reaction to form the corresponding L_1-Cl .
- Stoichiometric C-O bond forming reactions between $arylCu^{III}$ complex 1_{ClO_4} and oxygen nucleophiles (carboxylic acids, phenols and aliphatic alcohols) have been explored. The cleavage of the O-H bond of the nucleophile, reflected by the pK_A , has an important role in the reaction mechanism. However, different reactivity trends have been observed: a) the inhibitory effect of excess carboxylic acid and carboxylic acids with lower pK_A ; b) enhancing effect for the more acidic phenols (with the exception of *p*-nitrophenol). The latter observations, together with the detection of an adduct species between 1_{ClO_4} and carboxylic acids and *p*-cyanophenol, allowed us to propose a reliable reaction mechanism involving $aryl-Cu^{III}/HO-Nuc$ adduct formation, deprotonation and reductive elimination steps. A pK_A dependent change in the rate-determining step has been proposed based on all experimental data.
- Copper-catalyzed C-N and C-O bond-forming reactions have been developed in model L_1-X systems in the presence of nitrogen and oxygen nucleophiles (pyridone, 4-fluorophenol and acetic acid). In situ spectroscopic analysis showed evidences of the involvement of $arylCu^{III}-X$ intermediate as the resting-state. These results provide the first direct observation of a Cu^I/Cu^{III} catalytic cycle that may be relevant to Ullmann Condensation Reactions.
- The pH-dependent reactivity of $arylCu^{III}$ complex 1_{ClO_4} with nucleophiles has been evaluated. It has been found that coordinated secondary amines in 1_{ClO_4} are also prone to deprotonation in front a base or deprotonated oxygen nucleophiles, i.e. phenolates. The amine deprotonation to form species **3** causes a 1-fold increase in reactivity towards phenol substrates, thus highlighting the importance of understanding ligand multifunctionalities.

- An in-depth understanding of the copper-catalyzed aryl-heteroatom cross-coupling reactions at a molecular level is necessary for the development of new Ullmann-type catalysts which facilitate higher product conversions and TONs, under milder and more efficient conditions. This thesis uncovers the fundamental understanding of the key oxidative addition/reductive elimination $\text{Cu}^{\text{I}}/\text{Cu}^{\text{III}}$ catalytic cycle within model aryl halide substrates for C-heteroatom cross-coupling reactions occurring under very mild conditions, and that might be highly valuable for the design of new catalysts for Ullmann Condensation reactions.



Annex

1. Supplementary Information Chapter IV

1.1. Materials and Methods.....	189
1.2. Instrumentation	189
1.3. Synthesis and characterization of arylCu ^{III} -halide complexes	190
1.4. Synthesis and characterization of C-X reductive elimination products	193
1.5. Crystallographic characterization of arylCu ^{III} -halide complexes.....	195
1.6. General Procedure for Monitoring Catalytic Coupling of L₁-Br with Pyridone by NMR and UV-Vis Spectroscopy.....	198
1.7. Kinetic analysis of C-halogen reductive elimination triggered with CF ₃ SO ₃ H	199

1.1. Materials and Methods

Reagents and solvents used were commercially available reagent quality unless indicated otherwise. Solvents were purchased from SDS and were purified and dried by passing through an activated alumina purification system (MBraun SPS-800). Preparation and handling of air-sensitive materials were carried out in a N₂ drybox (MBraun-Unilab) with O₂ and H₂O concentrations < 1 ppm. Ligands **L₁-H** and **L₂-H** were synthesized following published procedures.¹

1.2. Instrumentation

UV-vis spectroscopy was performed on a Cary-50 (Varian) UV-vis spectrophotometer. Low temperature control was maintained with a cryostat from Unisoku Scientific Instruments, Japan. NMR data concerning product identity were collected on Bruker 600 MHz, Bruker 500 MHz or Bruker 400 MHz AVANCE spectrometers in DMSO, CDCl₃ or CD₃CN and calibrated relative to an internal reference, either the residual protons of the solvent or added tetramethylsilane. NMR data concerning the catalytic coupling of **L₁-Br** with pyridone were collected on a Bruker AC 300 MHz spectrometer. C, H, N elemental analyses were performed on a ThermoFinnigan Flash-EA1112 analyzer. ESI-MS experiments were collected and analyzed on a Bruker Daltonics Esquire 6000 spectrometer with acetonitrile or

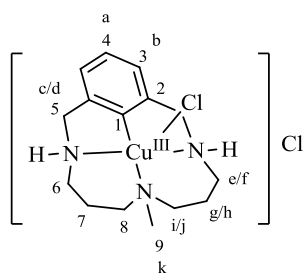
1. Xifra, R.; Ribas, X.; Llobet, A.; Poater, A.; Duran, M.; Solà, M.; Stack, T. D. P.; Benet-Buchholz, J.; Donnadieu, B.; Mahía, J.; Parella, T. *Chem.-Eur. J.* **2005**, *11*, 5146.

acetonitrile/water (80:20) as the mobile phase. Cyclic voltammetry (CV) experiments were performed in an IJ-Cambria HI-660 potentiostat using a three electrode cell. Glassy carbon disk electrodes (3mm diameter) from BAS were used as working electrode, platinum wire was used as auxiliary and SSCE electrode as the reference.

1.3. Synthesis and characterization of arylCu^{III}-halide complexes

Complexes **1_{Cl}**, **1_{Br}**, **2_{Cl}** and **2_{Br}** were prepared by modifying the synthetic procedure described in the literature.^{1,2} A solution of CuX₂ (X = Cl, Br) in acetone was added to a vigorously stirred solution of ligand **L₁-H** (for **1_{Cl}**, **1_{Br}**) or **L₂-H** (for **2_{Cl}**, **2_{Br}**) (1.1 equiv) in acetone. After 24 h stirring under O₂ atmosphere (1 atm), arylCu^{III}-halide complex precipitated from the solution that was isolated by centrifugation of the crude. The solid obtained was recrystallized in CH₃CN (**1_{Cl}**) or DMF (**1_{Br}**, **2_{Br}**, **2_{Cl}**) by slow diethyl ether diffusion over the resultant solution, affording crystals of the desired complexes.

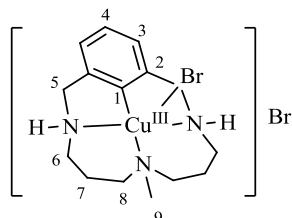
Complexes **1₁** and **2₁** were prepared by dropwise addition of a solution of AgClO₄ (2 equiv) in CH₃CN to a vigorously stirred solution of [L₁C-CuCl]Cl (**1_{Cl}**) or [L₂C-CuCl]Cl (**2_{Cl}**) in CH₃CN respectively. After a few seconds the solution became cloudy and a precipitate appeared. The solution is filtered through Celite and then through an Acrodisc[®] filter. The resultant solution is added dropwise to a stirred solution of KI (2 equiv) in CH₃CN (1 mL). After 10 minutes stirring, slow diethyl ether diffusion over the final solution dark green crystals corresponding to complexes **1₁** and **2₁** respectively.



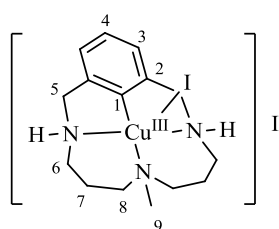
1_{Cl} (yield: 91 %). ¹H-NMR (DMSO-D₆, 500MHz) δ, ppm: 8.16 (s, 2H, Hⁱ), 7.14 (t, J = 7.4 Hz, 1H, H^a), 6.89 (d, J = 7.4 Hz, 2H, H^b), 4.37 (dd, J = 15.3, 5.6 Hz, 2H, H^c), 4.16 (dd, J = 15.3, 8.5 Hz, 2H, H^d), 3.21 (t, J = 13 Hz, 2H, H^e), 3.11 (t, J = 12.7 Hz, 2H, H^e), 2.80 (s, 3H, H^k), 2.72 (d, J = 11 Hz, 2H, H^j), 2.30 (d, J = 12.7 Hz, 2H, H^f), 2.03 (q, J = 13 Hz, 2H, H^g), 1.80 (d, J = 16 Hz, 2H, H^h). ¹³C-NMR (DMSO-D₆, 500MHz) δ, ppm: 179.7 (C₁), 146.1 (C₂), 128.3 (C₄), 121.8 (C₃),

2. Ribas, X.; Jackson, D. A.; Donnadieu, B.; Mahía, J.; Parella, T.; Xifra, R.; Hedman, B.; Hodgson, K. O.; Llobet, A.; Stack, T. D. P. *Angew.Chem. Int. Ed.* **2002**, *41*, 2991.

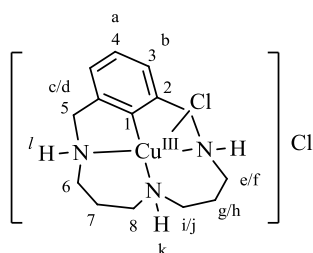
61.7 (C5), 57.8 (C6), 51.2 (C8), 40.7(C9), 23.1 (C7). **ESI-MS** (CH₃CN, m/z): 345(100) [C₁₅H₂₄CuClN₃]⁺. **Anal.** Calcd for **1_{Cl}** (%) 47.31 C, 11.03 N, 6.35 H; found: 47.01 C, 11.02 N, 6.14 H.



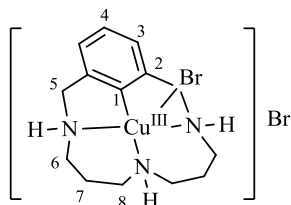
1_{Br} (yield: 82%). **¹H-NMR** (CH₃CN, 400MHz) δ, ppm: 7.98 (s, 2H), 7.13 (t, *J* = 7.4 Hz, 1H), 6.92 (d, *J* = 7.4 Hz, 2H), 4.35 (dd, *J* = 19.6, 5.6 Hz, 2H), 4.15 (dd, *J* = 15.6, 8.8 Hz, 2H), 3.35 (m, 2H), 3.17 (t, *J* = 12.4 Hz, 2H), 2.79 (s, 3H), 2.66 (d, *J* = 10.4 Hz, 2H), 2.38 (d, *J* = 12.8 Hz, 2H), 2.02 (q, *J* = 8.4 Hz, 2H), 1.83 (d, *J* = 16 Hz, 2H). **¹³C-NMR** (DMSO-D₆, 400MHz) δ, ppm: 181.31 (C1), 146.29 (C2), 128.8 (C4), 122.4 (C3), 62.2 (C5), 58.4 (C6), 51.6 (C8), 41.2 (C9), 23.7 (C7). **ESI-MS** (CH₃CN, m/z): 390.0 (100) [C₁₅H₂₄CuBrN₃]⁺. **Anal.** Calcd for **1_{Br}** (%) 38.35 C, 8.94 N, 5.14 H, found: 38.05 C, 8.65 N, 4.84 H.



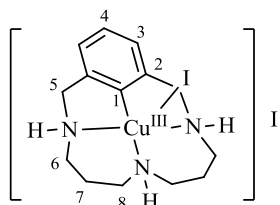
1_I (yield: 84%). **¹H-NMR** (CD₃CN, 300MHz) δ, ppm: 7.11 (t, *J* = 7.5 Hz, 1H), 6.86 (d, *J* = 7.5 Hz, 2H), 6.58 (s, br, 2H), 4.28 (dd, *J* = 15, 5.1 Hz, 2H), 4.17 (dd, *J* = 15, 8.1 Hz, 2H), 3.50 (q, *J* = 12.8 Hz, 4H), 2.85 (s, 3H), 2.52 (tt, *J* = 12.9, 3.3 Hz, 4H), 2.27 (m, 2H), 1.89 (m, 2H). **¹³C-NMR** (CD₃CN, 300MHz) δ, ppm: 182.5 (C1), 145.1 (C2), 128.5 (C4), 122.2 (C3), 61.7 (C5), 59.0 (C6), 51.0 (C8), 42.2 (C9), 23.4 (C7). **ESI-MS** (CH₃CN, m/z): 436.0 (100) [C₁₅H₂₄CuIN₃]⁺. **Anal.** Calcd for **1_I** (%) 31.96 C, 7.45 N, 4.29 H, found: 31.65 C, 7.38 N, 4.36 H.



2_{Cl} (yield: 94%). **¹H-NMR** (DMSO-D₆, 500MHz) δ, ppm: 7.42 (s, 2H, H^b), 7.11 (t, *J* = 7 Hz, 1H, H^a), 6.88 (d, *J* = 7 Hz, 2H, H^j), 4.36 (dd, *J* = 15, 5 Hz, 2H, H^c), 4.17 (dd, *J* = 14, 9 Hz, 2H, H^d), 4.17 (s, 1H, H^k), 3.04 (q, *J* = 12 Hz, 2H, H^e), 2.4-2.8 (m, 6H^f, Hⁱ, H^l), 1.85 (d, *J* = 15 Hz, 2H, H^g), 1.72 (q, *J* = 13 Hz, 2H, H^h). **¹³C-NMR** (DMSO-D₆, 500MHz) δ, ppm: 179.7 (C1), 145.5 (C2), 128.0 (C4), 121.6 (C3), 61.9 (C5), 51.3 (C6), 48.1 (C8), 26.2 (C7). **ESI-MS** (DMSO:CH₃CN, *m/z*): 330.1 (100) [C₁₄H₂₂CuClN₃]⁺. **Anal.** Calcd **2_{Cl}**·H₂O (%) 43.69 C, 10.92 N, 6.29 H, found: 43.76 C, 10.93 N, 6.32 H.

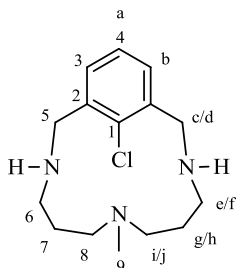


2_{Br} (yield: 86%). **¹H-NMR** (CH₃CN, 400MHz) δ, ppm: 7.23 (s, 2H), 7.10 (t, *J* = 7.2 Hz, 1H), 6.89 (d, *J* = 7.2 Hz, 2H), 4.32 (dd, *J* = 15.2, 5.6 Hz, 2H), 4.14 (dd, *J* = 15.2, 9.2 Hz, 2H), 4.10 (s, 1H), 3.05 (q, *J* = 11.2 Hz, 2H), 2.74 (m, 6H), 1.86 (d, *J* = 15.6 Hz, 2H), 1.69 (m, 2H). **¹³C-NMR** (DMSO-D₆, 400MHz) δ, ppm: 180.0 (C1), 145.7 (C2), 128.5 (C4), 122.2 (C3), 62.4 (C5), 51.6 (C6), 48.8 (C8), 26.7 (C7). **ESI-MS** (DMSO:CH₃CN, *m/z*): 376.0 (100) [C₁₄H₂₂CuBrN₃]⁺. **Anal.** Calcd for **2_{Br}**·1.5 DMF (%) 29.74 C, 7.43 N, 3.92 H, found: 29.39 C, 7.37 N, 3.80 H.

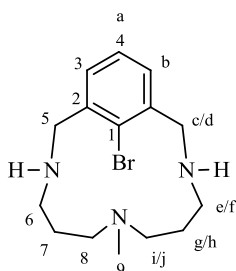


2_I (yield: 98%). **¹H-NMR** (CD₃CN, 400MHz) δ, ppm: 7.08 (t, *J* = 7.4 Hz, 1H), 6.83 (d, *J* = 7.4 Hz, 2H), 6.16 (s, 2H), 4.18 (m, 4H), 3.76 (s, 1H), 3.12 (m, 4H), 2.93 (d, *J* = 11.6 Hz, 2H), 2.54 (d, *J* = 12Hz, 2H), 1.99 (m, 4H). **¹³C-NMR** (CD₃CN, 400MHz) δ, ppm: 179.2 (C1), 144.4 (C2), 128.1 (C4), 122.1 (C3), 61.8 (C5), 51.0 (C6), 49.5 (C8), 26.1 (C7). **ESI-MS** (CH₃CN, *m/z*): 421.8 (100) [C₁₄H₂₂CuIN₃]⁺. **Anal.** Calcd for [L₂C-Cu^{III}I]I (%) 30.59 C, 7.64 N, 4.03 H, found: 30.33 C, 7.31 N, 3.82 H.

1.4. Synthesis and characterization of C-X reductive elimination products

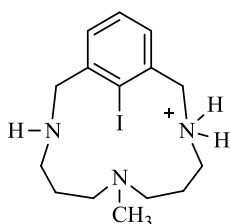


L₁-Cl. Under N₂ atmosphere, 2 equivalents of acid (CF₃SO₃H, 0.023 M, 1.4 mL, 0.032 mmols) are added dropwise to a stirred solution of complex **1_{Cl}** (6.1 mg, 0.016 mmols) in previously deoxygenated CH₃CN (3 mL), causing a color change from red to colorless in seconds (100% NMR yield). NH₄OH (1 mL, 28% in water) is added to the solution and the organic product is extracted with CH₂Cl₂. The organic phase is dried with MgSO₄ and then dried under vacuum overnight to obtain a yellow oil. **¹H-NMR** (CDCl₃, 400MHz) δ, ppm: 7.14 (m, 3H, H^a, H^b), 4.40 (d, *J* = 14 Hz, 2H, H^c or H^d), 3.53 (d, *J* = 14.4 Hz, 2H, H^c or H^d), 2.39 (m, 4H, H^e or H^f, Hⁱ or H^j), 2.31 (m, 2H, H^e or H^f), 2.01 (m, 2H, Hⁱ or H^j), 1.86 (s, 3H, CH₃), 1.46 (m, 4H, H^g, H^h). **¹³C-NMR** (CDCl₃, 400 MHz) δ, ppm: 138.9 (C2), 133.7 (C1), 130.8 (C3), 125.8 (C4), 55.3 (C8), 52.4 (C5), 43.4 (C6), 39.3 (C9), 26.6 (C7). **ESI-MS** (CH₃CN, *m/z*): 282.4 (100) [C₁₅H₂₅ClN₃]⁺.

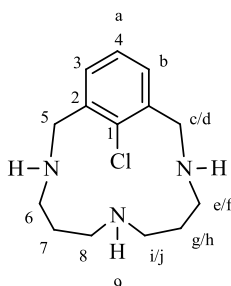


L₁-Br. Under N₂ atmosphere, 6 equivalents of acid (H₂SO₄ 1M, 33 μL, 0.033 mmols) are added dropwise to a stirred solution of complex **1_{Br}** (5.1 mg, 0.011 mmols) in previously deoxygenated CH₃CN (3 mL), causing a color change from purple to colorless in minutes (100% NMR yield). The organic product is extracted in NH₄OH/CH₂Cl₂. The organic phase is dried with MgSO₄ and then dried under vacuum overnight to obtain a yellow oil. **¹H-NMR** (CDCl₃, 400MHz) δ, ppm: 7.13 (m, 3H, H^a, H^b), 4.40 (d, *J* = 18.8 Hz, 2H, H^c or H^d), 3.57 (d, *J* = 18.8 Hz, 2H, H^c or H^d), 2.37 (m, 2H, Hⁱ or H^j), 2.33 (m, 2H, H^e or H^f), 2.16 (m, 2H, H^e or H^f), 1.97 (m, 2H, Hⁱ or H^j), 1.87 (s, 3H, CH₃), 1.52 (m, 4H, H^g, H^h). **¹³C-NMR** (CDCl₃, 400MHz) δ, ppm: 140.9 (C2), 130.8 (C3), 126.2 (C4), 125.5 (C1), 55.3 (C8), 54.5 (C5), 42.8 (C6), 39.2 (C9), 26.8 (C7). **ESI-MS** (CH₃CN, *m/z*): 326.1 (100) [C₁₅H₂₅BrN₃]⁺.

Alternative work-up for L₁-Br. After addition of acid to **1_{Br}** (400.8 mg, 85.14 μmol), 1,10-phenanthroline (150 mg, 160 μmol) was added to the acetonitrile solution, resulting in a color change from colorless to red. The acetonitrile was removed under vacuum, and approx. 100mL CH₂Cl₂ added to the resulting residue. The organic layer was washed with an HCl solution (pH~3) and the layers separated. The aqueous layer was basified (pH~13) and washed with CH₂Cl₂ to yield 240 mg (86 % yield) of **L₁-Br**.



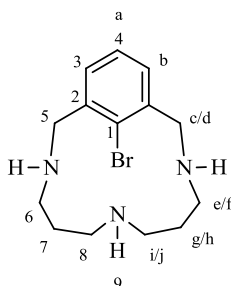
L₁-I. Under N₂ atmosphere 20 equivalents of HPF₆ 15.8 M (15 μL, 0.24 mmols) are added dropwise to a stirred solution of complex **1_I** (6.6 mg, 0.012 mmols) in previously deoxygenated CD₃CN (3 mL) causing a color change from green to pale-yellow. ¹H-NMR spectra of the resultant solution after 1 hour showed 85% yield of coupling product L₁-I(H⁺). ¹H-NMR (CDCl₃, 400MHz) δ, ppm: 7.70 (s, 3H), 4.67 (m, 4H), 3.22 (m, 2H), 3.06 (m, 2H), 2.92 (m, 4H), 2.74 (s, 3H), 1.74 (m, 2H), 1.39 (m, 2H). **ESI-MS** (CD₃CN, m/z): 374.0 (100) [C₁₅H₂₅IN₃]⁺.



L₂-Cl. Method 1: Under N₂ atmosphere, 6 equivalents of acid (H₂SO₄ 1 M, 38 μL, 0.038 mmols) are added dropwise to a stirred solution of complex **2_{Cl}** (4.6 mg, 0.013 mmols) in previously deoxygenated CH₃CN (3 mL), causing a color change from red to colorless in minutes. After stirring for 30 minutes, the solution became cloudy and a precipitate appeared quantitatively (no organic products remained in solution, as determined by ¹H-NMR). The solvent is decanted and the precipitate is extracted in NH₄OH/CH₂Cl₂. The organic phase is dried with MgSO₄, filtered and then dried under vacuum overnight to afford a white solid.

Method 2. Under N₂ atmosphere, 3 equivalents of acid (HCl 1M, 32 μL, 0.032 mmols) are added dropwise to a stirred solution of complex **2_{ClO4}** (5.6 mg, 0.011 mmols) in previously deoxygenated CH₃CN (3 mL), causing a color change from red to colorless in minutes. After stirring for 30 minutes, the solution became cloudy and a precipitate appeared quantitatively

(no organic products remained in solution, as determined by $^1\text{H-NMR}$). The solvent is decanted and the precipitate is extracted in $\text{NH}_4\text{OH}/\text{CH}_2\text{Cl}_2$. The organic phase is dried with MgSO_4 and then dried under vacuum overnight to yield a white solid. $^1\text{H-NMR}$ (CDCl_3 , 400MHz) δ , ppm: 7.14 (m, 3H, H^a , H^b), 4.41 (d, $J = 14$ Hz, 2H, H^c or H^d), 3.55 (d, $J = 14$ Hz, 2H, H^c or H^d), 2.6 (m, 4H, H^i , H^j), 2.4 (m, 2H, H^e or H^f), 2.15 (td, $J = 11.6$ Hz, $J = 2.8$ Hz, 2H, H^e or H^f), 1.7 (m, 2H, H^g or H^h), 1.65 (m, 2H, H^g or H^h). $^{13}\text{C-NMR}$ (CDCl_3 , 400MHz) δ , ppm: 139.0 (C2), 133.1 (C1), 131.2 (C3), 125.6 (C4), 52.3 (C8), 45.7 (C5), 41.5 (C6), 28.5 (C7). **ESI-MS** (CH_3CN , m/z): 268.2 (100) $[\text{C}_{14}\text{H}_{23}\text{ClN}_3]^+$.



L₂-Br. Under N_2 atmosphere, 6 equivalents of acid (H_2SO_4 1M, 72 μL , 0.072 mmols) are added dropwise to a stirred solution of complex **2_{Br}** (10.9 mg, 0.024 mmols) in previously deoxygenated CH_3CN (3 mL), causing a color change from purple to colorless in hours. After stirring overnight, the solution became cloudy and a precipitate appeared (no organic products remained in solution, as determined by $^1\text{H-NMR}$). The solvent is decanted and the precipitate is extracted in $\text{NH}_4\text{OH}/\text{CH}_2\text{Cl}_2$. The organic phase is dried with MgSO_4 and then dried under vacuum overnight to yield a white solid. $^1\text{H-NMR}$ (CDCl_3 , 400MHz) δ , ppm: 7.13 (m, 3H, H^a , H^b), 4.37 (d, $J = 14$ Hz, 2H, H^c or H^d), 3.57 (d, $J = 14$ Hz, 2H, H^c or H^d), 2.61 (t, $J = 12$ Hz, 2H, H^i or H^j), 2.53 (m, 2H, H^i or H^j), 2.40 (m, 2H, H^e or H^f), 2.09 (td, $J = 11.6$, 2.8 Hz, 2H, H^e or H^f), 1.7 (m, 2H, H^g or H^h), 1.59 (m, 2H, H^g or H^h). $^{13}\text{C-NMR}$ (CDCl_3 , 400MHz) δ , ppm: 140.7 (C2), 131.30 (C3), 126.2 (C4), 124.8 (C1), 54.2 (C5), 45.6 (C8), 41.1 (C6), 28.5 (C7). **ESI-MS** (CH_3CN , m/z): 312.0 (100) $[\text{C}_{14}\text{H}_{23}\text{BrN}_3]^+$.

1.5. Crystallographic characterization of aryl Cu^{III} -halide complexes

Crystals of complexes **1_I**, **2_{Cl}** and **2_I** were grown from slow diffusion of ethyl ether in a CH_3CN solution of the compound and crystals of complexes **1_{Cl}** and **1_{Br}** were grown from slow diffusion of ethyl ether in a DMF solution of the compound. All of them were used for room temperature (300(2) K) X-ray structure determination. The measurement was carried out on a *BRUKER SMART APEX CCD* diffractometer using graphite-monochromated $\text{Mo } K\alpha$ radiation ($\lambda = 0.71073 \text{ \AA}$) from an x-Ray Tube. Crystal data is found in Tables S4-S5. Programs used:

data collection, Smart version 5.631 (Bruker AXS 1997-02); data reduction, Saint + version 6.36A (Bruker AXS 2001); absorption correction, SADABS version 2.10 (Bruker AXS 2001). Structure solution and refinement was done using SHELXTL Version 6.14 (Bruker AXS 2000-2003). The structure was solved by direct methods and refined by full-matrix least-squares methods on F^2 . The non-hydrogen atoms were refined anisotropically. The H-atoms were placed in geometrically optimized positions and forced to ride on the atom to which they are attached, except N-H hydrogens which were located in the difference Fourier map and refined without constraints.

Crystal data for **1_{Cl}**, **1_{Br}**, **1_I**, **2_{Cl}** and **2_I** have been deposited as CCDC references 735508-735512, respectively, which contain the supplementary crystallographic data for each compound. These data can be obtained free of charge from CCDC via www.ccdc.cam.ac.uk/data_request/cif. Moreover, cif files of crystal structures of complexes can be found in the Supplementary Digital Information.

Table 1.5.1. Crystallographic data and structure refinement for complexes **1_{Cl}**, **1_{Br}**, **1_I**, **2_{Cl}**, **2_I**; CCDC codes are 735508-735512, respectively.

	1_{Cl}	1_{Br}	1_I	2_{Cl}·H₂O	2_I
Empirical formula	C ₁₅ H ₂₄ Cl ₂ CuN ₃	C ₁₅ H ₂₄ Br ₂ CuN ₃	C ₁₅ H ₂₄ I ₂ CuN ₃	C ₁₄ H ₂₄ Cl ₂ CuN ₃ O	C ₁₄ H ₂₂ I ₂ CuN ₃
Formula weight	380.81	469.73	563.71	380.4	549.69
Temperature, K	300(2)	300(2)	300(2)	300(2)	100(2)
Wavelength, Å	0.71073	0.71073	0.71073	0.71073	0.71073
Crystal system	orthorhombic	Orthorhombic	monoclinic	orthorhombic	triclinic
Space group	Pca21	Pca21	P21/c	Pca21	P-1
Unit cell dimensions					
a, Å	11.892(9)	12.3103(14)	7.1650(6)	12.470(2)	15.441(7)
α, deg	90	90	90	90	66.117(7)
b, Å	15.074(11)	15.3429(17)	17.7756(14)	15.254(7)	16.225(7)
β, deg	90	90	99.2740(10)	90	83.242(8)
c, Å	9.640(7)	9.6916(11)	15.0327(12)	9.0700(17)	16.686(8)
γ, deg	90	90	90	90	70.542(8)
Volume, Å ³	1728(2)	1830.5(4)	1889.6(3)	1725.3(6)	3603(3)
Density (calculated), g·cm ⁻³	1.464	1.704	1.982	1.481	2.026
Cell formula units_Z	4	4	4	4	8
Absorption coefficient, mm ⁻¹	1.570	5.556	4.421	1.577	4.634
Crystal size, mm ³	0.6 x 0.2 x 0.1	0.4 x 0.15 x 0.08	0.4 x 0.4 x 0.2	0.6 x 0.4 x 0.08	0.3 x 0.1 x 0.08
Reflections collected	25418	27574	29056	24670	55714
Independent reflections	4281 [R(int)= 0.0696]	4524 [R(int)= 0.0395]	4675 [R(int)= 0.0392]	4186 [R(int)= 0.0336]	17207 [R(int)= 0.0420]
Final R indices [I>2σ(I)]	R1= 0.0330, wR2= 0.0756	R1= 0.0266, wR2= 0.0547	R1= 0.0259, wR2= 0.0615	R1= 0.0455, wR2= 0.1358	R1= 0.0508, wR2= 0.1291
R indices (all data)	R1= 0.0442, wR2= 0.0805	R1= 0.0374, wR2= 0.0576	R1= 0.0367, wR2= 0.0644	R1= 0.0496, wR2= 0.1419	R1= 0.0971, wR2= 0.1489

1.6. General Procedure for Monitoring Catalytic Coupling of L₁-Br with Pyridone by NMR and UV-Vis Spectroscopy

In an inert-atmosphere glove box, stock solutions of L₁-Br/1,3,5-trimethoxybenzene (9.6/14.9 mM) and pyridone/Cu(CH₃CN)₄PF₆ (151/4.4 mM) were prepared in CD₃CN (5 mL each). The L₁-Br/1,3,5-trimethoxybenzene stock solution (700 μL) was added to an NMR tube and capped with a septum. To initiate the reaction, 50 μL of the pyridone/[Cu^I(CH₃CN)₄]PF₆ solution was added to the NMR tube, and the tube was placed in the NMR probe, pre-cooled to 15 °C. The dead time between addition and data acquisition was 2 min. The final concentrations were as follows: [L₁-Br] = 8.9 mM, [pyridone] = 10.1 mM, and [Cu^I(CH₃CN)₄]PF₆] = 0.3 mM. The same stock solutions were used to acquire the UV-Vis timecourse data. The L₁-Br/1,3,5-trimethoxybenzene stock solution (1.05 mL) was added to a 1-cm pathlength quartz cuvette and the solution was cooled to 15 °C in the sample holder. The reaction was initiated by addition of the pyridone/[Cu^I(CH₃CN)₄]PF₆ solution (75 μL).

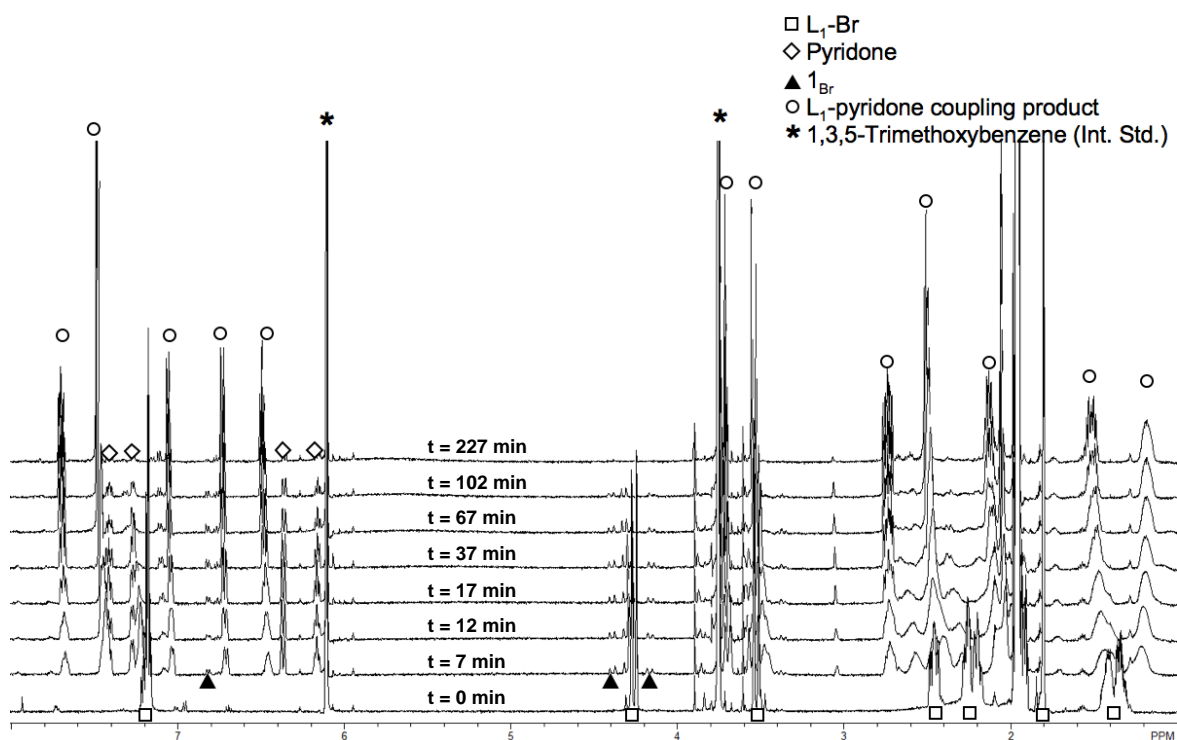


Figure 1.6.1. ¹H-NMR spectra acquired during the cross-coupling of pyridone with L₁-Br catalyzed by 3.3 mol % [Cu^I(CH₃CN)₄]PF₆.

1.7. Kinetic analysis of C-halogen reductive elimination triggered with $\text{CF}_3\text{SO}_3\text{H}$

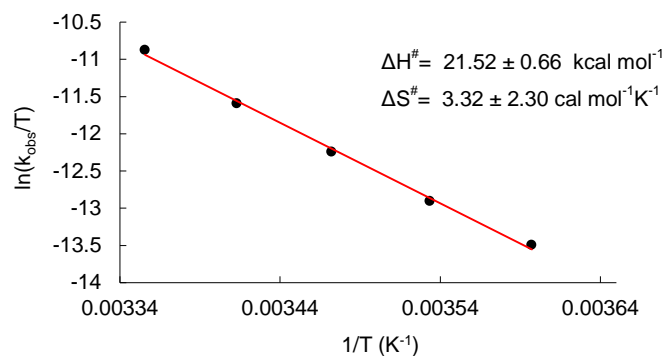


Figure 1.7.1. Eyring plot for the reaction of complex $\mathbf{1}_{\text{Br}}$ upon addition of 1.5 equiv of $\text{CF}_3\text{SO}_3\text{H}$. Conditions: $[\mathbf{1}_{\text{Br}}] = 0.5 \text{ mM}$, $[\text{CF}_3\text{SO}_3\text{H}] = 0.75 \text{ mM}$, CH_3CN , from 5 to 25 °C.

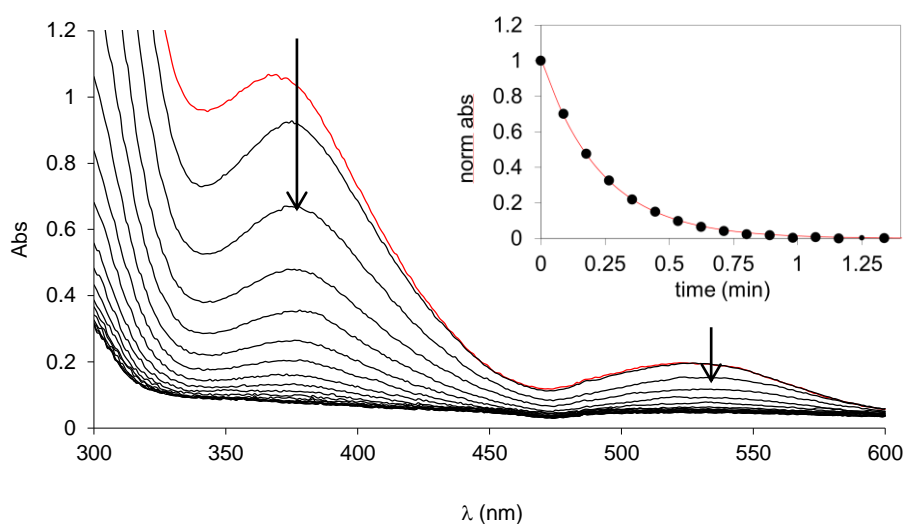


Figure 1.7.2. UV-vis monitoring of reductive elimination of complex $\mathbf{1}_{\text{Cl}}$ upon addition of 1.5 equiv of $\text{CF}_3\text{SO}_3\text{H}$. Inset shows decay profile at 274 nm (circles = experimental data, solid-line = first-order theoretical fit). Conditions: $[\mathbf{1}_{\text{Cl}}] = 0.1 \text{ mM}$, $[\text{CF}_3\text{SO}_3\text{H}] = 0.75 \text{ mM}$, CH_3CN , 10 °C.

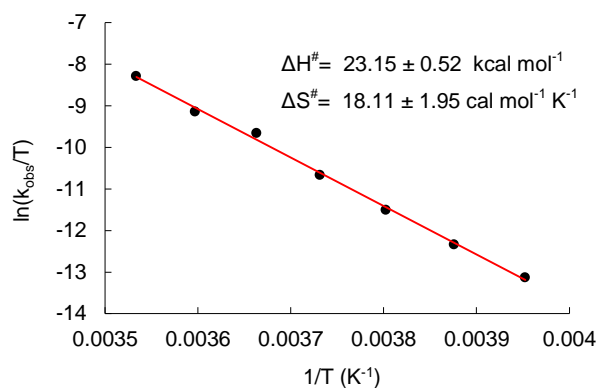


Figure 1.7.3. Eyring plot for the reaction of complex **1_{C1}** upon addition of 1.5 equiv of CF₃SO₃H. Conditions: [**1_{C1}**] = 0.5 mM, [CF₃SO₃H] = 0.75 mM, CH₃CN, from -20 to 10 °C.

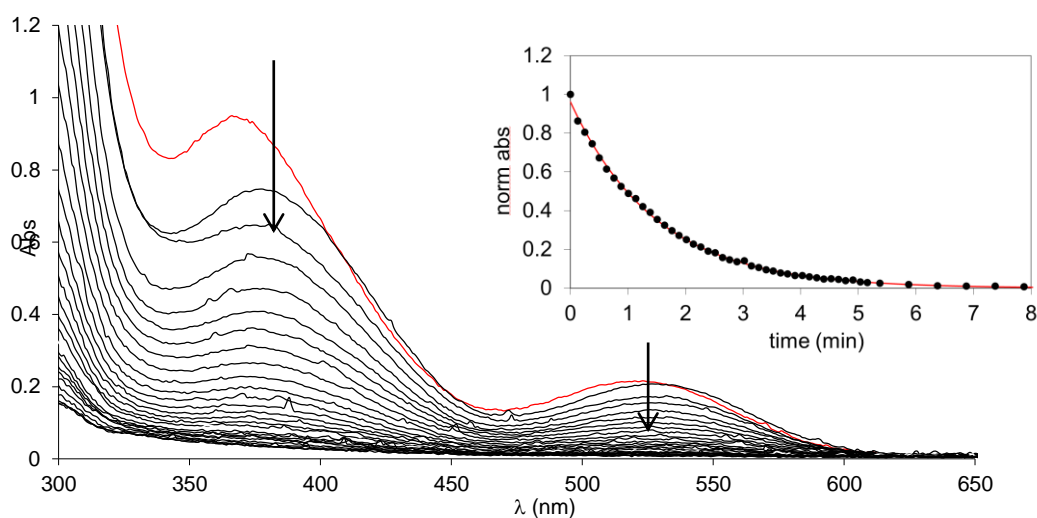


Figure 1.7.4. UV-vis monitoring of reductive elimination of complex **2_{C1}** upon addition of 1.5 equivalents of acid. Inset shows decay profile at 274 nm (circles = experimental data, solid-line = first-order theoretical fit). Conditions: [**2_{C1}**] = 0.1 mM, [CF₃SO₃H] = 0.75 mM, CH₃CN, 15 °C.

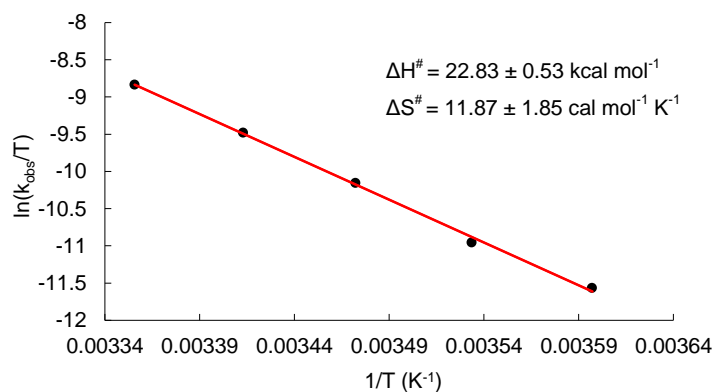


Figure 1.7.5. Eyring plot for the reaction of complex **2_{C1}** upon addition of 1.5 equiv of CF₃SO₃H. Conditions: [**2_{C1}**] = 0.5 mM, [CF₃SO₃H] = 0.75 mM, CH₃CN, from -5 to 25 °C.

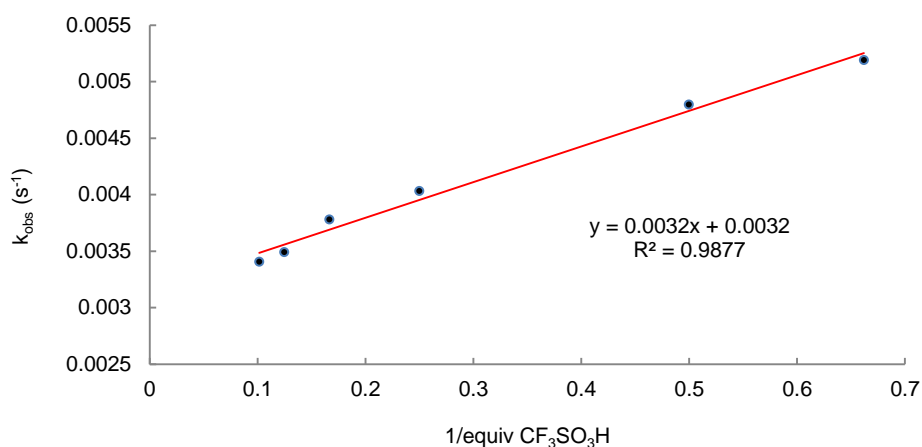


Figure 1.7.6. Dependence of k_{obs} on the $[\text{CF}_3\text{SO}_3\text{H}]$ obtained by monitoring the reaction of **1_{Br}** with $\text{CF}_3\text{SO}_3\text{H}$ by UV-visible spectroscopy. Conditions: $[\mathbf{1}_{\text{Br}}] = 0.3 \text{ mM}$, $[\text{CF}_3\text{SO}_3\text{H}] = 0.76\text{-}4.9 \text{ mM}$, CH_3CN , $24 \text{ }^\circ\text{C}$.

Table 1.7.1. Cathodic reduction potentials (E_{pc}) obtained by cyclic voltammeteries of **1_{Cl}**, **1_{Br}**, **2_{Cl}** and **2_{Br}** upon addition of 4.5 equiv of $\text{CF}_3\text{SO}_3\text{H}$ ($-10 \text{ }^\circ\text{C}$, CH_3CN , $[\mathbf{1}_x] = 1 \text{ mM}$, scan rate = 0.2 V/s , TBAP 0.1 M , using Fc/Fc^+ as a internal reference).

Complex	E_{pc} (V) neutral media	E_{pc} (V) acid media ^a	anionic shift (V)
1_{Cl}	-0.40	-0.28	0.12
1_{Br}	-0.37	-0.30	0.07
2_{Cl}	-0.46	-0.29	0.17
2_{Br}	-0.42	-0.35	0.07

2. Supplementary Information Chapter V

2.1. Materials, methods and instrumentation.....	203
2.2. Synthesis of complexes 1_{Cl} , 1_{Br} and 1_I	204
2.3. Synthesis and characterization of ligands	204
2.3.4. Synthesis of ligand L₁-Cl	204
2.3.5. Synthesis of ligand L₁-Br	206
2.3.6. Synthesis of ligand L₁-I	207
2.3.7. Synthesis of ligand L₁-F	208
2.3.8. Synthesis of ligands L₅-Cl and L₅-Br	210
2.4. Reaction of arylCu ^{III} -halide complexes with 1,10-phenanthroline	211
2.5. Catalytic halide exchange reactions	211
2.6. Aryl-F reductive elimination reactions.....	212
2.6.1. L₁-F synthesis: Stoichiometric reactions with complexes 1_{Cl} and 1_{Br}	212
2.6.2. Monitoring the formation of L₁-F by ¹ H-NMR spectroscopy.....	214
2.6.3. L₁-F synthesis: Catalytic reactions using L₁-Cl and L₁-Br	215
2.6.4. L₅-F synthesis: Catalytic reactions using L₅-Cl and L₅-Br	216
2.7. Stoichiometric aryl fluoride activation	217
2.8. Computational details	218

2.1. Materials, methods and instrumentation

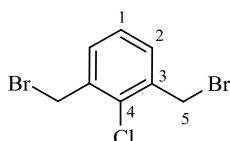
Reagents and solvents used were commercially available reagent quality unless indicated otherwise. Solvents were purchased from SDS-Carlo Erba and Scharlab and were purified and dried by passing through an activated alumina purification system (MBraun SPS-800). Preparation and handling of air-sensitive materials were carried out in a N₂ drybox (MBraun-Unilab) with O₂ and H₂O concentrations < 1 ppm. NMR data were collected on a Bruker 400 or 300 AVANCE in the corresponding deuterated solvent (CDCl₃, CD₃CN, acetone-d₆ or dmsO-d₆) and calibrated relative to an external reference (1,3,5-trimethoxybenzene). ESI-MS experiments were collected and analyzed on a Bruker Daltonics Esquire 6000 spectrometer with acetonitrile or acetonitrile/water (80:20) as solvent. C, H, N elemental analyses were performed on a ThermoFinnigan Flash-EA1112 analyzer.

2.2. Synthesis of complexes **1_{Cl}**, **1_{Br}** and **1_I**

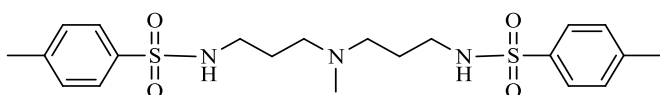
ArylCu^{III}-halide complexes **1_{Cl}**, **1_{Br}** and **1_I** were prepared following procedures described previously (see supporting information of Chapter IV).

2.3. Synthesis and characterization of ligands

2.3.1. Synthesis of ligand L₁-Cl



1,3-bis(bromomethyl)-2-chlorobenzene (1). Compound **1** is synthesized following an experimental procedure described in the literature.¹ A mixture of 2-chloro-1,3-dimethylbenzene (6.9 g, 47.6 mmol), *N*-bromosuccinimide (17.7, 99.4 mmol) and benzoyl peroxide (70 mg, 0.30 mmol) in CHCl₃ (150 mL) is heated under reflux for 12 h and then cooled down to room temperature. The white solid succinimide is removed by filtration. The solvent of the filtrate is evaporated under vacuum and the resulting solid is purified by column chromatography in silica gel using as mobile phase a hexane:CH₂Cl₂ (98:2) mixture, affording 4.1 g of product 1,3-bis(bromomethyl)-2-chlorobenzene (**1**) as a white solid in 29% yield. ¹H-NMR (CDCl₃, 400 MHz) δ, ppm: 7.42 (d, *J* = 7.6 Hz, 2H, H^b), 7.24 (t, *J* = 7.6 Hz, 1H, H^a), 4.61 (s, 4H, H^c). ¹³C-NMR (CD₃CN, 75.4 MHz) δ, ppm: 136.6 (C2), 134.4 (C1), 131.5 (C3), 127.3 (C4), 30.6 (C5).

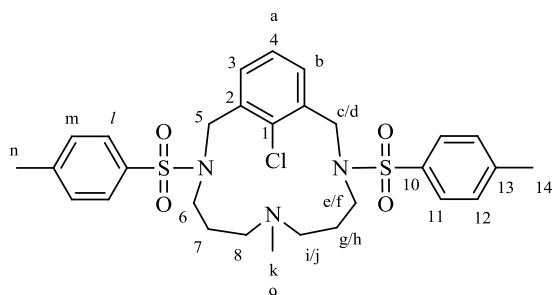


Compound 2. This compound has been synthesized following a reported procedure.² 3,3'-diamino-*N*-methyldipropylamine (6 g, 0.041 mols) and NaOH (10g, 0.25 mols) are added as solids in a 500 mL three-opening round-bottom flask. Then the reagents are dissolved with 150 mL of water and the resulting solution is heated to 80°C. Then, *p*-toluenesulfonyl chloride (15.8g, 0.083 mols) is dissolved in 95 mL of tetrahydrofuran (THF) and added dropwise with a compensated pressure funnel to the reaction mixture. After refluxing the final solution for 48 h,

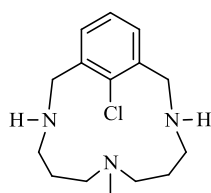
1. Krogh-Jespersen, K.; Czerw, M.; Zhu, K.; Singh, B.; Kanzelberger, M.; Darji, N.; Achord, P. D.; Renkema, K. B.; Goldman, A. S. *J. A. Chem. Soc.* **2002**, 124, 10797.

2. Xifra, R.; Ribas, X.; Llobet, A.; Poater, A.; Duran, M.; Solà, M.; Stack, T. D. P.; Benet-Buchholz, J.; Donnadiou, B.; Mahía, J.; Parella, T. *Chem.-Eur. J.* **2005**, 11, 5146.

the crude is cooled down to room temperature. Then, THF is rotavapored and the aqueous solution obtained is extracted with 150 mL CH₂Cl₂ (x3). The organic layer is dried with MgSO₄, filtered and rotavapored. The resulting oil is purified by column chromatography in silica gel using a CH₂Cl₂:MeOH (9:1) solvent mixture as mobile phase, affording 9.1 g of the desired product **1** in 49 % yield. ¹H-NMR (CDCl₃, 400 MHz) δ, ppm: 7.74 (d, *J* = 8.4 Hz, 4H), 7.29 (d, *J* = 8.8 Hz, 4H), 2.98 (t, *J* = 6 Hz, 4H), 2.45-2.35 (m, 10H), 2.13 (s, 3H), 1.64 (quint., *J* = 6.4 Hz, 4H). Full characterization of this ligand has been published previously (see reference 2).

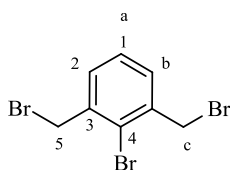


Compound 3. 2 (6.2 g, 13.7 mmol) is dissolved in 100 mL of CH₃CN in a round bottom-flask. Then Cs₂CO₃ is added as a solid to the reaction mixture, and the solution is refluxed at 90 °C. After reflux is initiated, 1,3-bis(bromomethyl)-2-chlorobenzene (**1**) (4.1 g, 13.7 mmol) in 100 mL of CH₃CN is added drop wise to the reaction mixture. After heating for 48 h under reflux, the crude is cooled down to room temperature and filtered. The solvent of the filtrate is evaporated under vacuum and the resulting solid is purified by column chromatography in silica gel using a CH₂Cl₂:MeOH (9:1) solvent mixture as mobile phase, affording 2.7 g of the desired product **3** in 68 % yield. ¹H-NMR (CDCl₃, 400 MHz) δ, ppm: 7.73 (d, *J* = 8.2 Hz, 4H, H^l), 7.51 (d, *J* = 7.6 Hz, 2H, H^b), 7.35 (d, *J* = 8.2 Hz, 4H, H^m), 7.29 (t, *J* = 7.6 Hz, 1H, H^a), 4.58 (d, *J* = 13.6 Hz, 2H, H^c or H^d), 4.30 (d, *J* = 13.6 Hz, 2H, H^c or H^d), 3.05 (quint., *J* = 7.0 Hz, 2H, H^e or H^f), 2.96 (quint., *J* = 7.0 Hz, 2H, H^e or H^f), 2.45 (s, 6H, Hⁿ), 2.05 (m, 2H, Hⁱ or H^j), 2.03 (s, 3H, H^k), 1.01 (m, 2H, 2.45 Hⁱ or H^j), 1.53 (m, 2H, H^g or H^h), 0.95 (m, 2H, H^g or H^h). ¹³C-NMR (CD₃Cl, 75.4 MHz) δ, ppm: 143.5 (C13), 135.6 (C2), 135.1 (C10), 134.5 (C1), 132.3 (C3), 129.9 (C12), 127.5 (C4), 127.4 (C11), 53.0 (C8), 50.7 (C5), 47.3 (C6), 43.7 (C9), 26.0 (C7), 18.5 (C14). **ESI-MS** (CH₃CN, *m/z*): 690.4 (100) [C₂₉H₃₇ClN₃O₄S₂]⁺.

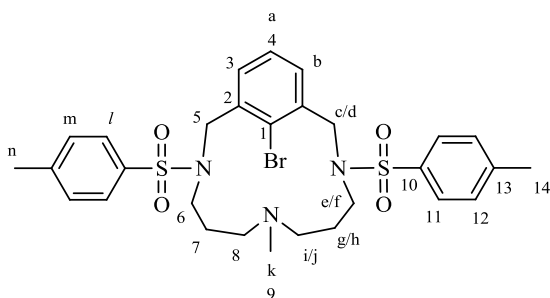


L₁-Cl. Compound **3** (4.0 g, 6.78 mmols) and phenol (16.40 g, 174.3 mmols) are added as solids into a flask. Then, 170 mL of HBr/AcOH 30 % are added to the flask and the resulting mixture is vigorously stirred and heated at 90 °C for 24 h. The crude is concentrated until the initial volume is reduced to the half part. Then, 20 mL of H₂O are added to the crude and the aqueous phase is extracted using CHCl₃ (3 x 80 mL). The aqueous phase is basified with NaOH aq until pH 14, and the resulting mixture is extracted with CHCl₃ (3 x 80 mL). The organic phase is separated, dried with MgSO₄ and concentrated. The obtained oil is purified by column chromatography in silica using a solvent mixture of CH₂Cl₂:CH₃OH:NH₄OH (90:10:2). Eluted fractions containing the product are combined, dried with MgSO₄ and solvent was removed under vacuum obtaining ligand L₁Cl in 51% yield. **¹H-NMR** (CDCl₃, 400 MHz) δ, ppm: 7.08 (m, 3H), 4.35 (d, 2H), 3.46 (d, 2H), 2.23 (m, 8H), 1.94 (m, 2H), 1.77 (s, 3H), 1.45 (m, 4H). Full characterization of this ligand has been published previously (see supporting information of Chapter IV).

2.3.2. Synthesis of ligand L₁-Br

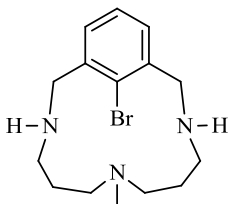


1,3-bis(bromomethyl)-2-bromobenzene (4). Same synthetic procedure as for compound **1** is used to obtain compound **4** but starting from 2-bromo-1,3-dimethylbenzene (Yield: 23 %). **¹H-NMR** (CDCl₃, 400 MHz) δ, ppm: 7.42 (d, *J* = 7.6 Hz, 2H, H^b), 7.29 (dd, *J* = 8.0, 7.2 Hz, 1H, H^a), 4.65 (s, 4H, H^c); **¹³C-NMR** (CDCl₃, 75.4 MHz) δ, ppm: 138.5 (C2), 131.4 (C3), 128.0 (C4), 126.6 (C1), 30.7 (C5).



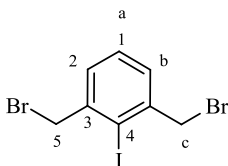
Compound 5. Same synthetic procedure as for compound **3** is used to obtain compound **5** but starting from 1,3-bis(bromomethyl)-2-bromobenzene **4** (Yield: 60 %). **¹H-NMR** (CDCl₃, 400 MHz) δ, ppm: 7.75 (d, *J* = 7.9 Hz, 4H, H^l), 7.52 (d, *J* = 7.6 Hz, 2H, H^b), 7.36 (d, *J* = 8.3 Hz, 4H, H^m), 7.33 (t, *J* = 7.6 Hz, 1H, H^a), 4.59 (d, *J* = 13.6 Hz, 2H, H^c or H^d), 4.36 (d, *J* = 14 Hz, 2H, H^c

or H^d), 3.01 (m, 4H, H^e, H^f), 2.45 (s, 6H, Hⁿ), 2.06 (s, 3H, H^k), 2.06 (m, 2H, Hⁱ or H^j), 1.93 (m, 2H, Hⁱ or H^j), 1.54 (m, 2H, H^g or H^h) 0.96 (m, 2H, H^g or H^h); ¹³C-NMR (CDCl₃, 75.4 MHz) δ, ppm: 143.6 (C13), 136.9 (C2), 135.4 (C10), 132.5 (C3), 129.9 (C12), 128.1 (C4), 127.3 (C11), 126.9 (C1), 53.5 (C5), 53.0 (C8), 47.3 (C6), 43.6 (C9), 26.0 (C7), 21.6 (C14); **ESI-MS** (CH₃CN, m/z): 636.2 (100) [C₂₉H₃₇BrN₃O₄S₂]⁺.

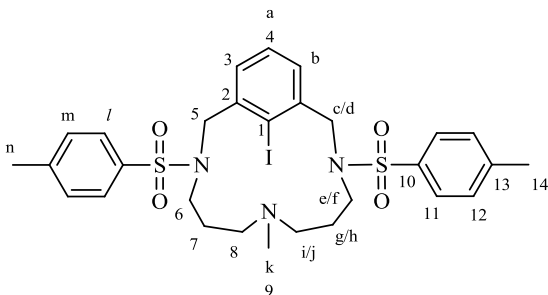


L₁-Br. Same synthetic procedure as for ligand **L₁-Cl** is used to obtain ligand **L₁-Br** but starting from cyclic tosylated compound **5** (Yield: 25%). ¹H-NMR (CDCl₃, 400 MHz) δ, ppm: 7.10 (t, 2H), 7.05 (d, 1H), 4.32 (d, 2H), 3.49 (d, 2H), 2.26 (m, 8H), 1.93 (m, 2H), 1.76 (s, 3H), 1.43 (m, 4H). Full characterization of this ligand has been published previously (see supporting information of Chapter IV).

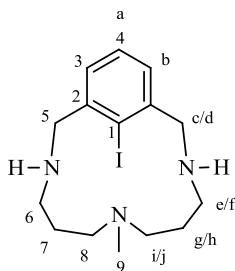
2.3.3. Synthesis of ligand L₁-I



1,3-bis(bromomethyl)-2-iodobenzene (6). Same synthetic procedure as for compound **1** is used to obtain compound **6** but starting from 2-iodo-1,3-dimethylbenzene (Yield: 19 %). ¹H-NMR (CDCl₃, 400 MHz) δ, ppm: 7.40 (d, *J* = 7.2 Hz, 2H, H^b), 7.30 (d, *J* = 6.8 Hz, 1H, H^a), 4.68 (s, 4H, H^c); ¹³C-NMR (CDCl₃, 75.4 MHz) δ, ppm: 142.0 (C2), 130.6 (C3), 129.0 (C4), 39.9 (C5).

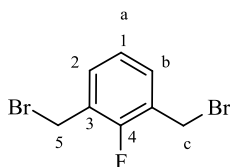


Compound 7. Same synthetic procedure as for compound **3** is used to obtain compound **7** but starting from 1,3-bis(bromomethyl)-2-iodobenzene **6** (Yield: 71 %). $^1\text{H-NMR}$ (CDCl_3 , 400MHz) δ , ppm: 7.74 (dt, $J = 8.4, 1.6$ Hz, 4H, H^l), 7.48 (d, $J = 7.2$ Hz, 2H, H^b), 7.35 (m, 5H, H^m , H^a), 4.49 (m, 4H, H^c , H^d), 2.98 (m, 4H, H^e , H^f), 2.46 (s, 6H, H^n), 2.08 (s, 3H, H^k), 2.08 (m, 2H, H^i or H^j), 1.95 (m, 2H, H^i or H^j), 1.52 (m, 2H, H^g or H^h), 0.96 (m, 2H, H^g or H^h); $^{13}\text{C-NMR}$ (CDCl_3 , 75.4 MHz) δ , ppm: 143.7 (C13), 140.2 (C2), 135.2 (C10), 132.0 (C3), 129.9 (C12), 128.1 (C4), 127.4 (C11), 58.8 (C5), 52.9 (C8), 47.2 (C6), 43.6 (C9), 26.1 (C7), 21.6 (C14); **ESI-MS** (CH_3CN , m/z): 682.1 (100) $[\text{C}_{29}\text{H}_{37}\text{IN}_3\text{O}_4\text{S}_2]^+$.

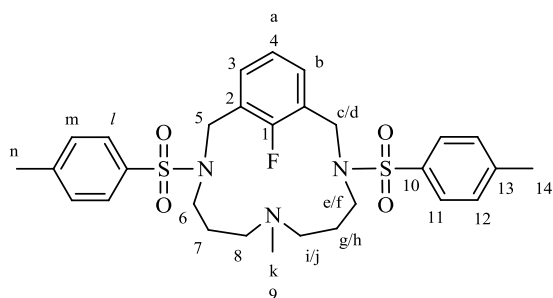


L₁-I. Same synthetic procedure as for ligand **L₁-Cl** is used to obtain ligand **L₁-I** but starting from cyclic tosylated compound **7** (Yield: 27%). Contains <5% of ligand **L₁-Br** which is formed during the amine detosylation step (HBr/AcOH) and cannot be separated from **L₁-I** because of their similar polarity. $^1\text{H-NMR}$ (CDCl_3 , 400MHz) δ , ppm: 7.16 (dd, $J = 6.8, 6.4$ Hz, 1H, H^a), 7.06 (d, $J = 7.2$ Hz, 2H, H^b), 4.30 (d, $J = 14.4$ Hz, 2H, H^c or H^d), 3.65 (d, $J = 14$ Hz, 2H, H^c or H^d), 2.44 (m, 2H, H^i or H^j), 2.35 (m, 2H, H^e or H^f), 2.21 (m, 2H, H^e or H^f), 1.98 (m, 2H, H^i or H^j), 1.83 (s, 3H, H^k), 1.42 (m, 4H, H^g , H^h); $^{13}\text{C-NMR}$ (CDCl_3 , 75.4 MHz) δ , ppm: 144.0 (C2), 130.1 (C3), 127.0 (C4), 104.0 (C1), 58.1 (C5), 55.3 (C8), 42.7 (C6), 39.3 (C9), 26.9 (C7); **ESI-MS** (CH_3CN , m/z): 374.1 (100) $[\text{C}_{15}\text{H}_{25}\text{IN}_3]^+$.

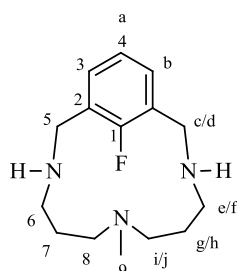
2.3.4. Synthesis of ligand **L₁-F**



1,3-bis(bromomethyl)-2-fluorobenzene (8). Same synthetic procedure as for compound **1** is used to obtain compound **8** but starting from 2-fluoro-1,3-dimethylbenzene (Yield: 26%). $^1\text{H-NMR}$ (CDCl_3 , 400MHz) δ , ppm: 7.36 (t, $J = 7.6$ Hz, 2H, H^b), 7.12 (t, $J = 7.6$ Hz, 1H, H^a), 4.52 (d, $J = 1.2$ Hz, 4H, H^c); $^{13}\text{C-NMR}$ (CDCl_3 , 100.6 MHz) δ , ppm: 158.5 ($J_{\text{C-F}} = 254.0$ Hz, C1), 131.7 ($J_{\text{C-F}} = 3.5$ Hz, C3), 125.7 ($J_{\text{C-F}} = 14.5$ Hz, C2), 124.7 (d, $J_{\text{C-F}} = 4.7$ Hz, C4), 25.2 (d, $J_{\text{C-F}} = 5.3$ Hz, C5).

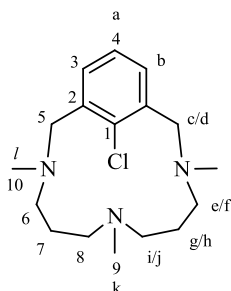


Compound 9. Same synthetic procedure as for compound **3** is used to obtain compound **9** but starting from 1,3-bis(bromomethyl)-2-fluorobenzene **8** (Yield: 65 %). **¹H-NMR** (CDCl₃, 400MHz) δ, ppm: 7.74 (d, *J* = 8.3Hz, 4H, H^l), 7.44 (t, *J* = 7.4 Hz, 2H, H^b), 7.34 (d, *J* = 8.3 Hz, 4H, H^m), 7.16 (t, *J* = 7.4 Hz, 1H, H^a), 4.32 (s, 4H, H^c, H^d), 3.06 (t, 4H, H^e, H^f), 2.45 (s, 6H, H^h), 2.00 (s, 3H, H^k), 2.01 (m, 4H, Hⁱ, H^j), 1.30 (quint., *J* = 7.2 Hz, 4H, H^g, H^h); **¹³C-NMR** (CDCl₃, 100.6 MHz) δ, ppm: 159.3 (d, *J*_{C-F} = 249 Hz, C1), 143.6 (C13), 135.8 (C10), 132.2 (C3), 129.9 (C12), 127.3 (C11), 125.2 (C4), 124.1 (d, *J*_{C-F} = 14.0 Hz, C2), 52.9 (C8), 47.4 (C5), 46.0 (C6), 43.7 (C9), 25.4 (C7), 21.5 (C14); **ESI-MS** (CH₃CN, *m/z*): 674.3 (100) [C₂₉H₃₇FN₃O₄S₂]⁺.

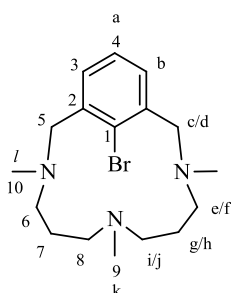


L₁-F. Same synthetic procedure as for ligand **L₁-Cl** is used to obtain ligand **L₁-F** but starting from cyclic tosylated compound **9** (Yield: 36%). **¹H-NMR** (CDCl₃, 400MHz) δ, ppm: 7.08 (t, *J* = 7.2 Hz, 2H, H^b), 6.99 (t, *J* = 7.2 Hz, 1H, H^a), 3.91 (s, 4H, H^c, H^d), 2.38 (t, *J* = 6 Hz, 4H, H^e, H^f), 2.21 (t, *J* = 6 Hz, 4H, Hⁱ, H^j), 2.10 (s, 2H, H_{amines}), 1.90 (s, 3H, CH₃), 1.56 (quint., *J* = 6 Hz, 4H, H^g and H^h); **¹³C-NMR** (CDCl₃, 100.6 MHz) δ, ppm: 160.9 (d, *J*_{C-F} = 244.7 Hz, C1), 130.1 (d, *J*_{C-F} = 5.7 Hz, C3), 128.01 (d, *J*_{C-F} = 14.4 Hz, C2), 123.2 (d, *J*_{C-F} = 3.9 Hz, C4), 55.6 (C8), 49.0 (d, *J*_{C-F} = 2.1 Hz, C5), 43.9 (C6), 40.1 (C9), 26.9 (C7); **¹⁹F-NMR** (CDCl₃, 282.4 MHz) δ, ppm: -124.5 ppm; **ESI-MS** (CH₃CN, *m/z*): 266.1 (100) [C₁₅H₂₅N₃F]⁺. **Anal.** Calcd for **L₁-F**·1/5(NH₄OH) (%) 66.14 C, 16.46 N, 9.25 H, found: 65.87 C, 16.44 N, 9.15 H.

2.3.5. Synthesis of ligands L₅-Cl and L₅-Br



L₅-Cl. 0.42 g of ligand **L₁-Cl** (1.5 mmols), 4.7 mL of HCOH 37 % (63.1 mmols) and 3.4 mL of HCO₂H 85 % (76.6 mmols) are mixed in a round-bottom flask and the resultant solution is refluxed at 100 °C. After 24 h the crude mixture is cooled to room temperature and the solvent is removed under vacuum. Then, extractions using CHCl₃/NaOH_{aq} 30% allowed to isolate a solid that was further purified by chromatography using silica gel and CH₂Cl₂/CH₃OH/NH₄OH (92:6:2) as a mobile phase. 0.315 g of a white solid corresponding to ligand **L₅-Cl** where obtained (yield: 69 %). **¹H-NMR** (CDCl₃, 400MHz) δ, ppm: 7.21 (d, *J* = 7.2 Hz, 2H, H^b), 7.11 (dd, *J* = 6.8, 6.4 Hz, 1H, H^a), 4.00 (d, *J* = 12 Hz, 2H, H^c or H^d), 3.20 (d, *J* = 12 Hz, 2H, H^c or H^d), 2.39 (s, 6H, H^l), 2.36 (m, 2H, Hⁱ or H^j), 2.28 (m, 2H, H^e or H^f), 2.08 (m, 2H, H^e or H^f), 1.90 (m, 2H, Hⁱ or H^j), 1.85 (s, 3H, H^k), 1.37 (m, 2 H, H^g or H^h), 1.15 (m, 2 H, H^g or H^h); **¹³C-NMR** (CDCl₃, 75.4 MHz) δ, ppm: 137.9 (C2), 136.2 (C1), 131.3 (C3), 125.6 (C4), 61.5 (C5), 55.6 (C8), 52.1 (C6), 44.3 (C10), 40.1 (C9), 25.7 (C7); **ESI-MS** (CH₃CN, *m/z*): 310.2 (100) [C₁₇H₂₉ClN₃]⁺. **Anal.** Calcd for L₅-Cl (%) 65.89 C, 13.56 N, 9.11 H, found: 65.62 C, 13.53 N, 9.41 H.



L₅-Br. Similar synthetic procedure than in ligand **L₅-Cl** but starting from ligand **L₁-Br** (Yield: 63 %). **¹H-NMR** (CDCl₃, 300MHz) δ, ppm: 7.15 (m, 3H, H^a, H^b), 4.00 (d, *J* = 16 Hz, 2H, H^c or H^d), 3.21 (d, *J* = 16 Hz, 2H, H^c or H^d), 2.43 (m, 2H, Hⁱ or H^j), 2.38 (s, 6H, H^l), 2.32 (m, 2H, H^e or H^f), 2.02 (m, 2H, H^e or H^f), 1.87 (m, 2H, Hⁱ or H^j), 1.84 (s, 3H, H^k), 1.35 (m, 2H, H^g or H^h) 1.10 (m, 2H, H^g or H^h); **¹³C-NMR** (CDCl₃, 75.5 MHz) δ, ppm: 139.9 (C2), 131.3 (C3), 129.1 (C1), 126.1 (C4), 63.9 (C5), 55.6 (C8), 51.9 (C6), 44.1 (C10), 40.9 (C9), 25.7 (C7); **ESI-MS** (CH₃CN, *m/z*):

454.3 (100) [C₁₇H₂₉BrN₃]⁺. **Anal.** Calcd for L₅-Br (%) 57.63 C, 11.86 N, 7.97 H, found: 57.78 C, 11.61 N, 8.24 H.

2.4. Reaction of arylCu^{III}-halide complexes with 1,10-phenanthroline

Representative experimental details for the reaction of arylCu^{III}-halide complexes **1_{Cl}**, **1_{Br}** and **1_I** with several equivalents of 1,10-phenanthroline is herewith explained. All reagents used were weighted in a precision balance (legibility 0.01 mg) and then entered into an inert-atmosphere glove box to perform the reaction. 3 mL of CH₃CN were added to a vial that contains 4.7 mg of complex **1_{Cl}** (0.012 mmols) obtaining a red suspension of the complex, which was vigorously stirred. Then, 6 equivalents of 1,10-phenanthroline (0.49 mL, 0.15 mM in CH₃CN) were added to the reaction mixture. Progressively, all the complex became soluble and the reaction mixture color changed from red to deep orange corresponding to [Cu(phen)₂]⁺ species. After 1 hour stirring, 50 μL of 1,3,5-trimethoxybenzene 3 mM were added to the crude reaction mixture. The solvent is evaporated and the solid obtained was dried under vacuum for. ¹H-NMR yield of the corresponding C_{aryl}-Cl coupling product (**L₁-Cl**) was obtained in DMSO-d₆ and was calculated using 1,3,5-trimethoxybenzene as internal standard. All products obtained in the reaction crude were identified by ESI-MS spectroscopy.

2.5. Catalytic halide exchange reactions

Ligand **L₁-I**, 1,3,5-trimethoxybenzene and Bu₄NX (X = Cl, Br) were weighted in vials using a precision balance (legibility: 0.01 mg) and then entered into an inert-atmosphere glove box, where stock solutions of **L₁-I**/1,3,5-trimethoxybenzene (24/1 mM) and Bu₄NX (0.36 M) (X = Cl, Br) were prepared in CD₃CN. A stock solution of [Cu^I(CH₃CN)₄]OTf (7.2 mM) was prepared inside the glove box weighting 15 mg of copper(I) salt and adding 5.5 mL of CD₃CN. The **L₁-I**/1,3,5-trimethoxybenzene stock solution (0.3 mL) was loaded into an NMR tube. Then 0.1 mL of [Cu(CH₃CN)₄]OTf 7.2 mM and 0.2 mL of Bu₄NX 0.36 M were added to the NMR tube. The final concentrations were as follows: [**L₁-I**] = 9 mM, [Bu₄NX] = 90 mM (10 equiv), and [Cu(CH₃CN)₄]OTf = 0.9 mM. The reaction was monitored by ¹H-NMR spectroscopy until reaction completion, and all yields were obtained using trimethoxybenzene as internal standard. In reactions using ligand **L₁-I** all calculations were done taking into account the corresponding 5 % of **L₁-Br** present as an impurity (see ligand **L₁-I** synthesis *vide supra*).

Similar procedures were followed for all halide exchange reactions except for the **L₁-Cl** interconversion to **L₁-Br** using NaBr due to the high insolubility of NaBr in CD₃CN. In that case, 3.9 mg of ligand **L₁-Cl** (0.014 mmol) in 1.35 mL of CH₃CN was added to a vial which contained

14.2 mg of NaBr (0.14 mmol). Then 0.19 mL of a solution of $[\text{Cu}(\text{CH}_3\text{CN})_4]\text{OTf}$ 7.2 mM (10 mol %) was added to the mixture, as well as 25 μL of 1,3,5-trimethoxybenzene 3 mM used as an internal standard. After stirring vigorously for 24 hours, the solvent was evaporated under vacuum and the solid crude obtained was redissolved in CD_3CN and filtered in order to remove the remaining solid (a mixture of NaCl and NaBr) before transferring the solution to the NMR tube.

Table 2.5.1. Study of the role of water in the copper-catalyzed halide exchange reactions. ^a $^1\text{H-NMR}$ yield using trimethoxybenzene as internal standard in CD_3CN . Conditions: $[\text{L}_1\text{-X}] = 20 \text{ mM}$ ($\text{X} = \text{Cl}, \text{I}$), $[\text{Cu}(\text{CH}_3\text{CN})_4\text{OTf}] = 2.1 \text{ mM}$ (11 mol%).

Entry	$\text{L}_1\text{-X}$	equiv H_2O	MY (equiv)	T ($^\circ\text{C}$)	time (h)	$\text{L}_1\text{-Y}$ % yield	2 % yield	% SM
1	$\text{L}_1\text{-Cl}$	0	NaI (10)	40	24	54	15	19
2		10	NaI (10)	40	24	56	16	17
3		50	NaI (10)	40	24	45	12	30
4		100	NaI (10)	40	24	27	9	51
5	$\text{L}_1\text{-I}$	0	Bu_4NCl (5)	25	1.5	99	-	-
6		10	Bu_4NCl (5)	25	1.5	99	-	-
7		50	Bu_4NCl (5)	25	1.5	96	-	-
8		100	Bu_4NCl (5)	25	1.5	96	-	-

2.6. Aryl-F reductive elimination reactions

2.6.1. $\text{L}_1\text{-F}$ synthesis: Stoichiometric reactions with complexes $\mathbf{1}_{\text{Cl}}$ and $\mathbf{1}_{\text{Br}}$

A representative experiment of stoichiometric C-F bond forming reactions with aryl- $\text{Cu}^{\text{III}}\text{-X}$ complexes $\mathbf{1}_{\text{Cl}}$, $\mathbf{1}_{\text{Br}}$ and $\mathbf{1}_{\text{I}}$ and using several equivalents of AgF is herewith explained. All reagents used are weighted in vials using a precision balance (legibility: 0.01 mg) and then entered into an inert-atmosphere glove box to perform the reaction. Then, 10 mL of CH_3CN are added to a vial that contains 9.5 mg of complex $\mathbf{1}_{\text{Cl}}$ (0.025 mmols). The resultant suspension was transferred to a vial that contains 25.4 mg of AgF (0.2 mmols), which was vigorously stirred for 8h. Then 50 μL of 1,3,5-trimethoxybenzene 3 mM were added to the mixture crude. The resultant solution was centrifuged in order to remove most of solid inorganic salts. Drops of NH_4OH were added to the mixture crude and the solution was dried with MgSO_4 and filtered. The solution was evaporated under vacuum and the solid obtained was dried under vacuum for

several hours. $^1\text{H-NMR}$ yield of the C-F coupling product ($\text{L}_1\text{-F}$) was obtained in DMSO-d_6 and was calculated using 1,3,5-trimethoxybenzene as internal standard.

A representative experiment of stoichiometric C-F bond forming reactions with aryl Cu^{III} -X complexes $\mathbf{1}_{\text{Cl}}$ and $\mathbf{1}_{\text{Br}}$ and using several equivalents of KF is herewith explained. 6 mL of solvent CH_3CN and 0.7 mL of dmsO-d_6 (ratio 89:11) were added to a vial that contains 9.9 mg of complex $\mathbf{1}_{\text{Cl}}$ (0.026 mmols) inside of a glove box. The resulting suspension was transferred to a vial that contains 7.5 mg of KF (0.13 mmols), which was vigorously stirred during 24h. Then 50 μL of 1,3,5-trimethoxybenzene 3 mM were added to the mixture crude. The resultant solution was centrifuged in order to remove most of solid inorganic salts. Drops of NH_4OH were added to the mixture crude and the solution was dried with MgSO_4 and filtered. The solution was evaporated under vacuum and the solid obtained was dried under vacuum for several hours. $^1\text{H-NMR}$ yield of the C-F coupling product was obtained in DMSO-d_6 and it was calculated using 1,3,5-trimethoxybenzene as internal standard.

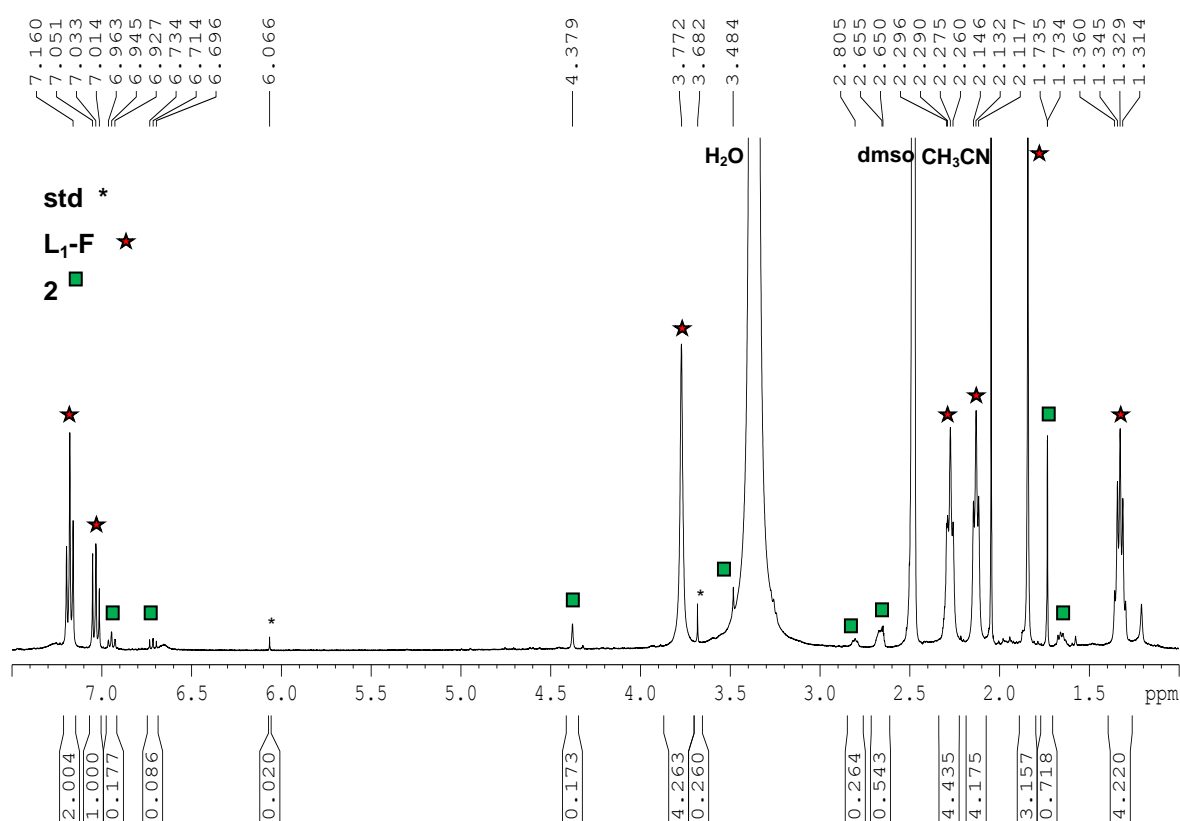


Figure 2.6.1. $^1\text{H-NMR}$ spectra of reaction of $\mathbf{1}_{\text{Cl}}$ with 8 equiv of AgF after copper extraction with NH_4OH in DMSO-d_6 .

2.6.2. Monitoring the formation of L₁-F by ¹H-NMR spectroscopy

All reagents used are weighted in vials using a precision balance (legibility: 0.01 mg) and then entered into an inert-atmosphere glove box to perform the reaction. In an inert-atmosphere glove box, 1.1 mg (0,0023 mmol) complex **1_{Br}** were dissolved in 0.65 mL of CD₃CN and 50 μL of 1,3,5-trimethoxybenzene 12.6 mM as internal standard obtaining a final concentration of complex **1_{Br}** of 2.34 mM. In a vial 0.6 mg (0.0047 mmol) of AgF were dissolved in 0.3 mL of CD₃CN and stirred for 10 min. To initiate the reaction, the solution of complex **1_{Br}** was added to the vial which contains AgF in CD₃CN. The resultant solution was filtered through *Celite*[®], loaded in an NMR tube and capped with a septum. Then, the tube was placed in the NMR probe at 35 °C and the reaction was monitored by ¹H-NMR. The dead time between the beginning of the reaction, taken as time of addition to the AgF solution, and data acquisition was 4 min. ¹⁹F-NMR at the end of the reaction shows only a peak at -122.8 ppm corresponding to the final product **L₁-F**.

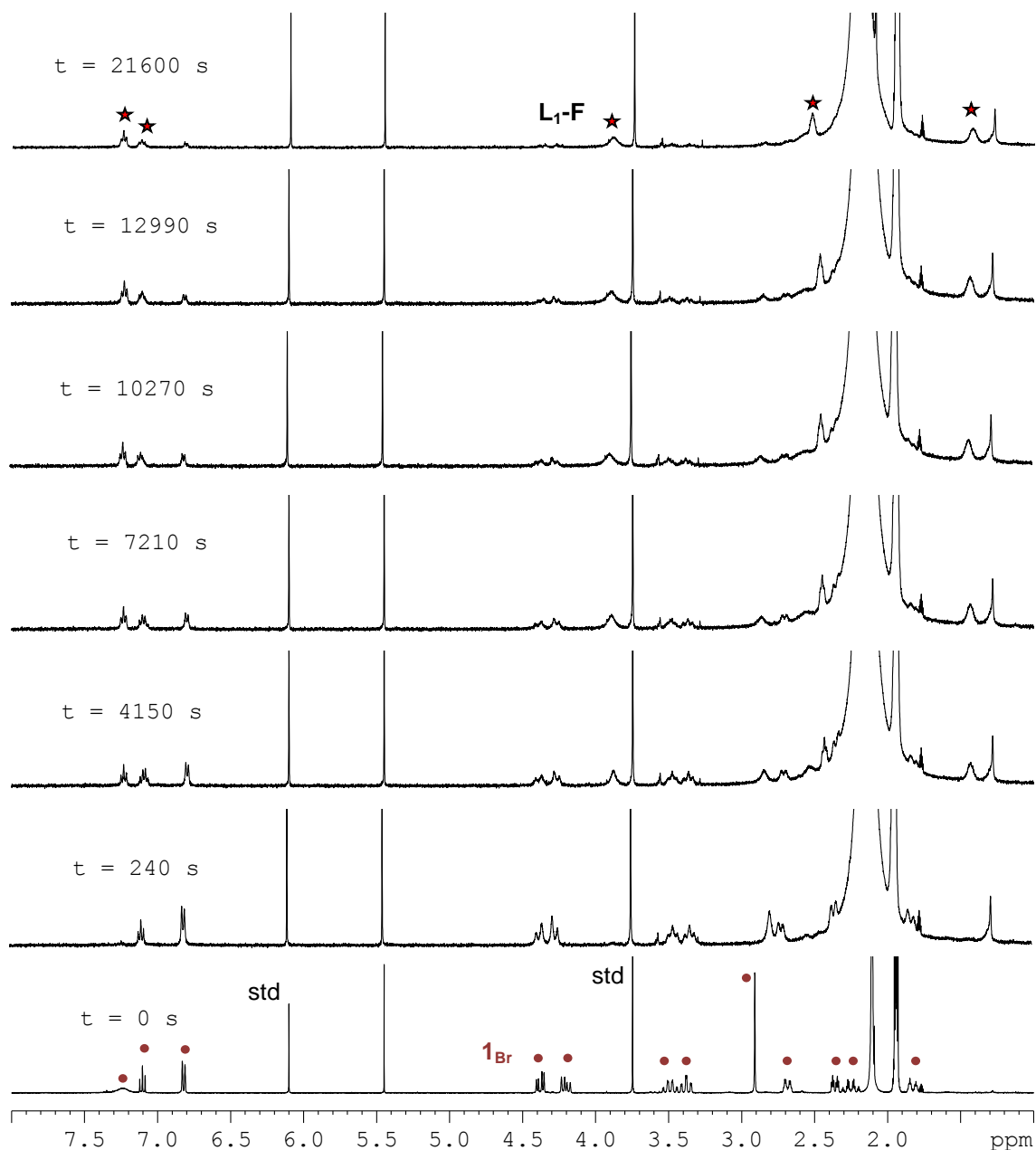


Figure 2.6.2. ¹H-NMR monitoring of the reaction of **1_{Br}** (red dots) with 2 equiv of AgF to afford **L₁-F** (stars) (CD₃CN at 35 °C).

2.6.3. **L₁-F** synthesis: Catalytic reactions using **L₁-Cl** and **L₁-Br**

A representative experiment of catalytic C-F bond forming reactions with ligands **L₁-Cl** and **L₁-Br** and using 10 % mol of [Cu(CH₃CN)₄]OTf and several equivalents of AgF is herewith explained. Ligand **L₁-X** (X = Cl, Br) and AgF were weighted in vials using precise balance (legibility: 0.01 mg) and entered into an inert-atmosphere glove box to perform the reaction. Stock solution of Cu^I(CH₃CN)₄OTf (50 mM) was prepared inside the glove box weighting 21.6

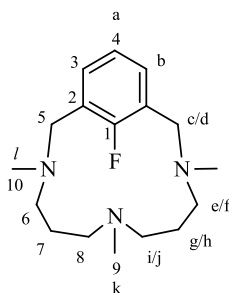
mg of copper(I) salt and adding 1.1 mL of CH₃CN. 10 mg of ligand **L₁-Cl** (0.035 mmols) were dissolved with 2 mL of CH₃CN in a vial. Then 71 μL of stock solution of [Cu(CH₃CN)₄]OTf 50 mM (3.5x10⁻³ mmols) was added and the colour solution change from colourless to red indicating the formation of the corresponding 10% mol of arylCu^{III}-halide complex **1_{Cl}**. In another vial which contains 9 mg of AgF (0.071 mmols), 4 mL of CH₃CN were added and the suspension was stirred vigorously without presence of light. This last solution was transferred drop by drop to the initial solution of **L₁-Cl** and 10% mol of [Cu(CH₃CN)₄]OTf for a period of time of 6h. 50 μL of 1,3,5-trimethoxybenzene 3 mM were added to the final colourless solution. Drops of NH₄OH were added to the mixture crude and the solution was dried with MgSO₄ and filtered. The solution was evaporated under vacuum and the solid obtained was dried under vacuum for several hours. ¹H-NMR yield of the C-F coupling product was obtained in DMSO-d₆ and it is calculated using 1,3,5-trimethoxybenzene as internal standard.

2.6.4. **L₅-F synthesis: Catalytic reactions using L₅-Cl and L₅-Br**

Representative experiment of catalytic C-F bond forming reactions with ligands **L₅-Cl** and **L₅-Br** and using 10 % mol of [Cu(CH₃CN)₄]OTf and several equivalents of AgF is herewith explained. Ligand **L₅-Cl** and AgF were weighted in vials using precise balance (legibility: 0.01 mg) and entered into an inert-atmosphere glove box to perform the reaction. Stock solution of Cu^I(CH₃CN)₄OTf (50 mM) was prepared inside the glove box weighting 22.3 mg of copper(I) salt and adding 1.2 mL of CH₃CN. In an inert-atmosphere glove box, 10 mg of ligand **L₅-Cl** (0.032 mmols) were dissolved in 6 mL of dry acetone in a vial. Then 65 μL of stock solution of [Cu(CH₃CN)₄]OTf 50 mM (3.3x10⁻³ mmols) were added to the solution obtaining a colour solution change from colourless to green. In another vial which contains 8.3 mg of AgF (0.065 mmols), 2 mL of CH₃CN were added and the suspension was stirred vigorously without presence of light. Then, the former solution, which contains **L₅-Cl** and copper, was transferred inside the vial which contains 2 equiv of AgF. The resultant solution was stirred for 12 h and then was centrifuged in order to remove most of solid inorganic salts. Drops of NH₄OH are added to the mixture crude and the solution was dried with MgSO₄ and filtered. The solution was evaporated under vacuum and the solid obtained was dried under vacuum for several hours. ¹H-NMR yield of the **L₅-F** coupling product was obtained in DMSO-d₆ and it was calculated using 1,3,5-trimethoxybenzene as internal standard.

A representative experiment of catalytic C-F bond forming reactions with ligands **L₅-Cl** and **L₅-Br** using 5 % mol of [Cu(CH₃CN)₄]OTf and several equivalents of AgF is herewith explained. In an inert-atmosphere glove box, 10.4 mg of ligand **L₅-Cl** (0.034 mmols) were dissolved with 4 mL of acetone in a vial. Then 34 μL of stock solution of [Cu(CH₃CN)₄]OTf 50 mM (1.7x10⁻³ mmols) were added and the colour solution change from colourless to green. In another vial which contains 8.6 mg of AgF (0.068 mmols), 2 mL of CH₃CN were added and the suspension was stirred vigorously without presence of light. This last solution was transferred

drop by drop to the initial solution of **L₅-Cl** and 10% mol of [Cu(CH₃CN)₄]OTf for a period of 24h. 50 μL of 1,3,5-trimethoxybenzene 3 mM were added to the final colourless solution. Drops of NH₄OH were added to the mixture crude and the solution was dried with MgSO₄ and filtered. The solution was evaporated under vacuum and the solid obtained was dried under vacuum for several hours. ¹H-NMR yield of the **L₅-F** coupling product was obtained in DMSO-d₆ and it was calculated using 1,3,5-trimethoxybenzene as internal standard.



L₅-F (yield: 98%). ¹H-NMR (dmsO-d₆, 400MHz) δ, ppm: 7.20 (t, *J* = 7.2 Hz, 2H, H^b), 7.05 (t, *J* = 7.6 Hz, 1H, H^a), 3.49 (s, 4H, H^c, H^d), 2.32 (s, 6H, Hⁱ), 2.19 (m, 8H, H^e, H^f, H^g, H^h), 1.89 (s, 3H, H^k), 1.29 (m, 4H, H^g, H^h); ¹³C-NMR (CD₃CN, 75.5 MHz) δ, ppm: 160.8 (C1, *J*_{C-F} = 249.0 Hz), 131.5 (C3, *J*_{C-F} = 5.1 Hz), 126.5 (C2, *J*_{C-F} = 14.87 Hz), 123.3 (C4, *J*_{C-F} = 4.22 Hz), 57.1 (C5), 55.6 (C8), 52.0 (C6), 43.3 (C10), 40.3 (C9), 24.9 (C7); ¹⁹F-NMR (dmsO-d₆, 282.4 MHz) δ, ppm: -119.3 ppm (CD₃CN, 282.4 MHz) δ, ppm: -120.1; **ESI-MS** (CH₃CN, *m/z*): 294.1 (100) [C₁₇H₂₈N₃F]⁺. **Anal.** Calcd for **L₅-F**·3/7(CH₂Cl₂) (%) 63.45 C, 12.74 N, 8.82 H, found: 63.14 C, 12.40 N, 8.82 H.

2.7. Stoichiometric aryl fluoride activation

A solution of [Cu(CH₃CN)₄]OTf (11 mg, 0.029 mmols) in acetone (1 mL) was added to a vial that contains ligand **L₁-F** (6.7 mg, 0.025 mmols) in 1 mL of acetone. The resulting solution was vigorously stirred for 12 h. Then, 2 equivalents of tetrabutylammonium chloride (13.9 mg, 0.050 mmols) and 100 μL of 1,3,5-trimethoxybenzene 10 mM were added to the mixture crude and the solvent was evaporated under vacuum. The mixture crude was dissolved in DMSO-d₆ and filtered through *Celite*[®] obtaining a deep red solution. ¹H-NMR yield of the complex **1_{C1}** was 75% (calculated using 1,3,5-trimethoxybenzene as internal standard).

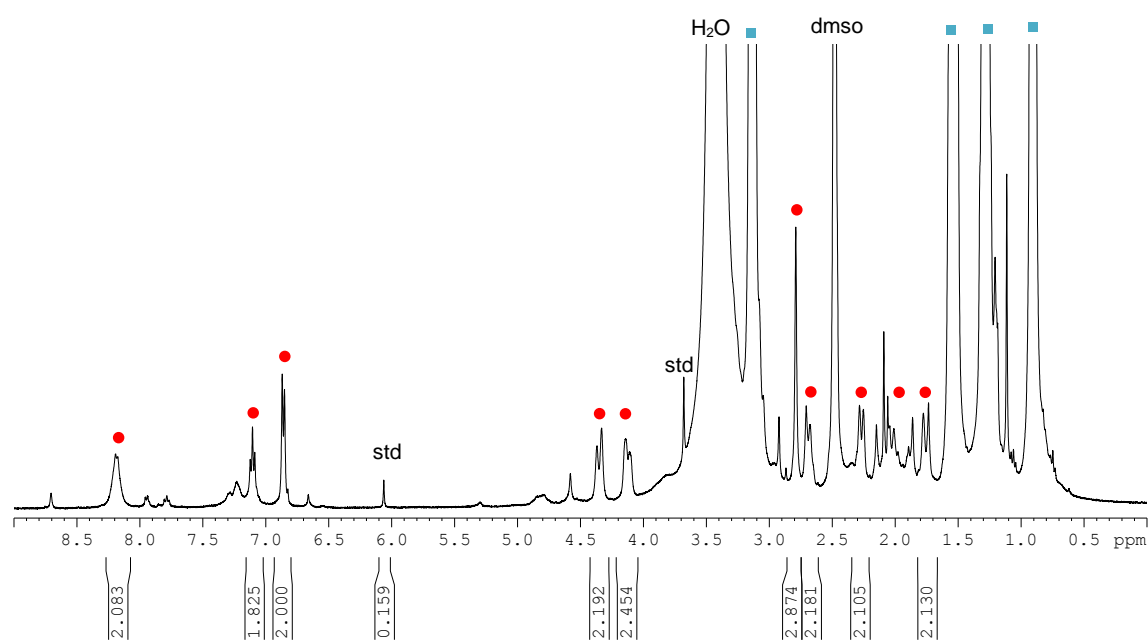


Figure 2.7.1. $^1\text{H-NMR}$ spectra in DMSO-d_6 of reaction crude of defluorination of ligand $\text{L}_1\text{-F}$ to afford complex 1_{Cl} (red circles). Blue squares indicate tetrabutylammonium anions used in the reaction.

2.8. Computational details

All geometry optimizations were performed at the B3LYP³ level, with a standard 6-31G(d) basis set⁴ in the Gaussian03 package.⁵ The geometry optimizations were performed

3. Becke, A. D. *J. Chem. Phys.* **1993**, *98*, 5648-5652; Lee, C.; Yang, W.; Parr, R. G. *Phys. Rev. B* **1988**, *37*, 785-789; Stevens, P. J.; Devlin, F. J.; Chabalowski, C. F.; Frisch, M. J. *J. Phys. Chem.* **1994**, *98*, 11623.

4. Hehre, W. J.; Ditchfield, R.; Pople, J. A. *J. Chem. Phys.* **1972**, *56*, 2257.

5. Frisch, M. J.; Trucks, G. W.; Schlegel, H. B.; Scuseria, G. E.; Robb, M. A.; Cheeseman, J. R.; Montgomery, J.; Vreven, T.; Kudin, K. N.; Burant, J. C.; Millam, J. M.; Iyengar, S. S.; Tomasi, J.; Barone, V.; Mennucci, B.; Cossi, M.; Scalmani, G.; Rega, N.; Petersson, G. A.; Nakatsuji, H.; Hada, M.; Ehara, M.; Toyota, K.; Fukuda, R.; Hasegawa, J.; Ishida, M.; Nakajima, T.; Honda, Y.; Kitao, O.; Nakai, H.; Klene, M.; Li, X.; Knox, J. E.; Hratchian, H. P.; Cross, J. B.; Adamo, C.; Jaramillo, J.; Gomperts, R.; Stratmann, R. E.; Yazyev, O.; Austin, A. J.; Cammi, R.; Pomelli, C.; Ochterski, J. W.; Ayala, P. Y.; Morokuma, K.; Voth, G. A.; Salvador, P.; Dannenberg, J. J.; Zakrzewski, V. G.; Dapprich, S.; Daniels, A. D.; Strain, M. C.; Farkas, O.; Malick, D. K.; Rabuck, A. D.; Raghavachari, K.; Foresman, J. B.; Ortiz, J. V.; Cui, Q.; Baboul, A. G.; Clifford, S.; Cioslowski, J.; Stefanov, B. B.; Liu, G.; Liashenko, A.; Piskorz, P.; Komaromi, I.; Martin, R. L.; Fox, D. J.; Keith, T.; Al-Laham, M. A.; Peng, C. Y.; Nanayakkara, A.; Challacombe, M.; Gill, P. M. W.; Johnson, B.; Chen, W.; Wong, M. W.; Gonzalez, C.; Pople, J. A.; Gaussian Inc.: Wallingford CT, **2004**.

without symmetry constraints and the stationary points found were characterized by analytical frequency calculations. Intrinsic reaction pathways⁶ were calculated to confirm the connection between the located transition states and the expected minima. Solvent effects including contributions of non electrostatic terms were estimated in single point calculations on the gas phase optimized structures, based on the polarizable continuous solvation model (PCM) using CH₃CN as a solvent.⁷ The cavity was created via a series of overlapping spheres.

6. Fukui, K. *Acc. Chem. Res.* **1981**, *14*, 363.

7. Barone, V.; Cossi, M. *J. Phys. Chem. A.* **1998**, *102*, 1995-2001; Tomassi, J.; Perisco, M. *Chem. Rev.* **1994**, *94*, 2027.

3. Supplementary Information Chapter VI

3.1. Materials and methods	220
3.2. Instrumentation	220
3.3. Synthesis of aryl-Cu ^{III} complex (1 _{ClO₄}).....	221
3.4. Synthesis and characterization of C-O coupling products.....	222
3.4.1. Carboxylic acid nucleophiles.....	222
3.4.2. Phenol nucleophiles	226
3.4.3. Aliphatic alcohol nucleophiles	229
3.5. General procedure for monitoring kinetics by NMR spectroscopy	229
3.6. General procedure for monitoring kinetics by UV-Vis spectroscopy	230
3.7. General procedure for catalytic experiments.....	235

3.1. Materials and methods

Reagents and solvents used were commercially available reagent quality unless indicated otherwise. Solvents were purchased from SDS and were purified and dried by passing through an activated alumina purification system (MBraun SPS-800). Preparation and handling of air-sensitive materials were carried out in a N₂ drybox (MBraun-Unilab) with O₂ and H₂O concentrations < 1 ppm. Ligand **L₁-H** was synthesized following procedure described in the literature.¹ Ligand **L₁-Br** was synthesized following procedure described in supporting information of Chapter V.

3.2. Instrumentation

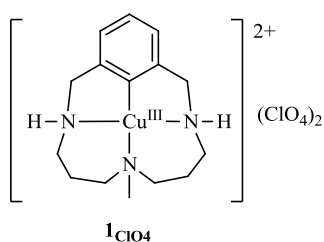
UV-Vis spectroscopy was performed on a Cary-50 (Varian) UV-Vis spectrophotometer. Low temperature control was maintained with a cryostat from Unisoku Scientific Instruments, Japan. Alternatively, low temperature was achieved with a dewar bath and electronic spectra taken using Helma dip probe (0.5 cm path length). NMR data concerning product identity were collected on Bruker 600 MHz, Bruker 500 MHz or Bruker 400 MHz AVANCE spectrometers in

1. Xifra, R.; Ribas, X.; Llobet, A.; Poater, A.; Duran, M.; Solà, M.; Stack, T. D. P.; Benet-Buchholz, J.; Donnadieu, B.; Mahía, J.; Parella, T. *Chem.-Eur. J.* **2005**, *11*, 5146.

CD₃CN and calibrated relative to an internal reference, either the residual protons of the solvent or added tetramethylsilane. ESI-MS experiments were collected and analyzed on a Bruker Daltonics Esquire 6000 spectrometer with acetonitrile or acetonitrile/water (80:20) as the mobile phase.

3.3. Synthesis of aryl-Cu^{III} complex (**1**_{ClO₄})

Caution: Perchlorate salts are potentially explosive and should be handled with care! Complex **1**_{ClO₄} was described in a previous work^{1,2} and here we present a modified synthetic method in order to enhance the final yield. A solution of CuCl₂ (45.5 mg, 0.33 mmol) in acetone (20 mL) was added to a vigorously stirred solution of ligand L₁-H (90.1mg, 0.36 mmols) in acetone (15 mL). After 5 h stirring under O₂ atmosphere (1 atm), the solution was centrifuged in order to separate the solid from the solution. Then, a solution of AgClO₄ in CH₃CN (137.2 mg, 0.66 mmol, 5 mL) is added dropwise to a vigorously stirred solution of the redissolved solid in CH₃CN (5mL). After a few seconds the solution became cloudy and a precipitate appeared. The solution is filtered through Celite and then through an Acrodisc[®] filter. Slow diethyl ether diffusion over the resultant solution in the anaerobic box afforded 102.3 mg of orange crystals. (0.20 mmols, 82%)



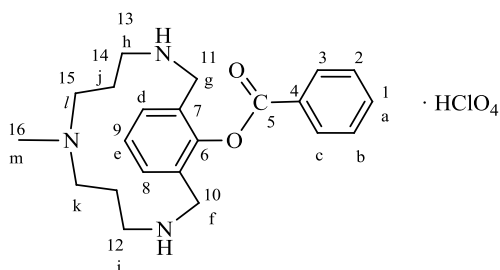
¹H-NMR (400 MHz, CD₃CN, 25°C) δ, ppm: 7.25 (t, *J* = 8 Hz, 1H), 6.98 (d, *J* = 8 Hz, 2H), 6.30 (s, 2H), 4.62 (d, *J* = 16 Hz, 2H), 4.47 (d, *J* = 16 Hz, 2H), 3.18 (t, *J* = 16 Hz, 2H), 3.05 (d, *J* = 8 Hz, 4H), 2.97 (d, *J* = 8 Hz, 4H), 2.68 (s, 3H), 2.56 (dt, *J* = 13.2, 2.8 Hz, 2H), 2.15 (m, 2H), 1.95 (m, 2H). **ESI-MS** (CH₃CN, *m/z*): 408.0 (100) [C₁₅H₂₄ClCuN₃O₄]⁺.

2. Ribas, X.; Jackson, D. A.; Donnadiou, B.; Mahía, J.; Parella, T.; Xifra, R.; Hedman, B.; Hodgson, K. O.; Llobet, A.; Stack, T. D. P. *Angew. Chem. Int. Ed.* **2002**, *41*, 2991.

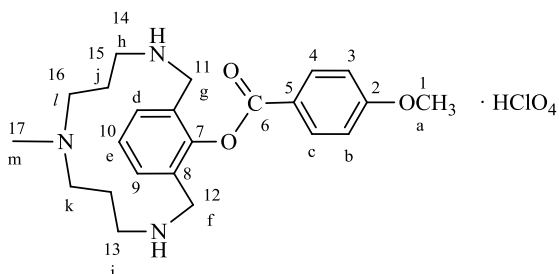
3.4. Synthesis and characterization of C-O coupling products

3.4.1. Carboxylic acid nucleophiles

In an inert-atmosphere glove box, a sample of the arylCu^{II} complex **1**_{ClO₄} (9 mg, 17 μmol) was dissolved in CD₃CN (2 mL). A portion of this solution (0.1 mL) was loaded into an NMR tube, and 1 or 10 equiv of the carboxylic acid nucleophile was added to the tube. The tube was sealed with a screw-cap and the reaction was monitored by ¹H-NMR spectroscopy. ¹H and ¹³C-NMR spectra and mass spectrometric analysis were obtained without isolation of the C-O coupling product. Reaction yields were obtained by integration of the ¹H-NMR spectra of the crude reaction mixtures relative to trimethoxybenzene as an internal standard (2.5 mM in CD₃CN).

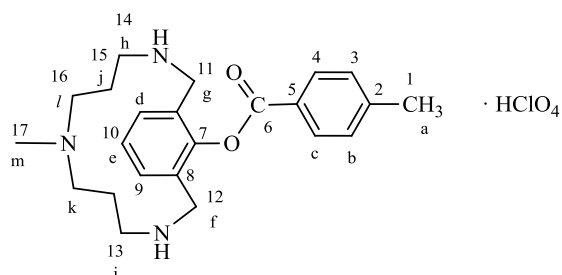


(100% yield) **¹H-NMR** (500.2 MHz, benzene-d₆, 70 °C) δ, ppm: 7.42 (br m, 2H, H^c), 7.06 (m, 3H, H^a, H^b), 6.68 (m, 3H, H^d, H^e), 4.97 (br m, 2H, H^f), 3.47 (s, 2H, H^h), 3.28 (br m, 2H, H^g), 2.19 (br m, 4H, Hⁱ), 2.11 (br m, 4H, H^j), 1.76 (br m, 2H, H^k), 1.72 (br m, 3H, H^m), 1.09 (br m, 2H, H^l). **¹³C-NMR** (125.7 MHz, benzene-d₆, 70 °C) δ, ppm: 173.5 (C5), 160.0 (C4), 141.2 (C7), 132.5 (C6), 131.0 (C1), 130.6 (C3), 129.6 (C2), 124.9 (C9), 121.8 (C8), 59.6 (C12), 55.7 (C10), 55.1 (C11), 46.3 (C13), 45.1 (C16), 30.3 (C15), 29.8 (C14). **ESI-HRMS** (*m/z*): [M+H]⁺ calculated for C₂₂H₃₀N₃O₂⁺, 368.2333, found: 368.2328.

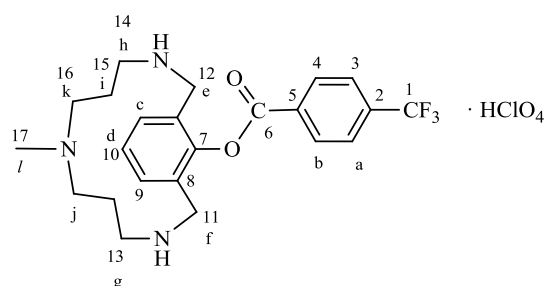


(100% yield) **¹H-NMR** (500.2 MHz, benzene-d₆, 70 °C) δ, ppm: 7.45 (d, *J* = 8.4 Hz, 2H, H^b), 7.37 (br m, 1H, H^e), 6.69 (m, 4H, H^c, H^d), 5.02 (br m, 2H, H^f), 3.46 (br m, 2H, H^h), 3.34 (br m, 2H, H^g), 3.28 (s, 3H, H^a), 2.19 (br m, 2H, Hⁱ), 2.12 (br m, 4H, H^j), 1.80 (br m, 2H, H^k), 1.73 (s, 3H, H^m),

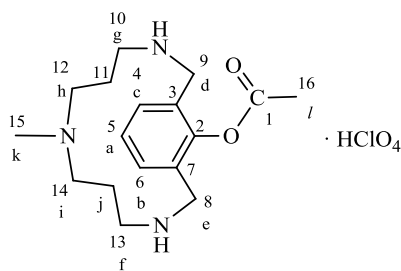
1.09 (m, 2H, H^l). **¹³C-NMR** (125.7 MHz, benzene-d₆, 70 °C) δ, ppm: 173.6 (C6), 162.9 (C5), 159.9 (C2), 133.4 (C8), 132.6 (C7), 131.5 (C4), 125.0 (C10), 121.9 (C3), 116.2 (C9), 59.7 (C13), 57.1 (C1), 55.8 (C11), 55.1 (C12), 46.4 (C14), 45.1 (C17), 30.3 (C16), 29.2 (C15). **ESI-HRMS** (*m/z*): [M+H]⁺ calculated for C₂₃H₃₂N₃O₃⁺, 398.2439, found: 398.2440.



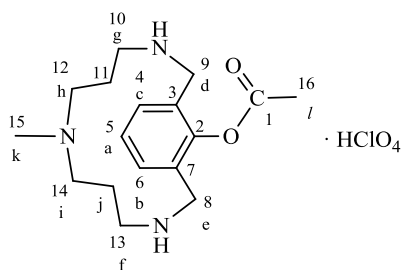
(100% yield) **¹H-NMR** (500.2 MHz, benzene-d₆, 70 °C) δ, ppm: 7.39 (m, J = 6.0 Hz, 2H, H^b), 6.92 (d, J = 5.9 Hz, 2H, H^c), 6.69 (m, 3H, H^d, H^e), 5.00 (br m, 2H, H^f), 3.46 (s, 2H, H^h), 3.33 (br m, 2H, H^g), 2.19 (s, 2H, Hⁱ), 2.12 (br m, 4H, H^j), 2.04 (s, 3H, H^a), 1.79 (br m, 2H, H^k), 1.72 (s, 3H, H^m), 1.10 (br m, 2H, H^l). **¹³C-NMR** (125.7 MHz, benzene-d₆, 70 °C) δ, ppm: 173.7 (C6), 160.0 (C5), 140.8 (C8), 138.3 (C7), 132.5 (C2), 131.3 (C4), 129.8 (C3), 125.0 (C10), 121.8 (C9), 59.7 (C13), 55.8 (C11), 55.1 (C12), 46.4(C14), 45.1 (C17), 30.3 (C16), 29.2 (C15), 23.2 (C1). **ESI-HRMS** (*m/z*): [M+H]⁺ calculated for C₂₃H₃₂N₃O₂⁺, 382.2490, found: 382.2491.



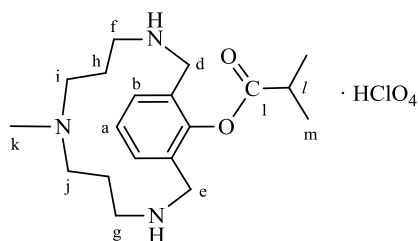
(100% yield) **¹H-NMR** (500.2 MHz, benzene-d₆, 70 °C) δ, ppm: 7.29 (br m, 5H, H^a, H^b, H^d), 6.69 (br m, 2H, H^c), 5.11 (v br m, 2H, H^e), 4.46 (v br m, 2H, NH), 3.44 (br m, 2H, H^g), 3.02 (v br m, 2H, H^b), 2.17 (s, 2H, H^h), 2.11 (br m, 4H, Hⁱ), 1.71 (br m, 5H, H^l, H^j), 1.08 (br m, 2H, H^k). **¹³C-NMR** (125.7 MHz, benzene-d₆, 70 °C) δ, ppm: 172.1 (C6), 160.0 (C5), 144.5 (C8), 133.2 (d, J_{C-F} = 32 Hz, C2), 132.4 (C7), (128.0, 125.8, 125.0, J_{C-F} = 370 Hz, 260 Hz, 106 Hz, C1), 127.7 (C4), 127.7 (C6), 121.8 (C9), 59.4 (C13), 55.8 (C11), 55.0 (C12), 46.3 (C14), 45.0 (C17), 30.2 (C16), 29.2 (C15). **ESI-HRMS** (*m/z*): [M+H]⁺ calculated for C₂₂H₂₉F₃N₃O₂⁺, 436.2207, found: 436.2212.



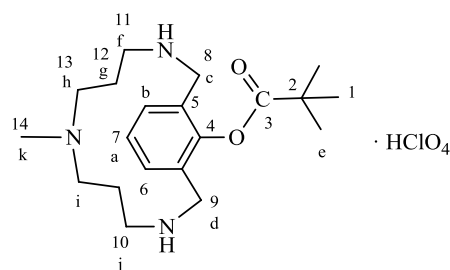
(100% yield) $^1\text{H NMR}$ (500.2 MHz, benzene- d_6 , 70 °C) δ , ppm: 7.77 (d, $J = 6.3$ Hz, 2H, H^a), 7.13 (m, 3H, H^b, H^d), 6.70 (m, 2H, H^c), 5.15 (br m, 2H, H^e), 4.34 (br m, 2H, **NH**), 3.45 (s, 2H, H^g), 2.91 (br m, 2H, H^f), 2.17 (br m, 2H, H^h), 2.12 (br m, 4H, H^i), 1.74 (s, 2H, H^j), 1.67 (br m, 3H, H^l), 1.09 (br m, 2H, H^k). $^{13}\text{C NMR}$ (125.7 MHz, benzene- d_6 , 70 °C) δ , ppm: 171.39 (C_5), 160.10 (C_4), 150.58 (C_7), 146.50 (C_2), 132.28 (C_1), 125.83 (C_9, C_8), 124.98 (C_6), 121.80 (C_3), 59.41 (C_{12}), 55.76 (C_{10}), 55.07 (C_{11}), 46.28 (C_{13}), 45.05 (C_{16}), 30.24 (C_{15}), 29.22 (C_{14}). **ESI-HRMS** (m/z): $[\text{M}+\text{H}]^+$ calculated for $\text{C}_{22}\text{H}_{29}\text{N}_4\text{O}_4^+$, 413.2184, found: 413.2189.



(100% yield) $^1\text{H-NMR}$ (499.9 MHz, CDCl_3 , 24 °C) Two conformations present, resonances for minor conformation indicated with prime symbol (Major isomer: 60%, Minor isomer: 40%). δ , ppm: 7.16 (d, $J = 7.0$ Hz, 1H, H^a), 7.06 (d, $J = 7.05$ Hz, 1H, H^a'), 6.95 (d, $J = 7.6$ Hz, 1H, H^b), 6.91 (d, $J = 7.6$ Hz, 1H, H^b'), 6.74 (t, $J = 7.9, 6.9$ Hz, 1H, H^c), 6.72 (t, $J = 8.3, 7.6$ Hz, 1H, H^c'), 4.83 (br m, 2H, H^d) 4.53 (br m, 2H, H^d'), 4.06 (br m, 2H, H^e), 3.25 (br s, H^e), 3.07 (t, $J = 6.8, 6.8$ Hz, 2H, H^f), 2.64 (m, 4H, H^g, H^h), 2.35 (s, 3H, H^i), 2.29 (m, 4H, H^j), 2.10 (s, 3H, H^l), 2.04 (s, 3H, H^k), 2.01 (s, 3H, H^k'), 1.56 (m, 2H, H^l). $^{13}\text{C-NMR}$ (125.7 MHz, CDCl_3 , 24 °C) δ , ppm: 173.0 (C_1), 160.0 (C_2), 159.7 (C_2'), 133.0 (C_6), 132.1 (C_7), 131.5 (C_3), 130.8 (C_6'), 127.4 (C_4), 126.3 (C_2'), 125.4 (C_3'), 124.7 (C_4'), 122.0 (C_5), 121.8 (C_5'), 59.8 (C_{10}), 58.2 (C_{10}'), 56.1 (C_9), 55.7 (C_8), 55.3 (C_9'), 55.2 (C_8'), 49.4 (C_{13}), 48.3 (C_{13}'), 47.0 (C_{14}), 46.6 (C_{14}'), 46.1 (C_{15}), 45.9 (C_{15}'), 44.9 (C_{11}), 30.3 (C_{12}), 30.1 (C_{12}'), 29.2 (C_{11}), 25.2 (C_{16}), 24.4 (C_{16}). **ESI-HRMS** (m/z): $[\text{M}+\text{H}]^+$ calculated for $\text{C}_{17}\text{H}_{28}\text{N}_3\text{O}_2^+$, 306.2177, found: 306.2173.



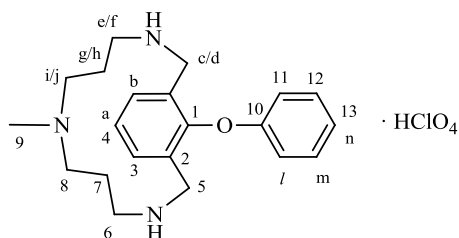
(100% yield) **¹H-NMR**: (499.9 MHz, CDCl₃, 24 °C) Two conformations present, resonances for minor conformation indicated with prime symbol. (Major isomer : 65%, Minor isomer: 35%). δ , ppm: 7.14 (d, $J = 7.13$ Hz, 1H, H^a), 7.06 (d, $J = 7.1$ Hz, 1H, H^{a'}), 6.95 (d, $J = 7.4$ Hz, 1H, H^b), 6.91 (d, $J = 6.8$ Hz, 1H, H^{b'}), 6.74 (t, $J = 7.4, 6.8$ Hz, 1H, H^c), 6.72 (t, $J = 7.4, 7.9$ Hz, 1H, H^{c'}), 4.60 (br m, 2H, H^d), 4.07 (br m, 2H, H^e), 3.23 (br sep, $J = 6.8, 6.8$ Hz, 1H, H^f), 3.11 (t, $J = 7.9$ Hz, 2H, H^{f'}), 2.74 (sep, $J = 6.5$ Hz, 1H, H^g), 2.64 (br m, 2H, H^g), 2.32 (t, 2H, Hⁱ), 2.28 (t, 2H, H^{i'}), 2.06 (s, 3H, H^k), 2.02 (s, 3H, H^{k'}), 1.56 (br m, 2H, H^h), 1.47 (br m, 2H, H^{h'}), 1.22 (d, $J = 6.3$ Hz, 6H, H^l), 1.14 (d, $J = 6.3$ Hz, 6H, H^{l'}). **¹³C-NMR** (125.7 MHz, CDCl₃, 24°C) δ , ppm: 179.7, 179.3, 160.0, 160.0, 132.9, 132.0, 131.4, 130.7, 127.9, 126.5, 125.4, 124.7, 122.1, 121.8, 79.9, 79.7, 79.4, 59.8, 58.7, 55.9, 55.8, 55.3, 55.2, 47.4, 47.2, 47.1, 46.6, 46.1, 45.9, 44.9, 42.5, 33.1, 33.0, 30.3, 30.2, 29.9, 28.9, 22.5, 22.4. **ESI-HRMS** (m/z): [M+H]⁺ calculated for C₁₉H₃₂N₃O₂⁺, 334.2490, found: 334.2490.



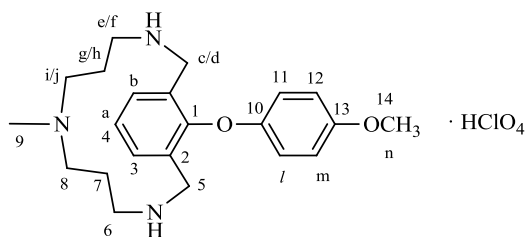
(100% yield) **¹H-NMR** (500.2 MHz, benzene-d₆, 70 °C) δ , ppm: δ 7.36 (m, 1H, H^a), 6.69 (m, 2H, H^b), 5.02 (br m, 2H, H^c), 3.46 (br m, 2H, H^f), 3.27 (br m, 2H, H^d), 2.20 (t, $J = 5.6$ Hz, 2H, H^h), 2.17 (br m, 4H, H^g), 1.83 (br m, 2H, Hⁱ), 1.79 (s, 3H, H^k), 1.31 (s, 9H, H^e), 1.09 (br m, 2H, H^j). **¹³C-NMR** (125.7 MHz, benzene-d₆, 70°C) δ , ppm: 178.9 (C3), 159.9 (C5), 132.2 (C4), 124.9 (C7), 121.9 (C6), 60.3 (C10), 55.6 (C8), 55.2 (C9), 46.4 (C11), 45.2 (C14), 41.5 (C2), 31.4 (C1), 30.3 (C13), 28.5 (C12). **ESI-HRMS** (m/z): [M+H]⁺ calculated for C₂₀H₃₄N₃O₂⁺, 348.2646, found: 348.2643.

3.4.2. Phenol nucleophiles

In an inert-atmosphere glove box, a sample of the arylCu^{II} complex **1**_{ClO₄} (49.2 mg, 17 μmol) was dissolved in CD₃CN (4.6 mL). A portion of this solution (0.4 mL) was loaded into an NMR tube, and 1.1 equiv of the corresponding phenol nucleophile was added to the tube (0.25 mL, 35 mM). 50 μL of 1,3,5-trimethoxybenzene was added as an internal standard. Final concentrations: [**1**_{ClO₄}] = 12 mM and [pX-phenol] = 12.5 mM. The tube was sealed with a screw-cap and the reaction was heated at 50 °C and monitored by ¹H-NMR spectroscopy till reaction completion. ¹H and ¹³C-NMR spectra and mass spectrometric analysis were obtained without isolation of the C-O coupling product. Reaction yields were obtained by integration of the ¹H-NMR spectra of the crude reaction mixtures relative to 1,3,5-trimethoxybenzene.

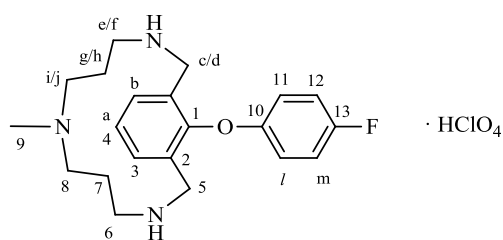


(100% yield) **¹H-RMN** (400 MHz, CD₃CN, 25 °C) δ, ppm: 7.32 (m, 5H, H^b, H^m, Hⁿ), 7.08 (tt, *J* = 7.4, 1 Hz, 1H, H^a), 6.86 (d, 2H, *J* = 7.7 Hz, H^l), 3.78 (d, *J* = 13.2 Hz, 2H, H^c or H^d), 3.49 (d, *J* = 13.6 Hz, 2H, H^e or H^f), 3.17 (m, 2H, Hⁱ or H^j), 2.83 (m, 2H, H^e or H^f), 2.76 (m, 2H, Hⁱ or H^j), 2.69 (m, 2H, H^e or H^f), 2.60 (s, 3H, H^k), 1.70 (m, 2H, H^g or H^h), 1.09 (m, 2H, H^g or H^h). **¹³C-RMN** (100 MHz, CD₃CN, 25 °C) δ, ppm: 157.1 (C10), 152.2 (C1), 133.7 (C2), 132.0 (C3), 130.0 (C12), 125.9 (C4), 122.4 (C13), 115.0 (C11), 55.9 (C8), 49.4 (C5), 46.6 (C6), 39.4 (C9), 24.2 (C7). **ESI-MS** (CH₃CN:H₂O (80:20), *m/z*): 340.2 (100) [C₂₁H₃₀N₃O]⁺.

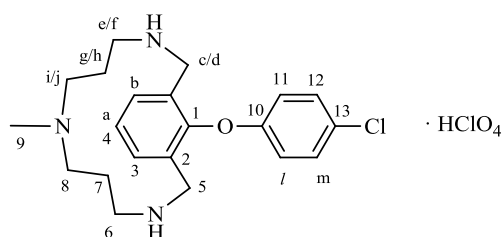


(100% yield) **¹H-NMR** (400 MHz, CD₃CN, 25 °C) δ, ppm: 7.36 (d, *J* = 7.4 Hz, 2H, H^b), 7.25 (t, *J* = 6.9 Hz, 1H, H^a), 6.88 (dt, *J* = 6.3, 2.5 Hz, 2H, H^m), 6.79 (dt, *J* = 9.3, 2.5 Hz, 2H, H^l), 3.80 (d, *J* = 13.3 Hz, 2H, H^c or H^d), 3.70 (s, 3H, Hⁿ), 3.49 (d, *J* = 13.3 Hz, 2H, H^c or H^d), 3.13 (m, 2H, Hⁱ or H^j), 2.82 (m, 2H, H^e or H^f), 2.72 (m, 4H, H^e or H^f, Hⁱ or H^j), 2.57 (s, 3H, H^k), 1.70 (m, 2H, H^g or H^h), 1.10 (m, 2H, H^g or H^h). **¹³C-RMN** (100 MHz, CD₃CN, 25 °C) δ, ppm: 155.0 (C13), 152.7 (C10), 151.0 (C1), 133.6 (C2), 132.0 (C3), 125.6 (C4), 115.9 (C11), 114.9 (C12), 55.9 (C8),

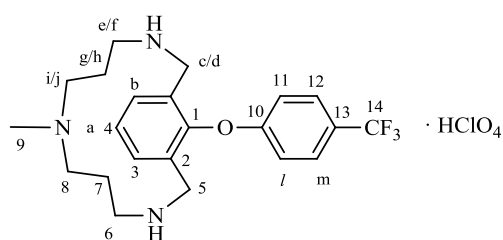
55.3 (C14), 49.4 (C5), 46.6 (C6), 39.4 (C9), 24.2 (C7). **ESI-MS** (CH₃CN, m/z): 370.3 (100) [C₂₂H₃₂N₃O₂]⁺.



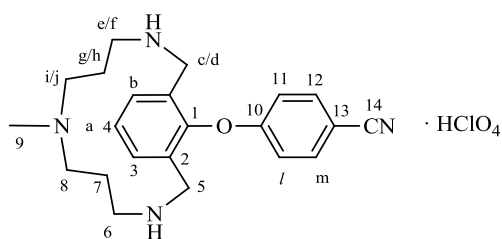
(100% yield) **¹H-NMR** (400 MHz, CD₃CN, 25 °C) δ, ppm: 7.37 (d, *J* = 7.4 Hz, 2H, H^b), 7.27 (dd, *J* = 6.8, 6.7 Hz, 1H, H^a), 7.07 (m, 2H, H^m), 6.86 (m, 2H, H^l), 3.79 (d, *J* = 14.3 Hz, 2H, H^c or H^d), 3.49 (d, *J* = 13.4 Hz, 2H, H^c or H^d), 3.17 (m, 2H, Hⁱ or H^j), 2.75 (m, 6H, H^e, H^f, Hⁱ or H^j), 2.60 (s, 3H, H^k), 1.69 (m, 2H, H^g or H^h), 1.06 (m, 2H, H^g or H^h). **¹³C-RMN** (100 MHz, CD₃CN, 25 °C) δ, ppm: 158.0 (d, *J*_{C-F} = 237.7 Hz, C13), 153.3 (d, *J*_{C-F} = 2.21 Hz, C10), 152.4 (C1), 133.7 (C2), 132.0 (C3), 125.9 (C4), 116.4 (d, *J*_{C-F} = 8.15 Hz, C11), 116.2 (d, *J*_{C-F} = 23.74 Hz, C12), 55.9 (C8), 49.4 (C5), 46.7 (C6), 39.4 (C9), 24.2 (C7). **ESI-MS** (CH₃CN, m/z): 358.3 (100) [C₂₁H₂₉FN₃O]⁺.



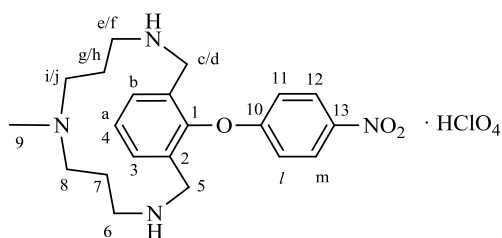
(100% yield) **¹H-RMN** (400 MHz, CD₃CN, 25 °C) δ, ppm: 7.37 (m, *J* = 7.2, 2H, H^b), 7.32 (dt, *J* = 9.0, 2.2 Hz, 2H, H^m), 7.28 (dd, *J* = 6.8, 6.8 Hz, 1H, H^a), 6.85 (dt, *J* = 9.0, 2.2 Hz, 2H, H^l), 3.77 (d, *J* = 13.6 Hz, 2H, H^c or H^d), 3.49 (d, *J* = 13.6 Hz, 2H, H^c or H^d), 3.18 (m, 2H, Hⁱ or H^j), 2.75 (m, 6H, H^e, H^f, Hⁱ or H^j), 2.60 (s, 3H, H^k), 1.68 (m, 2H, H^g or H^h), 1.06 (m, 2H, H^g or H^h). **¹³C-RMN** (100 MHz, CD₃CN, 25 °C) δ, ppm: 156.0 (C10), 152.0 (C1), 133.8 (C2), 132.0 (C3), 129.7 (C12), 126.7 (C13), 126.1 (C4), 116.1 (C11), 55.9 (C8), 49.4 (C5), 46.7 (C6), 39.4 (C9), 24.2 (C7). **ESI-MS** (CH₃CN:H₂O (80:20), m/z): 374.2 (100) [C₂₁H₂₉ClN₃O]⁺.



(100% yield) **¹H-RMN** (400 MHz, CD₃CN, 25 °C) δ, ppm: 7.66 (d, $J = 7.8$ Hz, 2H, H^m), 7.39 (d, $J = 7.2$ Hz, 2H, H^b), 7.31 (dd, $J = 6.6, 6.6$ Hz, 1H, H^a), 7.00 (d, $J = 8.4$ Hz, 2H, H^l), 3.74 (d, $J = 13.4$ Hz, 2H, H^c or H^d), 3.49 (d, $J = 13.5$ Hz, 2H, H^c or H^d), 3.23 (m, 2H, Hⁱ or H^j), 2.81 (m, 4H, H^e or H^f, Hⁱ or H^j), 2.70 (m, 2H, H^e or H^f), 2.63 (s, 3H, H^k), 1.70 (m, 2H, H^g or H^h), 1.05 (m, 2H, H^g or H^h). **¹³C-RMN** (100 MHz, CD₃CN, 25 °C) δ, ppm: 159.8 (C10), 151.6 (C1), 133.9 (C2), 132.0 (C3), 127.4 (d, $J_{C-F} = 3.80$ Hz, C12), 126.3 (C4), 115.6 (C11), 55.9 (C8), 49.5 (C5), 46.7 (C6), 39.5 (C9), 24.2 (C7). **ESI-MS** (CH₃CN:H₂O (80:20), m/z): 408.1 (100) [C₂₂H₂₉F₃N₃O]⁺.

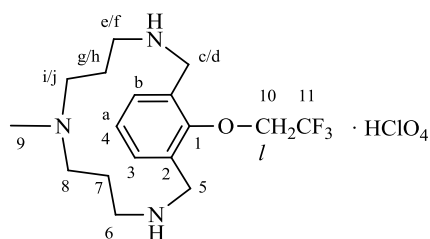


(100% yield) **¹H-NMR** (400 MHz, CD₃CN, 25 °C) δ, ppm: 7.70 (d, $J = 9.0$ Hz, 2H, H^m), 7.39 (d, $J = 7.5$ Hz, 2H, H^b), 7.31 (dd, $J = 6.6, 6.6$ Hz, 1H, H^a), 6.83 (d, 2H, $J = 6.6$ Hz, H^l), 3.72 (d, $J = 14.1$ Hz, 2H, H^c or H^d), 3.49 (d, $J = 13.6$ Hz, 2H, H^c or H^d), 3.22 (m, 2H, Hⁱ or H^j), 2.81 (m, 4H, H^e or H^f, Hⁱ or H^j), 2.64 (s, 3H, H^k), 2.67 (m, 2H, H^e or H^f), 1.68 (m, 2H, H^g or H^h), 1.03 (m, 2H, H^g or H^h). **¹³C-RMN** (100 MHz, CD₃CN, 25 °C) δ, ppm: 161.8 (C10), 153.0 (C1), 134.6 (C12), 133.9 (C2), 132.1 (C3), 126.4 (C4), (C14), 116.2 (C11), (C13), 55.9 (C8), 49.8 (C5), 46.7 (C6), 39.5 (C9), 24.3 (C7). **ESI-MS** (CH₃CN, m/z): 365.3 (100) [C₂₂H₂₉N₄O]⁺.

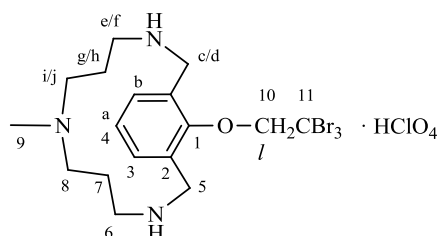


(100% yield) **¹H-NMR** (400 MHz, CD₃CN, 25 °C) δ, ppm: 8.21 (d, $J = 9.4$ Hz, 2H, H^m), 6.41 (d, $J = 7.4$ Hz, 2H, H^b), 7.33 (dd, $J = 6.6, 6.6$ Hz, 1H, H^a), 7.01 (d, $J = 9.2$ Hz, 2H, H^l), 3.74 (d, $J = 13.6$ Hz, 2H, H^c or H^d), 3.50 (d, $J = 13.6$ Hz, 2H, H^c or H^d), 2.25 (m, 2H, Hⁱ or H^j), 2.82 (m, 4H, Hⁱ or H^j, H^e or H^f), 2.69 (m, 2H, H^e or H^f), 2.66 (s, 3H, H^k), 1.70 (m, 2H, H^g or H^h), 1.03 (m, 2H, H^g or H^h). **¹³C-RMN** (100 MHz, CD₃CN, 25 °C) δ, ppm: 161.7 (C10), 151.5 (C1), 142.8 (C13), 133.8 (C2), 132.1 (C3), 126.6 (C4), 126.1 (C12), 115.7 (C11), 55.9 (C8), 49.5 (C5), 46.6 (C6), 39.5 (C9), 24.2 (C7). **ESI-MS** (CH₃CN, m/z): 385.3 (100) [C₂₁H₂₉N₄O₃]⁺.

3.4.3. Aliphatic alcohol nucleophiles



(yield 75%) **¹H-NMR** (400 MHz, CD₃CN, 25 °C) δ, ppm: 7.25 (d, *J* = 7.5 Hz, 2H, H^b), 7.11 (t, *J* = 7.5 Hz, 1H, H^a), 4.68 (q, *J* = 8.8 Hz, 2H, H^l), 4.26 (d, *J* = 13.9 Hz, 2H, H^c or H^d), 3.57 (d, *J* = 14.3 Hz, 2H, H^e or H^f), 3.08 (m, 2H, Hⁱ or H^j), 2.83 (m, 2H, H^e or H^f), 2.71 (m, 2H, Hⁱ or H^j), 2.64 (m, 2H, H^e or H^f), 2.51 (s, 3H, H^k), 1.63 (m, 2H, H^g or H^h), 1.04 (m, 2H, H^g or H^h); **¹³C-NMR** (100 MHz, CD₃CN, 25 °C) δ, ppm: 161.7 (C1), 131.8 (C3), 128.0 (C2), 125.1 (q, *J*_{C-F} = 278.5 Hz, C11), 68.3 (q, *J*_{C-F} = 34.0 Hz, C10), 55.6 (C8), 50.6 (C5), 46.8 (C6), 39.2 (C9), 24.2 (C7). **ESI-MS** (CH₃CN:H₂O (80:20), *m/z*): 346.1(100) [C₁₇H₂₇F₃N₃O]⁺.



(yield 85%) **¹H-NMR** (400 MHz, CD₃CN, 25 °C) δ, ppm: 7.45 (d, *J* = 7.6 Hz, 2H, H^b), 7.30 (t, *J* = 7.5 Hz, 1H, H^a), 4.86 (s, 2H, H^l), 4.54 (d, *J* = 13.8 Hz, 2H, H^c or H^d), 3.82 (d, *J* = 14.4 Hz, 2H, H^e or H^f), 3.05 (m, 2H, H^e or H^f), 2.80 (m, 4H, Hⁱ or H^j, H^e or H^f), 2.56 (m, 2H, Hⁱ or H^j), 2.44 (s, 3H, H^k), 1.80 (m, 2H, H^g or H^h), 1.22 (m, 2H, H^g or H^h); **¹³C-NMR** (100 MHz, CD₃CN, 25 °C) δ, ppm: 161.69 (C1), 133.56 (C3), 129.66 (C2), 126.28 (C4), 85.66 (C10), 55.45 (C8), 48.75 (C5), 46.85 (C6), 40.25 (C9), 36.18 (C11), 23.22 (C7). **ESI-MS** (CH₃CN:H₂O (80:20), *m/z*): 527.9(100) [C₁₇H₂₇Br₃N₃O]⁺.

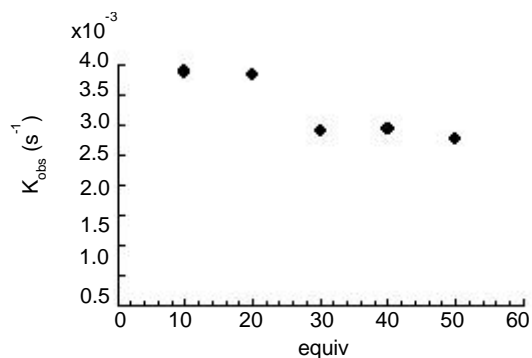
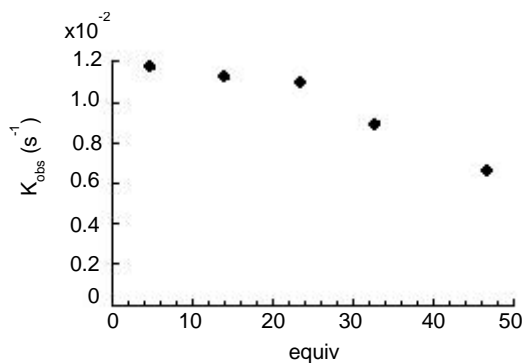
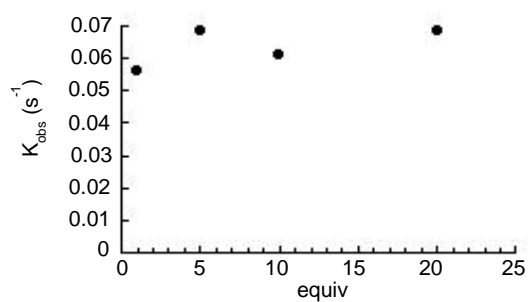
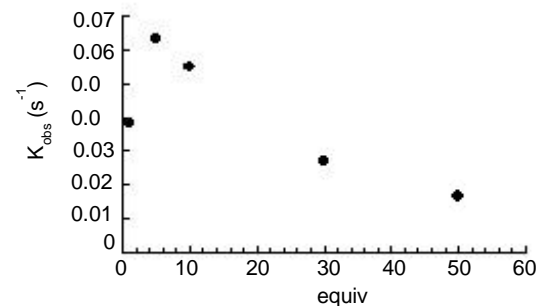
3.5. General procedure for monitoring kinetics by NMR spectroscopy

In an inert-atmosphere glove box, a stock solution of the arylCu^{III} complex **1**_{ClO₄} (26 mM) and 1,3,5-*tri-tert*-butylbenzene (1 mg, 4 μmol) as an internal standard was prepared in

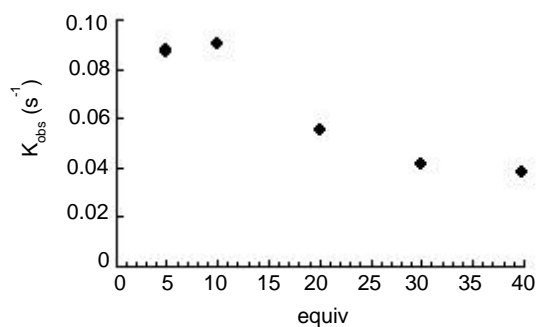
CD₃CN (1.0 mL). A stock solution of the corresponding carboxylic acid (75 mM) in CD₃CN (2.0 mL) was prepared. The concentration of each stock solution was confirmed by ¹H-NMR spectroscopy. Pulse widths and relaxation times were determined by using standard methods. To acquire the kinetic data, 0.3 mL of the nucleophile stock solution was added to a NMR tube and sealed with a septum, and the sample was placed in the NMR probe for 5 min to allow temperature equilibration. The reaction was initiated by addition of 0.1 mL of the arylCu^{III} stock solution to the NMR tube via syringe. The solution was mixed rapidly and the tube was inserted into the probe to begin data acquisition. The relaxation delay between acquisitions was set to 5xT₁ (T₁ ~ 2 s). Final concentrations: [**1**_{ClO₄}] = 6.5 mM. [carboxylic acid] = 56 mM.

3.6. General procedure for monitoring kinetics by UV-Vis spectroscopy

A UV-Visible cuvet equipped with a Teflon stopcock was dried in an oven and cooled under vacuum. Stock solutions of the oxygen nucleophile (40 mM) and the arylCu^{III} complex **1**_{ClO₄} (7.5 mM) were prepared in dry CH₃CN (50 mL). After backfilling the cuvet with dry N₂, 0.5 mL of the nucleophile stock solution was added via syringe, and it was diluted with CH₃CN to a total volume of 2.5 mL. The cuvet was inserted into the spectrometer and the temperature was allowed to equilibrate. The reaction was initiated by adding the arylCu^{III} stock solution (0.3 mL) to the cuvet followed by rapid mixing of the combined solutions. Final concentrations: [**1**_{ClO₄}] = 0.8 mM, [nucleophile] = 8mM. The average dead time was estimated to be seven seconds. The reaction progress was monitored by measuring the change in absorbance at 450 nm, and the data were fit to an exponential decay curve using Microsoft Excel.

a) *p*-nitrobenzoic acidb) *p*-trifluoromethylbenzoic acidc) *p*-Methylbenzoic acidd) *p*-Methoxybenzoic acid

e) Isobutyric acid



e) Pivalic acid

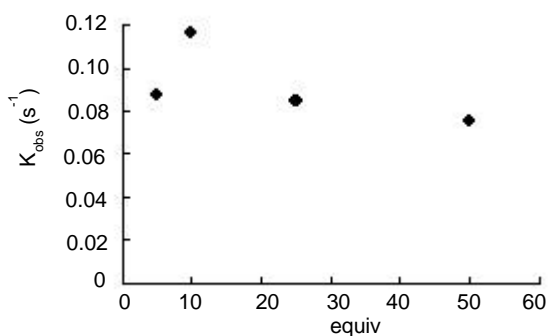


Figure 3.6.1. The dependence of reaction rate on increasing nucleophile concentration is shown for acid nucleophiles. Conditions for aromatic acids: $[\mathbf{1}_{\text{ClO}_4}] = 0.8 \text{ mM}$, $[\text{HO-Nu}] = 0.8 \text{ mM}$ to 40 mM , $15 \text{ }^\circ\text{C}$. Conditions for isobutyric and pivalic acid: $[\mathbf{1}_{\text{ClO}_4}] = 0.8 \text{ mM}$, $[\text{OH-Nu}] = 0.8 \text{ mM}$ to 40 mM , $0 \text{ }^\circ\text{C}$. Methyl benzoic acid was investigated up to only 20 equivalents due to

insolubility of the carboxylic acid. An exponential fit was used to estimate all the dependencies. Error determined by using the solver statistics macro written by Clark Landis in Microsoft Excel.

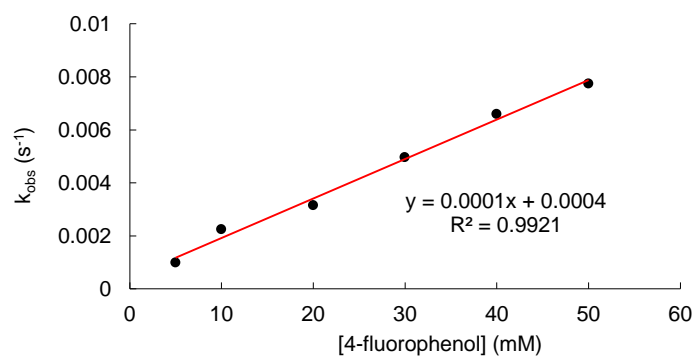


Figure 3.6.2. Dependence of k_{obs} on the [4-fluorophenol] obtained by monitoring the reaction of **1**_{ClO₄} with 4-fluorophenol by UV-Vis spectroscopy. Conditions: [**1**_{ClO₄}] = 1 mM, [4-fluorophenol] = 10-50 mM, CH₃CN, 25 °C

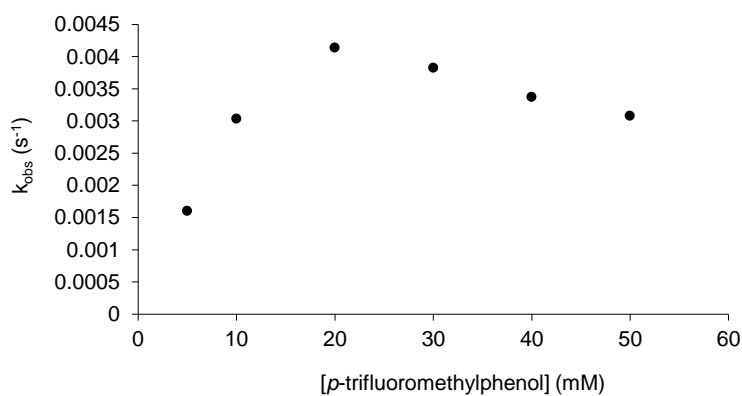


Figure 3.6.3. Dependence of k_{obs} on the [4-trifluoromethylphenol] obtained by monitoring the reaction of **2** with 4-trifluorophenol by UV-Vis spectroscopy. Conditions: [**1**_{ClO₄}] = 1 mM, [*p*-trifluoromethylphenol] = 10-50 mM, CH₃CN, 15 °C.

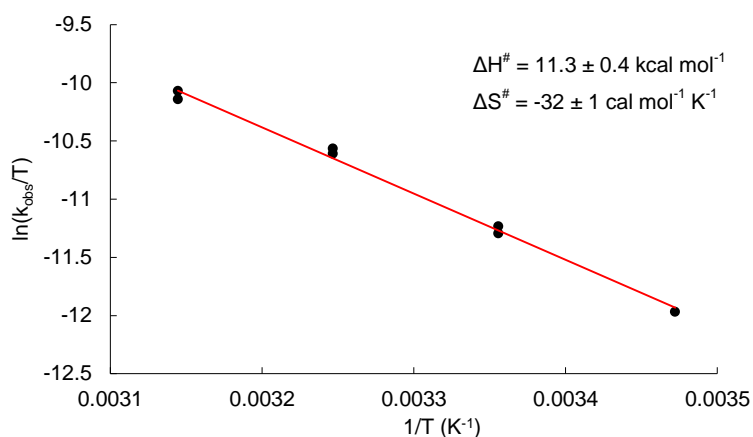


Figure 3.6.4. Eyring plot for the reaction of complex 1_{ClO_4} with *p*-methoxyphenol. Conditions: $[1_{\text{ClO}_4}] = 1 \text{ mM}$, $[p\text{-methoxyphenol}] = 10 \text{ mM}$, CH_3CN , from 15 to 45 °C.

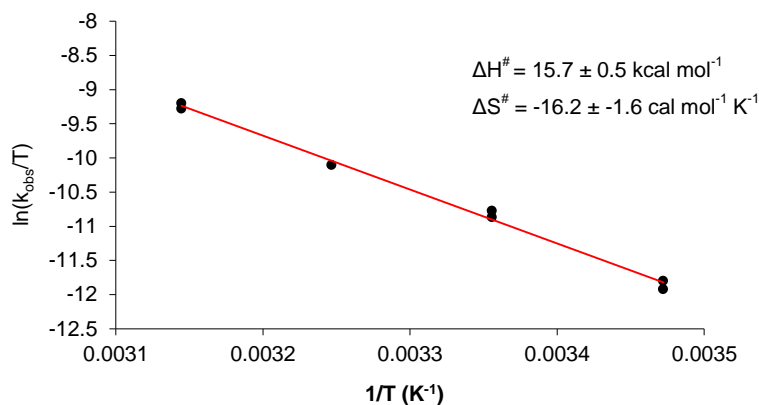


Figure 3.6.5. Eyring plot for the reaction of complex 1_{ClO_4} with *p*-nitrophenol. Conditions: $[1_{\text{ClO}_4}] = 1 \text{ mM}$, $[p\text{-nitrophenol}] = 10 \text{ mM}$, CH_3CN , from 15 to 45 °C.

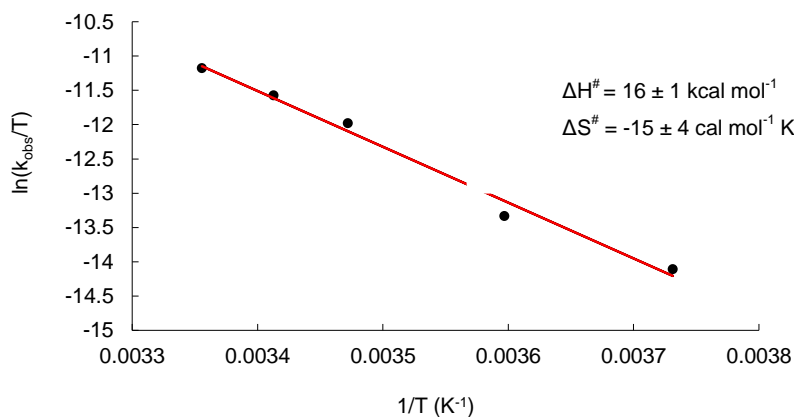


Figure 3.6.6. Eyring plot for reaction of 1_{ClO_4} with *p*-trifluoromethylphenol. Conditions: $[1_{\text{ClO}_4}] = 1 \text{ mM}$, $[p\text{-trifluoromethylphenol}] = 10 \text{ mM}$, CH_3CN , from -5 to 25 °C.

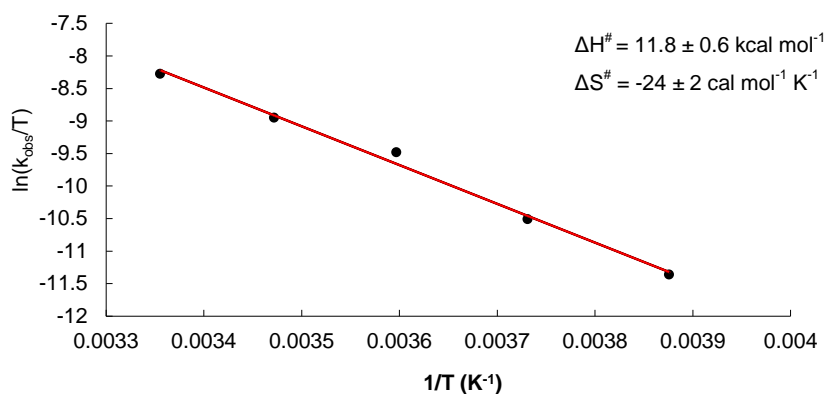


Figure 3.6.7. Eyring plots for reaction of 1_{ClO_4} with acetic acid. Conditions: $[1_{\text{ClO}_4}] = 0.8 \text{ mM}$, $[\text{CH}_3\text{COOH}] = 4 \text{ mM}$, from -15 to $25 \text{ }^\circ\text{C}$.

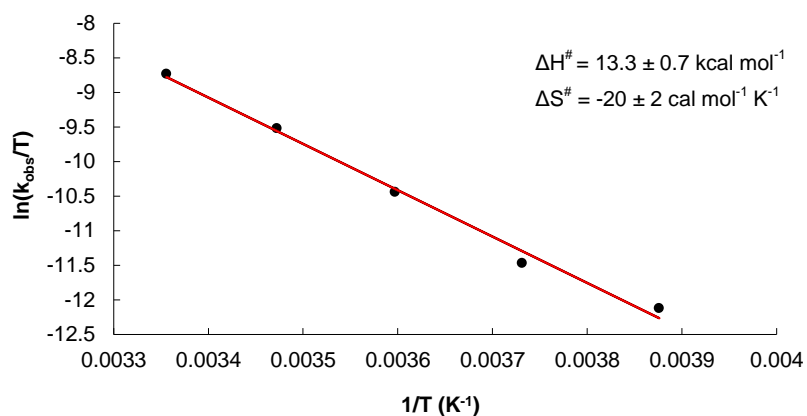


Figure 3.6.8. Eyring plots for reaction of 1_{ClO_4} with benzoic acid. Conditions: $[1_{\text{ClO}_4}] = 0.8 \text{ mM}$, $[\text{benzoic acid}] = 4 \text{ mM}$, from -15 to $25 \text{ }^\circ\text{C}$.

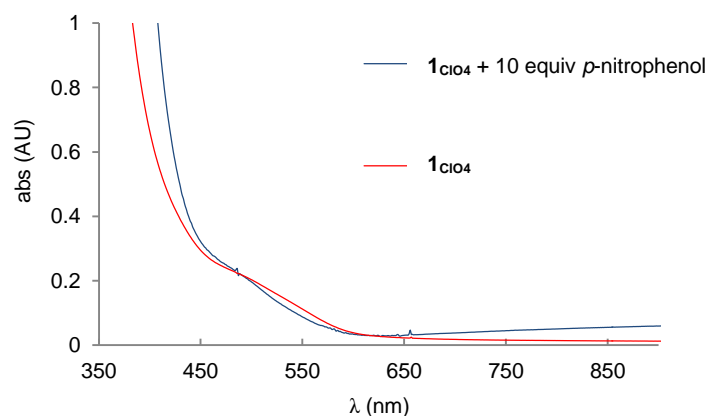


Figure 3.6.9. Volume corrected UV-Vis experiment monitoring the addition of 10 equiv of p -nitrophenol into a cooled solution of 1_{ClO_4} . Conditions: $[1_{\text{ClO}_4}] = 1 \text{ mM}$, at $-30 \text{ }^\circ\text{C}$.

3.7. General procedure for catalytic experiments

In an inert-atmosphere glove box, a vial was loaded with 0.5 mL of ligand **L₁-Br** 30 mM in CH₃CN and 10 mol % of Cu(CH₃CN)₄(CF₃SO₃) was added (0.2 mL of stock solution 7.5 mM in CH₃CN). The colourless solution became red indicating that oxidative addition takes place obtaining the corresponding complex arylCu^{III}-Br, complex **1_{Br}**. Then 2.3 mL of HO-nucleophile 13 mM in CH₃CN was added. Final concentrations: [**L₁-Br**] = 5 mM, [Cu(CH₃CN)₄OTf] = 0.5 mM and [HO-Nu] = 10 mM. After stirring the mixture crude for 24 hours, 50 μL of 1,3,5-trimethoxybenzene 3 mM in CH₃CN as internal standard is added and the solvent is rotavapored. The sample is redissolved in 0.5 mL of CD₃CN and NMR yields were obtained by ¹H-NMR using integration of benzylic protons respect to 1,3,5-trimethoxybenzene. In the case of acetic acid the corresponding equivalents were added by syringe pump in a period of 5 hours.

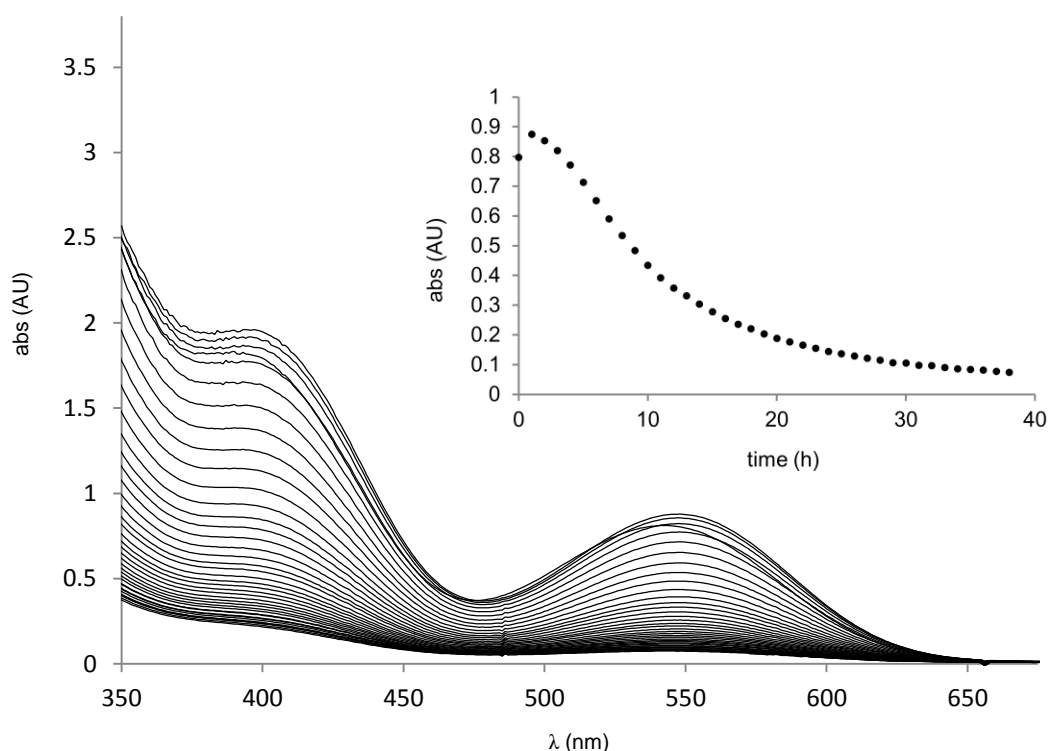


Figure 3.7.1. UV-Vis monitoring spectra of the cross coupling reaction between **L₁-Br** and acetic acid catalyzed by [Cu^I(CH₃CN)₄]OTf. Inset plot shows the timecourse of complex **2_{Br}** at 550 nm. Conditions: [**L₁-Br**] 10 mM, [CH₃COOH] = 20 mM, [[Cu(CH₃CN)₄]OTf] = 1.4 mM; CH₃CN, at 25 °C, N₂ atmosphere.

4. Supplementary Information Chapter VII

4.1. Synthesis of complex 1 _{ClO₄}	237
4.2. Synthesis of <i>para</i> -substituted phenolates.....	237
4.3. Stoichiometric reactions of complex 1 _{ClO₄} and phenolates.....	238
4.4. Stoichiometric reaction of complex 1 _{ClO₄} and Proton-sponge [®] and <i>p</i> -fluorophenol.....	240
4.5. Procedures for monitoring kinetics by UV-Vis spectroscopy.....	240
4.6. Procedures for monitoring kinetics by NMR spectroscopy.....	243
4.7. CW and Pulse-EPR experiments	248
4.7.4. Sample Preparation	248
4.7.5. EPR spectroscopy details	249
4.7.6. Quantification of the paramagnetic species	250
4.8. Identification of the paramagnetic species	250
4.8.4. ENDOR	250
4.8.5. ¹ H-HYSCORE	256
4.8.6. ¹⁴ N-HYSCORE	256

4.1. Synthesis of complex **1**_{ClO₄}

Arylcopper(III) complex **1**_{ClO₄} was prepared following procedures described previously (see supporting information of Chapter VI).

4.2. Synthesis of *para*-substituted phenolates

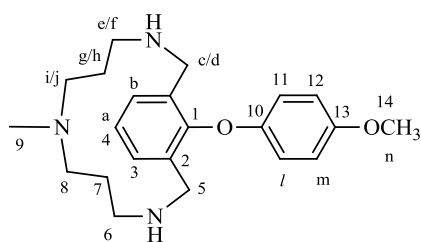
Para-substituted sodium phenolates *p*-X-phenolate (X= OCH₃, Cl, F, CN and NO₂) were prepared following procedures described in the literature previously.¹

1. Company, A.; Palavicini, S.; Garcia-Bosch, I.; Mas-Balleste, R.; Que, J. L.; Rybak-Akimova, E. V.; Casella, L.; Ribas, X.; Costas, M. *Chem. Eur. J.*, **2008**, *14*, 3535.

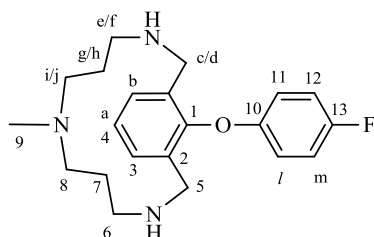
4.3. Stoichiometric reactions of complex 1_{ClO_4} and phenolates

Caution: Perchlorate salts are potentially explosive and should be handled with care!

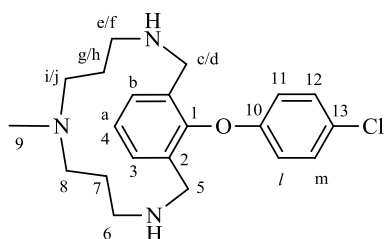
In an inert-atmosphere glove box, stock solutions of complex 1_{ClO_4} /1,3,5-trimethoxybenzene (10/1.8 mM) and sodium *para* substituted phenolates (X = OCH₃, F, Cl) (10 mM) were prepared in CD₃CN. The 1_{ClO_4} /1,3,5-trimethoxybenzene stock solution (0.3 mL) was loaded into an NMR tube. Then 0.3 mL of the corresponding *para* substituted phenolate was added to the NMR tube obtaining a deep violet solution that remains for 10 minutes. ¹H-NMR spectroscopy of the colourless solution showed that reaction was completed. Quantitative NMR yield of the corresponding C-O coupling product was obtained using 1,3,5-trimethoxybenzene as internal standard. The final concentrations were as follows: [1_{ClO_4}] = 5 mM, [*p*-X-phenolate] (X= OCH₃, F, Cl) = 5 mM. The same procedure was performed using sodium *p*-cyanophenolate and sodium *p*-nitrophenolate but due to their low solubility in CD₃CN, lower concentrations were used. In the case of *p*-cyanophenolate final concentrations were [1_{ClO_4}] = 2.5 mM and [*p*-cyanophenolate] = 2.5 mM. In the case of *p*-nitrophenolate final concentrations were [1_{ClO_4}] = 1.25 mM and [*p*-cyanophenolate] = 1.25 mM.



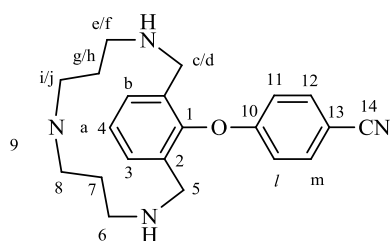
4a (yield: 100%). ¹H-NMR (CD₃CN, 400 MHz) δ , ppm: 7.20 (m, 3H, H^a, H^b), 6.86 (dt, J = 9, 2 Hz, 2H, H^m), 6.75 (dt, J = 9, 2 Hz, 2H, H^l), 3.87 (d, J = 14 Hz, 2H, H^c or H^d), 3.73 (s, 3H, Hⁿ), 3.31 (d, J = 14 Hz, 2H, H^c or H^d), 2.50 (m, 2H, H^e or H^f), 2.38 (m, 2H, Hⁱ or H^j), 2.26 (m, 2H, Hⁱ or H^j), 2.15 (under water solvent peak, 2H, H_{amines}), 2.03 (m, 2H, H^e or H^f), 1.89 (s, 3H, H^k), 1.56 (m, 4H, H^g and H^h). ¹³C-NMR (CD₃CN, 100 MHz) δ , ppm: 154.9 (C13), 152.5 (C10), 151.1 (C1), 134.4 (C2), 131.0 (C3), 124.9 (C4), 115.6 (C11), 114.9 (C12), 55.6 (C8), 55.3 (C14), 50.2 (C5), 44.7 (C6), 39.5 (C9), 26.0 (C7). **ESI-MS** (CH₃CN, m/z): 370.3 (100) [C₂₂H₃₂N₃O₂]⁺.



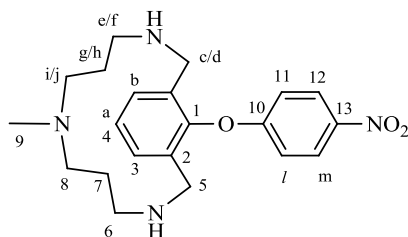
4b (yield: 100 %). $^1\text{H-NMR}$ (CD_3CN , 400MHz) δ , ppm: 7.22 (m, 3H, H^{a} , H^{b}), 7.04 (t, $J = 9$ Hz, 2H, H^{m}), 6.82 (m, 2H, H^{l}), 3.85 (d, $J = 14$ Hz, 2H, H^{c} or H^{d}), 3.31 (d, $J = 14$ Hz, 2H, H^{c} or H^{d}), 2.52 (m, 2H, H^{e} or H^{f}), 2.40 (m, 2H, H^{i} or H^{j}), 2.27 (m, 2H, H^{i} or H^{j}), 2.15 (under water solvent peak, 2H, H_{amines}), 2.04 (m, 2H, H^{e} or H^{f}), 1.92 (s, 3H, H^{k}), 1.54 (m, 4H, H^{g} , H^{h}). $^{13}\text{C-NMR}$ (CD_3CN , 100MHz) δ , ppm: 158.4 (d, $J_{\text{C-F}} = 145.8$ Hz, C13), 153.5 (C10), 152.1 (C1), 134.6 (C2), 130.9 (C3), 125.0 (C4), 116.4 (C11), 116.0 (d, $J_{\text{C-F}} = 8.9$ Hz, C12), 55.5 (C8), 50.1 (C5), 44.2 (C6), 39.6 (C9), 26.5 (C7). **ESI-MS** (CH_3CN , m/z): 358.3(100) [$\text{C}_{21}\text{H}_{29}\text{FN}_3\text{O}$] $^+$.



4c (yield: 100%). $^1\text{H-NMR}$ (CD_3CN , 400MHz) δ , ppm: 7.31 (dt, $J = 9$, 3 Hz, 2 H, H^{m}), 7.23 (m, 3 H, H^{a} , H^{b}), 6.81 (dt, $J = 9$ Hz, $J = 2$ Hz, 2H, H^{l}), 3.84 (d, $J = 14$ Hz, 2H, H^{c} or H^{d}), 3.31 (d, $J = 14$ Hz, 2H, H^{c} or H^{d}), 2.50 (m, 2H, H^{e} or H^{f}), 2.38 (m, 2H, H^{i} or H^{j}), 2.28 (m, 2H, H^{i} or H^{j}), 2.15 (under water solvent peak, 2 H, H_{amines}), 2.01 (m, 2H, H^{e} or H^{f}), 1.90 (s, 3H, H^{k}), 1.53 (m, 4H, H^{g} , H^{h}). $^{13}\text{C-NMR}$ (CD_3CN , 100MHz) δ , ppm: 156.1 (C10), 151.7 (C1), 134.6 (C2), 130.9 (C3), 129.8 (C12), 126.6 (C13), 125.2 (C4), 116.4 (C11), 55.5 (C8), 50.1 (C5), 44.2 (C6), 39.6 (C9), 26.4 (C7). **ESI-MS** (CH_3CN , m/z): 374.2 (100) [$\text{C}_{21}\text{H}_{29}\text{ClN}_3\text{O}$] $^+$.



4d (yield: 100 %). $^1\text{H-NMR}$ (CD_3CN , 400MHz) δ , ppm: 7.68 (d, $J = 9$ Hz, 2H, H^{m}), 7.25 (m, 3H, H^{a} , H^{b}), 6.96 (d, $J = 9$ Hz, 2H, H^{l}), 3.78 (d, $J = 14$ Hz, 2H, H^{c} or H^{d}), 3.34 (d, $J = 14$ Hz, 2H, H^{c} or H^{d}), 2.52 (m, 2H, H^{e} or H^{f}), 2.39 (m, 2H, H^{i} or H^{j}), 2.29 (m, 2H, H^{i} or H^{j}), 2.15 (under water solvent peak, 2H, H_{amines}), 2.04 (m, 2H, H^{e} or H^{f}), 1.93 (s, 3H, H^{k}), 1.50 (m, 4H, H^{g} , H^{h}). $^{13}\text{C-NMR}$ (CD_3CN , 100MHz) δ , ppm: 160.5 (C10), 151.1 (C1), 134.7 (C12), 134.6 (C2), 131.2 (C3), 125.7 (C4), 118.6 (C14), 115.9 (C11), 105.4 (C13), 55.6 (C8), 49.8 (C5), 44.6 (C6), 39.9 (C9), 26.2 (C7). **ESI-MS** (CH_3CN , m/z): 365.3 (100) [$\text{C}_{22}\text{H}_{29}\text{N}_4\text{O}$] $^+$.



4e (yield: 100 %). $^1\text{H-NMR}$ (CD_3CN , 400MHz) δ , ppm: 8.20 (d, $J = 9$ Hz, 2H, H^m), 7.27 (m, 3H, H^a , H^b), 6.97 (d, $J = 9$ Hz, 2H, H^l), 3.79 (d, $J = 14$ Hz, 2H, H^c or H^d), 3.35 (d, $J = 14$ Hz, 2H, H^c or H^d), 2.54 (m, 2H, H^e or H^f), 2.35 (m, 2H, H^i or H^j), 2.29 (m, 2H, H^i or H^j), 2.04 (m, 2H, H^e or H^f), 1.90 (s, 3H, H^k), 1.48 (m, 4H, H^g , H^h). $^{13}\text{C-NMR}$ (CD_3CN , 100MHz) δ , ppm: 162.0 (C10), 151.2 (C1), 142.8 (C13), 134.0 (C2), 131.5 (C3), 126.2 (C12), 126.0 (C4), 115.5 (C11), 55.7 (C8), 50.0 (C5), 45.3 (C6), 39.8 (C9), 25.7 (C7). **ESI-MS** (CH_3CN , m/z): 385.3 (100) [$\text{C}_{21}\text{H}_{29}\text{N}_4\text{O}_3$] $^+$.

4.4. Stoichiometric reaction of complex 1_{C104} and Proton-sponge[®] and *p*-fluorophenol

In an inert-atmosphere glove box, stock solutions of complex 1_{C104} /1,3,5-trimethoxybenzene (10/1 mM), Proton-sponge[®] (240 mM) and *p*-fluorophenol (60 mM) were prepared in dry CD_3CN at room temperature. The 1_{C104} /1,3,5-trimethoxybenzene stock solution (0.3 mL) and 0.2 mL of CD_3CN were loaded into an NMR tube and sealed with a septum. 50 μL of Proton-sponge[®] stock solution was added to the NMR tube obtaining a deep violet solution. Then 50 μL of *p*-fluorophenol stock solution was added into the NMR tube. $^1\text{H-NMR}$ spectroscopy of the colourless solution showed that reaction was completed. Quantitative NMR yield of the corresponding C-O coupling product was obtained using 1,3,5-trimethoxybenzene as internal standard. The final concentrations were as follows: [1_{C104}] = 5 mM, [Proton-sponge[®]] = 20 mM and [*p*-fluorophenol] = 5 mM.

4.5. Procedures for monitoring kinetics by UV-Vis spectroscopy

a) Reaction of complex 1_{C104} with Proton-sponge[®]

A UV-Visible cuvette (1 cm) equipped with a Teflon stopcock was dried in an oven and cooled under vacuum. Stock solutions of complex 1_{C104} (1 mM) and Proton-sponge[®] (24 mM) were prepared in dry CH_3CN in an inert glove box. Then 1.2 mL of stock solution of complex 1_{C104} and the corresponding volume of CH_3CN were loaded into the cuvette. The cuvette was inserted into the spectrometer and the temperature was allowed to equilibrate at 25 $^\circ\text{C}$. The

reaction was initiated by adding the corresponding volume of Proton-sponge[®] stock solution (50 μ L-0.6 mL) into the cuvette (3 mL of final volume). Final concentrations: [$\mathbf{1}_{\text{ClO}_4}$] = 0.6 mM, [Proton-sponge[®]] = 0.6-7.2 mM. ESI-MS of reaction mixture with 6 equiv of Proton-sponge[®] added shows a major copper-containing signal corresponding to species **3**: $m/z = 308.1$.

b) Reaction of complex $\mathbf{1}_{\text{ClO}_4}$ with sodium para substituted phenolates

A UV-Visible cuvette (1cm) equipped with a Teflon stopcock was dried in an oven and cooled under vacuum. Stock solutions of complex $\mathbf{1}_{\text{ClO}_4}$ (0.7 mM) and sodium *para* substituted phenolate (4.5 mM) (OCH₃, F, Cl, CN) were prepared in dry CH₃CN in an inert glove box. Then 2.6 mL of stock solution of complex $\mathbf{1}_{\text{ClO}_4}$ was loaded into the cuvette. The cuvette was inserted into the spectrometer and the temperature was allowed to equilibrate at 25 °C. The reaction was initiated by adding 0.4 mL of the phenolate stock solution into the cuvette. Final concentrations: [$\mathbf{1}_{\text{ClO}_4}$] = 0.6 mM, [phenolate] = 0.6 mM. Due to low solubility of sodium *p*-nitrophenolate salt, reaction of complex $\mathbf{1}_{\text{ClO}_4}$ and *p*-nitrophenolate were achieved mixing 2 mL of stock solution of complex $\mathbf{1}_{\text{ClO}_4}$ (0.9 mM) and 1 mL of *p*-nitrophenolate (1.8 mM) which is cooled previously with an ice bath.

c) Comparison between phenol and phenolate reactivity

A UV-Visible cuvette (0.5 cm) equipped with a Teflon stopcock was dried in an oven and cooled under vacuum. Stock solutions of complex $\mathbf{1}_{\text{ClO}_4}$ (6 mM) and sodium *para* substituted phenolate (24 mM) (OCH₃, F, CN) were prepared in dry CH₃CN in an inert glove box. Then 0.2 mL of stock solution of complex $\mathbf{1}_{\text{ClO}_4}$ and 0.75 mL of CH₃CN were loaded into the cuvette. The cuvette was inserted into the spectrometer and the temperature was allowed to equilibrate at 25 °C. The reaction was initiated by adding 50 μ L of the phenolate stock solution into the cuvette. Final concentrations: [$\mathbf{1}_{\text{ClO}_4}$] = 1.2 mM, [phenolate] = 1.2 mM.

For performing reactions with the corresponding *para*-substituted phenols, stock solutions of *para* substituted phenols (24 mM) (OCH₃, F, CN) were prepared in dry CH₃CN in an inert glove box. Then, 0.4 mL of stock solution of complex $\mathbf{1}_{\text{ClO}_4}$ and 1.5 mL of CH₃CN were loaded into the cuvette (1 cm). The cuvette was inserted into the spectrometer and the temperature was allowed to equilibrate at 25 °C. The reaction was initiated by adding 100 μ L of the 4-X-phenol stock solution into the cuvette. Final concentrations: [$\mathbf{1}_{\text{ClO}_4}$] = 1.2 mM, [phenol] = 1.2 mM.

In order to compare the reaction rate between *p*-fluorophenolate and *p*-fluorophenol/Proton-sponge[®], stock solution of Proton-sponge[®] (4.8 mM) was prepared in dry CH₃CN in an inert glove box. Then, 0.2 mL of stock solution of complex $\mathbf{1}_{\text{ClO}_4}$ was loaded into the cuvette (0.5 cm). The cuvette was inserted into the spectrometer and 0.75 mL of stock solution of Proton-sponge[®] was also loaded into the cuvette. After formation of the

corresponding band at 550 nm, 50 μ L of the *p*-fluorophenol stock solution was loaded into the cuvette. Final concentrations: [$\mathbf{1}_{\text{ClO}_4}$] = 1.2 mM, [*p*-fluorophenol] = 1.2 mM, [Proton-sponge[®]] = 3.6 mM (3 equiv).

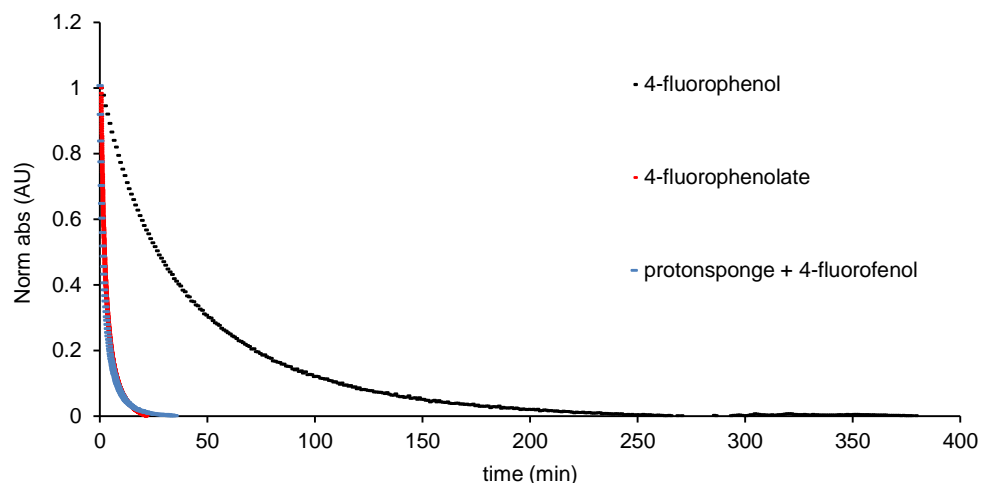


Figure 4.5.1. Decay profile plot of reaction of complex $\mathbf{1}_{\text{ClO}_4}$ with a) 1 equiv of *p*-fluorophenol (450 nm), b) sodium *p*-fluorophenolate (decay of 550 nm band corresponding to $\mathbf{3}$) and c) 3 equiv of Proton-sponge[®] and 1 equiv of *p*-fluorophenol (decay of 550 nm band corresponding to $\mathbf{3}$). Conditions: CH_3CN solvent, N_2 atmosphere, 25 $^\circ\text{C}$, [$\mathbf{1}_{\text{ClO}_4}$] = 1.2 mM, [*p*-fluorophenolate] = 1.2 mM, [*p*-fluorophenol] = 1.2 mM and [Proton-sponge[®]] = 3.6 mM.

d) Reaction of complex $\mathbf{1}_{\text{ClO}_4}$ with sodium *p*-fluorophenolate and $\text{CF}_3\text{SO}_3\text{H}$

A UV-Visible cuvette (1 cm) equipped with a Teflon stopcock was dried in an oven and cooled under vacuum. Stock solutions of complex $\mathbf{1}_{\text{ClO}_4}$ (1 mM), sodium *p*-fluorophenolate (24 mM) and $\text{CF}_3\text{SO}_3\text{H}$ (22 mM) were prepared in dry CH_3CN in an inert glove box. Then 2 mL of stock solution of complex $\mathbf{1}_{\text{ClO}_4}$ was loaded into the cuvette. The cuvette was inserted into the spectrometer and the temperature was allowed to equilibrate at 25 $^\circ\text{C}$. The reaction was initiated by adding 0.1 mL of the *p*-fluorophenolate stock solution (1 equiv) into the cuvette obtaining a deep violet intermediate. Then 0.1 mL of the trifluoromethanesulfonic acid (1 equiv) was added into the cuvette. This cycle was done two times more increasing the equivalents of base or acid in 0.5 equivalents each time in order to obtain the desired pH.

4.6. Procedures for monitoring kinetics by NMR spectroscopy

a) Reaction of complex 1_{ClO_4} with Proton-sponge®

In an inert-atmosphere glove box, a stock solution of the arylCu^{III} complex 1_{ClO_4} and 1,3,5-trimethoxybenzene as an internal standard was prepared in CD₃CN (10/1 mM). A stock solution of Proton-sponge (180 mM) was prepared in CD₃CN. Then, 0.3 mL of the stock solution of complex 1_{ClO_4} /1,3,5-trimethoxybenzene and 0.2 mL of CD₃CN were loaded into an NMR tube and sealed with a septum. The sample was placed in the NMR probe for 5 min to allow temperature equilibration at -30 °C. ¹H-NMR spectra of complex 1_{ClO_4} was obtained at -30 °C. Proton-sponge® stock solution was cooled to -30 °C using a CH₃CN/N₂(l) bath and 0.1 mL was added by syringe to the NMR tube. Final concentrations: [1_{ClO_4}] = 5 mM. [Proton-sponge®] = 30 mM. The solution was mixed rapidly and formation of violet intermediate was observed. The tube was inserted into the probe to begin data acquisition.

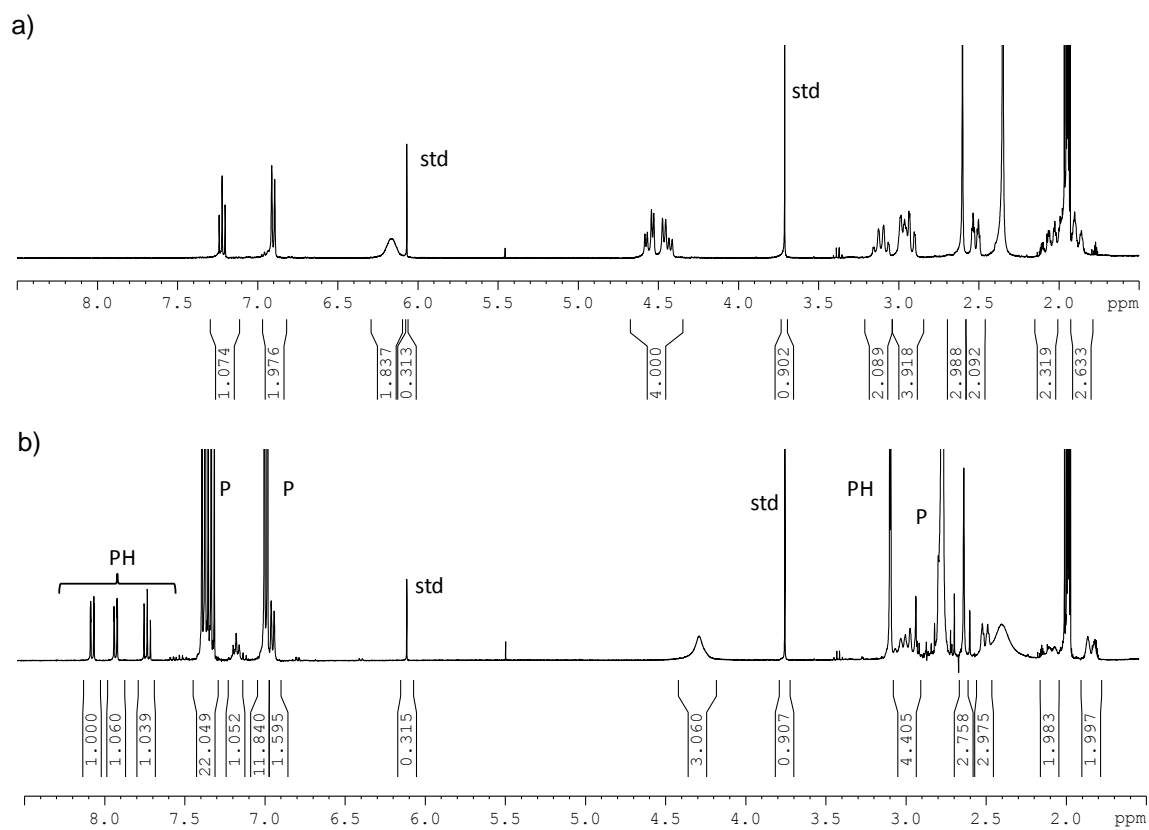


Figure 4.6.1. $^1\text{H-NMR}$ spectra of reaction of complex 1_{ClO_4} with 6 equiv of Proton-sponge[®] in CD_3CN at -30°C . a) 0.5 mL of complex 1_{ClO_4} , $[1_{\text{ClO}_4}] = 6 \text{ mM}$; b) addition of 0.1 mL of Proton-sponge[®] 180 mM, $[1_{\text{ClO}_4}] = 5 \text{ mM}$, $[\text{Proton-sponge}^{\text{®}}] = 30 \text{ mM}$ (6 equiv).

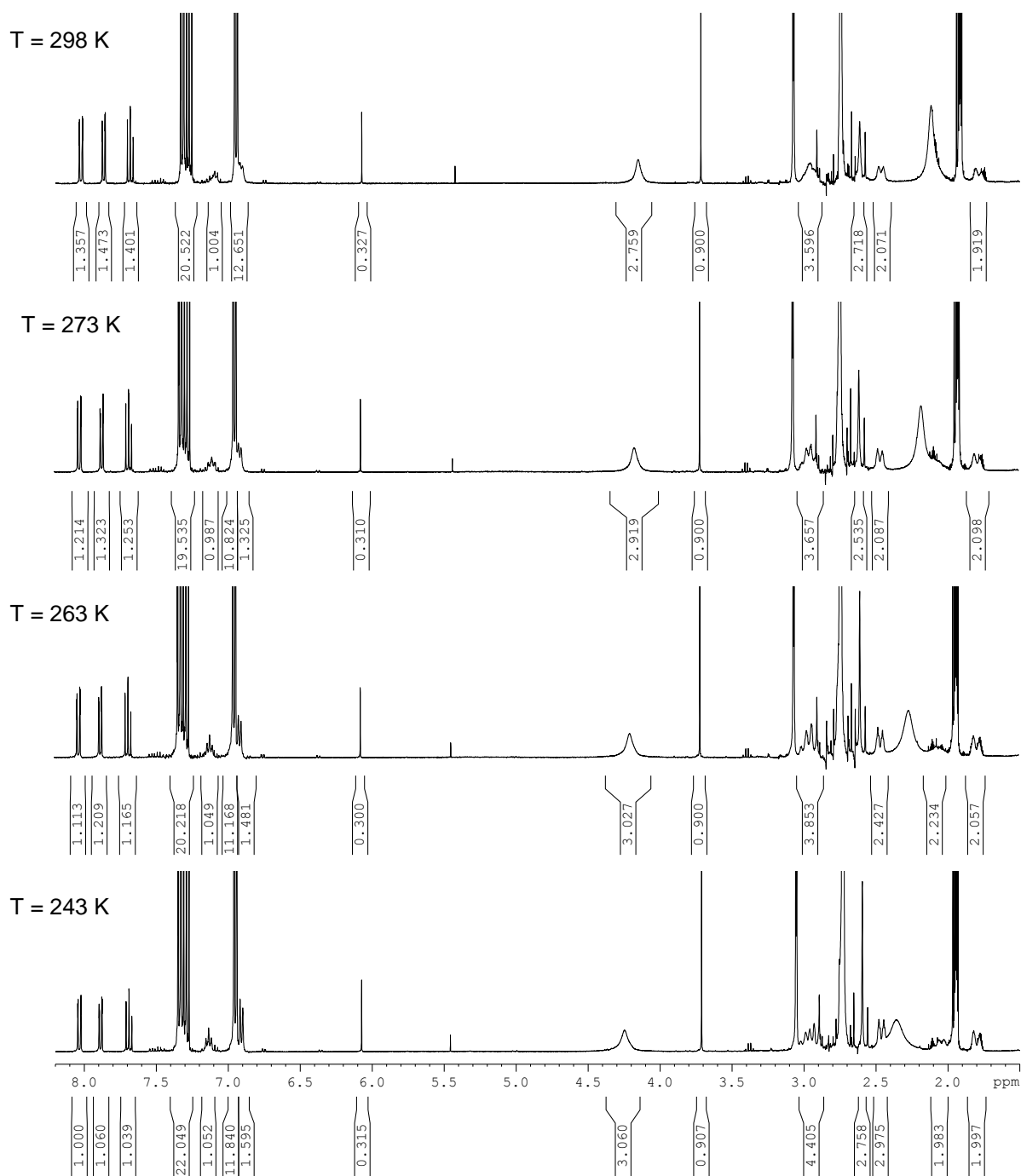


Figure 4.6.2. $^1\text{H-NMR}$ spectra of reaction of complex 1_{ClO_4} with 6 equiv of Proton-sponge[®] in CD_3CN at several temperatures (from -30 to 25 °C) in CD_3CN , $[1_{\text{ClO}_4}] = 5$ mM, $[\text{Proton-sponge}^{\text{®}}] = 30$ mM (6 equiv). Cooling the sample at 25 °C down to -30 °C again restores the same spectrum (see spectrum at the bottom).

*b) Reaction of complex $\mathbf{1}_{\text{ClO}_4}$ with sodium *p*-fluorophenolate*

In an inert-atmosphere glove box, a stock solution of the arylCu^{III} complex $\mathbf{1}_{\text{ClO}_4}$ and 1,3,5-trimethoxybenzene as an internal standard was prepared in CD₃CN (10/1 mM). A stock solution of *p*-fluorophenolate (30 mM) was prepared in CD₃CN. Then, 0.3 mL of the stock solution of complex $\mathbf{1}_{\text{ClO}_4}$ /1,3,5-trimethoxybenzene and 0.2 mL of CD₃CN were loaded into an NMR tube and sealed with a septum. The sample was placed in the NMR probe for 5 min to allow temperature equilibration at -30 °C. ¹H-NMR spectra of complex $\mathbf{1}_{\text{ClO}_4}$ was obtained at -30 °C. Sodium 4-fluorophenolate stock solution was cooled to -30 °C using a CH₃CN/N₂(l) bath and 0.1 mL was added by syringe to the NMR tube. Final concentrations: [$\mathbf{1}_{\text{ClO}_4}$] = 5 mM, [*p*-fluorophenolate] = 5 mM. The solution was mixed rapidly and formation of violet intermediate was observed. The tube was inserted into the probe to begin data acquisition.

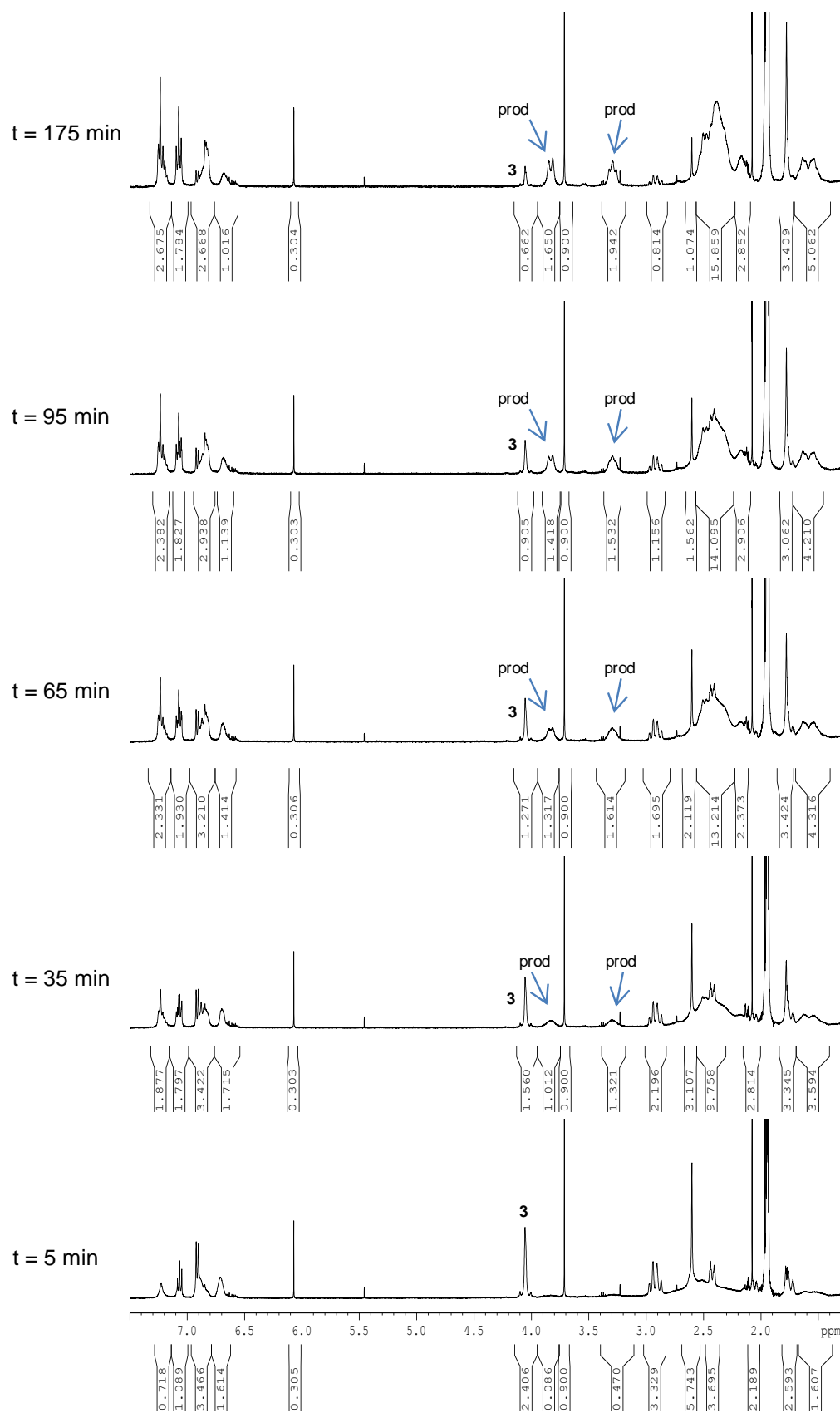


Figure 4.6.3. Monitoring the reaction of complex 1_{ClO_4} with 1 equiv of sodium *p*-fluorophenolate in CD_3CN at -30 °C by $^1\text{H-NMR}$ spectroscopy. Conditions: $[1_{\text{ClO}_4}] = 5$ mM, $[\text{phenolate}] = 5$ mM.

4.7. CW and Pulse-EPR experiments

4.7.4. Sample Preparation

a) Reaction with Proton-sponge®

Stock solutions of complex **1**_{ClO₄} (10 mM) and Proton-sponge® (50 mM) in CH₃CN were prepared under N₂. In vial sealed with a septum under N₂ atmosphere 1 mL of stock solution of complex **1**_{ClO₄} was added by syringe and 0.2 mL of CH₃CN. The solution mixture is cooled with a ice bath. Then 0.8 mL of stock solution of Proton-sponge® and color solution from orange to deep violet. Several aliquots of 0.3 mL were extracted from the reaction mixture at 2 min, 30 min, 1.5 h and 2.5 h and added into an EPR tube under N₂ atmosphere. Finally the EPR sample was frozen with N₂ liquid. Final concentrations were [**1**_{ClO₄}] = 5 mM and [Proton-sponge®] = 20 mM.

For obtaining samples at higher concentrations the following procedure was done. Solution of complex **1**_{ClO₄} (39.2 mg, 0.08 mmols) in 1.55 mL of CH₃CN was prepared in a vial sealed with a septum and under N₂ atmosphere. Then solution of Proton-sponge® (96.3 mg, 0.41 mmols) was prepared also under N₂ atmosphere. The Proton-sponge® solution was then added by syringe to a solution of **2** and stirred over time. Several aliquots of 0.3 mL were extracted from the reaction mixture at 2 min, 10 min and 20 min and added into an EPR tube under N₂ atmosphere. Finally the EPR sample was frozen with N₂ liquid. Final concentrations were [**1**_{ClO₄}] = 44 mM and [Proton-sponge®] = 220 mM.

b) Reaction with triethylenediamine

Stock solutions of complex **1**_{ClO₄} (10 mM) and triethylenediamine (100 mM) in CH₃CN were prepared under N₂. In vial sealed with a septum under N₂ atmosphere 1 mL of stock solution of complex **1**_{ClO₄} was added by syringe and 0.6 mL of acetonitrile. The solution mixture is cooled with an ice bath. Then 0.4 mL of stock solution of triethylenediamine were added and color solution changed from orange to deep violet. An aliquot of 0.3 mL was extracted from the reaction mixture at 2 min and added into an EPR tube under N₂ atmosphere. Finally the EPR sample was frozen with N₂ liquid. Final concentrations were [**1**_{ClO₄}] = 5 mM and [triethylenediamine] = 20 mM.

c) Reaction with sodium *p*-fluorophenolate

Stock solutions of complex **1**_{ClO₄} (10 mM) and sodium *p*-fluorophenolate (10 mM) in CH₃CN were prepared under N₂. In vial sealed with a septum under N₂ atmosphere 1 mL of

stock solution of complex 1_{ClO_4} was added by syringe and cooled with an ice bath. Then 1 mL of stock solution of sodium *p*-fluorophenolate was added and color solution changed from orange to deep violet. An aliquot of 0.3 mL was extracted from the reaction mixture immediately and added into an EPR tube under N_2 atmosphere. Finally the EPR sample was frozen with N_2 liquid. Final concentrations were $[1_{\text{ClO}_4}] = 5 \text{ mM}$ and [*p*-fluorophenolate] = 5 mM.

4.7.5. EPR spectroscopy details

CW EPR measurements at X-band were carried out on a Bruker ESP 380E spectrometer equipped with a rectangular ER 4102ST cavity. Experimental conditions: microwave (mw) frequency, 9.429 GHz; mw power incident to the cavity, 0.2 mW; modulation frequency, 100 kHz; modulation amplitude, 0.1 mT. Cooling of the sample was performed with a liquid-nitrogen finger Dewar ($T = 120 \text{ K}$).

CW EPR measurements at Q-band were carried out on a home-built spectrometer (at IMS Demokritos) equipped with an ER 5106 QT Bruker resonator. Experimental conditions: mw frequency, 34.6 GHz; mw power, 0.05 mW; modulation frequency, 100 kHz; modulation amplitude, 1 mT; temperature, 30 K.

Pulse EPR measurements at X-band (mw frequency 9.717 GHz) were performed at 30 K with a Bruker ESP 380E spectrometer equipped with an EN 4118X-MD4 Bruker resonator. The field-swept EPR spectrum (Figure 4.8.1, top trace) was recorded via the free induction decay (FID) following a pulse length of 500 ns. Davies electron-nuclear double resonance (ENDOR) experiments were carried out with the pulse sequence $\pi - T - \pi/2 - \tau - \pi - \tau - \text{echo}$, with selective ($\Delta t_\pi = 192 \text{ ns}$) or strong ($\Delta t_\pi = 32 \text{ ns}$) mw pulses and a radio-frequency (rf) pulse of length 10 μs . HYSORE experiments² were performed with the pulse sequence $\pi/2 - \tau - \pi/2 - t_1 - \pi - t_2 - \pi/2 - \tau - \text{echo}$ using the following parameters : $t_{\pi/2} = 16 \text{ ns}$; starting values of the two variable times t_1 and t_2 , 56 ns; time increment, $\Delta t = 16 \text{ ns}$ (data matrix 256×256). To avoid blind spots, spectra with different τ values were recorded and added. A four-step phase cycle was used to remove unwanted echoes. The data were processed with the program MATLAB 7.0 (The MathWorks, Natick, MA). The time traces were baseline corrected with a two-order exponential, apodized with a gaussian window and zero filled. After a two-dimensional Fourier transform the absolute-value spectra were calculated.

The CW EPR and ENDOR spectra were simulated with the EasySpin packag.³ HYSORE spectra were simulated with a program written in-house.⁴

2 Schweiger, A.; Jeschke, G. *Principles of pulse electron paramagnetic resonance*, Oxford University Press, Oxford, **2001**.

3. Stoll, S.; Schweiger, A. J. *J. Magn. Reson.*, **2002**, 178, 42.

4. Madi, Z. L.; Doorslaer, S. V.; Schweiger, A. *J. Magn. Reson.*, **2002**, 154, 181.

4.7.6. Quantification of the paramagnetic species

In order to quantify the paramagnetic species appeared after the reaction start, the cw EPR signal intensity (double integral) was compared to a standard Cu^{II} sample, namely $\text{Cu}^{\text{II}}(\text{acac})_2$ in chloroform.

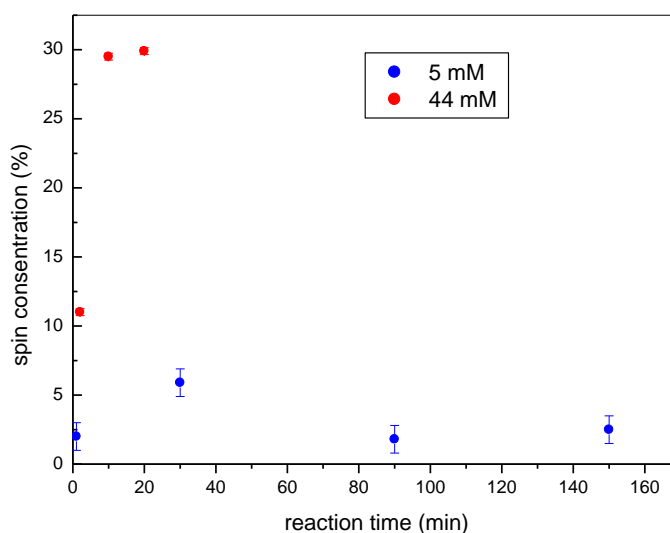


Figure 4.7.1. Relative concentration of paramagnetic species to the initial concentration of 1_{ClO_4} at different reaction times with Proton-sponge[®].

4.8. Identification of the paramagnetic species

4.8.4. ENDOR

All pulsed ENDOR spectra show proton (^1H) couplings ranging from 5 to 15 MHz. Spectrum (e) of Figure 4.8.1: there are clearly two sets of protons with couplings $A_1 = 6$ MHz and $A_2 = 13.5$ MHz. Using strong pulses two peaks at low frequencies appear. They are centered around 6 MHz and separated by approx. 2.5 MHz ($\approx 2\nu_{^{14}\text{N}} = 2.4$ MHz). This is consistent with a strongly coupled ^{14}N with $A = 12$ MHz. This assignment is also supported by the fact that we do not observe the symmetric peak of the 5 MHz peak about ν_{H} (expected around 26 MHz if this was a proton peak). Moreover, HYSORE measurements showed a strongly coupled N with identical parameters (Figures 4.8.3-4.8.5). Finally, the high frequency proton peak from the $A_2 = 13.5$ MHz set (higher intensity peak) is broader than its low-frequency counterpart and this implies an overlap with another peak, possibly arising from another strongly-coupled nucleus. This is in agreement with the spectrum (b) of Figure 4.8.1 showing two sets of proton couplings with an additional peak at 23 MHz. The counterpart of this

peak is missing; therefore it cannot be assigned to protons. A possible assignment is a strongly-coupled nitrogen with $A = 46$ MHz. This value is typical for directly coordinated N ligands in copper complexes, for example equatorially coordinated N ligands in square-planar Cu^{II} complexes. Overall, the ENDOR study shows at least two different sets of weakly coupled protons and presumably two strongly-coupled nitrogens, one with $A = 12$ MHz and another one with $A = 46$ MHz.

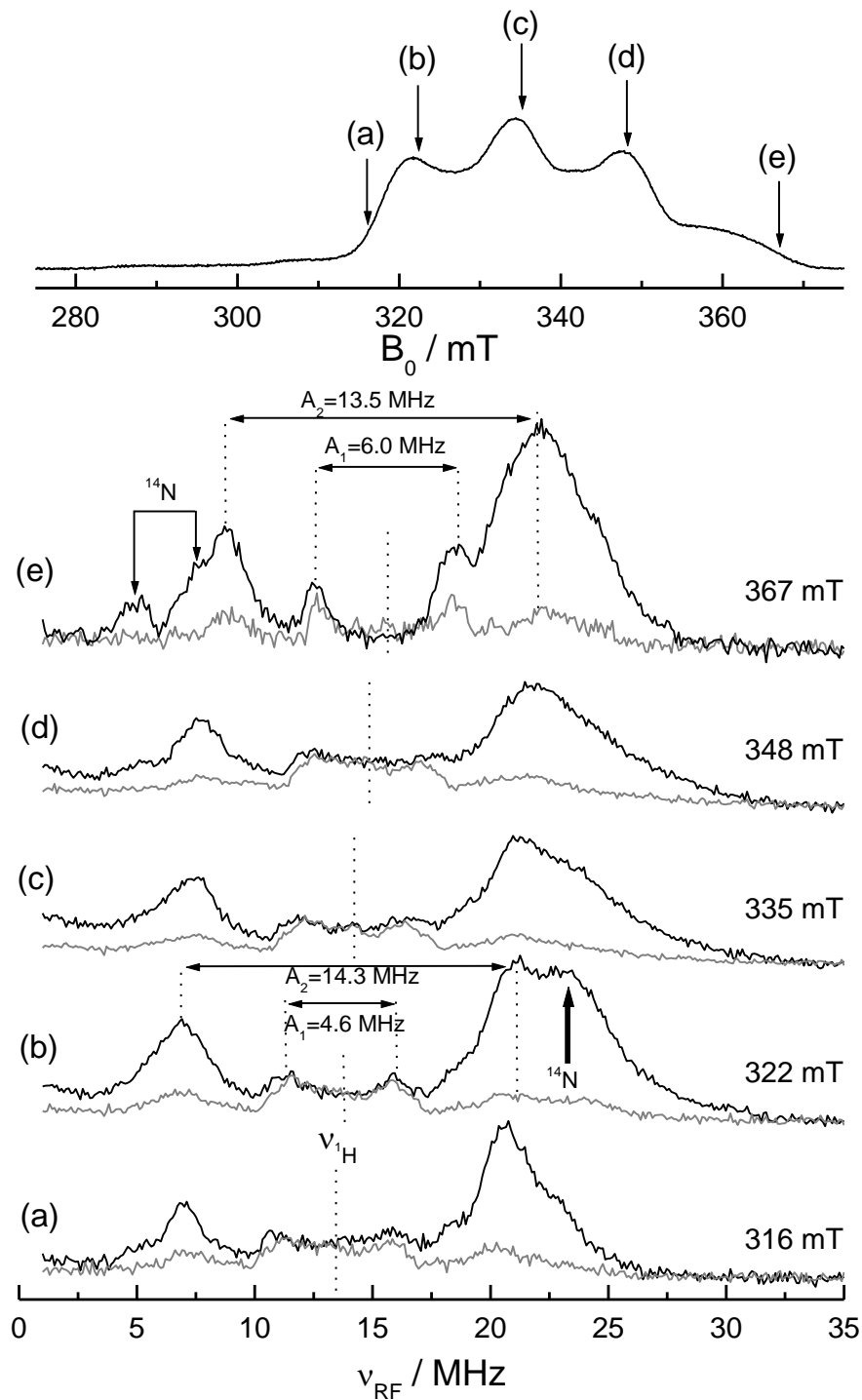


Figure 4.8.1. ENDOR spectra at different observer positions. Black traces: strong mw pulses in order to suppress weak hf couplings ($A < 10 \text{ MHz}$). Gray traces: selective (soft) mw pulses. Top trace: FID-detected field swept EPR spectrum.

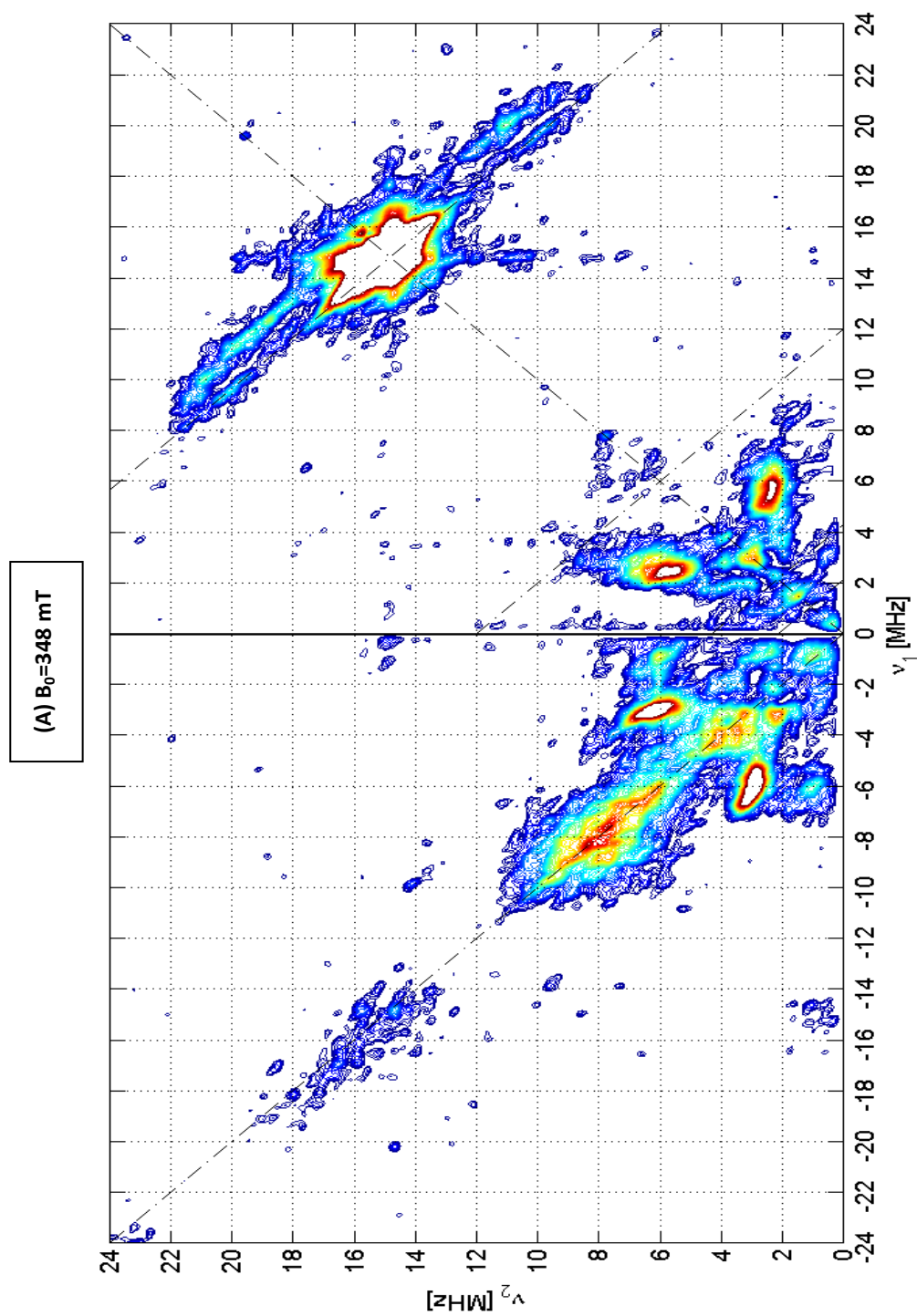
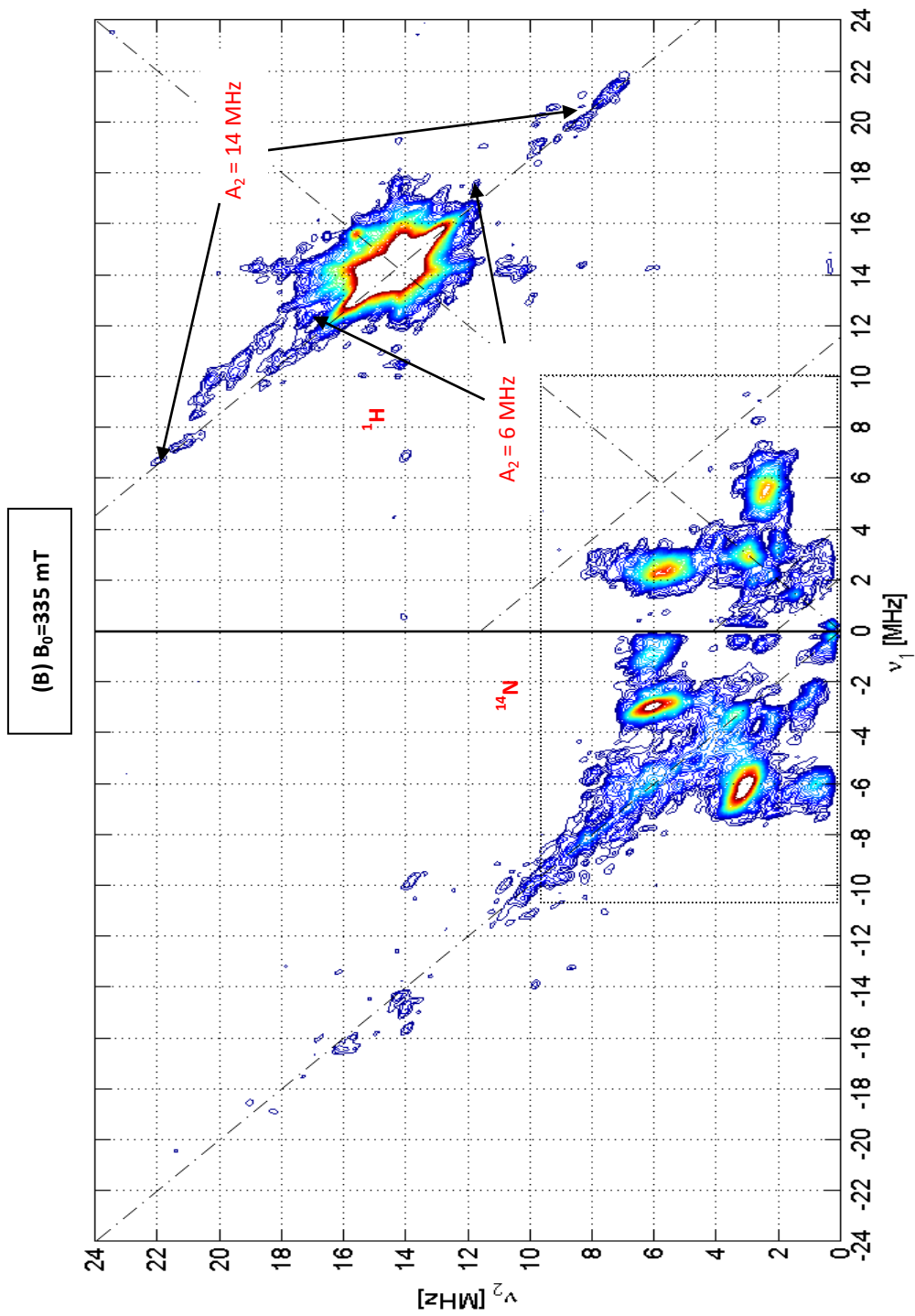


Figure 4.8.2. HSCORE spectrum of **3'** measured at $B_0 = 348$ mT.

Figure 4.8.3. HYSCORE spectrum of **3'** measured at $B_0 = 335$ mT.

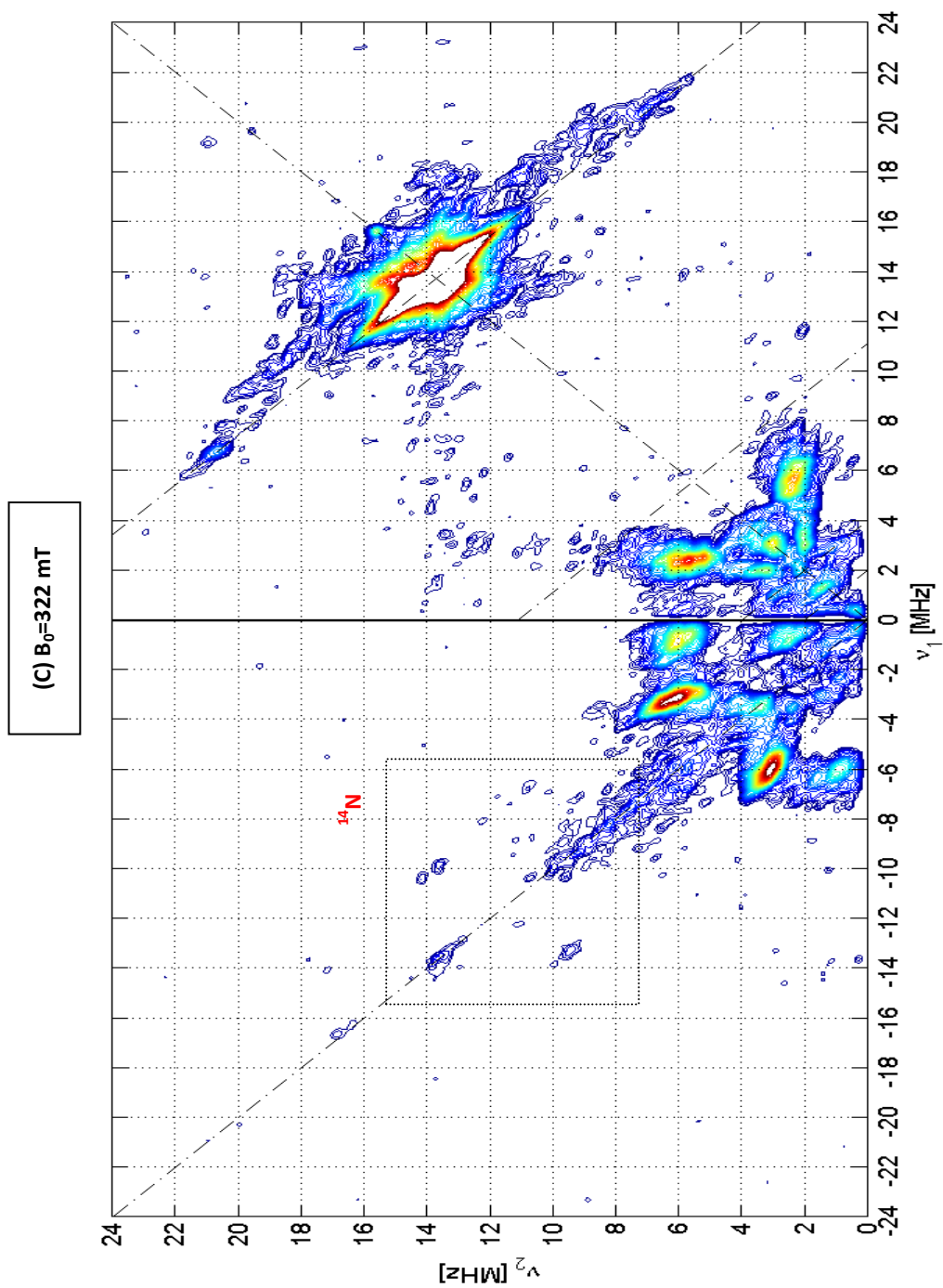


Figure 4.8.4. HYSCORE spectrum of **3'** measured at $B_0 = 322$ mT.

Figures 4.8.3-4.8.5 show three HYSCORE spectra at different observer positions (same as ENDOR, see Figure 4.8.1 upper part-field swept EPR). All spectra contain rich information and reveal proton and nitrogen couplings.

4.8.5. ^1H -HYSCORE

The correlation ridges around the anti-diagonal at 15 MHz are assigned to weakly coupled protons. The hf couplings are in agreement with the ones observed in ENDOR spectra. For example, in Figure 4.8.3 the two marked correlation peaks at (21.7) MHz and (7.21) MHz imply a proton coupling of $A = 21 - 7 = 14$ MHz with a modest anisotropy. This coupling agrees with the coupling A_1 of ENDOR spectra (comparison with spectrum (d) Figure 4.8.1). The stronger proton peaks appear close to diagonal and are marked by a circle (the contour plot cuts high intensity peaks in order to see better the low intensity peaks that are otherwise hidden in the baseline). The correlation peaks are spread up to 6 MHz and agree with the coupling A_2 of ENDOR spectra.

Finally, HYSCORE experiments revealed also a proton coupling with considerable anisotropy. The simulation of the spectrum at $B_0 = 348$ mT (position of correlation peaks, black arcs in figure Figure 4.8.5 below) give the principal values $[A_x, A_y, A_z] = [-3.65, -3.65, 14.8]$ MHz. Assuming an axial A tensor the anisotropic part is $T = 6.15$ MHz which implies a dipole-dipole distance of $r = 2.34$ Angstrom provided that the spin is 100% localized on Cu (this distance is reduced to 1.86 Angstrom if the spin density is 50% at Cu). The spectrum on the right-hand side of Figure 4.8.5 is the full HYSCORE simulation (in time domain, also including peak intensities) of this proton coupling.

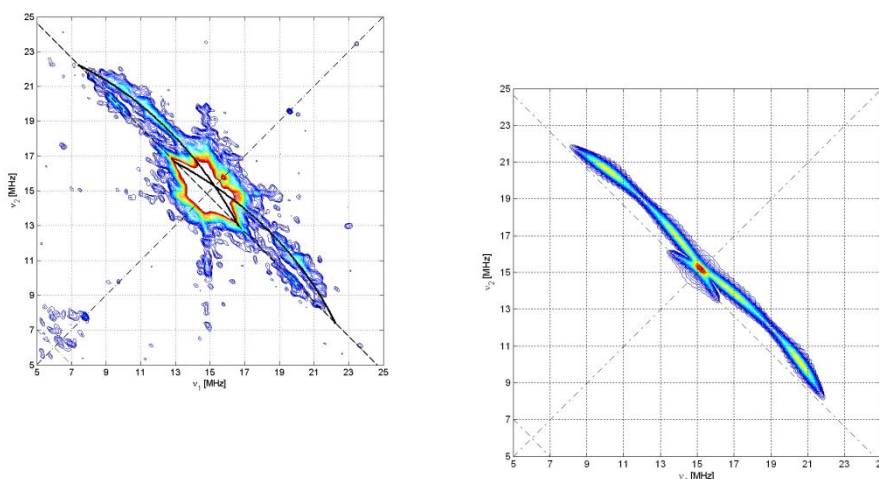


Figure 4.8.5. ^1H -HYSCORE spectrum of **3'** measured at $B_0 = 348$ mT (left) and the corresponding simulation (right).

4.8.6. ^{14}N -HYSCORE

In the (-, +) quadrant of all HYSCORE spectra there are two correlation peaks at (-9.9, 13.6) and (-13.3, 9.4) MHz, marked with a rectangular box in Figure 4.8.4. They are separated by approx. 3.9 MHz ($= 4\nu_N = 3.96$ MHz) and centred around 11.5 MHz. Therefore, these peaks are assigned to the double-quantum transitions of a strongly-coupled nitrogen with $A = 11.5$ MHz. This value nicely agrees with the one observed in ENDOR, see ^{14}N of Figure 4.8.1. In ENDOR spectrum we see the single-quantum transitions that contain information also about the nuclear quadrupole interaction (nqi). However, due to the limited resolution we cannot extract this interaction from ENDOR. Consequently, we cannot further identify this nitrogen.

Finally, in the area marked by a box in Figure 4.8.3, there are intense peaks in both quadrants (Figure 4.8.6). They are assigned to another nitrogen with $A = 4.0$ MHz and a relatively strong nuclear quadrupole coupling.

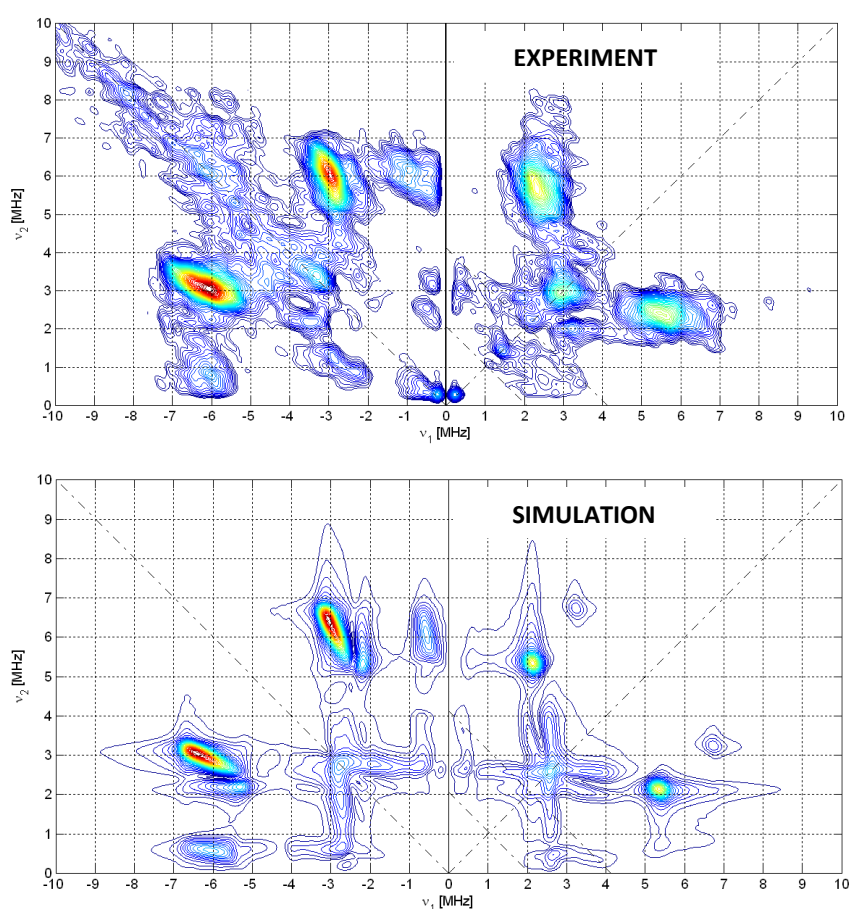


Figure 4.8.6. ^{14}N -HYSCORE spectrum of $\mathbf{3'}$ measured at $B_0 = 335$ mT (top) and the corresponding simulation (bottom). The simulation parameters for the hf coupling are $[A_x, A_y, A_z] = [2.7, 2.7, 4.2]$ MHz, whereas the nuclear quadrupole coupling constant is $|e^2qQ/h| = 3.0$ MHz with asymmetry parameter $\eta = 0.2$.